# ANALYZING SIGNALS OF SOME COMPRESSED SPECTRA IN SUPERSYMMETRY AT LHC

*By*

**JUHI DUTTA**

**PHYS08201205003**

**Harish-Chandra Research Institute, Prayagraj**

*A thesis submitted to the*

*Board of Studies in Physical Sciences*

*In partial fulfillment of requirements*

*for the Degree of*

**DOCTOR OF PHILOSOPHY**

*of*

**HOMI BHABHA NATIONAL INSTITUTE**

**May, 2019**

# Homi Bhabha National Institute[1]

## Recommendations of the Viva Voce Committee

As members of the Viva Voce Committee, we certify that we have read the dissertation prepared by Juhi Dutta entitled "Analyzing signals of some compressed spectra in Supersymmetry at LHC" and recommend that it may be accepted as fulfilling the thesis requirement for the award of Degree of Doctor of Philosophy.

| | | |
|---|---|---|
| Chairman - Prof. Raj Gandhi | | Date: 21/8/19 |
| Guide / Convener - Prof. Santosh Kumar Rai | | Date: 21/8/19 |
| Co-guide - Prof. B. Mukhopadhyaya | B Mukhopadhyay | Date: 21.8.19 |
| Examiner - Prof. Biplob Bhattacherjee | Biplob Bhattacherjee | Date: 21.8.2019 |
| Member 1- Prof. Sandhya Choubey | Sandhya Choubey | Date: 21/8/19 |
| Member 2- Prof. Anirban Basu | A. Basu | Date: 21/8/19 |
| Member 3- Prof. Aditi Sen (De) | Aditi Sen(De) | Date: 21.08.19 |

Final approval and acceptance of this thesis is contingent upon the candidate's submission of the final copies of the thesis to HBNI.

I/We hereby certify that I/we have read this thesis prepared under my/our direction and recommend that it may be accepted as fulfilling the thesis requirement.

**Date: 21.08.2019**

**Place: Prayagraj**

**Prof. B. Mukhopadhyaya**
**Co-guide**

**Prof. Santosh Kumar Rai**
**Guide**

[1] This page is to be included only for final submission after successful completion of viva voce.

# STATEMENT BY AUTHOR

This dissertation has been submitted in partial fulfillment of requirements for an advanced degree at Homi Bhabha National Institute (HBNI) and is deposited in the Library to be made available to borrowers under rules of the HBNI.

Brief quotations from this dissertation are allowable without special permission, provided that accurate acknowledgement of source is made. Requests for permission for extended quotation from or reproduction of this manuscript in whole or in part may be granted by the Competent Authority of HBNI when in his or her judgment the proposed use of the material is in the interests of scholarship. In all other instances, however, permission must be obtained from the author.

Juhi Dutta

Juhi Dutta

# DECLARATION

I, hereby declare that the investigation presented in the thesis has been carried out by me. The work is original and has not been submitted earlier as a whole or in part for a degree / diploma at this or any other Institution / University.

Juhi Dutta

Juhi Dutta

# List of Publications arising from the thesis

## Journal

1. "A Revisit to a Compressed Supersymmetric Spectrum with 125 GeV Higgs", Juhi Dutta, Subhadeep Mondal, Partha Konar, Biswarup Mukhopadhyaya, Santosh Kumar Rai, *JHEP*, **2016**, *01*,051.
2. "Search for a compressed supersymmetric spectrum with a light Gravitino", Juhi Dutta, Subhadeep Mondal, Partha Konar, Biswarup Mukhopadhyaya, Santosh Kumar Rai, *JHEP*, **2017**, *09*,026.
3. "Natural SUSY at LHC with Right-Sneutrino LSP", Arindam Chatterjee, Juhi Dutta, Santosh Kumar Rai, *JHEP*, **2018,** *06*, 042.

## Preprints

1. "Identification Higgsino-like neutralino with a keV-scale dark matter", Juhi Dutta, Biswarup Mukhopadhyaya, Santosh Kumar Rai, arXiv: 1904.08906.

# List of Publications not included in the thesis

## Journal

1. "SModelS extension with the CMS supersymmetry search results from Run 2", Juhi Dutta, Sabine Kraml, Andre Lessa, Wolfgang Waltenberger, *LHEP*, **2018,** *1*, 5-12.

### Conferences

1. Presented a talk "Analyzing signals of Compressed spectra in SUSY", SUSY, 2017, TIFR, Mumbai, India.
2. Presented a talk "Light Higgsinos at the LHC with Right-Sneutrino LSP", XXIII DAE-BRNS HEP Symposium, 2018, IIT Madras, India

Juhi Dutta

Juhi Dutta

**Dedicated to**

**Ma, Baba and Dada**

# ACKNOWLEDGEMENTS

First and foremostly I am grateful to my supervisor Prof. Santosh Kumar Rai for giving me an opportunity to work under his supervision for the last five years. His constant support, timely guidance and patience along with critical insights and suggestions have been instrumental in completing my work. I am grateful to my thesis co-supervisor Prof. Biswarup Mukhopadhyaya for his constant support, guidance, insights and encouragement during my thesis work. I am thankful to both of them for introducing me to the problems studied in this thesis and their patience without which this thesis would not have been possible.

I express my sincere gratitude to all my collaborators who have helped me learn. I am grateful to Prof. Partha Konar, Dr. Subhadeep Mondal and Dr. Arindam Chatterjee for sharing their knowledge and their help throughout. I thank Prof. Sabine Kraml for involving me in the SModelS collaboration. It was a learning experience for me. I also thank the SModelS group Andre, Wolfgang, Ursula, Jan, Jory among others who made the stay at Grenoble during this period enjoyable.

I am grateful to my graduate committee members Prof. Raj Gandhi, Prof. Sandhya Choubey, Prof. Aditi (Sen) De and Prof. Anirban Basu for their constant support during the duration of my PhD and their comments and suggestions on my work. My teachers Prof. Sumathi Rao, Prof. Raj Gandhi, Prof. Anirban Basu, Prof. Rajesh Gopakumar, Prof. Satchidananda Naik, Prof. Prasenjit Sen, Prof. Sandhya Choubey, Prof. Dileep Jatkar, Prof. Ashoke Sen, Prof. Asesh Krishna Datta and Dr. Pratishruti Saha have offered great courses and advice over the years. I am indebted to the HEP group at HRI over the years who have helped me learn actively from discussions and workshops organised frequently. I express my gratitude to Siddharth, Kasinath, Jyotiranjan, Ushoshi, Shankha, Nabarun, Indrani, Atri, Anushree, Mehedi, Avirup, Arpan, Atri, Jayita, Toushik, Arif, Satadal, Titas, Ankur and Ruchi for their tolerance and support as well as advice over academic and non-academic issues over the years during our daily life at HRI making my stay at HRI enjoyable.

I thank RECAPP for supporting my academic travels to schools and conferences during my PhD as well as to the HRI administration, computer centre and office-staff who took care of the practical aspects of my stay at HRI. Last, but definitely not the least, I thank my family, especially Ma, Baba, Dada, Mamu, Masimoni, Boromasi and Mesomosai for their love, care, patience, support, encouragement and motivation without which this often arduous journey would never have been possible. I also thank my friends Swagata, Pallabi, Madhurima and Promita for their patience and support. I am indebted to HRI for being a second home to me over the years.

# CONTENTS

# SUMMARY

The discovery of a Standard Model (SM)-like 125 GeV Higgs boson at the Large Hadron Collider (LHC) [1], has more or less confirmed SM as the theory that accounts for almost all known particle interactions. However there still remain various unexplained phenomena in Nature which implore us to seek answers beyond the SM (BSM). Supersymmetry (SUSY) is one of the most well motivated extensions of SM to address some of the issues [2]. Weak scale SUSY allows rich phenomenology of signals to be tested at experiments. However, the absence of any new physics signal is a source of exasperation to those in search of BSM physics.

This lack of evidence for any low scale SUSY events prompted the idea of a compressed sparticle spectrum [3–5], where the lightest SUSY particle (LSP) and the heavier sparticle states may be nearly degenerate. The resulting final state jets and leptons from the decay cascades of the parent particles are expected to be very soft, including the overall missing transverse energy ($\not{E}_T$) which is a manifestation of the available visible transverse momenta. Thus, such signals allow a much lighter SUSY spectrum compared to the conventional channels with hard leptons, jets and large missing transverse momentum [6].

In many recent studies, experimental as well as theoretical, the deciding factor is assumed to be the mass splitting between the colored members such as gluino/squarks and the LSP. However, given the manifold diversity of an MSSM spectrum, *we have preferred to think not in terms of some compression parameter(s) in a somewhat simplified spectrum but to work with a wide assortment of benchmark points, which reflect as many different possibilities as possible.* We have presented results for some benchmark points where the *entire spectrum* lies tightly compressed. After a detailed study of this variety of benchmarks, consistent with the Higgs mass as well as collider and dark matter constraints, we reach the conclusion that signals comprising multi-jets are likely to be more useful in the 13/14 TeV runs, as compared to those depending upon mono-jets [7].

Such a compressed spectrum when augmented with a light gravitino ($\widetilde{G}$) as the LSP, as in gauge mediated SUSY breaking (GMSB) models [8], leads to significantly different signatures. The $\widetilde{\chi}_1^0$ is now the next-to-lightest SUSY particle (NLSP) which decays into a $\widetilde{G}$ and a gauge/Higgs boson depending on its composition. Taking a bino-dominated $\widetilde{\chi}_1^0$ NLSP, one or more hard photons are expected in the final state. On the other hand, the

presence of a higgsino-dominated NLSP leads to a preponderance of $Z$ or Higgs bosons in the final state.We investigate such signals at the 13 TeV LHC in presence of compressed SUSY spectra [9, 10]. In the bino-dominated NLSP case, we analyse and compare the discovery potential in different benchmark scenarios consisting of both compressed and uncompressed SUSY spectra, considering different levels of compression and intermediate decay modes. Our conclusion is that compressed spectra upto few TeV are likely to be probed even before the high luminosity run of LHC. Kinematic variables are also suggested, which offer distinction between compressed and uncompressed spectra yielding similar event rates for photons + multi-jets + $\not{E}_T$. We also distinguish between a higgsino-dominated and gaugino-dominated NLSP scenario using the polarisation information of the $Z$ boson and new variables enhancing the asymmetry in the angular distributions have been proposed in order to characterize a longitudinally polarised $Z$ boson in the former case in comparison to a transversely polarised $Z$ boson in the latter case.

Therefore, we observe that the presence of non-standard LSP candidates, such as a light $\widetilde{G}$, renders the $\widetilde{\chi}_1^0$ to be the NLSP thereby providing alternate modes of discovery of such scenarios. In the same spirit, a naturally occuring compressed sector in the MSSM, namely the low-lying electroweakino sector dominated by higgsinos, may be probed in simple extensions of the MSSM. In this direction, an extension of the MSSM with additional right-handed singlet neutrino superfields opens up the possibility of having the right-sneutrinos ($\widetilde{\nu}_R$). It also provides a mechanism for generation of light neutrino masses. We give a detailed account of how the decay of the light electroweakinos depend on the various supersymmetric parameters that govern the mixing, mass-splitting and in which region of the parameter space the decays are prompt. We also highlight how even the smallest gaugino admixture plays a significant role in their decays. We then look at possible signals that arise from such a spectrum and analyse them at LHC. The presence of a mixed right-sneutrino as the LSP can lead to a very different signature from the compressed higgsino-like states, mostly due to the leptonic decay of the light chargino ($\widetilde{\chi}_1^{\pm}$) leading to multi-leptonic channels along with $\not{E}_T$ [11].

In conclusion, this thesis primarily looks into ways of discovering largely as well as partially compressed SUSY scenarios within the phenomenological MSSM framework and also in its extensions yielding different LSP candidates such as $\widetilde{\chi}_1^0$, $\widetilde{G}$ or $\widetilde{\nu}_R$. We analyse signals of such spectra and observe that multi-jets, multi-leptons as well as photonic signals, with appropriate event selection criteria, are promising signatures at LHC. We also observe that using polarisation of gauge bosons, one can determine the nature of the parent NLSP.

# List of Figures

# List of Tables

# Chapter 1

# Introduction

## 1.1 The Standard Model

Experiments have established the presence of fundamental spin-$\frac{1}{2}$ fermions, spin-1 gauge bosons and a spin-0 scalar in the observable universe. The matter content of the universe and three of the four fundamental forces in nature, electromagnetism, weak and the strong force are described by gauge interactions in the framework of a quantum field theory known as the Standard Model (SM) of Particle Physics. The SM has withstood rigorous experimental scrutiny over the years at experiments such as the Large Electron-Positron Collider (LEP) and Tevatron, and now at the Large Hadron Collider (LHC), all making discoveries consistent with the predictions of SM. It is amazing that we have not observed any appreciable deviations from the SM predictions as yet.

The SM is a gauge theory where the underlying symmetry is described by the gauge groups $SU(3)_C \times SU(2)_L \times U(1)_Y$ corresponding to the color, weak isospin and hypercharge gauge groups respectively. The matter content of the SM consists of six flavours of spin-$\frac{1}{2}$ quarks and leptons. The six fundamental quarks and leptons are divided into three generations, each generation being exact copies of one another under the SM gauge symmetry, whereas the interactions between the matter particles are mediated by gauge bosons which correspond to the generators of the SM gauge group. To begin with, all SM fermions and gauge bosons are massless, respecting the gauge symmetry. They obtain mass after a phenomenon called spontaneous symmetry breaking (SSB) occurs, commonly known as the Higgs mechanism where the $SU(2)_L \times U(1)_Y$ symmetry breaks down to $U(1)_{em}$.

The particle content of the SM and the quantum numbers under the gauge groups are summarized in Table 1.1. The left-handed quarks and leptons are doublets of $SU(2)_L$ and are denoted by $q_L^i$ and $\ell_L^i$ respectively. The right-handed counterparts are singlets with the quarks denoted by $u_R^i$ and $d_R^i$ for the up-type and down-type quark respectively while the leptons are denoted by $e_R^i$ where $i = 1, 2, 3$ is the generation index. Note that there is no right-handed neutrino ($\nu_R^i$) in the SM. All quarks participate in the strong interactions and

| Name | $SU(3)_C$ | $SU(2)_L$ | $U(1)_Y$ |
|---|---|---|---|
| $q_L^i = \begin{pmatrix} u_L^i \\ d_L^i \end{pmatrix}$ | 3 | 2 | 1/3 |
| $u_R^i$ | 3 | 1 | 4/3 |
| $d_R^i$ | 3 | 1 | -2/3 |
| $\ell_L^i = \begin{pmatrix} \nu_L^i \\ e_L^i \end{pmatrix}$ | 1 | 2 | -1 |
| $e_R^i$ | 1 | 1 | -2 |
| $\phi = \begin{pmatrix} \phi^+ \\ \phi^0 \end{pmatrix}$ | 1 | 2 | 1 |
| $G_\mu$ | 8 | 1 | 0 |
| $W_\mu$ | 1 | 3 | 0 |
| $B_\mu$ | 1 | 1 | 0 |

Table 1.1: The particle content of the SM.

are represented as color triplets of $SU(3)$ whereas all leptons are color singlets. The massless gauge bosons in the SM are the color octet gluons $G_\mu$, $SU(2)_L$ triplet $W_\mu$ and $U(1)_Y$ singlet $B_\mu$.

The electric charge $Q$ of the particles is defined as

$$Q = I_3 + \frac{Y}{2} \tag{1.1.1}$$

where $I_3$ and $Y$ represent the quantum numbers for third component of weak isospin and hypercharge respectively. The up-type quark with $I_3 = \frac{1}{2}$ and $Y = \frac{1}{3}$ has charge $Q = \frac{2}{3}$ whereas the down-type quark with $I_3 = -\frac{1}{2}$ and $Y = \frac{1}{3}$ carry $Q = -\frac{1}{3}$. Similarly, for the charged leptons ($e_i$) $Q = -1$ whereas the neutrinos are chargeless. In addition, SM has a scalar $\phi$, which is a color singlet $SU(2)_L$ doublet with weak hypercharge $Y = 1$ and is responsible for giving mass to all SM particles. The SSB happens when the neutral component of this scalar doublet $\phi$ obtains a vacuum expectation value ($vev$) which breaks the electroweak symmetry in vacuum (Higgs mechanism) leading to mass terms for the quarks and charged leptons while the neutrinos remain massless. The massive spin-1 bosons, namely, the $W^{\pm}$ and $Z$ bosons correspond to the broken generators which mediate the electroweak interactions while the massless gauge bosons corresponding to the unbroken generators are photon and gluons which mediate the electromagnetic and strong force respectively.

The full gauge invariant SM Lagrangian is [12]

$$\mathcal{L}_{SM} = \mathcal{L}_f + \mathcal{L}_G + \mathcal{L}_H + \mathcal{L}_Y \tag{1.1.2}$$

where $\mathcal{L}_f$ constitutes the fermionic Lagrangian, $\mathcal{L}_G$ stands for the Lagrangian describing the gauge bosons, $\mathcal{L}_H$ constitutes the Higgs part of the Lagrangian, and $\mathcal{L}_Y$ describes the Yukawa interactions involving the fermions and the Higgs doublet. The fermionic part of the Lagrangian (generation and color indices are suppressed) is

$$\mathcal{L}_f = \bar{q}_L i\not{D} q_L + \bar{u}_R i\not{D} u_R + \bar{d}_R i\not{D} d_R + \bar{\ell}_L i\not{D} \ell_L + \bar{e}_R i\not{D} e_R \quad . \tag{1.1.3}$$

Here $D_\mu$ is the covariant derivative.

$$D_\mu = \partial_\mu + ig'\frac{Y}{2}B_\mu + ig\frac{\vec{\sigma}}{2}.\vec{W}_\mu + i\frac{g_s}{2}\lambda_a G^a_\mu \tag{1.1.4}$$

for the quark doublets, where $\vec{\sigma} = (\sigma_1, \sigma_2, \sigma_3)$ refers to the Pauli matrices, $\lambda_a$ refer to the Gell-Mann matrices where $a = 1, .., 8$. The coefficients $g'$, $g$ and $g_s$ refer to the gauge coupling constants while $B_\mu$, $W_\mu$ and $G^a_\mu$ refer to the massless gauge bosons of $U(1)_Y$, $SU(2)_L$ and $SU(3)_C$ respectively. Note that the last term in Eq. 1.1.4 is absent for the lepton doublets. The covariant derivate for the $SU(2)_L$ and $SU(3)_C$ singlet fermions take a simpler form, defined without the corresponding terms in Eq. 1.1.4. The Lagrangian for the gauge bosons is

$$\mathcal{L}_G = -\frac{1}{4}G^{a\mu\nu}G_{a\mu\nu} - \frac{1}{4}B^{\mu\nu}B_{\mu\nu} - \frac{1}{4}W^{k\mu\nu}W^k_{\mu\nu} \tag{1.1.5}$$

where $G^{a\mu\nu}$ is the gluon field strength tensor. It is defined as

$$G^a_{\mu\nu} = \partial_\mu G^a_\nu - \partial_\nu G^a_\mu - g_s f^{abc} G^b_\mu G^c_\nu \tag{1.1.6}$$

where $a, b, c$ are the color indices and $f^{abc}$ refer to the totally antisymmetric structure constants of $SU(3)_C$. Also,

$$B_{\mu\nu} = \partial_\mu B_\nu - \partial_\nu B_\mu,$$
$$W^k_{\mu\nu} = \partial_\mu W^k_\nu - \partial_\nu W^k_\mu - g\epsilon^{ijk} W^i_\mu W^j_\nu$$

are the field strength tensors corresponding to the hypercharge and electroweak gauge fields, while $\epsilon^{ijk}$ represents the totally antisymmetric structure constants for $SU(2)_L$ and $i, j, k = 1, 2, 3$ are the $SU(2)_L$ indices.

The Higgs Lagrangian is defined as

$$\mathcal{L}_H = |D_\mu \phi|^2 + \mu^2 \phi^\dagger \phi - \lambda(\phi^\dagger \phi)^2 \tag{1.1.7}$$

while the Yukawa Lagrangian is

$$\mathcal{L}_Y = -y_u^{ij} \bar{Q}_i.\phi^c u_{R_j} - y_d^{ij} \bar{Q}_i.\phi \, d_{R_j} - y_l^{ij} \bar{L}_i.\phi \; e_{R_j} + h.c. \tag{1.1.8}$$

where $i, j = 1, 2, 3$ are the family indices of the SM fermions. Here $y_f$ ($f = u, d, e$) refer to the $3 \times 3$ matrices for the Yukawa couplings of the up-type quarks, down-type quarks and the leptons. Note that all the quarks and leptons obtain masses after spontaneous symmetry breaking (SSB) occurs when the neutral component of the Higgs doublet, i.e, $\phi^0$ obtains vacuum expectation value (*vev*). Note that the down-type quarks and leptons obtain mass from the Higgs doublet $\phi$ while the up-type quarks obtain mass from $\phi^c = i\sigma^2\phi^*$ where $\phi^c$ has $Y = -1$. The electroweak gauge bosons mix with one another and obtain mass from the Higgs field after spontaneous symmetry breaking. We discuss the phenomena of SSB briefly in the following section.

### 1.1.1 Spontaneous Symmetry Breaking

In this section, we briefly outline the phenomena of *spontaneous symmetry breaking* [13–15] *viz.*, the Higgs mechanism. The Higgs Lagrangian in Eq. 1.1.7 can be rewritten as

$$\mathcal{L}_H = |D_\mu \phi|^2 - V_H$$

where $V_H$ is the Higgs potential given by

$$V_H = -\mu^2 \phi^\dagger \phi + \lambda(\phi^\dagger \phi)^2 \,. \tag{1.1.9}$$

The complex Higgs doublet is defined as

$$\phi = \begin{pmatrix} \phi^+ \\ \phi^0 \end{pmatrix}$$

where $\phi^+$ and $\phi^0$ are complex scalars which can be written out in terms of real scalars ($\phi_i\,;\, i = 1, 2, 3, 4$) as

$$\phi = \frac{1}{\sqrt{2}} \begin{pmatrix} \phi_1 + i\phi_2 \\ \phi_3 + i\phi_4 \end{pmatrix}.$$

The term proportional to $\lambda$ describes the self interaction of the Higgs field. Note that for $\lambda > 0$ the Higgs potential is bounded from below. The minimum of $V_H$ corresponds to a non-vanishing $\phi$ for $\mu^2 > 0$ given by

$$\frac{v}{\sqrt{2}} = \frac{\sqrt{\mu^2}}{2\lambda} \tag{1.1.10}$$

where $\phi^\dagger \phi = \frac{v^2}{2}$. Writing $\phi$ in the unitary gauge as

$$\phi = \frac{1}{\sqrt{2}} \begin{pmatrix} 0 \\ v + h \end{pmatrix}$$

in the Higgs potential, one obtains the mass of the Higgs as

$$m_h = v\sqrt{2\lambda}\,. \tag{1.1.11}$$

The recent measurements of Higgs mass at LHC give $m_h \sim 125$ GeV [1,16] and using $v = 246$ GeV one gets the self-interaction strength of the Higgs boson as $\lambda \sim 0.13$. Note that in SM both $\mu^2$ and $\lambda$ are free parameters. Once the Higgs field obtains a *vev*, the quarks and leptons obtain mass through the Yukawa interaction terms, whereas the gauge bosons acquire mass by absorbing the massless Goldstone bosons which constitute their *longitudinal* modes. The mass of the fermions and gauge bosons after SSB are given by

$$m_f = y_f \frac{v}{\sqrt{2}} \tag{1.1.12}$$

$$m_W = \frac{1}{2} g\ v \tag{1.1.13}$$

$$m_Z = \frac{1}{2} \sqrt{(g^2 + g'^2)}\ v \tag{1.1.14}$$

where $m_f$, $m_W$ and $m_Z$ are the masses of the fermions, $W^\pm$ and $Z$ bosons respectively. Note that the SU(2)$_L$ and U(1)$_Y$ gauge couplings get related after SSB as $\tan\theta_W = g'/g$ where

$\theta_W$ is the weak mixing angle. The SU$(2)_L$ coupling constant $g = \frac{e}{\sin\theta_W}$ where $e$ is the electric charge and the weak mixing angle is measured to be $\sin^2\theta_W \sim 0.231$ [17].

Note that the above masses are predicted at the tree-level. However, SM being a quantum theory would imply radiative corrections to these masses at higher orders in perturbation theory. Large corrections are avoided for fermions and gauge bosons in SM by symmetry principles. Chiral symmetry (i.e, invariance under $\psi \to e^{i\alpha\gamma_5}\psi$) plays an important role in protecting the tree-level masses of quarks and leptons from large radiative corrections while gauge bosons are also protected from radiative corrections by gauge symmetry. However, scalars such as the Higgs boson are not protected under any such symmetry and therefore susceptible to large quantum corrections to the Higgs mass which may lead to the instability of the electroweak scale. We discuss this issue in the following section.

## 1.2 Going Beyond Standard Model

Despite its success, there are pertinent reasons to think beyond SM for a complete description of Nature. We briefly review some of these reasons below:

1. **Free parameters of the SM:**

   Although the SM provides an accurate description of Nature it is plagued by a number of free parameters in the theory whose values do not have any underlying justification. Among the 18 free parameters are the six quark masses, three lepton masses, three gauge coupling constants, three quark mixing angles, one CP-phase for the quark mixing matrix, Higgs mass and the QCD theta ($\theta$) term. SM does not explain why there are three generations of quarks and leptons and the reason for the observed mass hierarchy among the quarks and leptons. The flavor mixing structure of the quarks is also not explained within the SM and motivates one to think beyond SM.

2. **Neutrino Mass:**

   Measurements of neutrino oscillation phenomena have established affirmatively that neutrinos have a small ($\lesssim \mathcal{O}(0.1)$ eV) but non-zero mass [18]. However in absence of a right-handed neutrino the SM does not account for a gauge invariant mass term for the neutrinos. SM also fails to explain the mixing amongst the light neutrinos, namely the Pontecorvo-Maki-Nakagawa-Sakata (PMNS) matrix. However if one considers lepton number non-conservation as observed in neutrino oscillation, a lepton number violating ($\Delta L = 2$) effective dimension five operator $\frac{1}{\Lambda_M}\bar{L}\phi\phi L^c$ [19] gives rise to a Majorana mass

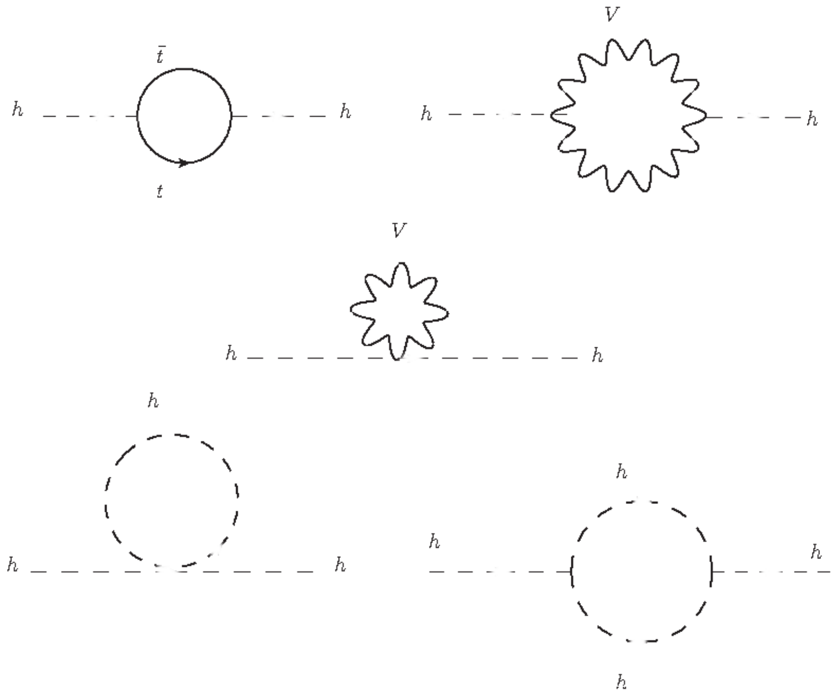


Figure 1.1: Contribution from SM top quark and gauge bosons $V = W^{\pm}, Z, h$ to the Higgs mass [27].

term for the neutrinos once the Higgs obtains a *vev*. Here, $\Lambda_M$ is the heavy scale after which effects of the new physics giving rise to this operator should be accounted for. Neutrino masses may be generated in minimal extensions of the SM such as in the Type-I seesaw mechanism [20–22] using gauge singlet right-handed neutrinos, in Type-II seesaw mechanism using a scalar triplet [23, 24] or in Type-III seesaw mechanism using fermion triplets [25, 26].

3. **Naturalness problem**:

   Radiative corrections to the tree level Higgs mass, $\Delta m_h^2$, arises from contributions involving the SM top quark, $W^{\pm}$ bosons, $Z$ boson as well as self coupling of the Higgs bosons [12] as seen in Figure 1.1 and expressed as

$$\Delta m_h^2 = \frac{3}{16}\frac{\lambda}{\pi^2}\Lambda^2[m_h^2 + 2m_W^2 + m_Z^2 - 4m_t^2]. \tag{1.2.1}$$

   The quadratically divergent term is proportional to $\Lambda^2$, where $\Lambda$ is the cut off scale at which new physics effects start appearing. This implies that the Higgs mass may be radiatively raised to, say, the Planck scale, if the SM continues to hold all the way.

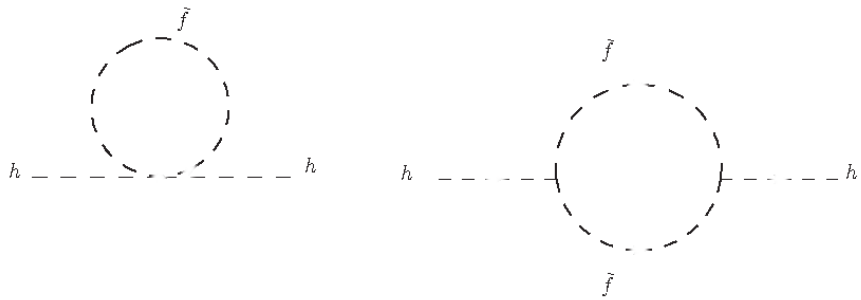


Figure 1.2: Contribution from $\widetilde{f}(=\widetilde{t}_L, \widetilde{t}_R)$ to the Higgs mass [27].

However such a consequence may be avoided if there are cancellations up to 30 decimal places among the various parameters contributing to the radiative contributions. Such a large cancellation is rather fine-tuned and undesirable for a physical theory. This is referred to as the naturalness problem. This primarily motivates us to think beyond SM in order to resolve this issue. As an example, Supersymmetry, a symmetry between fermion and bosons, is one of the best candidates to resolve the naturalness problem of the Higgs mass. It provides two extra complex scalars in the theory corresponding to the SM top, namely, the left-handed and right-handed superpartners of the top, $\widetilde{t}_L$ and $\widetilde{t}_R$ respectively. Contribution from the Lagrangian term $\lambda_S|\widetilde{t}_L|^2|\phi|^2$ to the Higgs mass as seen in Figure 1.2 is

$$\Delta m_h^2 = \frac{\lambda_S}{16\pi^2}[\Lambda_S^2 - 2m_S^2 \log \Lambda_S/m_S + \text{finite terms}] \tag{1.2.2}$$

where $\Lambda_S$ is the SUSY scale and $m_S$ the stop mass. Note that a judicious choice of the couplings involved i.e, $|y_t^2| = \lambda_S$ for $\widetilde{t}_L$ and $\widetilde{t}_R$ leads to a cancellation of the quadratic divergences retaining only the mild logarithmic divergent term. Such a cancellation also occurs for the contribution arising from the $W$ and $Z$ bosons notably due to the contributions of their fermionic superpartners to the Higgs mass at all loop orders owing to the symmetry relating fermions and bosons.

4. **Dark Matter and Dark Energy:**

Observation of galactic rotation curves show that rotational velocity of the galaxies remains rather flat as the distance of the star from the center of the galaxy increases [28]. However, Newtonian gravity predicts that the velocity ($v$) must decrease as the distance from the center of the galaxy increases such that

$$v \propto \sqrt{\frac{M}{R}} \tag{1.2.3}$$

where $M$ is the mass of the galaxy and $R$ is the distance from the center of the galaxy. Thus the observation of the flat rotation curves indicates that the mass of the galaxy must also increase as one moves away from the center of the galaxy. Current observations show that the requisite mass is nearly five times the visible mass of the galaxy. This unobserved mass is referred to as the dark matter (DM). On the other hand, observations from the Bullet cluster, a consortium of two galaxies which collided with each other, has been experimentally observed using gravitational lensing techniques [29]. It has been found to have a greater accumulation of mass as opposed to the observed visible mass from stars at the edges of the Bullet cluster leading to a greater gravitiational bending of light at the edges of the Bullet cluster. This is one of the best known evidence of dark matter. Finally, analysis of the anisotropies of the cosmic microwave radiation (CMB) from the Big Bang together with baryon-acoustic oscillation (BAO) data as measured by Planck [30] provides the most accurate measurement of the relic abundance of the matter content of the universe showing that non-baryonic, non-luminous dark matter is nearly five times that of the ordinary matter. The current measurement of the DM relic density is [30]

$$\Omega h^2 = 0.1193 \pm 0.00091 \tag{1.2.4}$$

Observations from the Hubble telescope have unequivocally established that the universe is accelerating. The acceleration is attributed to the presence of dark energy, which is hypothesized as a repulsive potential to counter the gravitational attraction between the stars. It has been estimated from the CMB data that the current universe has a preponderance of dark energy contributing nearly 71.4% of the total energy content of the universe while dark matter forms nearly 24% and matter consists of 4.6% [31]. SM does not explain the dark matter and dark energy content of the universe. This forces one to think beyond the SM in order to incorporate dark matter and dark energy.

5. **Matter-Antimatter Asymmetry:**

   There is a predominance of matter over antimatter in the universe referred to as baryon asymmetry. This asymmetry is quantified in terms of the parameter $\eta_B$ defined as

$$\eta_B = \frac{n_B - n_{\bar{B}}}{n_\gamma} \tag{1.2.5}$$

   where $n_B$, $n_{\bar{B}}$ and $n_\gamma$ refer to the number densities corresponding to matter, anti-matter and photons. Experiments indicate $5.7 \times 10^{-10} \leq \eta_B \leq 6.7 \times 10^{-10}$ [32,33] as measured from the abundances of light elements produced during Big Bang Nucleosynthesis. Since the Big Bang is expected to produce equal amount of baryons and anti-baryons, a theory would require to obey Sakharov's conditions [34] in order to explain the observed baryon asymmetry. Sakharov's conditions require

- Departure from thermal equilibrium
- Baryon number violation
- C and CP violation

Although SM does allow CP violation in the quark sector via the Cabibo-Kobayashi-Maskawa (CKM) phases, the generated CP violation is insufficient to explain the required asymmetry parameter $\eta_B$ [35]. This therefore forces one to think beyond the SM in order to the explain the observed baryon asymmetry of the universe.

6. **Gravity**

   Among the four fundamental interactions in Nature, namely, gravity, electromagnetism, strong force and weak force, SM describes the latter three forces. It however does not incorporate gravitational interactions. In order to motivate a complete theory which encompasses all the four interactions, one must think of extensions to the minimal version of SM. Such a theory would be desirable as it points towards a unified picture of the fundamental interactions in Nature providing a complete description of the current universe at all energy scales.

All of these outstanding issues implore us to think beyond the SM. In this regard, Supersymmetry, which is the topic of my thesis, has been one of the prime contenders of BSM physics to answer some of these issues.

# Chapter 2

# Supersymmetry Phenomenology

Supersymmetry (SUSY) has been one of the best motivated candidates for physics Beyond the Standard Model (BSM). Several excellent articles [2,27,36] and text books [37–39] exist on the subject, covering the basics and theoretical aspects of supersymmetry. As our focus in this thesis will be on SUSY phenomenology, we only discuss the relevant aspects of SUSY formalism applicable for this thesis. Supersymmetry is a special symmetry connecting fermions and bosons which postulates a superpartner for every SM particle, differing by spin-$\frac{1}{2}$. It addresses the naturalness problem, also known as the gauge hierarchy problem as discussed in Chapter 1. R-parity, a discrete symmetry when conserved in SUSY also offers a dark matter candidate which is the lightest of all SUSY particles and usually taken to be the lightest neutralino $\widetilde{\chi}_1^0$.

In this chapter we discuss briefly the Minimal Supersymmetric Standard Model (MSSM), the supersymmetrized version of the SM. The MSSM retains the same gauge group as the SM, i.e, $SU(3)_C \times SU(2)_L \times U(1)_Y$. The SM particle and its superpartner are arranged in the form of supermultiplets, namely, chiral supermultiplets for SM fermions and the Higgses whereas vector (gauge) supermultiplets for the SM gauge bosons. SUSY algebra demands that the number of fermionic and bosonic degrees of freedom are the same in a supermultiplet. In addition, the members of the supermultiplet should have the same gauge quantum numbers apart from spin, as well as same mass as its SM partner in the absence of SUSY breaking. Table 2.1 and 2.2 summarise the particle content of MSSM [2]. We discuss the primary motivations for SUSY in the following section.

## 2.1 Motivations for Supersymmetrization of the Standard Model

The primary motivations for studying the MSSM as a potential BSM theory are [2, 27]:

- **Resolving the naturalness problem**: SUSY helps resolve the naturalness problem as discussed in Chapter 1. Radiative contributions to the Higgs mass have quadratic divergences which require large cancellations amongst the parameters involved to fit the observed Higgs mass. However, in the presence of unbroken SUSY, contributions from one of the superpartners of the top, namely stop ($\widetilde{t}$) with mass $m_S$ to the Higgs mass is as follows:

$$\Delta m_h^2 = \frac{\lambda_S}{16\pi^2}[\Lambda_{UV}^2 - 2m_S^2 \log \Lambda_{UV}/m_S + \text{finite terms}]$$

  The top and stop contributions differ by an overall negative sign owing to the fermion loop in the former case and in the magnitude of the couplings involved, i.e, $\lambda_S$ and $y_t$. A judicious choice of the couplings such that they are correlated, namely, $|y_t|^2 = \lambda_S$, would cancel the quadratic divergence piece of the radiative corrections. However a mild dependence on the cut-off scale $\Lambda_{UV}$ which is the SUSY scale remains via the logarithmic divergent pieces involving the mass of the particles in the loop and the cut-off energy scale which suggest that the SUSY scale should not be very high. This however applies to the scale when all SM particles and their superpartners are degenerate. A mass-splitting will cause a consequent Higgs mass shift which is of the order of the mass-squared difference between the fermions and bosons mediating the mass corrections.

- **Dark Matter candidate**: As discussed at the end of the Chapter 1, experimental observations unequivocally support the presence of dark matter in the universe. The nature of dark matter remains however undetermined. If a particle nature of dark matter is assumed, R-parity conserving SUSY provides a dark matter candidate, mostly the lightest neutralino, $\widetilde{\chi}_1^0$, as the lightest SUSY particle (LSP) where R-parity is defined as

$$P_R = (-1)^{(3B-L+2S)} \tag{2.1.1}$$

  where $B, L, S$ refer to baryon number, lepton number and spin quantum number respectively. The SM particles have $P_R = +1$ (R-even) whereas the sparticles, differing from the SM particles by spin $\frac{1}{2}$, have $P_R = -1$ (R-odd). Hence the sparticles can only be pair produced at the colliders. The heavier sparticles cascade down to the LSP along with SM particles. If R-parity is conserved the LSP is stable and serves as a dark matter candidate.

- **Gauge coupling unification**: The MSSM particle content contributes to the running of the SM gauge couplings modifying their high-scale behaviour. MSSM provides a mechanism for unification of the gauge couplings in SM at high scale thereby suggesting a possible unification of all three fundamental forces [2].

This motivates one to look for SUSY as a new physics scenario to address at least some of the unexplained phenomena in Nature. In the following subsections, we discuss the SUSY algebra, followed by a brief introduction to the MSSM, its particle content and phenomenological implications. We conclude the chapter with an outline of some of the important motivations which lead us to think beyond the minimal SUSY scenario and some alternate DM candidates in such scenarios.

## 2.2 SUSY Algebra

Haag, Lopuzanski and Sohnius postulated that the spacetime symmetry could be extended with fermionic generators by a combination of commutation and anticommutation relations [40]. This was in response to Coleman-Mandula's no-go theorem [41] which stated that it was impossible to extend Poincare algebra with generators having commutation relations. The SUSY generators $Q$ and $Q^\dagger$ transform a boson into a fermion and vice versa and thereby are fermionic in nature. The algebra followed by the SUSY generators is

$$
\begin{aligned}
\{Q_\alpha, Q^\dagger_{\dot\beta}\} &= 2\sigma^\mu_{\alpha\dot\beta} P^\mu \\
\{Q_\alpha, Q_\beta\} = \{Q^\dagger_{\dot\alpha}, Q^\dagger_{\dot\beta}\} &= 0 \\
[Q_\alpha, P^\mu] = [Q^\dagger_{\dot\beta}, P^\mu] &= 0
\end{aligned}
\tag{2.2.1}
$$

$(Q, Q^\dagger)$ are the fermionic SUSY generators whereas $P^\mu$ is the momentum four-vector and $\sigma^\mu = (\mathbf{1}, \vec\sigma)$ where $\mathbf{1}$ is the $2\times2$ identity matrix and $\vec\sigma$ are the Pauli matrices. Here $\alpha, \dot\beta = 1, 2$ are the dotted and undotted indices respectively referring to the left-handed Weyl spinor and right-handed Weyl spinor components. From the above relations we see that SUSY generators commute with $P^\mu$. Therefore they also commute with $P^2$. This leads to the fact

| Name | spin-0 | spin-$\frac{1}{2}$ | $SU(3)_C$ | $SU(2)_L$ | $U(1)_Y$ |
|---|---|---|---|---|---|
| $\mathcal{Q}^i$ | $\widetilde{Q}^i_L = \begin{pmatrix} \widetilde{u}^i_L \\ \widetilde{d}^i_L \end{pmatrix}$ | $Q^i_L = \begin{pmatrix} u^i_L \\ d^i_L \end{pmatrix}$ | 3 | 2 | 1/3 |
| $\bar{\mathcal{U}}^i$ | $\widetilde{\bar{U}} = \widetilde{u}^{i\,c}_R$ | $\bar{U} = u^{i\,c}_R$ | 3 | 1 | - 4/3 |
| $\bar{\mathcal{D}}^i$ | $\widetilde{\bar{D}} = \widetilde{d}^{i\,c}_R$ | $\bar{D} = d^{i\,c}_R$ | 3 | 1 | 2/3 |
| $\mathcal{L}^i$ | $\widetilde{L}^i = \begin{pmatrix} \widetilde{\nu}^i_L \\ \widetilde{e}^i_L \end{pmatrix}$ | $L^i = \begin{pmatrix} \nu^i_L \\ e^i_L \end{pmatrix}$ | 1 | 2 | -1 |
| $\bar{\mathcal{E}}^i$ | $\widetilde{\bar{E}}^i = \widetilde{e}^{i\,c}_R$ | $\bar{E}_i = e^{i\,c}_R$ | 1 | 1 | 2 |
| $\mathcal{H}_u$ | $H_u = \begin{pmatrix} H^+_u \\ H^0_u \end{pmatrix}$ | $\widetilde{H}_u = \begin{pmatrix} \widetilde{H}^+_u \\ \widetilde{H}^0_u \end{pmatrix}$ | 1 | 2 | 1 |
| $\mathcal{H}_d$ | $H_d = \begin{pmatrix} H^0_d \\ H^-_d \end{pmatrix}$ | $\widetilde{H}_d = \begin{pmatrix} \widetilde{H}^0_d \\ \widetilde{H}^-_d \end{pmatrix}$ | 1 | 2 | -1 |

Table 2.1: Chiral supermultiplets in the MSSM. All the spin 1/2 Weyl fermions are left-handed while the spin 0 particles are complex scalars [2] .

| Name | spin-$\frac{1}{2}$ | spin-1 | $SU(3)_C$ | $SU(2)_L$ | $U(1)_Y$ |
|---|---|---|---|---|---|
| $\mathcal{G}$ | $\widetilde{g}$ | $g$ | 8 | 1 | 0 |
| $\mathcal{W}$ | $\widetilde{W}^{\pm}\ \widetilde{W}^0$ | $W^{\pm}\ W^0$ | 1 | 3 | 0 |
| $\mathcal{B}$ | $\widetilde{B}^0$ | $B^0$ | 1 | 1 | 0 |

Table 2.2: Vector supermultiplets in the MSSM. All the spin 1/2 superpartners of SM gauge bosons are Weyl fermions [2].

that within a supermultiplet, formed by the SM particle and its superpartner differing by spin-$\frac{1}{2}$, the fermion and bosons are degenerate in mass. The SUSY generators also commute with other internal symmetry operators such as gauge symmetry. Therefore the members of a supermultiplet differ only in their spins but have all other quantum numbers the same as the SM partners. We discuss the structure of a supermultiplet in the following section for the MSSM.

## 2.3 The Minimal Supersymmetric Standard Model

The simplest extension to the SM is the supersymmetrized version of the SM, namely the Minimal Supersymmetric Standard Model (MSSM). This scenario has the bare minimum of field content consistent with supersymmetry. In addition, all parameters related to SUSY breaking (to be discussed later) are phenomenologically introduced and are not related apriori. The MSSM consists of both chiral and gauge superfields in order to accomodate the SM particle content as summarised in Table 2.1 and 2.2 along with their gauge quantum numbers. $\mathcal{Q}$ and $\mathcal{L}$ are the left-handed chiral superfields for quarks and leptons respectively whereas $\bar{\mathcal{U}}, \bar{\mathcal{D}}, \bar{\mathcal{E}}$ are the the left-chiral fields corresponding to the right-handed up-type quarks, down-type quarks and charged lepton superfields. The chiral supermultiplets in the MSSM with their gauge quantum numbers are summarised in Table 2.1 with the index $i$ denoting the generation index where $i = 1, 2, 3$. Each of the SM particles has a SUSY partner differing by spin-$\frac{1}{2}$. Due to the construction of the SUSY invariant superpotential being holomorphic, two Higgs doublets with opposite hypercharges are required to give masses to the up and down quarks as well as leptons. $H_u, H_d$ are the two Higgs doublets with opposite hypercharges, $Y = 1, -1$ respectively while $\mathcal{H}_u$, $\mathcal{H}_d$ denotes the chiral superfields corresponding to the Higgs doublets. For the quark and lepton superfields the tilde notation denotes the scalar doublets and singlet superpartners of the corresponding SM partners while for the Higgses it refers to the spin-$\frac{1}{2}$ higgsino doublets. Analogous to the SM, no right-handed neutrinos are present to contribute to the neutrino mass term after EWSB occurs. Table 2.2 refers to the set of gauge superfields in the MSSM. The partners of the gluons are the spin-$\frac{1}{2}$ gluinos while that of the $\mathrm{U}(1)_Y$ and $\mathrm{SU}(2)_L$ gauge bosons are the binos and winos respectively.

In this section we focus on the R-parity conserving MSSM, where R-parity is defined as

$$P_R = (-1)^{3B-L+2S} \tag{2.3.1}$$

The R-parity conserving MSSM Lagrangian consists of

$$\mathcal{L}_{MSSM} = \mathcal{L}_{SUSY} + \mathcal{L}_{soft} \tag{2.3.2}$$

where $\mathcal{L}_{SUSY}$ is the SUSY invariant part of the Lagrangian denoted by

$$\mathcal{L}_{SUSY} = \mathcal{L}_{chiral} + \mathcal{L}_{gauge} + \mathcal{L}_{int} \tag{2.3.3}$$

while $\mathcal{L}_{soft}$ is the soft SUSY breaking part of the Lagrangian $\mathcal{L}_{int}$. Note that the presence of fermions and gauge bosons in the SM motivates the presence of both chiral and gauge superfields in the MSSM.

### SUSY invariant Lagrangian

The SUSY invariant part of the Lagrangian $\mathcal{L}_{SUSY}$ is specified in terms of the chiral superfields, gauge superfields and interactions between the chiral and gauge superfields as below.

$$\mathcal{L}_{SUSY} = \mathcal{L}_{chiral} + \mathcal{L}_{gauge} + \mathcal{L}_{int} \,. \tag{2.3.4}$$

Here

$$\mathcal{L}_{chiral} = -\frac{1}{2} W^{ij} \psi_i \psi_j + W^i F_i + h.c. \tag{2.3.5}$$

denotes the interactions of the chiral superfields in the MSSM where

$$W^{ij} = \frac{\partial^2 W_{MSSM}}{\partial \phi_i \partial \phi_j} \tag{2.3.6}$$

and

$$W^i = \frac{\partial W_{MSSM}}{\partial \phi_i} \tag{2.3.7}$$

and $W_{MSSM}$ is the superpotential with the generation indices suppressed [2]

$$W_{MSSM} = y_u \mathcal{Q} H_u \bar{\mathcal{U}} - y_d \mathcal{Q} H_d \bar{\mathcal{D}} - y_l \mathcal{L} H_d \bar{\mathcal{E}} + \mu \mathcal{H}_u \mathcal{H}_d \tag{2.3.8}$$

where $y_k$ are the $3 \times 3$ Yukawa coupling matrices ( $k = u, d, l$) for the quarks and leptons, $\mu$ is the higgsino mass parameter. The chiral superfields $\Phi_i = (\phi_i \ \psi_i \ F_i)^T$ where $\phi_i$ is the bosonic degree of freedom, $\psi_i$ is the fermionic degree of freedom of the chiral supermultiplet, $F_i$ is the auxilliary field required for SUSY algebra to close off-shell and $i$ is the number of such chiral superfields in the theory. In the MSSM, $\phi_i \equiv \widetilde{Q}_i, \widetilde{L}_i, H_u$ and $H_d$, ie., squarks, sleptons and Higgs doublets.

The gauge part of the Lagrangian is

$$\mathcal{L}_{gauge} = -\frac{1}{4} F^a_{\mu\nu} F^{a\mu\nu} + i\lambda^{\dagger a} \bar{\sigma}^\mu D_\mu \lambda^a + \frac{1}{2} D^a D^a \tag{2.3.9}$$

where $F_{\mu\nu}$ is the field strength tensor, $V$ is the vector boson, $\lambda$ is the gaugino, $D$ is the auxilliary field required such that the SUSY algebra closes off-shell while $a$ index is summed over the gauge groups of MSSM. Note that the color and family indices are suppressed in the Lagrangian definition for simplicity. $T^a$ are the generators of the gauge groups while $g^a$ are the gauge couplings of the specific gauge group. The covariant derivative $D_\mu$ is given by

$$D_\mu \lambda^a = \partial_\mu + g^a f^{abc} V^b_\mu \lambda^c \tag{2.3.10}$$

where $f^{abc}$ are the totally antisymmetric structure constants of the gauge groups. The most general renormalizable interaction terms involving the chiral and vector superfields are

$$\mathcal{L}_{int} = -\sqrt{2}g^a(\phi^* T^a \psi)\lambda^a - \sqrt{2}g^a \lambda^{a\dagger}(\psi^\dagger T^a \phi) + g^a(\phi^* T^a \phi)D^a \tag{2.3.11}$$

Recall that both $F$ and $D$ are auxilliary fields with no kinetic terms. They contribute to the scalar potential $\mathcal{V}$ given by

$$\mathcal{V} = V_F + V_D = F^i F_i^* + \frac{1}{2}D^a D^a \tag{2.3.12}$$

where $V_F$ refers to the contribution from the F-term and $V_D$ refers to the contribution from the D-term. After solving the equation of motions, the $F$ and $D$ are derivable directly from the superpotential $W^i$ and $\mathcal{L}_{int}$ respectively as given below

$$F_i = -W_i^* = -\frac{\partial W_{MSSM}}{\partial \phi_i^*} \tag{2.3.13}$$

wheras

$$D^a = -g^a(\phi^* T^a \phi) \tag{2.3.14}$$

There is an additional contribution to the MSSM Lagrangian, namely the softly broken part of the Lagrangian which we discuss next.

## Soft SUSY breaking Lagrangian

If SUSY were to be an exact symmetry, masses of the SUSY particles would be the same as their SM partners. Non-observation of such light SUSY particles requires the presence of heavier sparticle states, thereby requiring breaking of supersymmetry. However this breaking has to be such that the hierarchy problem is still resolved. Recall that in order to resolve the naturalness problem the coupling of the superpartners and their SM partner were correlated, which led to the cancellation of the quadratic divergent piece. In order to retain this feature the couplings must still remain correlated while the masses may differ leading to finite corrections to the Higgs mass proportional to the mass squared differences of the fermion and bosons contributing to the Higgs mass. Therefore soft SUSY breaking is needed, i.e, SUSY breaking via mass and not couplings of the superpartners. Therefore the mass dimension of these soft SUSY breaking parameters must be positive and not dimensionless to avoid worsening the naturalness problem. However the origin of SUSY breaking is not known yet. SUSY breaking may occur via the $F$-term such that the auxilliary field $F$ obtains a vev (

$< F >\neq 0$ ) and/or via the $D$-term such that $D$ obtains a vev ($< D >\neq 0$) [2]. In both cases one requires to go beyond the MSSM [2].

Note that if one were to consider spontaneous SUSY breaking using renormalizable terms, analogous to the Higgs mechanism in the SM, the SUSY breaking masses in a renormalizable theory obey the supertrace theorem at tree level [2] which will not lead to a phenomenologically consistent spectrum. A useful way to bypass this issue would be by considering that SUSY breaking occurs at the loop level and the fields responsible for SUSY breaking do not couple to the MSSM sparticles at the tree-level. Another possibility for SUSY breaking to occur is via non-renormalizable terms. Therefore SUSY breaking may be communicated to the MSSM in the following ways so it may still survive the supertrace theorem if it occurs, for example,

- via gravitational interactions of particles in a hidden sector to the MSSM particles, as in Gravity Mediated SUSY breaking, commonly referred to as mSUGRA,
- via flavor blind interactions between particles in the hidden sector to the MSSM particles as in Gauge-Mediated SUSY Breaking (GMSB) where the SM gauge interactions are responsible for mediating the SUSY breaking to the MSSM sector

Thus popular SUSY breaking scenarios are mSUGRA, where non-renormalizable gravitational interactions mediate SUSY breaking or GMSB where SUSY breaking is communicated to the visible sector radiatively using gauge interactions of the SM via members of a new messenger sector. In both cases the supertrace theorem ceases to hold for reasons discussed above.

A popular way of parametrizing the SUSY breaking parameters without making assumptions about how SUSY breaking occurs and is communicated to MSSM, is by adding the SUSY breaking terms explicitly to the Lagrangian at the weak scale as free parameters of the Lagrangian. In the MSSM the most general soft SUSY breaking terms added to the Lagrangian at the weak scale are

$$\mathcal{L}_{soft} = (\frac{1}{2}M_3\widetilde{g}\ \widetilde{g} + \frac{1}{2}M_1\widetilde{B}^0\ \widetilde{B}^0 + \frac{1}{2}M_2\widetilde{W}\ \widetilde{W} + c.c.) - \widetilde{Q}^\dagger m_Q^2\widetilde{Q} - \widetilde{L}^\dagger m_L^2\widetilde{L} - \widetilde{\bar{E}}^\dagger m_{\bar{E}}^2\widetilde{\bar{E}} - \widetilde{\bar{U}}^\dagger m_U^2\widetilde{\bar{U}}$$
$$-\widetilde{\bar{D}}^\dagger m_D^2\widetilde{\bar{D}} + (B\mu H_u H_d + c.c.) - m_{H_u}^2 H_u^\dagger H_u - m_{H_d}^2 H_d^\dagger H_d + A_u\widetilde{Q}H_u\widetilde{\bar{U}} + A_d\widetilde{Q}H_d\widetilde{\bar{D}} + A_l\widetilde{L}H_d\widetilde{\bar{E}}$$

where $M_1, M_2, M_3$ are the soft SUSY breaking masses for the gauginos. The squarks and sleptons have explicit mass terms involving squared-mass matrices $m_U^2$ , $m_D^2$ , $m_E^2$ , $m_L^2$ and $m_Q^2$ for the right handed up-type and down-type squarks, right-handed sleptons, left-handed sleptons and left-handed squarks respectively. The soft SUSY breaking terms corresponding to the $\mu$ term and mass-squared parameters for the Higgs doublets are $B\mu\,, m^2_{H_u}$ and $m^2_{H_d}$ respectively. Note that spin-0 squarks and sleptons also couple to the Higgs fields $H_u, H_d$ via the soft trilinear terms involving $A_u, A_d, A_l$ respectively similar to the Yukawa interaction terms and obtain masses after EWSB occurs. All in all, this introduces a multitude of free parameters in the theory. Including masses, mixing angles and phases there are nearly 105 free parameters in the MSSM which is not desirable in a physical theory and therefore begs for an underlying justification of the many free parameters.

In this thesis, we focus on scenarios with non-universal SUSY breaking, i.e, soft SUSY breaking terms explicitly added to the MSSM Lagrangian with no underlying assumptions about their behaviour at high scale and study their phenomenological consequences. In such a generic extension, the SUSY preserving as well as soft SUSY breaking parameters are specified at the weak scale. While such a soft breaking of SUSY maintains the cancellation of quadratic divergences, the masses of the SUSY particles differ from their SM partners.

### 2.3.1 Sparticle spectrum of the MSSM

The MSSM consists of the SM particles and their SUSY partners commonly referred to superpartners differing in spin by half-integer units. For example, spin-$\frac{1}{2}$ quarks have spin-0 superpartners known as scalar quarks or *squarks*. There are also *sleptons* corresponding to leptons. Note that the Higgs sector of the MSSM is similar to a Type II two Higgs Doublet Model (2HDM) [42,43] with two Higgs doublets, $H_u$ and $H_d$ respectively. The up-type quarks obtain their masses from $H_u$ while the down-type quarks and leptons obtain their masses from $H_d$.

In MSSM the presence of two Higgs doublets necessitates the presence of their spin-$\frac{1}{2}$ counterparts, namely the higgsinos, $\widetilde{H}_u$ and $\widetilde{H}_d$. After EWSB the gauge bosons $W^{\pm}, Z$ obtain masses while the photon ($\gamma$) remains massless. The gauginos which are spin $\frac{1}{2}$ partners of the SM gauge bosons mix with the higgsinos after EWSB. The mass eigenstates are $\widetilde{\chi}^{\pm}_i$ and $\widetilde{\chi}^0_i$ referred to as the *charginos* and *neutralinos* respectively, together constituting the *electroweakino* sector of the MSSM. The superpartners of the gluons are color octet *gluinos*. We discuss the MSSM spectrum as below.

#### Higgs sector

Motivated by the holomorphicity of the superpotential as required by the SUSY invariant part of the Lagrangian, it is imperative that the up and down type quarks receive masses from two different Higgs doublets with opposite hypercharges. The MSSM has two $SU(2)_L$ Higgs doublets, namely, $H_u$ and $H_d$ with hypercharge $Y = 1$ and $-1$ respectively. $H_u$ and $H_d$ are defined as

$$H_u = \begin{pmatrix} H_u^+ \\ H_u^0 \end{pmatrix}$$

$$H_d = \begin{pmatrix} H_d^0 \\ H_d^- \end{pmatrix}$$

After electroweak symmetry breaking, two of the eight real degrees of freedom are the Goldstone bosons which are eaten up by the $W^\pm$ and $Z$ bosons and constitute their longitudinal modes while the other five degrees of freedom form five physical states: two CP-even Higgses $h$ and $H$, a CP-odd pseudoscalar Higgs $A$ and a charged Higgs $H^\pm$. The *vev*'s of the Higgses $v_u, v_d$

$$< H_0^u >= \frac{1}{\sqrt{2}} v_u \ , < H_0^d >= \frac{1}{\sqrt{2}} v_d \tag{2.3.15}$$

constitute the electroweak vacuum expectation value $v$ such that

$$v_u^2 + v_d^2 = v^2 \tag{2.3.16}$$

Note that $v_u = v \sin\beta$ and $v_d = v\cos\beta$ where $\tan\beta = \frac{v_u}{v_d}$ is the ratio of the *vev's* of the $H_u$ and $H_d$. Conventionally $0 < \beta < \pi/2$ and $\alpha$ is the mixing angle between the CP-even Higgses. In the decoupling limit, $m_A >> m_h$ where $h$ resembles the SM Higgs boson properties, $\beta - \pi/2 \simeq \alpha$. The masses of the physical Higgses at tree-level are as follows [2]

$$m_A^2 = 2B\mu / \sin(2\beta)$$
$$m_{H^\pm}^2 = m_A^2 + m_W^2$$

$$m_{h,H}^2 = \frac{1}{2}(m_A^2 + m_Z^2 \mp \sqrt{(m_A^2 - m_Z^2)^2 + 4m_Z^2 m_A^2 \sin^2(2\beta)}).$$

where $B\mu$ is the soft SUSY-breaking term in $\mathcal{L}_{soft}$ corresponding to $\mu$. The above relations imply an upper bound on the light Higgs mass

$$m_h \leq m_Z \cos(2\beta) \tag{2.3.17}$$

and therefore the light Higgs mass is bounded from above by the $Z$ boson mass at the tree-level in the MSSM. The observed mass of the Higgs at 125 GeV [1, 16] therefore indicates that a substantial contribution to the Higgs mass arises from quantum corrections in the form of logarithmic contributions from top-stop loops.

### Squarks

The six flavors of squarks mix amongst each other in case the mass matrices are non-diagonal. In order to avoid stringent constraints from flavor violating decays, it is imperative that the off-diagonal terms in the squark mixing matrix amongst the generations are small. In such a case, the left-handed and right-handed squarks of a specific generation and flavor mix. The mixing in the stop sector is the most appreciable due to the large top Yukawa coupling. The mass term in the Lagrangian in the basis $\widetilde{Q} = (\widetilde{u}_L \;\; \widetilde{u}_R)$ is as follows

$$\mathcal{L}_{\widetilde{Q}} = -\,\widetilde{Q}^\dagger M^2_{\widetilde{Q}_u}\,\widetilde{Q}$$

where $M^2_{\widetilde{Q}_u}$ is the squark squared-mass matrix as follows

$$M^2_{\widetilde{Q}_u} = \begin{pmatrix} m^2_{Q_u} + m^2_u + \Delta_{u_L} & v(A^*_u \sin\beta - \mu y_u \cos\beta) \\ v(A_u \sin\beta - \mu^* y_u \cos\beta) & m^2_U + m^2_u + \Delta_{u_R} \end{pmatrix}$$

in the flavor eigenbasis. The diagonal terms arise from the soft squared mass terms, F-term and the D-term contributions ($\Delta_{u_L} = (I_3 - Q_u \sin^2\theta_W) m^2_Z \cos(2\beta)$, $\Delta_{u_R} = -Q_u \sin^2\theta_W m^2_Z \cos(2\beta)$ where $Q_u$ is the charge of the squark while $I_3$ is its isospin). The off-diagonal terms receive contributions from both the SUSY respecting and SUSY breaking Lagrangian. The former contributions are proportional to $\mu y_u$ while the latter come from the soft trilinear terms proportional to $A_u$. The presence of the off-diagonal terms induce mixing among the left-right flavor eigenstates, with the mixing being most pronounced for the third generation sector due to the large Yukawa couplings of the top quark as compared to the first and second generation squarks. Therefore depending upon the choice of the soft mass parameters, the lightest squark in the MSSM could be the lightest stop $\widetilde{t}_1$ while the first and second generation squarks are heavy.

The mass matrix for the down type squarks sector is given by

$$M^2_{\widetilde{Q_d}} = \begin{pmatrix} m^2_{Q_d} + m^2_d + \Delta_{d_L} & v(A^*_d \cos\beta - \mu y_d \sin\beta) \\ v(A_d \cos\beta - \mu^* y_d \sin\beta) & m^2_D + m^2_d + \Delta_{d_R} \end{pmatrix}$$

with analogous terms as before. Since $\widetilde{t}_L$ and $\widetilde{b}_L$ form a doublet a light stop indicates the presence of a light sbottom nearby in mass.

### Sleptons

The left and right handed sleptons of a specific generation and flavor mix via the Yukawa interaction terms. The mass term in the Lagrangian in the gauge eigen-basis $\widetilde{L} = (\widetilde{l}_L \;\; \widetilde{l}_R)$ is given by

$$\mathcal{L}_{\widetilde{L}} = -\widetilde{L}^\dagger \ M^2_{\widetilde{L}} \ \widetilde{L} \tag{2.3.18}$$

The slepton mass matrix is denoted as

$$M^2_{\widetilde{L}} = \begin{pmatrix} m^2_L + m^2_l + \Delta_{l_L} & v(A^*_l \cos\beta - \mu y_l \sin\beta) \\ v(A_l \cos\beta - \mu^* y_l \sin\beta) & m^2_{\widetilde{E}} + m^2_l + \Delta_{l_R} \end{pmatrix}$$

in the flavor eigenbasis with $l = e, \mu, \tau$. The diagonal elements of the mass matrix receive contributions from the F-term, D-term and soft-mass squared terms while the off-diagonal elements receive contributions from the SUSY invariant terms as well as the trilinear coupling terms in the soft SUSY breaking part of the Lagrangian. The slepton mixing in the squark sector is appreciable in the third generation $\widetilde{\tau}$ due to the large $y_\tau$ as compared to $y_e$ or $y_\mu$. Therefore, amongst the sleptons, for all the soft masses are chosen to be equal, the first and second generation sleptons will be nearly degenerate whereas the lighter stau ($\widetilde{\tau}$) would be the lightest amongst the sleptons.

**Neutralinos**

The higgsinos, bino and wino have the same $SU(2)_L \times U(1)_Y$ quantum numbers, and mix amongst themselves after EWSB occurs to form the neutral mass eigenstates *neutralinos*. In the neutral gauge eigenstate basis, $\psi^0 = (\widetilde{B}^0, \widetilde{W}^0, \widetilde{H}^0_d, \widetilde{H}^0_u)$, the mass term for the neutralinos in the Lagrangian is

$$\mathcal{L}_{\widetilde{N}} = -\frac{1}{2}(\psi^0)^T \ M_{\widetilde{N}} \ \psi^0 + c.c. \tag{2.3.19}$$

where $M_{\widetilde{N}}$, the mass matrix of the neutralinos is

$$M_{\widetilde{N}} = \begin{pmatrix} M_1 & 0 & -M_Z \sin\theta_W \cos\beta & M_Z \sin\theta_W \sin\beta \\ 0 & M_2 & M_Z \cos\theta_W \cos\beta & -M_Z \cos\theta_W \sin\beta \\ -M_Z \sin\theta_W \cos\beta & M_Z \cos\theta_W \cos\beta & 0 & -\mu \\ M_Z \sin\theta_W \sin\beta & -M_Z \cos\theta_W \sin\beta & -\mu & 0 \end{pmatrix}. \tag{2.3.20}$$

The mass eigenstates are $\widetilde{\chi}^0_1$, $\widetilde{\chi}^0_2$, $\widetilde{\chi}^0_3$, $\widetilde{\chi}^0_4$ such that $m_{\widetilde{\chi}^0_1} < m_{\widetilde{\chi}^0_2} < m_{\widetilde{\chi}^0_3} < m_{\widetilde{\chi}^0_4}$. The lightest neutralino, $\widetilde{\chi}^0_1$ is the most popular choice for the LSP in MSSM and preferred candidate for cold dark matter. Depending on the composition of the neutralino, the LSP may be predominantly bino-dominated, wino-dominated or higgsino-dominated.

### Charginos

In the charged gauge eigenstate basis, $\psi^+ = (\widetilde{W}^+, \widetilde{H_u^+})$ and $\psi^- = (\widetilde{W}^-, \widetilde{H_d^-})$, the mass term for the charginos in the Lagrangian is

$$\mathcal{L}_{\widetilde{C}} = -\frac{1}{2}(\psi^\pm)^T M_{\widetilde{C}}\, \psi^\pm + c.c \tag{2.3.21}$$

where $M_{\widetilde{C}}$, the mass matrix of the charginos is

$$M_{\widetilde{C}} = \begin{pmatrix} M_2 & \sqrt{2}M_W \sin\beta \\ \sqrt{2}M_W \cos\beta & \mu \end{pmatrix}.$$

where $M_2$ and $\mu$ are the wino and higgsino mass parameters respectively. Diagonalising the chargino mass matrix yields the mass eigenstates $\widetilde{\chi}_1^\pm, \widetilde{\chi}_2^\pm$ where $m_{\widetilde{\chi}_1^\pm} < m_{\widetilde{\chi}_2^\pm}$. In general there are higgsino-like and wino-like charginos.

## Gluinos

The gluinos are color octets and $SU(2)_L \times U(1)_Y$ singlets and thereby couple only to quark-squark pairs. The mass term in the Lagrangian for the gluinos is:

$$\mathcal{L}_{\widetilde{g}} = \frac{1}{2} M_3\, \widetilde{g}\, \widetilde{g} \tag{2.3.22}$$

## 2.3.2 Phenomenological Implications

Minimal models of SUSY such as mSUGRA and GMSB advocate relations amongst all the soft parameters at the high-scale indicating a sense of universality amongst all the SUSY breaking parameters. In mSUGRA, there are five free parameters of interest dictating the MSSM spectrum: $m_0, m_{1/2}, A_0,\ \tan\beta, sgn(\mu)$, where $m_0$ is the universal scalar mass, $m_{1/2}$ universal fermion mass, $A_0$ universal trilinear coupling, $\tan\beta = \frac{v_u}{v_d}$, ratio of the *vev*'s of the up-type and down-type Higgs doublets and $sgn(\mu)$ refers to the sign of the $\mu$ parameter. The magnitude of the $\mu$ parameter is already fixed from the EWSB condition. This scenario is also popularly known as the constrained MSSM (cMSSM) scenario due to the economy in the number of parameters in the theory.

After renomalisation group running from high scale to low scale, the soft parameters give rise to a hierarchical spectrum, as observed from the following relation [2]:

$$M_3 : M_2 : M_1 = 6 : 2 : 1 \tag{2.3.23}$$

with $M_1/g_1^2 = M_2/g_2^2 = M_3/g_3^2 = \kappa$ where $\kappa$ is a constant. Thus the kind of spectrum advocated in mSUGRA has a large mass hierarchy amongst the sparticles. For compressed spectrum such a mass hierarchy amongst the sparticles is not respected and leads to closely spaced sparticles. Similar mass hierarchy is observed for gauge-mediated SUSY breaking (GMSB) where one has the following free parameters: $\tan\beta$, sign($\mu$), $M$, $\Lambda$, $N_M$ where $\Lambda$ is proportional to the SUSY breaking scale, $M$ is the messenger mass scale whereas $N_M$ refers to the number of messengers[1]. However note that the discovery of a light 125 GeV Higgs boson stringently constrains the GMSB parameter space requiring stop masses to be as heavy as 4-5 TeV in absence of large mixing values of $A_t$ at the tree or one loop level [8, 44–46].

We now briefly review the general phenomenological implications of the MSSM part of the spectrum in such scenarios. The heavier sparticle decays to lighter sparticles along with SM particles, cascading down to the lightest SUSY particle. For R-parity conserving SUSY, where R-parity is defined as $P_R = (-1)^{3B-L+2S}$, SM particles have $P_R = +1$ whereas SUSY particles have $P_R = -1$. SUSY particles decay to the LSP which remains stable for a R-parity conserving SUSY scenario. The large mass hierarchy amongst the sparticles has prompted searches for SUSY in final states with large missing energy and hard jets and leptons at past and present colliders. Although most SUSY searches are inspired by mSUGRA/GMSB-like spectra to observe signals at experiments with high $p_T$ jets and/or leptons and large missing transverse energy carried away by the LSP, such signatures differ drastically from SM since the SUSY particles are heavier compared to the SM. However no signals of SUSY have been observed at the LHC in such channels with multiple jets/leptons and large missing transverse energy as predicted for conventional SUSY scenarios like mSUGRA and current searches at LHC push the bounds on mSUGRA to the multi-TeV range. Bounds on cMSSM are summarised in Fig. 2.1 with the particle spectrum being pushed up to $\sim 6$ TeV for LSP masses $\sim 500$ GeV at the Run 1 of LHC with the centre-of-mass energy $\sqrt{s} = 8$ TeV by the ATLAS experiment [47].

In the light of the current data being collected at LHC [48, 49], it is imperative to inves-

[1]Note that both mSUGRA and GMSB have additional particle content beyond the MSSM. Namely, both mSUGRA and GMSB accomodate gravity in SUSY by including a spin-2 graviton and its spin-$\frac{3}{2}$ superpartner, the gravitino and therefore include a free parameter $m_{\widetilde{G}}$, namely the mass of the gravitino. While in mSUGRA the SUSY breaking scale is near the Planck scale $M_{Pl}$, the gravitino is massive and not a good candidate for LSP, in GMSB the SUSY breaking scale is low enough such that gravitino mass $m_{\widetilde{G}}$ is light. In such a case the $\widetilde{G}$ is the LSP [8]. The presence of such a LSP candidate would modify the phenomenology of the MSSM sparticles significantly as we discuss in Chapter 4 and 5.

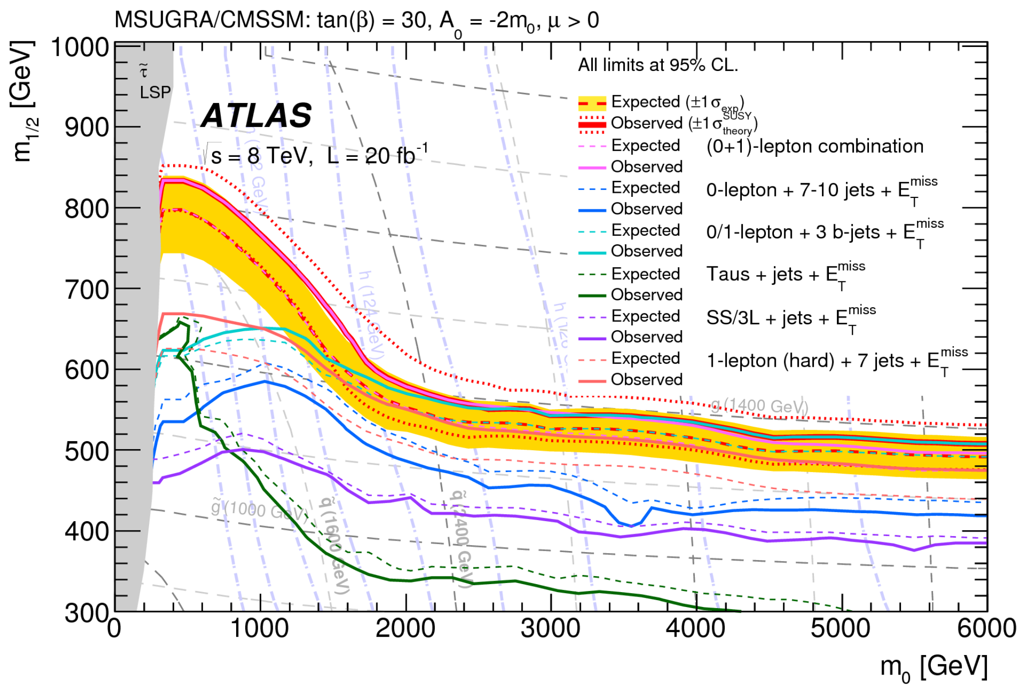


Figure 2.1: Limits on mSUGRA from the ATLAS experiment at LHC [47].

tigate the underlying assumption of unification of soft parameters for cMSSM. The assumption, although an economical choice, is not enforced from any underlying principle. This prompted searches for alternate scenarios where the mass hierarchy amongst the sparticles are not robustly enforced to be large. Such spectra have closely spaced sparticles and are commonly referred to as *compressed* spectra which do not have large mass gaps amongst the sparticles. Although the LSP is massive, since the ensuing daughter particles inherit transverse momentum proportional to the available phase space, the absence of substantial mass difference amongst the sparticles including the LSP leads to the presence of soft jets and leptons as its characteristic feature. The missing transverse energy balancing the visible transverse momenta of the particles is also degraded and consequently a compressed spectra has low missing energy ($\not{E}_T$). Therefore, signals of a compressed spectra typically are devoid of hard jets/leptons and large missing energy. This makes it particularly difficult to investigate the collider signatures of the compressed spectra and leads to reduced limits from searches optimized to signatues of mSUGRA-like spectra and thus lead to weaker limits on compressed spectra. Therefore a much lighter SUSY spectrum is allowed from current limits compared to the limits from searches for conventional channels with hard leptons, jets and large missing transverse momentum.

In the absence of hard visible objects to trigger upon, the traditional signature of a compressed spectrum was thought to be monojet and missing energy. The source of the monojet is the initial state radiation (ISR) or final state radiation (FSR) jet which recoils against the system of the produced sparticles decaying to the soft visible particles and the invisible massive LSP. It also helps boost the recoil system. In absence of hard triggerable objects in the event, the hard ISR jet is tagged upon to balance the invisible new physics sector thus leading to the presence of a large missing transverse energy. Thus monojet and missing transverse energy has been traditionally the best channel for discovery of a compressed spectra. Also, in most studies the compression in the mass is studied with respect to simplified spectra with part of the spectrum decoupled.

The work in this thesis encompasses the following aspects of study:

- Scenarios where SUSY spectrum, fully or partially compressed, have been explored indicating that the SUSY breaking masses are correlated and therefore one needs to go beyond the MSSM particle structure.

- We have discussed implications of scenarios where the LSP is not an MSSM particle but gravitino or a right-sneutrino. It is thus relevant to summarise below some motivations for going beyond MSSM.

## 2.4 Motivations for going beyond MSSM

We briefly review some of the motivations for going beyond the MSSM:

- **To bring order in chaos**: The MSSM leads to a proliferation of free parameters (>100). It is a legitimate aspiration to have them connected, using some overseeing principle.

  (a) mSUGRA: The most common example is the constrained MSSM (cMSSM) based on a minimal supergravity (mSUGRA) scenario. There the breakdown of SUSY in a 'hidden sector' gets communicated to the 'observable sector' via gravitational interaction. One thus obtains high-scale universal scalar and gaugino as well as trilinear soft breaking parameter $A_0$. Upon evolution down to the TeV scale, these generate the entire low-energy MSSM spectrum, buttressed by $sgn(\mu)$ and $\tan\beta$, the ratio of the vaccuum expectation values of the two Higgs doublets. This remains an appealing paradigm, although the current cosmological and collider data put rather strong constraints on such scenarios.

(b) Gauge mediation: In gauge-mediated SUSY breaking (GMSB) [8], SUSY breaking occuring in the 'hidden sector' is communicated to a 'messenger sector' which in turn transmits the breaking information to the observable sector via loop effects mediated by SM gauge interactions. The messenger sector holds the SUSY breaking information in the scalar and auxilliary component vev's of some chiral superfield. The minimal GMSB model with $N_M$ messenger superfields, consisting of vector-like quark and lepton chiral supermultiplets, couple to a singlet superfield S whose scalar and auxilliary fields obtain *vev*. After SUSY breaking is communicated to the visible sector, the gauginos acquire masses at one-loop level (via contributions from the messenger fields in the loop) while the scalars receive masses at two-loop level. Note that the soft trilinear coupling is generated at the higher loop level at the messenger scale. Therefore the entire low-energy spectrum is generated entirely from the free parameters $\Lambda, N_M, M, sgn(\mu)$ and $\tan\beta$ where $\Lambda$ is $\frac{<F_S>}{<S>}$, $< F_S >$ is the SUSY breaking scale while $M \sim< S >$. Therefore GMSB also advocates an economy in the number of free parameters in the theory. An attractive feature of GMSB is that the SUSY breaking scale may be much lighter than the Planck scale (as in mSUGRA) depending on the model parameters, i.e, $\sqrt{F} \propto \sqrt{m_{\widetilde{G}} M_{Pl}}$. This not only reduces the undesirable flavor-changing neutral currents, but also enables the gravitino to be much lighter ( $\lesssim$ keV) than the sparticle masses and motivates it to be a possible LSP candidate. However, minimal models of GMSB fail to fit the Higgs mass. This is because it fails to generate non-zero trilinear couplings at the lower loop levels. Thus the protagonists of GMSB need to turn to non-minimal scenarios.

- **Mechanism for generating neutrino masses**: The MSSM does not include right-handed neutrinos thereby leading to massless neutrinos after electroweak symmetry breaking. However, extensions to MSSM with right-handed neutrino superfields give rise to potential mechanisms for generating neutrino masses via Type-I Seesaw mechanism [20–22].

- **Alternate DM candidates**: In the light of the current data disfavouring WIMPs as cold dark matter candidates from direct searches [50, 51], it is worthwhile to study alternate candidates for the LSP or alternate mechanisms of production of dark matter, focusing not only on thermal but non-thermal production mechanisms as well. Gravitino, in the keV mass range, is a potential warm dark matter candidate [52, 53] whereas the right-sneutrinos with masses close to the weak scale may serve as a thermal or non-thermal DM candidates [54–63] depending on the left-right sneutrino mixing and mass-splitting with respect to the MSSM sparticles.

- $\mu$ **problem**: The naturalness of the Higgs mass demands that the value of the $\mu$ parameter should be close to the electroweak scale in order to avoid large fine-tuning amongst the parameters contributing to the Higgs mass. However $\mu$ being a SUSY preserving parameter is not restricted to be near the electroweak scale as demanded by the naturalness problem. This is commonly referred to as the $\mu$ problem and bears no explanation in the MSSM.

- **Spontaneous SUSY breaking**: It is imperative to go beyond the MSSM if SUSY is to be broken spontaneously analogous to the Higgs mechanism. Since the mechanism of SUSY breaking is unknown it could very well be spontaneously broken and similar to SSB as in SM. Therefore if spontaneous SUSY breaking is to occur via the F-term or the D-term would require one to explore non-minimal SUSY scenarios [2]. This is especially true in the light of the supertrace theorem which underlines the requirement of non-renormalisable interactions, thus hinting that the MSSM is perhaps an effective theory at best. It is also rather difficult to fit the Higgs data in the MSSM necessitating the presence of at least one or more heavy stops or a large soft trilinear parameter $A_t$ leading to a large mixing in the stop sector and therefore challenging the naturalness paradigm.

- **R-parity conservation**: Baryon and Lepton number conservation is an accidental symmetry in the SM and the same is respected in the MSSM. However in the absence of any dynamical principles to motivate the conservation of baryon and lepton number, solely limiting ourselves to such specialised cases could be an oversimplification. R-parity violating SUSY scenarios [64] respecting the upper limits on the lifetime of the proton allows the LSP to be unstable. Although unstable the LSP may still be a valid DM candidate if it has a lifetime larger than the age of the universe and the prospects of observing such a SUSY scenario at the colliders in such cases can be completely different from that in the R-parity conserving case.

## 2.5 Alternate Candidates for LSP in Beyond MSSM scenarios

The lightest neutralino has been the most preferred candidate for cold dark matter although absence of signals at experiments indicates we should also think beyond and look for alternate dark matter candidates for the LSP, such as gravitinos, axinos and right-sneutrino among other possibilities. A light gravitino LSP candidate, for example, arises in GMSB-like models where the SUSY breaking scale is low enough. This leads to new signatures of the MSSM spectra and the limits on the MSSM sector are in turn affected. We first briefly discuss few of the possible candidates for the lightest SUSY particle (LSP) and in the subsequent chapters, probe alternate novel signatures of compressed and partially compressed spectra in MSSM and its extensions. We discuss some of the alternate candidates for the LSP such as gravitino and right-sneutrino relevant for my thesis as below.

**Gravitino ($\widetilde{G}$)**

Local supersymmetric theories incorporate gravitational interaction by introducing a graviton (spin-2) and its superpartner gravitino (spin-$\frac{3}{2}$). Spontaneuos breaking of local SUSY gives rise to a massless Nambu Goldstone Weyl fermion, the goldstino, which subsequently gets absorbed as the longitudinal component of the gravitino after EWSB similar to the Higgs mechanism. For a light gravitino, at energies greater than the gravitino masses, the longitudinal mode of the gravitino, i.e, the goldstino couples to an SM particle and its superpartner with a coupling enhanced by a factor $(m_{\widetilde{G}})^{-1}$ as compared to the transverse modes and hence dominates the interactions of a gravitino. In such a scenario, it is the goldstino mode of the gravitino which plays an important role in collider phenomenology[2]. The sparticle-particle-goldstino ($\widetilde{G}$) Lagrangian is as follows [2]:

$$\mathcal{L}_{goldstino} = i\widetilde{G}^{\dagger}\bar{\sigma}^{\mu}\partial_{\mu}\widetilde{G} - \frac{1}{< F >}\widetilde{G}\partial_{\mu}j^{\mu} + c.c \tag{2.5.1}$$

where $< F >$ refers to the *vev* obtained by the SUSY breaking auxilliary field $F$ and $j^{\mu}$ refers to the current involving all other sparticles and SM particles. The couplings of the gravitino are inversely proportional to $(M_{Pl}\, m_{\widetilde{G}})$ such that light gravitinos coupled with stronger interaction strengths to particle-sparticle pairs. A light gravitino of mass in the keV range is also a candidate for warm dark matter and favoured by structure formation.

[2] We use $\widetilde{G}$ to refer to the gravitino henceforth.

Such a light $\widetilde{G}$ occurs as a LSP in gauge mediated SUSY breaking (GMSB) models [8, 65–71]. Since GMSB fails to explain the Higgs mass in its minimal version [44–46], the particle spectra we study in this thesis does not conform to the GMSB in its minimal form. Also, a keV-scale gravitino, too, may not be easy to fit into a minimal GMSB structure. We have therefore used a phenomenologically adapted spectrum including a light gravitino DM, which is consistent with all observations so far. We discuss the relevant couplings and interaction strengths of the gravitino to other MSSM sparticle-SM particles in Chapter 4 and 5.

### Right-Sneutrino ($\widetilde{\nu}_R$)

Neutrino oscillation experiments have affirmatively established the presence of light neutrino masses. However neither SM nor its supersymmetric counterpart MSSM, in its simplest reincarnation accomodates neutrino masses. There exist beyond MSSM scenarios which may accomodate neutrino masses. One such case is that of extending the MSSM with a right-handed neutrino superfield $N$ [20–22]. In addition to providing a mechanism to incorporate neutrino mass, it also opens up the prospect of the presence of an alternate dark matter candidate, namely, the presence of a right-sneutrino as the lightest SUSY particle. This aspect will be discussed in more detail in Chapter 6 while in the subsequent Chapters 3, 4 and 5 of this thesis we present our works with compressed scenarios in MSSM and beyond, including different LSP candidates.

# Chapter 3

# Revisiting Compressed Supersymmetry with 125 GeV Higgs

## 3.1 Introduction

Despite the very pertinent candidature of TeV-scale SUSY as the solution to the Higgs naturalness problem, and the possibility of solving the DM problem with its help, the LHC experiment is yet to reveal any hint of SUSY. As we have discussed in Chapter 2, the conventional SUSY scenarios like mSUGRA and GMSB, bearing the tell-tale signatures of SUSY had garnered considerable attention over the past few decades however without success. Although model independent results are published by the ATLAS and CMS collaborations, the signal search strategies are mostly optimized using the characteric signatures of such constrained scenarios and thus any departure from such conventional forms of SUSY may not be captured efficiently by the current search strategies.

A way of retaining one's hope in this direction is to think of some version(s) of SUSY, broken around the TeV-scale, but with such spectra as can suppress the usually expected signals. One such version is where the sparticle masses are compressed within a rather small range, a situation whose theoretical justification and phenomenological analyses have already generated some efforts [4, 5, 72, 73]. The compressed spectrum causes the jets and leptons produced in SUSY cascades to be relatively soft, and also downgrades the missing transverse energy ($\not{E}_T$) somewhat, thus potentially suppressing signals that pass the acceptance criteria at the LHC. One can therefore envision allowed regions in the parameter space after the 8 TeV run, with relatively low-lying superparticles but small spacing between the squark/gluino masses and that of the lightest SUSY particle (LSP)[1].

It was initially thought that the best way to look for compressed SUSY was to focus on the mono-jet $+\not{E}_T$ signal [3,74–88]. Subsequent investigations in the context of run-I showed that the 'conventional' multi-jet $+\not{E}_T$ signals (with or without accompanying leptons) could be more useful if appropriate event selection criteria were followed [76,77,79]. It is important to see how such (multi-jet $+\not{E}_T$) signals fare against the mono-jet $+\not{E}_T$ ones in the 13 and 14 TeV runs of the LHC.

A few things, however, remain to be noted carefully in such an investigation. In many recent studies, experimental as well as theoretical, the deciding factor is assumed to be the mass splitting between the coloured members such as gluino/squarks and the LSP, the role of the rest of the spectrum being relatively inconsequential. It is also sometimes customary to focus on the mass gap between the LSP and the next-to-LSP (NLSP). This kind of an approach has often been prompted by attempts to parametrize the spectrum in terms of some 'compression factor' [4, 5] that straightjackets the entire spectrum in a little oversimplified manner. However, one should take an equally serious note of the rest of the minimal SUSY standard model (MSSM) spectrum where even non-coloured particles (or third family squarks) can have substantial splitting with the LSP, thus producing additional hard jets and/or leptons after all.

Another vital issue that needs to be addressed is the undeniable presence of the lighter CP-even Higgs boson around 125-126 GeV. In a SUSY extension of the standard model (SM), one can only consider spectra where this mass value is replicated, its behaviour being most likely SM-like. As we know, the mass of this scalar in the MSSM, taking radiative corrections into account, is highly dependent on the two stop masses as well as the stop left-right mixing angle. Hence the degree of compression of the entire MSSM spectra is expected to be strongly constrained, if the lighter CP-even Higgs mass has to be in the right value. Therefore, the compressed spectra proposed in the earlier works need to be revisited in the aftermath of the Higgs boson discovery. This is not thoroughly done in most existing studies; it is often implied that either the spectrum is only partly compressed [3, 74–88], or some physics beyond MSSM is responsible for the observed value of the Higgs mass [1,16,89]. In contrast, we have proceeded assuming the intervention of only the MSSM fields in deciding the Higgs mass(es).

In addition, the constraints from the relic density of the universe as well as those arising from direct DM search experiments are important requirements of a SUSY spectrum. We

[1] The lightest neutralino ($\widetilde{\chi}_1^0$) has been assumed to be the LSP in this study.

have taken these constraints into account while selecting the benchmark points in the parameter space. For more detailed study of DM in the context of compressed SUSY scenario, see [90–92].

On the whole, given the manifold diversity of an MSSM spectrum, *we have preferred to think not in terms of some compression parameter(s) in a somewhat simplified spectrum but to work with a wide assortment of benchmark points, which reflect as many different possibilities as possible.* We have kept the heavier stop mass and/or the higgsino mass parameter $\mu$ somewhat above the compressed spectrum in some cases. The latter choice may perhaps be justified by the observation that $\mu$ does not have the same origin as the SUSY-breaking mass parameters; it is in fact a SUSY-invariant parameter, though destined to be in the TeV scale by the electroweak symmetry breaking requirement. In any case we have also presented results for some benchmark points where the *entire spectrum* lies tightly compressed. After a detailed study of this variety of benchmarks, we reach the conclusion that signals comprising multi-jets are likely to be more useful in the 13/14 TeV runs, as compared to those depending upon mono-jets. The contents of this chapter are based on the work [7].

The subsequent sections are organized as follows. In section 3.2, we discuss the existing experimental limits on the MSSM parameter space. We further discuss the status of compressed SUSY search at the LHC. Then we look for a truly compressed SUSY spectrum keeping the lightest CP-even Higgs boson mass in its allowed range around 125 GeV. While doing so, we carry out a detailed scan of the relevant parameter space keeping all the collider, DM and flavour physics constraints in consideration. We then provide some benchmark points to showcase our results with different squark-gluino mass hierarchy keeping the lightest neutralino as the LSP. In section 3.3, we explore the collider aspects of such scenarios in the context of run II of the LHC. We look for both multi-jet $+\not{E}_T$ and mono-jet $+\not{E}_T$ final states arising from all possible squark-gluino production channels and compare the sensitivities of these two signals to such compressed spectrum and conclude.

## 3.2 Status of SUSY search and a compressed spectrum

The generic SUSY search channels at the LHC involve the strongly interacting sector comprising of squarks ($\widetilde{q}$) and gluino ($\widetilde{g}$), all of which have large production rates. In the CMSSM/mSUGRA scenario, the mass spectrum for the squarks, gluino and other sparticles have a predetermined hierarchy dictated by the renormalization group (RG) evolutions, once the free parameters are chosen at the unification scale. Once a mass-ordering is thus established, this simplifies the search strategies, since the observed jets or charged leptons originating from the SUSY cascades would carry the imprint of the mass spectrum. One usually associates the signal to contain jets and charged leptons with large transverse momenta along with substantial missing transverse energy ($\not{E}_T$) carried away by the stable lightest SUSY particle (LSP). As a result, the final states are easily separated from their respective SM backgrounds and the exclusion limits derived on the coloured sparticles come out stronger in this framework. Both CMS and ATLAS have put bounds which are close to around 1 TeV on the squark masses and 1.4 TeV on the gluino masses respectively for simplified models [93]. In the case of degenerate squarks and gluinos, the exclusion limit extends up to 1.7 TeV in CMSSM models [94].

### 3.2.1 Current limits on MSSM from ATLAS and CMS

However, the MSSM in general poses a bigger challenge for LHC to put similar exclusion limits. Since the number of free parameters increases many fold, possibilities for different mass ordering of the SUSY particles open up. In such situations, it not only becomes very difficult to put absolute bounds on the masses of the sparticles, but the guiding principles to search for SUSY at LHC also become ambiguous. Because of this, the bounds are always associated with some simplified assumptions for the decay pattern of the produced particles and therefore, one has to be careful while implementing these limits. In such scenarios, gluino mass ($m_{\widetilde{g}}$) is excluded upto 1.3 - 1.5 TeV when the lightest neutralino (LSP) mass ($m_{\widetilde{\chi}_1^0}$) is not heavier than 500 - 600 GeV [94], provided the first two generation squarks are lighter than gluino. When the squarks are much heavier than the gluino, the $m_{\widetilde{g}}$ decays via off-shell squarks. The decay to three-body final state comprising of two quarks and the LSP leads to softer jets in the final state which dilute the $m_{\widetilde{g}}$ exclusion limit to about 1.4 TeV for $m_{\widetilde{\chi}_1^0} \leq 300$ GeV [94]. Just as above, all such available limits from run-I data of the LHC are expected to weaken further if the mass difference between the parent and daughter particles gets reduced as this would result in less $\not{E}_T$ and softer jets/leptons in the final state. For example, if $m_{\widetilde{g}} - m_{\widetilde{\chi}_1^0}$ is very small, the exclusion limit on $m_{\widetilde{g}}$ reduces to 550-600 GeV [94]. Thus, a light spectrum with small mass gaps among the SUSY particles might have escaped Run-I scrutiny, thereby prompting increased interest in a *compressed SUSY scenario* [4, 5].

Summarizing the other available bounds on MSSM, for a much heavier gluino, lighter squark (first 2 generations) masses are excluded below 850 GeV when $m_{\widetilde{\chi}_1^0} \leq 350$ GeV [94]. Lighter stop masses ($m_{\widetilde{t}_1}$) are excluded upto 600-700 GeV provided $\widetilde{t}_1$ decays into a top quark ($t$) and $\widetilde{\chi}_1^0$ where $m_{\widetilde{\chi}_1^0} < 250$ GeV [95, 96]. When the $\widetilde{t}_1$ decays into a bottom quark ($b$) and the lighter chargino ($\widetilde{\chi}_1^{\pm}$), any $m_{\widetilde{t}_1}$ below 500-600 GeV is excluded for $m_{\widetilde{\chi}_1^0}$ below 200-250 GeV [95, 97], the exact limits being dependent on the chargino mass. For other decay modes of $\widetilde{t}_1$ (flavor violating or $>$ 2-body modes), the exclusion limits reduce to 240-260 GeV [95, 97, 98]. Similarly, a lighter sbottom mass ($m_{\widetilde{b}_1}$) below 620 GeV is excluded for $m_{\widetilde{\chi}_1^0} \leq 150$ GeV [99]. When $m_{\widetilde{b}_1} - m_{\widetilde{\chi}_1^0}$ is small, the exclusion limit on $m_{\widetilde{b}_1}$ is lowered to 250 GeV [98].

Since for our present work we consider a relatively compressed spectrum, it turns out that the weakly interacting sector of MSSM has a relatively less important role to play. Therefore, we shall focus on the production and decay of the coloured sparticles. For a more detailed discussion, we refer the readers, for example, to Ref. [100, 101].

### 3.2.2 SUSY with the entire spectrum compressed

Compressed SUSY spectra has been studied in the context of LHC quite extensively with special emphasis on the smallness of the mass gap between the coloured sparticles and the LSP. A coloured NLSP (be it a squark or a gluino) is often assumed, and the role of the other sparticles in SUSY signals is considered to be of secondary importance. In an un-compressed spectrum one probably can accept that the significant contribution to the rates come from lightest colour sparticle production (where the other coloured modes are heavier), but in a compressed scenario contributions from the heavier modes cannot be ignored anymore. Understandably, hard jets or leptons are difficult to obtain in the final state for small mass gaps. This results in weaker limits on the parameter space, when compared to the standard SUSY searches. However, such effects do not always presume the entire spectrum to be compressed. In most cases, a part of the strongly interacting sector (for example, the third family squarks) is ignored by decoupling it from the low lying spectrum. In addition, many extant studies do not pay enough attention to parts of the coloured spectrum, which may not be entirely decoupled, but whose participation vis-a-vis that of the gluino may have bearing on the SUSY signals, especially on the kinematic profiling of the events arising out of sparticle production. For example, the contribution to the final state may dominantly come from the hard processes comprising of the production of squarks in association with gluinos. Now, inspite of having a small gluino-LSP mass gap, the squarks may have a substantial mass gap with the LSP. These sparticles will then start contributing to the final state giving rise to harder jets or leptons along with relatively larger $\not{E}_T$.

Hence the question we really need to ask is, how would a really compressed SUSY spectrum, with almost all sparticles rubbing shoulders with each other, play out at the LHC.

Such a SUSY spectrum, however, has to obey some guiding principles. The first of these is to reproduce the lighter neutral CP-even Higgs mass in the neighbourhood of 125 GeV. The next constraint to be taken into account is the contribution to the relic density of the universe. These, in addition to various limits arising from flavour physics and/or direct search results till date, guide one towards some allowed spectra that are either fully compressed or have to leave out some relatively heavy states above the compressed band.

We discuss these issues in the next subsection, based on which we finally choose specific benchmarks from the viable parameter space which highlight different mass hierarchies among the gluino and the squark states. We use the benchmarks to carry out a detailed collider simulation for both multi-jet $+\not{E}_T$ and mono-jet $+\not{E}_T$ final states, to determine which search strategy may help us better to discover or rule out various SUSY spectra that are compressed to the utmost.

### 3.2.3 A spectrum constrained by Higgs mass and Dark matter

We recall that the tree-level mass of the lightest CP-even Higgs boson as obtained in the MSSM framework has an upper bound:

$$m_h^{\texttt{tree}} \leq m_Z \, |\cos 2\beta| \tag{3.2.1}$$

where $\tan\beta = v_u/v_d$ is the ratio of the two Higgs *vev*'s. Since Eq. 3.2.1 cannot allow a Higgs mass greater than the $Z$ boson mass, one has to rely on substantial contribution through higher order (loop) corrections to reach the neighbourhood of 125 GeV, the experimentally measured mass of what could be the lighter CP-even neutral scalar in a SUSY scenario. The dominant higher-order contribution comes from stops in the loop due to a large Yukawa coupling of the Higgs boson with the top quark. The one-loop contribution to the $m_h^{\texttt{tree}}$ is approximately [102]:

$$(\Delta m_h^2)^{\texttt{1-loop}} \simeq \frac{3m_t^4}{4\pi^2 v^2}\left(\ln\frac{M_S^2}{m_t^2} + \frac{X_t^2}{M_S^2} - \frac{X_t^4}{12M_S^4}\right), \tag{3.2.2}$$

where $v$ is the up-type Higgs VEV, $M_S = \sqrt{m_{\widetilde{t}_L} m_{\widetilde{t}_R}}$ is the geometric mean of the stop left-right masses and $X_t = A_t - \mu\cot\beta$, which governs $\widetilde{t}_L - \widetilde{t}_R$ mixing as well as the splitting between the two stop mass eigenstates. Thus the radiatively corrected Higgs mass crucially depends on two parameters, namely, $M_S$ and $X_t$, along with $\mu$ and $\tan\beta$. We note that in order to have one of the CP-even Higgs mass as 125 GeV Higgs boson in the theory, one requires large stop masses and large stop mixing ($X_t \simeq \pm\sqrt{6}M_S$) [103, 104].

One has the freedom to choose soft-breaking SUSY parameters in the MSSM for each sfermion generation separately. Also, maximum mass splitting is possible in the third family (due to the larger Yukawa couplings) which again contributes most significantly to the Higgs mass correction. Thus one concludes that obtaining a significant compression in the *entire spectrum* is difficult, since achieving $m_h \approx 125$ GeV requires (at least) one stop eigenstate to be heavy.

At the same time, we find a somewhat large $\mu$, too, is favourable in achieving $m_h \approx 125$ GeV. However, this also entails the possibility of having the higgsino-dominated chargino and neutralinos on the heavier side, thus jeopardising the degree of compression in the entire MSSM spectrum. This also affects the higgsino component in the LSP, which in turn may reduce the annihilation rate far too much, leading to excess relic density.

We thus use the following constraints in our scan of the parameter space :

- The lightest CP-even Higgs mass should be in the range $122 < m_h < 128$ GeV [1,16,89].
- The LEP lower bound on the lightest chargino mass, *viz.* $m_{\widetilde{\chi}_1^\pm} > 103.5$ GeV [105].
- Constraints from branching ratios of rare decays such as $\mathrm{BR}(\mathrm{b} \to \mathrm{s}\gamma) = (3.55 \pm 0.24 \pm 0.09) \times 10^{-4}$ [106] and $\mathrm{BR}(\mathrm{B_s} \to \mu^+\mu^-) = (3.2^{+1.4}_{-1.2}\,{}^{+0.5}_{-0.3}) \times 10^{-9}$ [107,108].
- The LSP, $\widetilde{\chi}_1^0$, which is the cold dark matter candidate, satisfies the observed thermal relic density, $0.092 < \Omega_{\widetilde{\chi}} h^2 < 0.138$ [109].

  However, for our parameter scan we have considered only the upper limit of $\Omega h^2$, taking the view that it is plausible to have multi-component DM. [110–118]. However, substantial portions in the parameter space have been identified, where a single-component DM satisfies it. We also include the constraints from direct dark matter searches, as obtained from the LUX data [119].

In order to achieve spectra which are as compressed as can be, consistent with the above constraints, we have taken into consideration the following points in our prediction of the LHC signal:

- The mass gap within the stop pair being large, overall compression can be reduced in situations where one stop eigenstate, $\widetilde{t}_1$, lies just above the neutralino LSP.
- Gluino can be light and both cases are considered when gluino mass is above or below the lighter stop.

- The non-strongly interacting sfermions and gauginos are assigned various orders in the compressed spectrum. Though they have less of a role in the LHC signals (except for SUSY cascades which reduce rates of the signal consisting purely of jets), they may have a bearing on the relic density as well as cascade decays.

- The heavier stop mass as well as $\mu$ are kept both outside and inside the most compressed part of the spectrum. The latter possibility (*i.e.* no sparticle outside the compressed region) works for relatively heavy spectra only.

We parameterize the compression using the mass gap between the LSP ($m_{\widetilde{\chi}_1^0}$) and the heaviest sparticle ($\widetilde{X}$) in the spectrum, defined as $\Delta M = m_{\widetilde{X}} - m_{\widetilde{\chi}_1^0}$, where $\widetilde{X} \in \widetilde{g}$, $\widetilde{t}_2$, $\widetilde{b}_2$, $\widetilde{\tau}_2$, $\widetilde{\chi}_2^0$ and $\widetilde{\chi}_1^{\pm}$ [2]. We scan over the relevant parameters shown in Table 3.1.

| Parameters | Ranges |
|---|---|
| $M_1$, $M_2$, $M_3$ | (100, 2500) GeV |
| $A_t$ | (-3000, 3000) GeV |
| tan$\beta$ | (2, 50) |
| $M_L = M_R$ | $(M_1, M_1 + 200)$ GeV(if $\mathrm{M_1 < M_2}$) |
| | $(M_2, M_2 + 200)$ GeV(if $\mathrm{M_2 < M_1}$) |

Table 3.1: Ranges of the relevant parameters for the scan. $M_1$, $M_2$, $M_3$ are the gaugino mass parameters, varied in the same range but independent of each other. $M_L$ and $M_R$ are the left-handed and the right-handed soft mass parameters of squarks and sleptons.

Here $M_L$ and $M_R$ represent the soft mass parameters of the left and right handed squarks and sleptons respectively[3]. As Table 3.1 suggests, we chose same $M_L$ and $M_R$ for all flavours. For our scan, we have used `SPheno` ($v$3.3.6) [120,121] which calculates all sparticle masses at one-loop level while the Higgs mass is calculated at two-loop in order to generate the SUSY spectrum and consequently `micrOMEGAs` ($V$4.1.7) [122] to calculate the DM relic density and direct-detection cross-section, flavour physics constraints and muon g-2. In Fig. 3.1, we plot $m_{\widetilde{\chi}_1^0}$ as a function of $\Delta M$. As evident, a $\mu$-value close to or above 4 TeV allows a $\Delta M$ as low

[2]Note that the higgsino dominated states may lie outside our compressed spectrum when $\mu$ is chosen to be very large.

[3]Although the soft mass parameters for the squarks and sleptons are kept equal by choice, this does not significantly affect the hadronic signals.

as 100 GeV. This figure gives a clear idea of the heaviness of the MSSM spectra as we keep compressing the whole spectrum. To give some estimate, in order to restrict the spectrum with $\Delta M \sim 100$ GeV, one obtains a lower limit on the LSP mass close to 1800 GeV for $\mu = 5$ TeV.

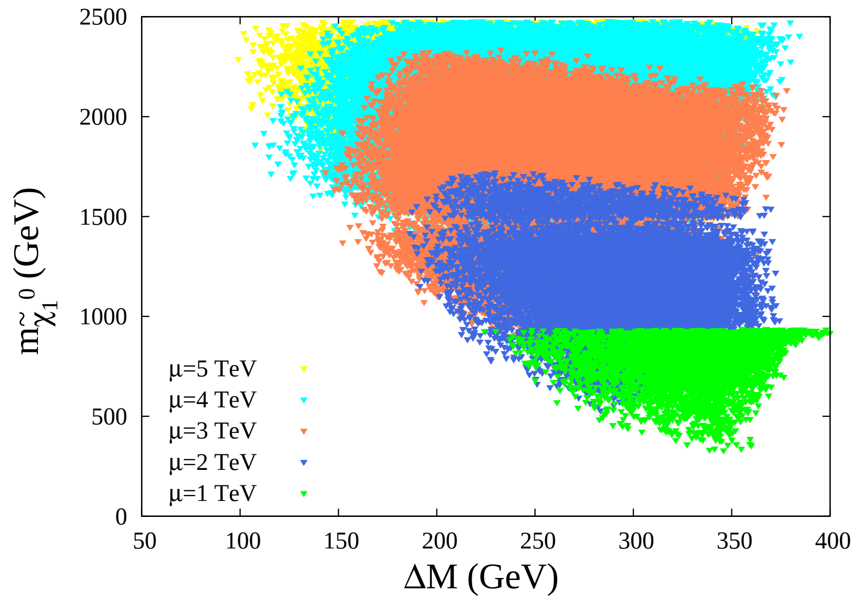


Figure 3.1: Distribution of $m_{\widetilde{\chi}_1^0}$ as a function of $\Delta M$ at different $\mu$ values. The five colours (yellow, cyan, brown, blue and green) indicate five different values of $\mu$. The points in the plot satisfy all the relevant constraints mentioned in the text.

We examine next how the the constraints from relic density$(\Omega h^2)$ and the spin-independent cross-sections $(\sigma_{SI})$ in direct search experiments affect the allowed parameter space. Since we are considering a compressed MSSM scenario, there are always some sparticles whose masses lie close enough to the LSP to produce sufficient co-annihilation to bring down the relic density to permissible limits. For a wino-like LSP, the $\widetilde{\chi}_1^0$ mainly co-annihilates with the $\widetilde{\chi}_1^{\pm}$. In addition, if there are sparticles nearby, e.g, $\widetilde{g}$, $\widetilde{t}_1$, $\widetilde{b}_1$, $\widetilde{\tau}_1$, in the spectrum, all the annihilation channels combine to produce underabundance of the DM relic density. Similar situation may occur in case of a bino-like or a bino-wino mixed LSP state. Hence $\Omega h^2$ is not a very serious constraint for such a scenario.

Direct search limits, $(\sigma_{SI})$, however, can rule out some of the relevant parameter space. Fig. 3.2 shows the distribution of $\sigma_{SI}$ as a function of the DM mass$(m_{\widetilde{\chi}_1^0})$. Note that in this

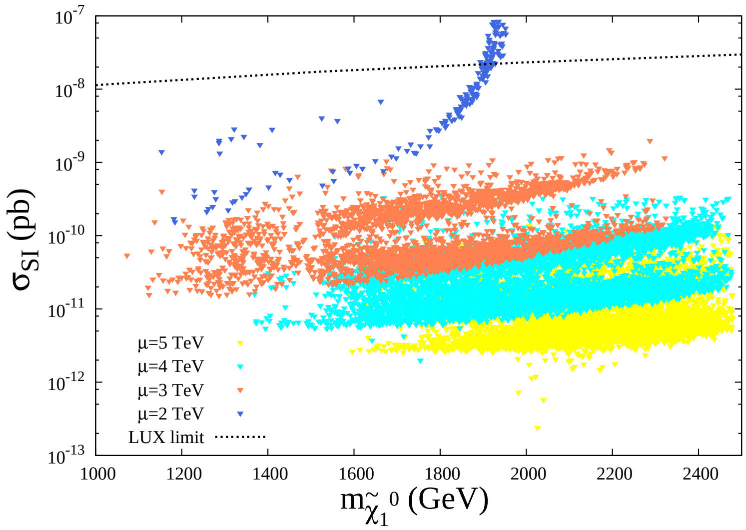


Figure 3.2: The direct detection cross-section as a function of the LSP mass. Since we are interested in small $\Delta M$ we have plotted the points only when $\Delta M \leq 200$ GeV. Colour labels follow Fig. 3.1. The black dotted line represents the most updated LUX bound.

plot we only show those points in the parameter space, which produce $\Delta M \leq 200$ GeV. Understandably, there are no points corresponding to $\mu = 1$ TeV in the distribution, since Fig. 3.1 clearly shows the maximum compression we can reach in this case is close to 220 GeV. The black dotted line represents the most recent bound on $\sigma_{SI}$ provided by the LUX experiment as a function of the DM mass [119]. As expected, all the points obtained in the scan with $\mu \geq 3$ TeV lie well below the exclusion line, the LSP in these scenarios have almost zero contribution from higgsino components and as a result, the Z-boson coupling of the LSP is reduced to a very small value, resulting in such small DM-nucleon scattering cross-sections. However, if we keep decreasing the $\mu$ value, $\sigma_{SI}$ increases. When the bino or wino mass parameters become comparable to the $\mu$ parameter, as happens in part of the parameter space in the $\mu = 2$ TeV case [4], the LSP turns out to be a mixed state with substantial higgsino component. This results in enhancement of $\sigma_{SI}$ which is manifested in the few blue points in the figure which violate the LUX limit.

To demonstrate how the stop mixing parameters behave under the Higgs mass constraint,

[4] This is a result of our choice of the scan ranges of $M_1$ and $M_2$ as indicated in Table 3.1. In section. 3.2.4, we show two such sample benchmark points with non-negligible higgsino component (e.g. 8% in BP6). However, we have not considered higgsino-like LSP for our present work.

we chose one particular LSP mass close to 1100 GeV ($M_1 = 1100$ GeV) and vary $A_t$ in the range $(-3000, 3000)$ GeV and $\widetilde{t}_L$ and $\widetilde{t}_R$ soft masses, $M_L^{Q_3}$ and $M_R^{U_3}$, such that $M_1 < M_{L/R}^{Q_3/U_3} < M_1 + 200$ GeV.[5] with $M_2 = 1200$ GeV . We further impose the constraint that the light stop mass ($m_{\widetilde{t}_1}$) is never heavier than the LSP by more than 30 GeV. Gluino mass and all the other squark and slepton soft masses are kept fixed at a uniform value, about 100 GeV above the LSP mass. These other scalar masses and the gluino mass can be lower than their fixed values. However, we are interested in minimising the mass gap between $m_{\widetilde{t}_2}$ and $m_{\widetilde{t}_1}$. This largely determines the compression factor in the whole SUSY parameter space. We have, therefore, kept them at an intermediate value in order to reduce the number of parameters to scan. The scan is carried out for two different values of $tan\beta$, namely, 10 and 25 each for two different $\mu$-values (2 TeV and 3 TeV) to ascertain their effect on the compression of the relevant parameter space.

Fig. 3.3 showcases the correlation between the stop mixing parameters once the Higgs boson mass constraint is implemented for two different $\mu$ values. As already discussed, the mass difference between the two stop states, $\Delta m_{\widetilde{t}}$, is an important factor in enhancing the radiative Higgs mass correction. In Fig. 3.3 (a) and (b) we show the variation of $\Delta m_{\widetilde{t}}$ with $A_t$ at two different $\tan\beta$ values (Green and Blue points) for $\mu = 2$ and 3 TeV respectively. As expected, with the increase of $\tan\beta$ smaller $|A_t|$ is allowed from Higgs mass constraint as a result of increased mixing in stop sector. Fig. 3.3 (b) indicates that slightly smaller $|A_t|$ values are permissible with increase in $\mu$. In a nutshell, the minimum allowed value of $\Delta m_{\widetilde{t}}$ decreases as we increase $\tan\beta$ or $\mu$ indicating the possibility of getting more and more compressed spectrum. The minimum $\Delta m_{\widetilde{t}}$ obtained is about 180 GeV with $m_{\widetilde{t}_1}$ close to 1400 GeV and $\mu = 2$ TeV whereas with $\mu = 4$ TeV this minimum value reduces to about 100 GeV.

Fig. 3.3 (c) and (d) show the distribution of $m_h$ as a function of $\Delta m_{\widetilde{t}}$. These distributions give a clear idea about the range of Higgs mass we obtaine for a certain value of $\Delta m_{\widetilde{t}}$. Fig. 3.3 (d) shows one can squeeze $\Delta m_{\widetilde{t}}$ to about 160 GeV. However, to ascertain the whole sparticle spectrum mass window, one needs to look at the difference between the LSP mass and the heaviest sparticle in the spectrum. Mass gap of the heavier stop/sbottom and the LSP is denoted as $\Delta M$. Fig. 3.3 (e) and (f) show the distribution of $m_h$ as a function of $\Delta M$. As evident from the plots, the minimum $\Delta m_{\widetilde{t}}$ is almost similar to the minimum $\Delta M$ that is obtained here indicating that at the periphery of this minima, $m_{\widetilde{\chi}_1^0} \approx m_{\widetilde{t}_1}$.

[5]For this scan, we only consider bino-like LSP, i,e, $M_1 < M_2$.

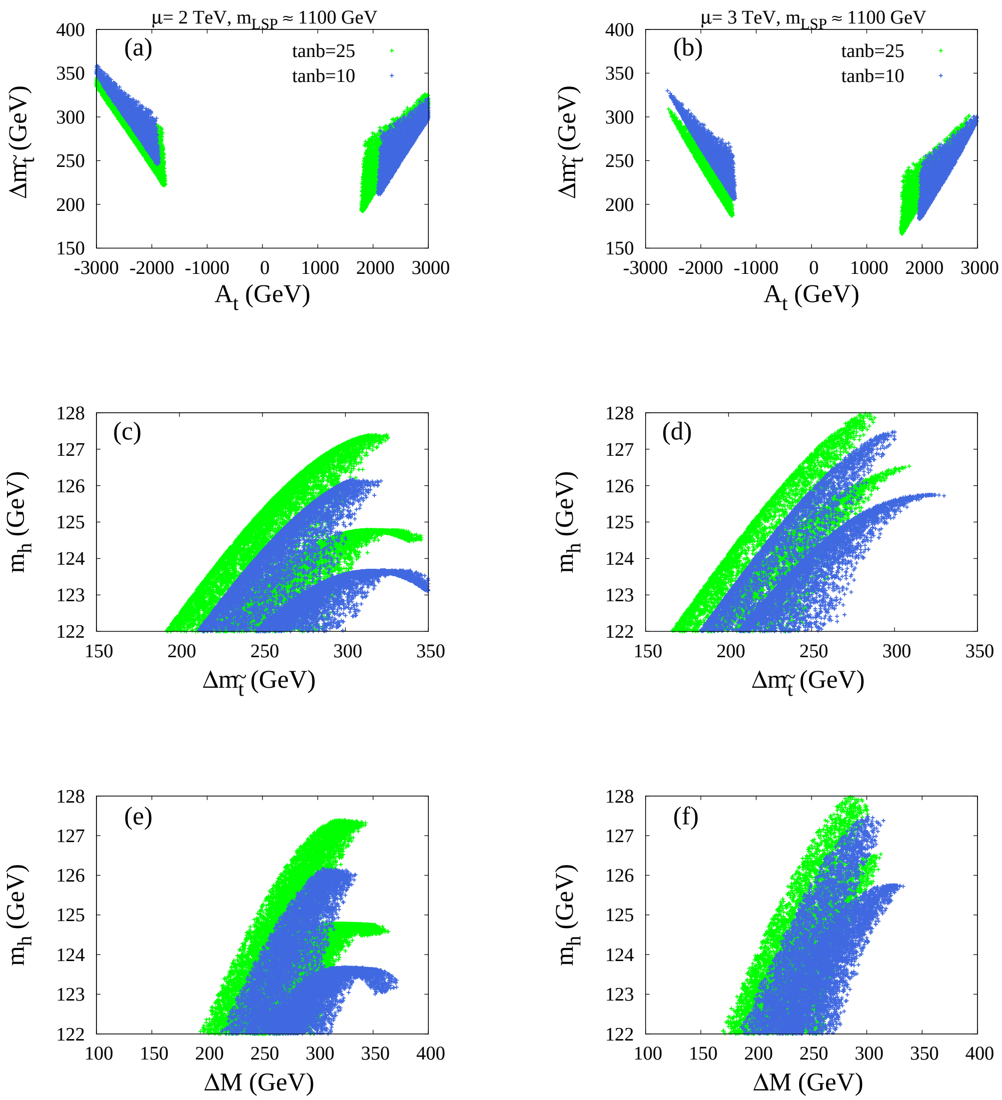


Figure 3.3: The various distributions obtained in our scan are shown. Fig. (a), (c) and (e) are obtained with $\mu = 2$ TeV while Fig. (b), (d) and (f) show the same set of plots obtained with $\mu = 3$ TeV. All the points shown in these plots respect the set of constraints mentioned in the text. The scan is done for two different tan$\beta$ values: 25 (green points) and 10 (blue points).

### 3.2.4 Benchmark points

In choosing the benchmark points for our collider study, we have considered a range of LSP masses varying from 840 GeV to 1862 GeV. The benchmark choices also take into account a varied mass hierarchy for squarks and gluinos, thus allowing different possible decay cascades down to the LSP. We also consider situations where the $\widetilde{g}$ is the NLSP instead of $\widetilde{t}_1$. An illustrative representation of our choice of benchmark points, keeping in mind the different ways the sparticles can be arranged in their masses, is presented in Figure 3.4 where we have classified the benchmarks into the four types of representations as shown. To study the

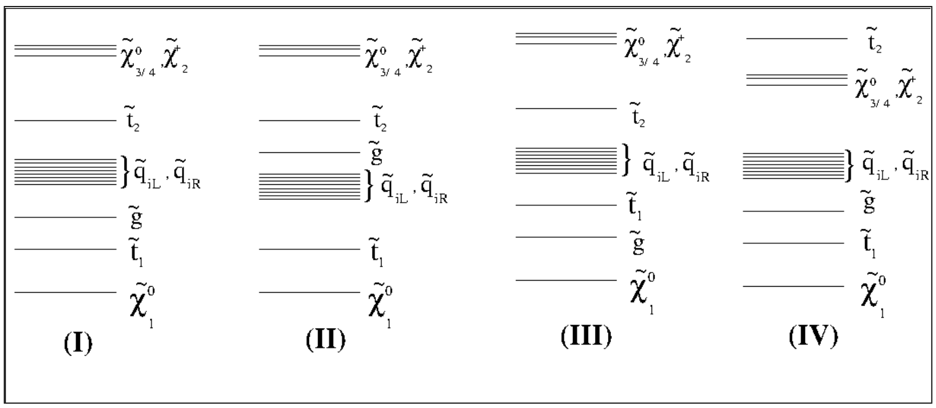


Figure 3.4: Different benchmark scenarios considered in our study: Type I (BP1,BP3, BP5, BP10), Type II (BP4, BP7, BP8, BP9), Type III (BP2) and Type IV (BP6). (In all cases, $\widetilde{q}_{iL/R}$=$\widetilde{u}_{iL/R}, \widetilde{d}_{iL/R}$ with $i = 1, 2$. Sleptons, $\widetilde{\chi}_2^0$ and $\widetilde{\chi}_1^\pm$ not indicated in the figure, lie below $\widetilde{t}_2$ in all cases. Additionally, the mass gaps shown between different sparticles are not to scale).

signal from the above class of spectrum within a compressed SUSY scenario, we have chosen ten benchmark points from the allowed parameter space in the model. The relevant input parameters, mass spectra and the values of the constraints are summarised in Table 4.1.

Since having at least one heavy ($\sim$ TeV) stop in the spectrum helps in achieving a Higgs boson mass of 125 GeV, it is quite natural to expect more and more compression in the whole SUSY spectrum if we keep increasing the LSP mass. In order to showcase this, we have chosen benchmark points with different LSP masses for different choices of the $\mu$-parameter. BP2, with the lightest LSP mass at 842.4 GeV, gives $\Delta M \sim 300$ GeV while BP6 has the heaviest $\widetilde{\chi}_1^0$ at 1861.9 GeV and $\Delta M \sim 184$ GeV. However, note that in BP6, we are able to even pull down the $\widetilde{\chi}_{3/4}$ and the $\widetilde{\chi}_2^\pm$ masses within a 200 GeV mass window from the LSP. A heavier spectrum with $M_1/M_2$ closer to $\mu$ may give rise to more compressed spectrum, but they run into trouble with the DM direct detection constraint. In addition we note that spectra with very heavy squarks and gluino would be out of the 13/14 TeV LHC reach with perhaps some hope for the *very high luminosity* run. We also take some similar LSP masses with different squark-gluino mass hierarchies, like in `BP1, BP5` and `BP3, BP9` to study how the different decay modes and hardness of jets are affected. It should be noted here that we have focussed on final states with zero lepton; one-lepton, two-lepton and three-lepton states have in general highly suppressed rates when they arise in cascade decays of coloured sparticles. Besides, the leptonic final states often entail backgrounds with harder lepton as well as $\not{E}_T$ spectra, which survive the cuts in a relatively, more abundant manner. Thus the exact location of the sleptons in our spectra are somewhat inconsequential, so far as the multi-jet $+\not{E}_T$ signal is concerned.

## 3.3 Probing a compressed spectrum at the LHC

We explore the possibility of finding such a scenario with jet(s) + $\not{E}_T$ final state at the 13 TeV run of the LHC and also perform a detailed background simulation for the same. We consider all possible squark/gluino production channels. We must point out that among all the subprocesses contributing to the signal, the squark-gluino associated production channel has the largest cross-section closely followed by squark pair production cross-section in most of the cases. To study the signal we look at final states with both mono-jet + $\not{E}_T$ and multi-jets ($\geq$ 2-jets) + $\not{E}_T$ in order to compare the relative statistical significance factors.

Note that there have been some significant studies [4, 5, 74–79] that deal with collider signatures of a compressed spectrum. However, all these studies consider either squark or gluino pair production and their subsequent decays into the LSP neutralino. The compression is highlighted through the mass gap between the squark/gluino and the LSP being small, begging the explanation that the final state jets in such cases are too soft to be detected at the colliders. In order to observe any signal, one then has to rely on the ISR-FSR jets and/or photons. While such an observation may shed light on a somewhat fine tuned compression in the SUSY spectrum, one cannot fathom that no other SUSY particle will be in similar mass ranges. We believe that we have already highlighted that an equally probable spectrum, where almost all SUSY particles are squeezed within a relatively small mass gap between the LSP and the heaviest coloured sparticle, meets the strictest of experimental constraints there is to offer. Such a scenario, therefore, presents a situation where one can envisage additional contributions to the final states in consideration through production of the closely lying

| Parameters | BP1 | BP2 | BP3 | BP4 | BP5 | BP6 | BP7 | BP8 | BP9 | BP10 |
|---|---|---|---|---|---|---|---|---|---|---|
| $M_1$ | 1470.0 | 850.0 | 1107.0 | 1334.5 | 1476.3 | 1890.3 | 1200.0 | 1510.0 | 1105.0 | 1730.0 |
| $M_2$ | 1400.5 | 880.0 | 1200.0 | 1328.6 | 1402.6 | 1971.3 | 1250.0 | 1550.0 | 1150.0 | 1770.0 |
| $M_3$ | 1312.0 | 780.0 | 1015.0 | 1405.5 | 1387.7 | 1737.1 | 1180.0 | 1420.0 | 1080.0 | 1600.0 |
| $A_t$ | 2200.8 | -1650.0 | 1897.0 | -1535.1 | 1840.8 | 2800.2 | 2050.0 | 2300.0 | 2000.0 | 2720.0 |
| $\mu$ | 2000.0 | 3000.0 | 2000.0 | 3000.0 | 3000.0 | 2000.0 | 2500.0 | 3000.0 | 3000.0 | 2000.0 |
| $\tan\beta$ | 20.0 | 20.0 | 25.0 | 23.9 | 24.2 | 16.87 | 18.0 | 20.0 | 20.0 | 35.0 |
| $m_{\widetilde{g}}$ | 1430.0 | 861.6 | 1111.6 | 1497.4 | 1500.4 | 1882.0 | 1275.9 | 1534.7 | 1165.6 | 1737.8 |
| $m_{\widetilde{q}_L}$ | 1475.1 | 893.7 | 1159.0 | 1451.2 | 1532.8 | 1912.6 | 1271.4 | 1523.4 | 1127.5 | 1789.1 |
| $m_{\widetilde{q}_R}$ | 1473.6 | 887.4 | 1158.1 | 1450.9 | 1531.9 | 1909.9 | 1269.9 | 1520.4 | 1128.8 | 1789.1 |
| $m_{\widetilde{t}_1}$ | 1412.3 | 871.7 | 1097.9 | 1330.6 | 1426.1 | 1865.0 | 1192.4 | 1507.6 | 1100.4 | 1711.3 |
| $m_{\widetilde{t}_2}$ | 1595.9 | 1136.8 | 1300.4 | 1509.0 | 1581.3 | 2045.6 | 1390.5 | 1686.6 | 1308.3 | 1903.2 |
| $m_{\widetilde{b}_1}$ | 1459.7 | 861.6 | 1125.1 | 1407.4 | 1493.5 | 1966.7 | 1241.9 | 1521.9 | 1130.4 | 1761.3 |
| $m_{\widetilde{b}_2}$ | 1525.3 | 1044.1 | 1222.3 | 1494.5 | 1570.3 | 2011.6 | 1321.7 | 1619.5 | 1229.4 | 1838.4 |
| $m_{\widetilde{\ell}_L}$ | 1432.2 | 880.9 | 1121.2 | 1400.7 | 1482.7 | 1916.4 | 1221.5 | 1543.1 | 1132.5 | 1745.3 |
| $m_{\widetilde{\ell}_R}$ | 1426.2 | 871.0 | 1114.7 | 1400.7 | 1482.7 | 1907.6 | 1215.1 | 1535.5 | 1121.3 | 1736.9 |
| $m_{\widetilde{\tau}_1}$ | 1430.3 | 890.3 | 1113.5 | 1353.2 | 1438.0 | 1893.7 | 1220.0 | 1529.1 | 1105.6 | 1725.4 |
| $m_{\widetilde{\tau}_2}$ | 1483.8 | 1003.3 | 1209.5 | 1446.6 | 1526.0 | 1928.4 | 1289.1 | 1602.2 | 1198.2 | 1803.8 |
| $m_{\widetilde{\nu}_L}$ | 1429.8 | 876.5 | 1117.6 | 1398.6 | 1480.6 | 1914.4 | 1218.3 | 1540.5 | 1128.9 | 1743.1 |
| $m_{\widetilde{\chi}_1^0}$ | 1406.7 | 842.4 | 1096.1 | 1323.9 | 1417.6 | 1861.9 | 1188.9 | 1496.3 | 1095.4 | 1709.3 |
| $m_{\widetilde{\chi}_2^0}$ | 1453.9 | 889.1 | 1200.6 | 1342.9 | 1463.6 | 1934.7 | 1256.9 | 1559.0 | 1158.4 | 1764.9 |
| $m_{\widetilde{\chi}_1^\pm}$ | 1407.0 | 889.3 | 1200.8 | 1342.9 | 1417.6 | 1929.1 | 1257.1 | 1559.1 | 1158.5 | 1764.3 |
| $m_h$ | 122.6 | 122.0 | 122.2 | 122.5 | 122.8 | 123.9 | 122.0 | 122.4 | 122.1 | 124.6 |
| $\Omega h^2$ | 0.092 | 0.032 | 0.036 | 0.113 | 0.099 | 0.113 | 0.062 | 0.105 | 0.073 | 0.110 |
| $\sigma_{SI} \times 10^{11}$ (pb) | 115.78 | 50.11 | 35.95 | 4.65 | 9.08 | 744.98 | 7.64 | 0.13 | 9.56 | 280.97 |
| $\Delta M$ (GeV) | 189.2 | 294.4 | 204.3 | 185.1 | 163.7 | 183.7 | 201.6 | 190.3 | 212.9 | 193.9 |
| $\Delta M_i$ (GeV) | 68.4 | 51.3 | 41.6 | 173.5 | 115.2 | 50.7 | 87.0 | 38.4 | 70.2 | 79.8 |

Table 3.2: Low scale input parameters and the relevant sparticle masses along with the values of the relevant constraints for some of the chosen benchmark points satisfying all the collider, DM and low energy constraints discussed in this section. All the mass parameters are written in GeV unit. Here, $\Delta M_i = m_i - m_{\widetilde{\chi}_1^0}$, where $i$ represents a gluino or the $1^{st}/2^{nd}$ family squarks (whichever is the heaviest).

coloured sparticles. Through this work we try to show how this could lead to modifications in the signal topologies and what optimisations in kinematic selections may be required to study such a compressed SUSY signal at the LHC.

### 3.3.1 Analysis setup and simulation details

We consider all possible production channels of the coloured sparticles, *i.e.*

$$pp \to \widetilde{q}_i\,\widetilde{q}_j,\;\; \widetilde{q}_i\,\widetilde{q}_j^{\,*},\;\; \widetilde{g}\,\widetilde{g},\;\; \widetilde{q}_i\,\widetilde{g},\;\; \widetilde{q}_i^{*}\,\widetilde{g}$$

where the respective sparticles would cascade down to the LSP, giving a multi-particle final state comprising of leptons and quarks along with $\not{E}_T$ associated with the invisible LSP. It turns out that for the compressed spectrum, the jets and charged leptons originating from cascade decays are expected to be quite soft. Therefore it becomes quite likely that events observed from such productions could be observed through jets originating from initial-state radiation (ISR). As a trigger threshold for such jets would naturally include situations where the jets may actually be coming from hard partons produced in association with the pair of SUSY particles at the parton-level. Hence one necessarily requires to produce hard jet(s) at the parton level along with the coloured sparticles and match the events with the ISR jet events. We perform a parton level event generation simulation using `MadGraph5-v2.2.3`) [123, 124]. For our analysis we have chosen `CTEQ6L` [125] as the parton distribution function (PDF). The factorization scale is set following the default option of `MadGraph5`. The generated events are passed through `Pythia-v6.4` [126] to simulate showering and hadronisation effects, including fragmentation. The matching between shower jets and jets produced at the parton level is done using `MLM` matching [127, 128] based on *shower*-$k_T$ algorithm with $p_T$-ordered showers. The matching scale, defined as `QCUT`, differs for the signal where heavy SUSY particles are produced in association with jets when compared to the scale chosen for the SM background. Typical choice of this scale is set between $\simeq 20-30$ GeV for the SM backgrounds, and $\simeq 100-120$ GeV for the MSSM processes after careful investigation of the matching plots generated for different `QCUT` values. Then we pass the events through `Delphes-v3.2.0` [129–131] for jet formation, using *anti*-$k_T$ jet clustering algorithm [132] (via `FastJet` [133]), and detector simulation with default ATLAS selection cuts.

As the signal under consideration is either mono-jet $+\not{E}_T$ or multi-jet $+\not{E}_T$, we need to identify the dominant SM subprocesses that can contribute to the above. For hadronic final states, the most dominant contribution comes from the pure QCD processes such as multi-jet production where $\not{E}_T$ comes either from the jets fragmenting into neutrinos or simply from mismeasurement of the jet energy. Other significantly large contributions can come from $W$ + jets where the $W$ decays leptonically and the charged lepton is missed, $Z$ + jets where the $Z$ decays to neutrinos and $t\bar{t}$ production. Additional modes that may also contribute include $t$ + jets and $VV$ + jets where $V = W^{\pm}, Z$. For reasons already stated in section

3.2.4, a lepton veto in the final state helps to suppress quite a few of the above backgrounds. The matching scheme has been also included for the SM background wherever necessary.

### Primary selection criteria

To identify the charged leptons ($e, \mu$), photon ($\gamma$) and jets, we put the following basic selection criteria (**C0**) on the final state particles for both signal and background:

- Leptons ($\ell = e, \mu$) are selected with $p_T^\ell > 10$ GeV, $|\eta^e| < 2.47$ and $|\eta^\mu| < 2.40$, excluding the transitional pseudorapidity region between the barrel and end cap of the calorimeter $1.37 < |\eta^\ell| < 1.52$.
- Photons are identified with $p_T^\gamma > 10$ GeV and $|\eta^\gamma| < 2.47$ excluding the same transition window as before.
- We demand hard jets having $p_T^j > 40$ GeV within $|\eta^j| < 2.5$.
- All reconstructed jets are required to have an azimuthal separation with $\vec{\not{E}}_T$ given by $\Delta\phi(\text{jet}, \vec{\not{E}}_T) > 0.2$.

Once the primary selection criteria are set for the signal and background events, we now need to identify specific kinematic characteristics that would differentiate the SUSY events from that of the SM background. To highlight the differences, we choose for illustration a few benchmark points, namely `BP4, BP8` and `BP10`. In Fig. 3.5 we show the normalised distributions of some relevant kinematic variables where one can expect significant differences between the signal events of SUSY and the SM, after imposing the above selection criteria **C0**. Note that events with all jet multiplicities have been included in these plots. As the SUSY signal arises from production of heavy coloured sparticles and is expected to carry large missing energy due to the invisible heavy LSP's in the final state, the effective mass ($M_{Eff}$) and $\not{E}_T$ are expected to help in differentiating the SUSY events from SM. In Fig. 3.5(a) we present the effective mass ($M_{Eff}$) distribution for these channels where

$$M_{Eff} = \sum_i |\vec{p}_{T_i}| + \not{E}_T$$

and $i$ runs over all the states present in the event including the reconstructed jets. This global variable, without utilising any topology information, can be extremely efficacious from the understanding that, contrary to most of the SM background processes, production of heavy SUSY particles require significantly larger parton level center-of-mass (CM) energy. Thus

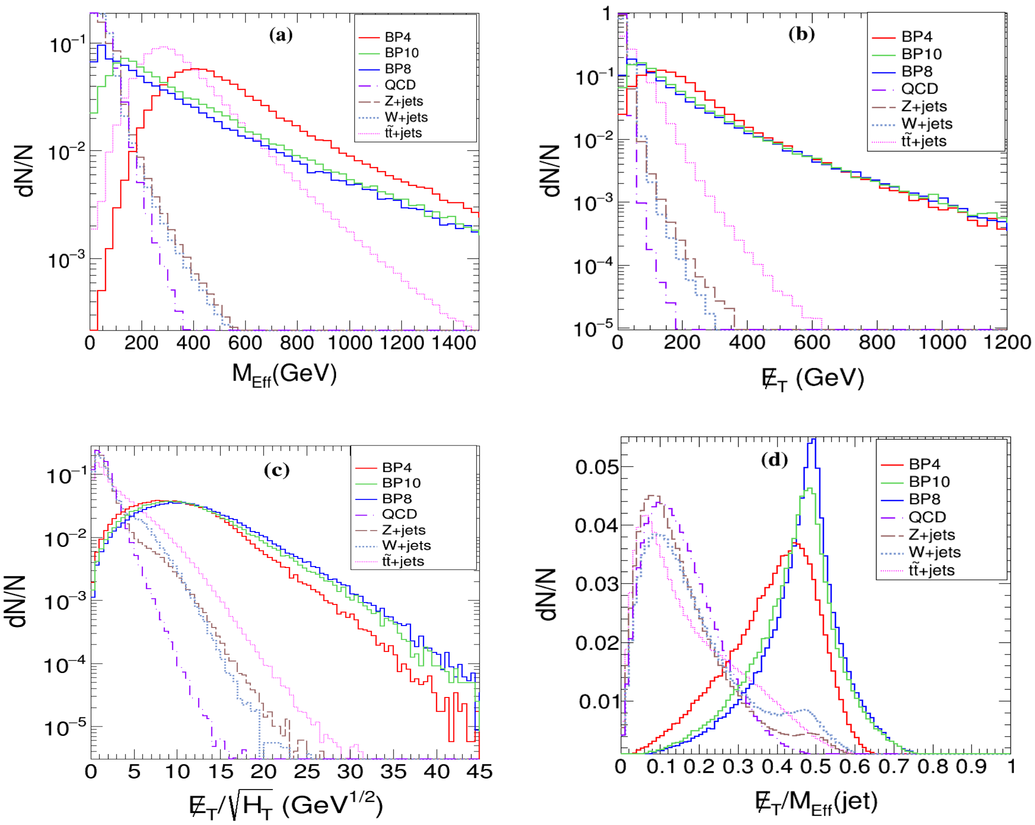


Figure 3.5: Normalised differential distributions of a few relevant kinematic variables for our analysis of compressed spectra after imposing the event selection cuts **C0**. For illustration, signals `BP4`, `BP8` and `BP10` are compared to the SM Backgrounds. The scalar sum of the transverse momenta of the jets, $H_T = \sum_{j=jets} p_{T_j}$. See the draft for the description of $M_{Eff}(jet)$.

one expects a larger $M_{Eff}$ for all benchmark scenarios as shown in Fig. 3.5(a). In Fig. 3.5(b) we show the expected missing transverse energy distributions for the SUSY signal and SM background. Quite clearly, the distributions in both the above variables seem to peak at lower values for the SM background (except $t\bar{t}$+jets) when compared to the SUSY signal. Note that we have plotted the normalized distributions which gives a qualitative idea on the additional cuts required on these variables, rather than a quantitative one.

In addition we find two more kinematic variables of interest used by the ATLAS Collaboration [88,94], *viz.* $\not{E}_T/\sqrt{H_T}$ and $\not{E}_T/M_{Eff}(jet)$, which show clear difference between signal and background. These are shown in Fig. 3.5(c) and Fig. 3.5(d) respectively. Here, $H_T$

represents the scalar sum of all isolated jet $p_T$'s while $M_{Eff}(jet)$ is defined to be constructed out of the first two leading jets and $\not{E}_T$:

$$M_{Eff}(jet) = p_T^{j_1} + p_T^{j_2} + \not{E}_T$$

These plots also show some distinct characteristic distributions for signals. We thus find that appropriate cuts on the above variables, shown in Fig. 3.5, would serve to optimise the signal vis-a-vis the SM background. We now proceed to analyse the multi-jets + $\not{E}_T$ and mono-jet + $\not{E}_T$ signals in the next section.

### 3.3.2 Multi-jets $+\not{E}_T$

As discussed earlier, a compressed SUSY spectra such as ours can lead to high multiplicity of jets in the final state. We observe that significant signal events are found when the jet-multiplicity ($n_j$) is at least two ($n_j \geq 2$) after selecting events using **C0**. This multi-jet scenario is dependent on the hardness of the selected jets and therefore one requires optimised event selection criteria to see how it stands against the SM background. We list below the different cuts which help us in achieving an improved signal to background ratio:

- **C1**: Since we are only considering squark and gluino production channels, no hard lepton or photon are expected in the final state. We, therefore, select final states with two or more jets, vetoing any qualified lepton or photon in such events.

The multi-jet signal is defined for events that satisfy **C0 + C1**. Note that for a compressed SUSY spectrum, the jet multiplicity would start falling when more hard jets are selected in the final state. An optimised choice in our case is to have only a few very hard jets with the following requirements on their transverse momenta:

- **C2**: The hardest jet should have $p_T(j_1) > 130$ GeV and the next hardest jet $p_T(j_2) > 80$ GeV.

We find that the above requirement does not affect the signal significantly while giving appreciable suppression to the SM background (see Table 3.3 and Table 3.4).

- **C3**: We demand larger azimuthal separations between the leading two jets and $\vec{\not{E}}_T$ $\left(\Delta\phi(\text{jet}, \vec{\not{E}}_T) > 0.4\right)$. This requirement is necessary to reduce the chance of contamination in the $\not{E}_T$ coming from missing parts of these hard jets.

| Signal | | Effective cross-section after the cuts (in fb) | | | | | | |
|---|---|---|---|---|---|---|---|---|
| Benchmark Points | Production cross-section(fb) | **C0 + C1** | **C2** | **C3** | **C4** | **C5** | **C6** | **C7** |
| BP1 | 155.56 | 87.38 | 24.32 | 23.34 | 11.49 | 11.29 | 8.28 | 8.22 |
| BP2 | 4202.42 | 1877.45 | 588.58 | 564.81 | 260.89 | 255.29 | 176.81 | 175.21 |
| BP3 | 835.49 | 414.61 | 126.64 | 121.58 | 58.32 | 57.12 | 40.96 | 40.66 |
| BP4 | 126.93 | 118.79 | 62.85 | 59.72 | 20.74 | 19.84 | 9.99 | 9.93 |
| BP5 | 93.77 | 81.83 | 41.58 | 39.57 | 13.64 | 13.17 | 7.18 | 7.13 |
| BP6 | 29.66 | 14.39 | 5.49 | 5.30 | 2.76 | 2.71 | 2.03 | 2.01 |
| BP7 | 364.38 | 248.29 | 82.04 | 77.54 | 32.81 | 31.99 | 20.16 | 20.04 |
| BP8 | 95.58 | 40.62 | 12.86 | 12.45 | 6.34 | 6.24 | 4.72 | 4.68 |
| BP9 | 731.08 | 453.91 | 117.84 | 112.37 | 55.17 | 53.86 | 35.92 | 35.62 |
| BP10 | 29.60 | 19.21 | 5.20 | 4.99 | 2.37 | 2.33 | 1.65 | 1.64 |

Table 3.3: The cut-flow table for the (multi-jet $+\not{E}_T$) final state, showing the change in signal cross-sections for the ten different benchmark points. The cuts (**C0 − C7**) are defined in the text in section 3.3.2.

We note that the above set of requirements (**C0 − C3**) not only helps in refining the signal against the SM background but also helps us in determining more precise quantitive cuts on the kinematic variables shown in Fig. 3.5 to improve the signal significance (see Table 3.3 and Table 3.4). Naively, Fig. 3.5(d) would suggest that an appropriate cut on $\not{E}_T/M_{Eff}(jet)$ itself can help us completely eliminate the background. However, on close inspection, we find that the tail of the large QCD background still survives this cut. We, therefore, find a more optimised cut flow to improve the signal significance as shown below.

- **C4**: We demand $M_{Eff} > 800$ GeV. This turns out to be quite crucial in significantly suppressing almost all contributions for the SM background while moderately affecting the signal events.

- **C5**: We demand $\not{E}_T > 160$ GeV which helps in completely eliminating the remnant QCD multi-jet background while suppressing all the other SM background channels. Note that this cut hardly affects the signal for any of the benchmark points.

- **C6**: Larger missing energy and softer jets in our scenario results in a larger $\not{E}_T/\sqrt{H_T}$ ratio compared to the SM background channels. We find that with $\not{E}_T/\sqrt{H_T} > 15$

| SM Backgrounds | | Effective cross-section after the cuts (in pb) | | | | | | |
|---|---|---|---|---|---|---|---|---|
| Channels | Production (in pb) | **C0** + **C1** | **C2** | **C3** | **C4** | **C5** | **C6** | **C7** |
| $t\bar{t}$ +≤ 2 jets | 722.94 | 542.67 | 167.2 | 141.63 | 15.54 | 2.47 | 0.16 | 0.151 |
| t +≤ 3 jets | 330.57 | 227.0 | 36.23 | 29.84 | 1.09 | 0.123 | 0.01 | 0.009 |
| QCD(≤4 jets) | 2E+08 | 1.8E+07 | 312747 | 251865 | 2765.52 | ∼0 | ∼0 | ∼0 |
| Z +≤ 4 jets | 57088 | 6660.86 | 325.92 | 265.45 | 13.39 | 2.10 | 0.666 | 0.666 |
| W + ≤4 jets | 197271 | 14206.3 | 896.76 | 734.47 | 36.93 | 3.98 | 0.485 | 0.485 |
| WZ + ≤2 jets | 53.8 | 24.44 | 5.74 | 4.81 | 0.67 | 0.16 | 0.037 | 0.036 |
| ZZ + ≤2 jets | 13.69 | 5.77 | 0.79 | 0.66 | 0.069 | 0.019 | 0.00549 | 0.00548 |
| Total background | | | | | | | | 1.352 |

Table 3.4: The cut-flow table for the (multi-jet $+\not{E}_T$) final state, showing the change in cross-sections for the different subprocesses contributing to the SM background. The cuts ($\mathbf{C0} - \mathbf{C7}$) are defined in the text in section 3.3.2.

GeV$^{1/2}$ the signal significance can be improved further.

- **C7**: The ratio $\not{E}_T/M_{Eff}(jet)$ is shown to peak at smaller values for the SM background and therefore we demand $\not{E}_T/M_{Eff}(jet) > 0.35$ which further improves our signal significance.

We present the numerical results for the ten aforementioned benchmark points and the SM background to the multi-jet $+\not{E}_T$ signal at LHC with $\sqrt{s} = 13$ TeV. In Table 3.3 we summarise the effects of the cuts ($\mathbf{C0} - \mathbf{C7}$) on signal cross-sections. It is worth pointing out here that we have used next-to-leading order (NLO) cross-section for the production rates of squarks and gluinos in our signal analysis by multiplying the leading-order cross-sections of `MadGraph5` by NLO $K$-factors obtained using Prospino 2.1 [134–138]. The cut-flow table for the same set of cuts is shown for the SM background processes in Table 3.4. Note that we have also used the NLO cross-section for SM background processes provided in `MadGraph5` [123]. It is quite clear to see from Tables 3.3 and 3.4 that our choice of cuts is quite efficient in suppressing a seemingly huge SM background such that the signal may be observed at the LHC. The statistical significance ($\mathcal{S}$) of the observed signal ($s$) over the total

| | | Statistical significance ($\mathcal{S}$) | | | Required luminosity (in $fb^{-1}$) | |
|---|---|---|---|---|---|---|
| Signal | $\mathrm{m}_{\widetilde{\chi}_1^0}$(GeV) | $\mathcal{L} = 100$ | $\mathcal{L} = 500$ | $\mathcal{L} = 1000$ | $\mathcal{S} = 3\sigma$ | $\mathcal{S} = 5\sigma$ |
| BP1 | 1406.7 | 2.23 | 4.99 | 7.06 | 180.98 | 502.72 |
| BP2 | 842.4 | 46.67 | 104.37 | 147.60 | 0.41 | 1.15 |
| BP3 | 1096.3 | 11.00 | 24.61 | 34.80 | 7.44 | 20.66 |
| BP4 | 1323.89 | 2.70 | 6.03 | 8.53 | 123.46 | 342.94 |
| BP5 | 1417.56 | 1.94 | 4.33 | 6.13 | 239.13 | 664.26 |
| BP6 | 1862.2 | 0.55 | 1.22 | 1.73 | 2975.21 | 8264.46 |
| BP7 | 1189.04 | 5.44 | 12.16 | 17.19 | 30.41 | 84.48 |
| BP8 | 1496.3 | 1.27 | 2.84 | 4.02 | 558.00 | 1550.00 |
| BP9 | 1095.38 | 9.65 | 21.57 | 30.50 | 9.66 | 26.85 |
| BP10 | 1709.33 | 0.45 | 1.00 | 1.41 | 4444.44 | 12345.68 |

Table 3.5: Statistical significance of the signal for different benchmark points in the multi-jet $+\not{E}_T$ analysis at 13 TeV LHC. The significance is estimated for three values of integrated luminosity ($\mathcal{L} = 100, 500$ and $1000$ fb$^{-1}$). We also estimate the required integrated luminosity to achieve a $3\sigma$ and $5\sigma$ excess for each benchmark point at LHC with $\sqrt{s} = 13$ TeV.

SM background ($b$) has been calculated using

$$\mathcal{S} = \sqrt{2 \times \left[(s+b)\ln(1+\frac{s}{b}) - s\right]}. \tag{3.3.1}$$

We show the significance of the signal for different benchmark points in the multi-jet $+\not{E}_T$ channel in Table 3.5. We choose three different values for the integrated luminosity ($\mathcal{L} = 100, 500$ and $1000$ fb$^{-1}$) to highlight the significance for the benchmark points. We find that the signal corresponding to `BP6` and `BP10` are practically scenarios within a compressed SUSY spectrum which would be very hard to observe in the multi-jet $+\not{E}_T$ channel. In fact an integrated luminosity of over 3000 fb$^{-1}$ would be required for any hope of observing a notable excess for the SUSY spectrum given by the above benchmark points. This is however understandable as the corresponding spectra is very heavy leading to smaller production rates compared to the other benchmark points. The lightest spectrum amongst all the benchmark points, *viz.* `BP2` is the most robust of all and should be observable at the present run of

LHC with luminosity as low as 1 $\mathrm{fb}^{-1}$. The rest of the benchmark points too lead to $3\sigma$ and $5\sigma$ excess over the SM backgrounds with relatively nominal to slightly higher integrated luminosities as shown in the last two columns of Table 3.5 [6].

### 3.3.3 Mono-jet $+\not{E}_T$

The mono-jet $+\not{E}_T$ signal is considered as a favourable channel to probe a compressed spectrum at the LHC [3, 74–81, 86]. Therefore it is quite logical to explore how the mono-jet final state in our scenario stands against the SM background. Both ATLAS and CMS have investigated mono-jet signals in the context of compressed SUSY spectra [83–85, 87, 88]. Note that, these analyses consider only such scenarios where the compression is between the NLSP and LSP, and the signal arises through the NLSP pair production and its subsequent decay. Since we consider almost the entire SUSY spectrum to be compressed, all SUSY processes (dominated, of course, by coloured sparticle production channels) are of interest to us. Thus our analysis requires revisiting the standard cuts suggested in the literature. As in the case of multi-jet $+\not{E}_T$ final state, we demand a leptonically quiet mono-jet final state (after **C0**) where:

- **D1**: Events are selected having at least one hard jet in the final state with no charged lepton or photon.

Since mono-jet searches rely on hard ISR jet, the leading jet is required to be considerably hard with large transverse momentum and well separated from the direction of $\vec{\not{E}}_T$:

- **D2**: The leading jet has $p_T(j_1) > 130$ GeV (as before) with a significantly larger azimuthal separation with $\vec{\not{E}}_T$ given by $\Delta\phi(j_1, \vec{\not{E}}_T) > 1.0$.

- **D3**: In order to accommodate a hard jet coming from ISR, but not rule out cases with another jet arising due to its fragmentation, we demand the second hardest jet to have $p_T(j_2) < 80$ GeV, but with $\Delta\phi(j_2, \vec{\not{E}}_T) > 1.0$.

We thus define our mono-jet + $\not{E}_T$ signal for events which satisfy cuts (**C0, D1 – D3**). Moreover, for events where the leading jet is hard enough, a sizeable $\not{E}_T$ is seen, which also serves as an useful discriminator for the SUSY signal from the SM background.

- **D4**: We demand $\not{E}_T > 160$ GeV. In our case, this decreases the SM background substantially, as opposed to the SUSY signals (see Table 3.6 and 3.7).

[6] The current LHC run 2 data [139] should have seen **BP2**, **BP3**, **BP7** and **BP9**.

| Signal | | Effective cross-section after the cuts (in fb) | | | | |
|---|---|---|---|---|---|---|
| Benchmark Points | Production cross-section(fb) | **C0 + D1** | **D2** | **D3** | **D4** | **D5** |
| BP1 | 155.56 | 136.11 | 51.85 | 14.19 | 11.64 | 3.01 |
| BP2 | 4202.42 | 3262.38 | 1334.47 | 321.74 | 256.86 | 58.14 |
| BP3 | 835.49 | 686.61 | 277.70 | 70.70 | 57.26 | 13.76 |
| BP4 | 126.93 | 126.70 | 79.36 | 12.06 | 8.22 | 0.88 |
| BP5 | 93.77 | 88.93 | 55.13 | 9.16 | 6.23 | 0.78 |
| BP6 | 29.66 | 23.81 | 11.58 | 2.58 | 2.13 | 0.58 |
| BP7 | 364.38 | 308.97 | 126.35 | 27.61 | 20.34 | 5.15 |
| BP8 | 95.58 | 71.47 | 30.46 | 7.48 | 6.20 | 1.63 |
| BP9 | 731.08 | 650.39 | 241.20 | 69.16 | 54.65 | 13.63 |
| BP10 | 29.60 | 27.11 | 10.32 | 2.91 | 2.32 | 0.60 |

Table 3.6: The cut-flow table for the (mono-jet $+\not{E}_T$) final state, showing the change in signal cross-sections for the ten different benchmark points. The cuts (**C0, D1 – D5**) are defined in the text in section. 3.3.3.

We also find that a hard effective mass ($M_{Eff}$) cut is also quite efficient in suppressing the SM background as compared to SUSY signal events for the mono-jet+$\not{E}_T$ channel.

- **D5**: We set $M_{Eff} > 800$ GeV for the analysis which again helps to remove the huge QCD background as well as reduce the other dominant contributions. Although the signal events are also reduced considerably, the signal-to-background ratio improves significantly after the $M_{Eff}$ cut.

Tables 3.6 and 3.7 summarise the effect of the cuts (**C0, D1 – D5**) on the SUSY signals and SM background cross-sections respectively. For both signal and background, we have used the NLO cross-sections as before. It is clear from Tables 3.6 and 3.7 that our choice of cuts for the mono-jet $+\not{E}_T$ final state, although quite helpful in suppressing the SM background to improve the signal significance is however not an improvement over the multi-jet $+\not{E}_T$ channel. We show the significance of the signal for all the benchmark points in the mono-jet $+\not{E}_T$ channel in Table 3.8 with the same integrated luminosity ($\mathcal{L} = 100, 500$ and 1000 fb$^{-1}$).

For the mono-jet $+\not{E}_T$ channel too, we find that the lightest spectrum, `BP2` will be discovered at the earliest. The heavier spectra, `BP6 and BP10` are no more better observable

| SM Backgrounds | | Effective cross-section after the cuts (in pb) | | | | |
|---|---|---|---|---|---|---|
| Channels | Production (in pb) | **C0** + **D1** | **D2** | **D3** | **D4** | **D5** |
| $t\bar{t}$ $+\leq$ 2 jets | 722.94 | 573.89 | 171.12 | 21.52 | 2.135 | 0.119 |
| t $+\leq$ 3 jets | 330.57 | 278.05 | 41.14 | 6.17 | 0.355 | 0.011 |
| QCD($\leq$4 jets) | 2E+08 | 7.6E+07 | 417461 | 46034 | 2584 | $\sim$0 |
| Z $+\leq$ 4 jets | 57088 | 18924.1 | 446.41 | 52.25 | 6.66 | 0.255 |
| W + $\leq$4 jets | 197271 | 50478.5 | 1167.56 | 139.332 | 8.98 | 0.534 |
| WZ + $\leq$2 jets | 53.8 | 37.92 | 6.896 | 0.953 | 0.208 | 0.0161 |
| ZZ + $\leq$2 jets | 13.69 | 9.77 | 1.03 | 0.158 | 0.0498 | 0.00264 |
| Total background | | | | | | 0.938 |

Table 3.7: The cut-flow table for the (mono-jet $+\not{E}_T$) final state, showing the change in cross-sections for the different subprocesses contributing to the SM background. The cuts (**C0, D1 − D5**) are defined in the text in section. 3.3.3.

in the mono-jet $+\not{E}_T$ channel as they were in the multi-jet $+\not{E}_T$ channel. Among others, large number of signal spectra such as, `BP4, BP5, BP8`, have low significances even at 1000 fb$^{-1}$ whereas `BP3, BP9, BP7 and BP1` may be observed at moderate ($\sim$45 fb$^{-1}$) to high ($\sim$1000 fb$^{-1}$) luminosities at the LHC. It is important to note that the squark-gluino masses and hierarchy dictate the hardness of the cascade jets. As per our selection criteria, **D2** rejects events with additional hard jets while retaining many more with softer accompanying jets, thereby enhancing the significance in general. However, it adversely affects cases such as `BP4` which have larger mass gaps.

Thus, although the multi-jet + $\not{E}_T$ channel provides increased signal significances for all the benchmark points, mono-jet + $\not{E}_T$ channel still remains a viable window for observing compressed spectra. Overall, the efficacy of both these channels depends on the splitting among the LSP, lighter stop, gluino and first two generation squark masses. The benchmark points where the masses of the first two generation squarks and the gluino are separated from the LSP by about 50 GeV at most are found to have better signal to background ratio in the multi-jet $+\not{E}_T$ final state when compared to mono-jet $+\not{E}_T$. However, two spectra with similar $\widetilde{q}$-$\widetilde{g}$ masses resulting in similar production cross-sections, are expected to differ in their relative sensitivities to the two final states depending upon the $\widetilde{q}$-$\widetilde{g}$-$\widetilde{\chi}_1^0$ mass gaps.

| | | Statistical significance ($\mathcal{S}$) | | | Required Luminosity (in $fb^{-1}$) | |
|---|---|---|---|---|---|---|
| Signal | $\mathrm{m}_{\widetilde{\chi}_1^0}$(GeV) | $\mathcal{L} = 100$ | $\mathcal{L} = 500$ | $\mathcal{L} = 1000$ | $\mathcal{S} = 3\sigma$ | $\mathcal{S} = 5\sigma$ |
| BP1 | 1406.7 | 0.98 | 2.19 | 3.10 | 937.11 | 2603.08 |
| BP2 | 842.4 | 18.98 | 42.44 | 60.02 | 2.50 | 6.94 |
| BP3 | 1096.3 | 4.49 | 10.03 | 14.20 | 44.64 | 124.00 |
| BP4 | 1323.89 | 0.29 | 0.64 | 0.91 | 10926.44 | 30351.22 |
| BP5 | 1417.56 | 0.25 | 0.57 | 0.81 | 14400 | 40000 |
| BP6 | 1862.2 | 0.19 | 0.42 | 0.60 | 24930.75 | 69252.08 |
| BP7 | 1189.04 | 1.68 | 3.76 | 5.31 | 318.88 | 885.77 |
| BP8 | 1496.3 | 0.53 | 1.19 | 1.68 | 3203.99 | 8899.96 |
| BP9 | 1095.38 | 4.45 | 9.95 | 14.07 | 45.44 | 126.25 |
| BP10 | 1709.33 | 0.20 | 0.44 | 0.62 | 22500 | 62500 |

Table 3.8: Statistical significance of the signal for different benchmark points in the mono-jet $+\not{E}_T$ analysis at 13 TeV LHC. The significance is estimated for three values of integrated luminosity ($\mathcal{L} = 100, 500$ and $1000$ fb$^{-1}$). We also estimate the required integrated luminosity to achieve a $3\sigma$ and $5\sigma$ excess for each benchmark point at LHC with $\sqrt{s} = 13$ TeV.

Let us consider `BP5` and `BP8` for example. Although the $\widetilde{q}$'s and the $\widetilde{g}$ masses are very similar, $\Delta M_i$ in `BP8` is much smaller than that in `BP5` because of their different LSP masses. Naturally, `BP5` provides a better signal significance than `BP8` when multi-jet + $\not{E}_T$ final state is considered but the situation is reversed when we do a mono-jet + $\not{E}_T$ analysis. `BP3` and `BP9` despite having similar LSP mass, are different in terms of the $\widetilde{q}$-$\widetilde{g}$ mass hierarchy. `BP3`, as a consequence of having smaller gluino mass, has a larger production cross-section, but due to the presence of more number of softer jets in `BP9`, it does slightly better than `BP3` in terms of signal significance in the mono-jet analysis. `BP4` despite having smaller production cross-section than `BP1`, has a better signal significance for multi-jet + $\not{E}_T$ final state due to the presence of more number of harder jets. On the other hand, `BP1` does better if mono-jet + $\not{E}_T$ final state is considered. `BP2` prevails over all the other benchmark points in terms of signal significance in both the final states due to its large production cross-section. `BP6` and `BP10` having very heavy $\widetilde{q}$-$\widetilde{g}$ spectrum, are unlikely to be probed even at high luminosities.

## 3.4 Summary and Conclusions

In this chapter, we have considered the compressed SUSY scenario within the phenomenological MSSM framework that is consistent with all the present collider and DM data. We observe that achieving a substantial compression in the whole SUSY spectrum while being consistent with the observed Higgs boson mass requires relatively heavy masses for the sparticles. Since at least one of the stop masses needs to be heavy (above TeV) in order to enhance the lightest CP-even Higgs boson mass to the allowed range, better compression in the parameter space is obtained as we consider heavier LSP masses which nonetheless address the naturalness problem. Such mass ranges, we emphasize, are beyond the reach of the 8 TeV run, and therefore, warrant a close investigation in the context of 13/14 TeV LHC. We observe that having a large $\mu$-parameter, too, can achieve tighter compression in the remaining spectrum.

We select ten representative benchmark points from the currently allowed parameter space with all kinds of mass hierarchies and explore their detection possibility at the 13 TeV run of the LHC. Similar results can be expected if the upgrade to 14 TeV takes place. We analyse both the conventional multi-jet $+\not{E}_T$ channel and the mono-jet $+\not{E}_T$ channel. We observe that although mono-jet $+\not{E}_T$ channel may be a viable option for this kind of scenario, a multi-jet $+\not{E}_T$ final state provides better statistical significance over the SM background for all our benchmark points.

# Chapter 4

# Search for a compressed spectrum with gravitino LSP

## 4.1 Introduction

From our discussion in Chapter 3 we recall that the lack of evidence for any low scale SUSY events had prompted the idea of a compressed sparticle spectrum where the LSP, mostly the lightest neutralino $\widetilde{\chi}_1^0$, and the heavier sparticle states may be nearly degenerate. In the absence of hard leptons or jets arising from the cascade, one has to rely on tagging the jets or photons originating from the ISR or FSR to detect such events where the available missing transverse momenta are characterized by the stability of the LSP in the cascades. Thus, such signals allow a much lighter SUSY spectrum compared to the conventional channels with hard leptons, jets and large missing transverse momentum [6,83–85,87,88,94,140–143].

However, in the presence of a light gravitino ($\widetilde{G}$) in the spectrum, the $\widetilde{\chi}_1^0$ is quite often the next-to-lightest SUSY particle (NLSP), which decays into a $\widetilde{G}$ and a gauge/Higgs boson. Search strategy for such scenarios, therefore, is expected to be significantly different. In this case, one would always expect to find one or more hard leptons/jets/photons in the final state originating from the $\widetilde{\chi}_1^0$ decay, irrespective of whether the SUSY mass spectrum is compressed or not. Hence detecting events characterizing such a signal is expected to be much easier, with the preferred channel being the photon mode. Given the fact that the hard photon(s) can easily be tagged for these events in a relatively compressed spectrum of the SUSY particles with the NLSP, one need not rely on the radiated jets for signal identification, thereby improving the cut efficiency significantly. If one considers a fixed gravitino mass, the photon(s) originating from the $\widetilde{\chi}_1^0$ decay will be harder as $\widetilde{\chi}_1^0$ becomes heavier. Hence these hard photon associated signals can be very effective to probe a heavy SUSY spectrum with a light gravitino as there would rarely be any SM events with such hard photons in the final state.

While the light gravitino scenario yields large transverse missing energy ($\not{E}_T$) as well as hard photon(s) and jet(s), the question remains as to whether its presence obliterate the information on whether the MSSM part of the spectrum is compressed or not. In this chapter, the contents of which are based on [9], we have demonstrated how such information can be extracted. Our study in this direction contains the following new observations:

- A set of kinematic observables are identified involving hardness of the photon(s), the transverse momenta ($p_T$) of the leading jets and also the $\not{E}_T$, which clearly brings out the distinction between a compressed and an uncompressed spectrum with similar signal rates. We have studied different benchmarks with varied degree of compression in the spectrum in this context.

- The characteristic rates of the $n$-$\gamma$ (where $n \geq 1$) final state in a compressed spectrum scenario have been obtained and the underlying physics has been discussed.

- The circumstances under which, for example, a gluino in a compressed MSSM spectrum prefers to decay into a gluon and a gravitino rather than into jets and a neutralino have been identified. In this context, we have also found some remarkable effects of a eV-scale gravitino though such a particle can not explain the cold dark matter (DM) content of the universe.

The experimental collaborations have considered light gravitino scenarios and derived bounds on the colored sparticles [144–150]. The ATLAS collaboration recently published their analysis on a SUSY scenario with a light $\widetilde{G}$ with the 13 TeV data accumulated at an integrated luminosity of 13.3 fb$^{-1}$ [150]. In this analysis, $m_{\widetilde{\chi}_1^0}$ is considered to be a bino-higgsino mixed state decaying into $\gamma\widetilde{G}$ and(or) $Z\widetilde{G}$ resulting in the final state "$n_1\gamma + n_2$ jets + $\not{E}_T$" where the photon multiplicity $n_1 \geq 1$ and the jet multiplicity $n_2 > 2$. The 13 TeV data puts a stringent constraint on the sparticle masses excluding $m_{\widetilde{g}}$ up to 1950 GeV subject to the lightest neutralino mass close to 1800 GeV [146, 149, 150], which is a significant improvement on the bounds obtained after the 8 TeV run with 20.3 fb$^{-1}$ integrated luminosity [145, 147]. We note that, in order to derive the limits from the collider data, the experimental collaboration considers signal events coming from gluino pair production only, while assuming the rest of the colored sparticles *viz.* squarks to be much heavier to contribute to the signal. The robustness of the signal however does not differentiate whether such a heavy SUSY spectrum (leaving aside the gravitino) is closely spaced in mass or has a widely split mass spectrum, and whether it is just a single sparticle state that contributes to the signal or otherwise. We intend to impress through this work that such a signal would also be able to distinguish such alternative possibilities quite efficiently.

In Chapter 3 while assuming a similar compression in the sparticle spectrum [7] we had shown that in order to get a truly compressed[1] pMSSM spectrum consistent with a 125 GeV Higgs boson and the flavour and dark matter (DM) constraints, one has to have the $m_{\widetilde{\chi}_1^0}$ mass at or above 2 TeV with the entire colored sector lying slightly above. Such a spectrum is now seemingly of interest given the present experimental bounds obtained in $\widetilde{G}$ LSP scenario[2]. In this work, we aim to extend our previous study by adding to the spectrum, a $\widetilde{G}$ LSP with mass, at most, in the eV-keV range. The rest of the pMSSM spectrum lies above the TeV range to be consistent with the experimental bounds. This is in contrast to existing studies done earlier for gravitino LSP which we compare by studying the prospects of uncompressed spectra having relatively larger mass gaps between the colored sparticles and $m_{\widetilde{\chi}_1^0}$, but with event rates similar to that of the compressed spectra. Since the kinematics of the decay products in the two cases are expected to be significantly different, we present some kinematical variables which clearly distinguish a compressed spectrum from an uncompressed one, in spite of comparable signal rates in both cases.

The subsequent sections are organised as follows. In section 4.2 we discuss about the phenomenological aspects of a SUSY spectrum with gravitino LSP and then move on to study the variation of the branching ratios of squark, gluino and the lightest neutralino (predominantly bino-like) into gravitino associated and other relevant decay modes. In section 4.3 we present some sample benchmark points representative of our region of interest consisting of both compressed and uncompressed spectra that are consistent with the existing constraints. Subsequently, in section 4.4 we proceed to our collider analysis with these benchmark points and present the details of our simulation and obtained results. Finally, in section 4.5 we summarise our results and conclude.

[1]Mass gap between the heaviest colored sparticle and the LSP neutralino has to be around 100 GeV.

[2]Note that the bounds on the squark-gluino masses in the compressed region with $m_{\widetilde{\chi}_1^0}$ LSP are still much weaker. In such cases, the gluinos and first two generation squarks are excluded up to 650 GeV and 450 GeV respectively [142].

## 4.2 Compressed spectrum with a gravitino LSP

The NLSP decaying into a gravitino and jets/leptons/photons give rise to very distinct signals at the LHC. Both the ATLAS and CMS collaborations have studied these signal regions for a hint of GMSB-like scenarios [144–151]. Note that, a pure GMSB like scenario is now under tension after the discovery of the 125 GeV Higgs boson [44–46]. It is very difficult to fit a light Higgs boson within this minimal framework, mostly because of small mixing in the scalar sector. As a consequence, the stop masses need to be pushed to several TeV in order to obtain the correct Higgs mass, thus rendering such scenarios uninteresting in the context of LHC. However, some variations of the pure GMSB scenario are capable of solving the Higgs mass issue and can still give visible signals within the LHC energy range [152,153]. Since we are only interested in the phenomenology of these models here, a detailed discussion on their theoretical aspects is beyond the scope of this paper.

Although the lightest neutralino ($\widetilde{\chi}_1^0$) is the more popular DM candidate in SUSY theories, gravitino ($\widetilde{G}$) as the LSP has its own distinct phenomenology. The $\widetilde{G}$ is directly related to the effect of SUSY breaking via gauge mediation and all its couplings are inversely proportional to the Planck mass ($\sim 10^{18}$ GeV) and thus considerably suppressed. The hierarchy of the sparticle masses depend on the SUSY breaking mechanism and can result in $\widetilde{G}$ getting mass which is heavier, comparable or lighter than the other superpartners. Thus if it happens to be the LSP in the theory, $\widetilde{G}$ can also be a good DM candidate [154–159] making such scenarios of considerable interest in the context of the LHC. In addition, having $\widetilde{G}$ as a DM candidate also relaxes the DM constraints on the rest of the SUSY spectrum by a great deal, allowing them to be very heavy while being consistent with a light $\widetilde{G}$ DM. However, a very light $\widetilde{G}$ is mostly considered to be warm DM. Present cosmological observations require a light gravitino to have a mass close to a few keV [52,53] at least, if it has to explain the cold DM relic density. However, the kinematic characteristics of events when the NLSP decays into a gravitino are mostly independent of whether the gravitino is in the keV range or even lower in mass. Some special situations where the difference is of some consequence have been discussed in Section 4.4.3. Of course, the presence of a gravitino much lighter than a keV will require the presence of some additional cold DM candidate.

Note that with $\widetilde{G}$ as the LSP decay branching ratios (BR) of the sparticles can be significantly modified since they can now decay directly into $\widetilde{G}$ instead of decaying into $\widetilde{\chi}_1^0$, which may significantly alter their collider signals. The decay width ($\Gamma$) of a sparticle, scalar($\widetilde{f}$) or gaugino($\widetilde{V}$), decaying into their respective SM counterparts, chiral fermion($f$)

or gauge boson($V$), and $\widetilde{G}$ is given by [37]

$$\Gamma(\widetilde{f} \to f\widetilde{G}) = \frac{1}{48\pi}\frac{m_{\widetilde{f}}^5}{M_{Pl}^2 m_{\widetilde{G}}^2}\left[1-\left(\frac{m_{\widetilde{G}}}{m_{\widetilde{f}}}\right)^2\right]^2 \tag{4.2.1}$$

$$\Gamma(\widetilde{V} \to V\widetilde{G}) = \frac{1}{48\pi}\frac{m_{\widetilde{V}}^5}{M_{Pl}^2 m_{\widetilde{G}}^2}\left[1-\left(\frac{m_{\widetilde{G}}}{m_{\widetilde{V}}}\right)^2\right]^3 \tag{4.2.2}$$

where $M_{Pl}$ is the Planck scale. Thus it is evident that this decay mode starts to dominate once the sparticles become very heavy and the $\widetilde{G}$ becomes light.

### 4.2.1 Relevant Branching Ratios

In this section, we discuss the variation of the branching ratios (BR) of various sparticles into the LSP gravitino. Since in this analysis we aim to study the production of the colored sparticles and their subsequent decays into the $\widetilde{G}$ via $\widetilde{\chi}_1^0$, the decay modes of $\widetilde{g}$, $\widetilde{q}$ and $\widetilde{\chi}_1^0$ are of our primary interest. While considering the decay modes, we focus on a simplified assumption that the decaying colored sparticle is the next-to-next-lightest supersymmetric particle (NNLSP) with $\widetilde{\chi}_1^0$ as the NLSP and $\widetilde{G}$ as the LSP. The BR computation and spectrum generation was done using `SPheno` [120, 121, 160] for a phenomenological MSSM (pMSSM) like scenario with one additional parameter, i.e, the gravitino mass ($m_{\widetilde{G}}$).

#### Variation of BR($\widetilde{g} \to g\widetilde{G}$)

In Fig. 4.1 we show the variation of two relevant gluino decay mode channels *viz.* $\widetilde{g} \to g\widetilde{G}$ and $\widetilde{g} \to q\bar{q}\widetilde{\chi}_1^0$ where all the squarks are heavier, as a function of $\Delta m_{\widetilde{g}} - m_{\widetilde{\chi}_1^0} = m_{\widetilde{g}} - m_{\widetilde{\chi}_1^0}$ and $m_{\widetilde{G}}$. The gluino mass has been fixed to $m_{\widetilde{g}} = 2500$ GeV while $m_{\widetilde{\chi}_1^0}$ has been varied such that $\Delta m_{\widetilde{g}\widetilde{\chi}_1^0}$ varies within 10-1500 GeV. Note that the $\widetilde{\chi}_1^0$ is considered to be dominantly bino-like. In the absence of its two-body decay mode into squark-quark pairs, the gluino can only decay via $\widetilde{g} \to g\widetilde{G}$ or $\widetilde{g} \to q\bar{q}\widetilde{\chi}_1^0$. The other two-body decay mode $\widetilde{g} \to g\widetilde{\chi}_1^0$ being loop suppressed, remains mostly subdominant compared to these two decay modes. Hence, only the two relevant channels are shown in the figure. Note that, BR($\widetilde{g} \to q\bar{q}\widetilde{\chi}_1^0$) includes the sum of all the off-shell contributions obtained from the first two generation squarks which in this case lie about 100 GeV above $m_{\widetilde{g}}$. As the gravitino mass gets heavier, BR($\widetilde{g} \to g\widetilde{G}$) decreases since, the corresponding partial width is proportional to the inverse square of $m_{\widetilde{G}}$. Similarly, as $m_{\widetilde{\chi}_1^0}$ keeps increasing, BR($\widetilde{g} \to q\bar{q}\widetilde{\chi}_1^0$) goes on decreasing. Note that, the BR for the 3-body decay mode can decrease further with increase in the corresponding squark

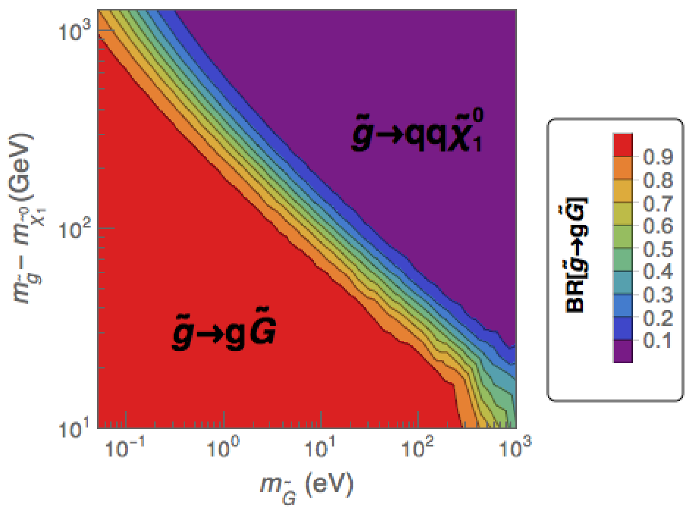


Figure 4.1: Variation of BR($\widetilde{g} \to g\widetilde{G}$) and BR($\widetilde{g} \to q\bar{q}\widetilde{\chi}_1^0$) shown color coded in $\Delta m_{\widetilde{g}\,\widetilde{\chi}_1^0} - m_{\widetilde{G}}$ plane.

masses. However, even for a keV $\widetilde{G}$, BR($\widetilde{g} \to g\widetilde{G}$) can remain significantly large provided there is sufficient compression in the mass gap ($\Delta m_{\widetilde{g}\widetilde{\chi}_1^0}$ ∼10 GeV) as seen in Fig. 4.1.

### Variation of BR($\widetilde{q}_{L/R} \to q\widetilde{G}$)

Next we look into the relevant decay modes of the first two generation squarks[3] when they are the NNLSP's. In this case, we assume that the gluino is heavier than the squarks, so that the dominant two-body decay modes available to the squarks are $\widetilde{q}_{L/R} \to q\widetilde{G}$ and $\widetilde{q}_{L/R} \to q\widetilde{\chi}_1^0$. Unlike the previous case, here the gravitino decay branching ratio has competition from another two-body decay mode. Although the decay into $\widetilde{G}$ does not depend on the L and R-type of the squarks, BR($\widetilde{q}_{L/R} \to q\widetilde{\chi}_1^0$) is expected to be different depending on the composition of the $\widetilde{\chi}_1^0$. For simplicity, we choose the $\widetilde{\chi}_1^0$ to be purely bino-like as before. The squark masses are fixed at $m_{\widetilde{q}} = 2500$ GeV and the NLSP mass, $m_{\widetilde{\chi}_1^0}$ is varied as before such that $\Delta m_{\widetilde{q}\widetilde{\chi}_1^0} = m_{\widetilde{q}} - m_{\widetilde{\chi}_1^0}$ varies in a wide range, 10-1500 GeV. The branching probabilities are shown in Fig. 4.2 where the plots on the left (right) show the decay branching ratios of $u_{L/R}$ ($d_{L/R}$). As the coupling of $\widetilde{q}_L$ with the SM-quark and bino-component of $\widetilde{\chi}_1^0$ is proportional to $\sqrt{2}g\ \tan\theta_W(I_{3q} - e_q)$ while that of $\widetilde{q}_R$ is proportional to $\sqrt{2}g\ \tan\theta_W e_q$, where

[3]Since the production cross-section of the third generation squarks are substantially smaller than those of the first two generations, we do not consider the production of the stop and sbottom states. Hence we only discuss the decays of $\tilde{u}_{L/R}$ and $\tilde{d}_{L/R}$.

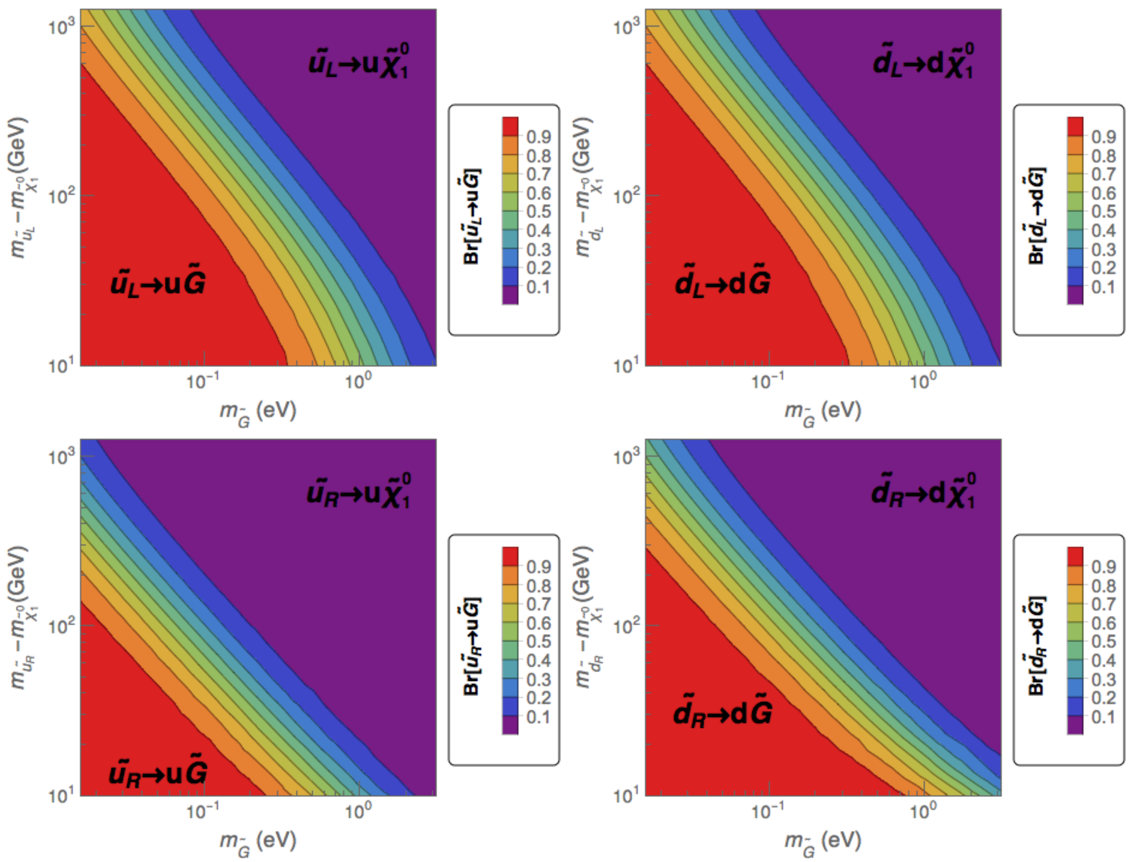


Figure 4.2: Variation of BR($\widetilde{q}_{L/R} \to q\widetilde{G}$) and BR($\widetilde{q}_{L/R} \to q\widetilde{\chi}_1^0$) in the plane $\Delta m_{\widetilde{q}m_{\widetilde{\chi}_1^0}}$ - $m_{\widetilde{G}}$. The plots on the left show the distributions corresponding to the up-squarks and the plots on the right show the same for the down-squarks.

$g, e_q$ and $I_{3q}$ represents SU(2) gauge coupling, electric charge of the SM-quark and its isospin respectively [37], we find a noticeable variation in decay probabilities of $\widetilde{q}_L$ and $\widetilde{q}_R$ for the same choice of mass spectrum. This implies that the right-handed squarks couple more strongly with the $\widetilde{\chi}_1^0$ compared to the left-handed ones. As a result, although the partial decay widths of the squarks decaying into gravitino and quarks are identical for squarks of similar mass, the corresponding BR vary slightly depending on their handedness. This feature is evident in Fig. 4.2. The coupling strength of $\widetilde{u}_R$ with $\widetilde{\chi}_1^0$ is larger by a factor of four compared to that of $\widetilde{u}_L$. The same coupling corresponding to $\widetilde{d}_R$ is larger by a factor of two compared to that of $\widetilde{d}_L$. Hence the difference in the BR distributions is more manifest for the up-type squarks. The magnitude of the coupling strengths corresponding to $\widetilde{u}_L$ and $\widetilde{d}_L$ are exactly same and hence we have obtained similar distributions corresponding to those.

The BR distributions indicate that as we go on compressing the SUSY spectrum, the gravitino decay mode becomes more and more relevant but only if its mass is around or below the eV range. We, therefore, conclude that for a keV $\widetilde{G}$, the decay mode $\widetilde{g} \to g\widetilde{G}$ may be of importance but only for the cases where the gluino mass lies very close to the NLSP neutralino mass. For the first two generation squarks and a keV $\widetilde{G}$, the BR($\widetilde{q}_{L/R} \to q\widetilde{G}$) is very small and the decay of the squarks into $\widetilde{\chi}_1^0$ dominates in the absence of a lighter gluino. As evident, the gravitino decay mode can be of significance for LHC studies if $m_{\widetilde{G}} \sim$ eV. However, such a light $\widetilde{G}$ is strongly disfavoured from DM constraints as mentioned before.

### Variation of BR($\widetilde{\chi}_1^0 \to X\widetilde{G}$)

The last two subsections point out the situations where the NLSP can be bypassed in the decay of strongly interacting superparticles. Such events tend to reduce the multiplicity of hard photons in SUSY-driven final states. In contrast, in the case where the SUSY cascades lead to a $\widetilde{\chi}_1^0$ NLSP, the $\widetilde{\chi}_1^0$ may further decay into gravitino along with a $Z$, $\gamma$ or the Higgs boson ($h$) depending upon its composition[4]. The $h$-associated decay width is entirely dependent on the higgsino component of $\widetilde{\chi}_1^0$ while $\Gamma(\widetilde{\chi}_1^0 \to \gamma\widetilde{G})$ depends entirely on the bino and wino component of $\widetilde{\chi}_1^0$ whereas the $Z$-associated decay width has a partial dependence on all the components that make up the $\widetilde{\chi}_1^0$. The functional dependence on the different composition strengths of $\widetilde{\chi}_1^0$ in its decay width can be summarised as [37]:

$$\Gamma(\widetilde{\chi}_1^0 \to \gamma\widetilde{G}) \quad \propto |N_{11}\cos\theta_W + N_{12}\sin\theta_W|^2 \tag{4.2.3}$$

$$\Gamma(\widetilde{\chi}_1^0 \to Z\widetilde{G}) \quad \propto \left(|N_{11}\sin\theta_W - N_{12}\cos\theta_W|^2 + \frac{1}{2}|N_{14}\cos\beta - N_{13}\sin\beta|^2\right) \tag{4.2.4}$$

$$\Gamma(\widetilde{\chi}_1^0 \to h\widetilde{G}) \quad \propto |N_{14}\sin\alpha - N_{13}\cos\alpha|^2 \tag{4.2.5}$$

where, $N_{ij}$ are the elements of the neutralino mixing matrix, $\theta_W$ is the Weinberg mixing angle, $\alpha$ is the neutral Higgs mixing angle and $\beta$ corresponds to the ratio of the up and down type Higgs vacuum expectation values (VEVs). Note that the partial decay widths are proportional to $m_{\widetilde{\chi}_1^0}^5/(M_{Pl}^2\, m_{\widetilde{G}}^2)$ and hence if $m_{\widetilde{G}}$ is too large, the total decay width of $\widetilde{\chi}_1^0$ may become too small such that it will not decay within the detector. Although the decay width is also dependent upon $m_{\widetilde{\chi}_1^0}$, one finds that for a 2500 GeV $\widetilde{\chi}_1^0$, and a MeV $\widetilde{G}$ the neutralino becomes long-lived. In Fig. 4.3 we show the variation of the three relevant BRs with the composition of the $\widetilde{\chi}_1^0$. Here we have varied $M_1$, $M_2$ and $\mu$ in the range [2 : 2.5] TeV with the condition $\mu > M_2 > M_1$ such that $\widetilde{\chi}_1^0$ is bino-like most of the time with different admixtures of wino and higgsino components. The other relevant mixing parameter tan$\beta$ is

[4]In principle, $\widetilde{\chi}_1^0$ may decay into the other neutral Higgs states also which we assume to be heavier.

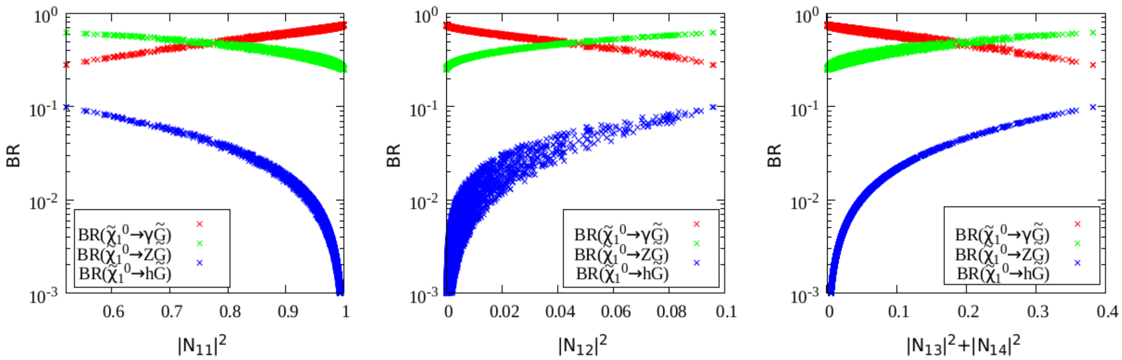


Figure 4.3: Vatiation of the three relevant BRs of $\widetilde{\chi}_1^0$ decay modes with its bino, wino and higgsino components. The red, green and blue lines correspond to BR($\widetilde{\chi}_1^0 \to \gamma\widetilde{G}$), BR($\widetilde{\chi}_1^0 \to Z\widetilde{G}$) and BR($\widetilde{\chi}_1^0 \to h\widetilde{G}$) respectively.

kept fixed at 10. The red, green and blue colors correspond to BR($\widetilde{\chi}_1^0 \to \gamma\widetilde{G}$), BR($\widetilde{\chi}_1^0 \to Z\widetilde{G}$) and BR($\widetilde{\chi}_1^0 \to h\widetilde{G}$) respectively. $|N_{11}|^2$ indicates the bino-fraction in the composition of $\widetilde{\chi}_1^0$. Similarly, $|N_{12}|^2$ and $|N_{13}^2|+|N_{14}|^2$ represent the wino and higgsino components respectively. As can be clearly seen from the plots, obtaining 100% BR($\widetilde{\chi}_1^0 \to \gamma\widetilde{G}$) is not possible even if the bino and(or) wino components are close to 1, since the $Z$-mode is always present. However, the $h$-associated decay channel can be easily suppressed with a relatively larger $\mu$. Motivated by this behaviour of the BRs, we choose to work with a signal consisting of at least one photon for our collider analysis. In our case, the $\widetilde{\chi}_1^0$ being dominantly bino-like, it decays mostly into a $\gamma$ and a $\widetilde{G}$. However, the $Z\widetilde{G}$ decay mode has a substantial BR ($\sim 25\%$). The higgsino admixture in $\widetilde{\chi}_1^0$ being small, the $h\widetilde{G}$ decay mode is not considered in this work. However it is worth noting that this particular channel can be the dominant mode for a higgsino-dominated NLSP and could also be an interesting mode of study, which we leave for future work.

## 4.3 Benchmark Points

For our analysis we choose a few benchmark points that would represent the salient features of a compressed sparticle spectrum with varying compression strengths while also categorically defining a few points that are more in line with current SUSY searches with $\widetilde{G}$ LSP by the CMS and ATLAS collaborations at the LHC. We insure that our benchmark choices are consistent with all existing experimental constraints. We consider both compressed and uncompressed spectra, with bino-like $\widetilde{\chi}_1^0$ as the NLSP and a keV gravitino as the LSP and warm dark matter candidate. For one of the benchmarks, we also show the effect of an eV mass gravitino LSP. The final benchmarks used in this study are shown in Table 4.1.

The mass spectrum and decays of the sparticles are computed using `SPheno` (v3.3.6) [120, 121, 160]. We restrict the light CP-even Higgs mass to be in the range 122-128 GeV, i.e, within 3-$\sigma$ range of the measured Higgs mass [1, 16, 89, 161] and including theoretical uncertainty of $\sim 4$ GeV. Note that when the mass spectrum is compressed, all squark/gluino (which are nearly degenerate in mass) production channels contribute significantly to the signal. For all the benchmark points, the squarks and gluino decay directly or via cascades to the bino-like $\widetilde{\chi}_1^0$ NLSP. The $\widetilde{\chi}_1^0$ then dominantly decays to a photon and gravitino and, to a lesser extent, a $Z$ boson and gravitino. This leads to either a mono-photon or a diphoton signal with jets and $\not{E}_T$ which defines our signal. To evade constraints from photon(s) searches at the LHC for simplified models [144–150, 162], we require the sparticles in a compressed spectrum such as ours, to be much heavier than the existing experimental limits. We have checked this for our spectra represented by the benchmark points, with the NLSP mass lying in the range $2.4 - 2.6$ TeV with varied masses and hierarchy of the colored sparticles with respect to the NLSP. Amongst them, **C6** is the utmost compressed spectra, with a mass gap, $\Delta M_i \sim 6$ GeV between the colored sparticles and the NLSP of mass 2462 GeV, followed by **C2**, **C5** where the mass gap is in the range of 40-50 GeV and the NLSP masses are 2428 and 2526 GeV respectively. We have also considered benchmarks **C1**, **C3** and **C4** such that the mass gap between the colored sparticles and NLSP are slightly higher and lie in the range of 100-200 GeV.

We also choose various possible mass hierarchical arrangements of the squarks and gluino to accommodate different cascades contributing to the signal. For example, **C1** and **C3** have different squark-gluino mass hierarchical stuctures in the strong sector. This leads to different jet distributions in the two cases. **C2** and **C5**, on the other hand, are similar in the arrangement of the sparticles, however placed within 50 GeV from the NLSP, which represents a much more compressed scenario. Finally we consider two uncompressed spectra **U1**, **U2** with NLSP mass $\sim$ 700 GeV and $\sim$ 1200 GeV and gluinos with mass $\sim$1.4 TeV and $\sim$1 TeV above the NLSP respectively. Since the photons arise from the NLSP decays, a heavier NLSP gives rise to a harder photon, having better chances of passing the analysis cuts. Thus the difference in the signal cross-sections differ on account of the difference in hardness of the photons and the resulting cut efficiencies in these two cases.

Benchmark points **U1**, **U2** are in fact replications of the simplified scenarios that are considered by experimental collaborations to put limits on SUSY particle masses. For for both these benchmark points, we have kept the squarks very heavy ($\sim 4-5$ TeV) so that the gluino pair production is the only dominant contributing channel. However, we have only focussed on uncompressed spectra with event rates comparable to those of the compressed spectra. Since the large mass gap between the gluino and NLSP allow for multiple hard jets to be produced as opposed to the compressed case, we further exploit this feature to differentiate compressed from uncompressed scenarios with comparable event rates during signal analysis.

## 4.4 Collider Analysis

We look for multi-jet signals associated with very hard photon(s) and missing transverse energy ($\not{E}_T$) in the context of SUSY with gravitino as the LSP. For such GMSB kind of models with a keV gravitino, a very clear signature arises from the decay of the NLSP neutralino into a photon and a gravitino. If the NLSP-LSP mass difference is large enough, two hard photons would appear in the final state at the end of a SUSY cascade. The lightest neutralino, if bino-like, decays dominantly into a photon and gravitino (∼75%) while a small fraction decays into $Z$ boson and gravitino ($\sim$ 25%). For cases with $\widetilde{\chi}_1^0$ having a significant higgsino component, we get comparable branching fractions for its decay into $Z$ boson or a Higgs boson, besides photons, along with $\widetilde{G}$. For simplicity, we have considered a bino-like $\widetilde{\chi}_1^0$ as the NLSP. Note that the signal strength consisting of very hard photons in the final state can be affected by the composition of the NLSP as we have discussed before. The $\widetilde{\chi}_1^0$ decay into a $Z\widetilde{G}$ however still remains relevant for the bino-like $\widetilde{\chi}_1^0$ and as a result, gives rise to a monophoton signal at the LHC along with the diphoton channel, associated with large missing transverse energy. The existing LHC constraints in such scenarios have already pushed the $\widetilde{\chi}_1^0$-$\widetilde{q}$-$\widetilde{g}$ mass bounds above 1.5 TeV which automatically result in a large $m_{\widetilde{\chi}_1^0}$ - $\widetilde{G}$ mass gap. This gives rise to very high $p_T$ photons in the final states, which are very easy to detect and also highly effective to suppress the SM background events.

In this work, we consider six benchmark points for compressed spectra (**C1 - C6**) such that the entire colored sector (apart from $\widetilde{t}_2$ and $\widetilde{b}_2$) lie within 200 GeV of the $\widetilde{\chi}_1^0$ ($m_{\widetilde{\chi}_1^0} \sim$ 2.4 - 2.6 TeV). We then estimate signal rates of final state events with at least one or more hard photons arising from all possible squark-gluino pair production modes. We also study a couple of uncompressed spectra (**U1,U2**) such that both the compressed and uncompressed

| | Compressed spectra | | | | | | Uncompressed spectra | |
|---|---|---|---|---|---|---|---|---|
| **Parameters** | **C1** | **C2** | **C3** | **C4** | **C5** | **C6** | **U1** | **U2** |
| $M_1$ | 2623 | 2451 | 2671 | 2608 | 2550 | 2486 | 704 | 1200 |
| $M_2$ | 2710 | 2610 | 2710 | 2710 | 2610 | 2610 | 2310 | 2310 |
| $M_3$ | 2480 | 2280 | 2560 | 2601 | 2380 | 2285 | 1747 | 1747 |
| $A_t$ | 2895 | 2895 | -3295 | -3750 | -3197 | -2895 | 2895 | 2895 |
| $\mu$ | 4000 | 4000 | 4000 | 4000 | 3500 | 4000 | 3000 | 3000 |
| $\tan\beta$ | 15 | 15 | 9 | 6 | 25 | 15 | 15 | 15 |
| $M_A$ | 2500 | 2500 | 1800 | 1800 | 2500 | 2500 | 2500 | 2500 |
| $m_{\widetilde{g}}$ | 2678 | 2456 | 2746 | 2783 | 2562 | 2468 | 2102 | 2102 |
| $m_{\widetilde{q}_L}$ | 2729 | 2468 | 2734 | 2753 | 2571 | 2467 | 4721 | 4721 |
| $m_{\widetilde{q}_R}$ | 2727 | 2466 | 2730 | 2751 | 2574 | 2468 | 4742 | 4742 |
| $m_{\widetilde{t}_1}$ | 2707 | 2457 | 2652 | 2625 | 2532 | 2543 | 4680 | 4678 |
| $m_{\widetilde{t}_2}$ | 2837 | 2593 | 2857 | 2863 | 2718 | 2725 | 4767 | 4765 |
| $m_{\widetilde{b}_1}$ | 2787 | 2501 | 2782 | 2778 | 2594 | 2598 | 4560 | 4558 |
| $m_{\widetilde{b}_2}$ | 2846 | 2570 | 2846 | 2846 | 2677 | 2669 | 4746 | 4744 |
| $m_{\widetilde{\ell}_L}$ | 2703 | 2452 | 2703 | 2703 | 2572 | 2503 | 4335 | 4336 |
| $m_{\widetilde{\ell}_R}$ | 2700 | 2455 | 2700 | 2700 | 2585 | 2495 | 4365 | 4366 |
| $m_{\widetilde{\tau}_1}$ | 2706 | 2443 | 2707 | 2709 | 2600 | 2576 | 4332 | 4332 |
| $m_{\widetilde{\tau}_2}$ | 2882 | 2514 | 2882 | 2881 | 2671 | 2622 | 4375 | 4375 |
| $m_{\widetilde{\nu}_L}$ | 2701 | 2450 | 2701 | 2701 | 2570 | 2501 | 4335 | 4335 |
| $m_{\widetilde{\chi}_1^0}$ | 2600 | 2428 | 2646 | 2585 | 2526 | 2462 | 699 | 1191 |
| $m_{\widetilde{\chi}_2^0}$ | 2726 | 2614 | 2724 | 2724 | 2619 | 2617 | 2383 | 2383 |
| $m_{\widetilde{\chi}_1^\pm}$ | 2726 | 2614 | 2725 | 2724 | 2619 | 2617 | 2382 | 2382 |
| $m_h$ | 123 | 123 | 124 | 124 | 125 | 124 | 125 | 125 |
| $\Delta M_i$ | 129 | 40 | 100 | 198 | 48 | 6 | 1403 | 911 |

Table 4.1: Low energy input parameters and the relevant sparticle masses, (in GeV), for the compressed ($\mathbf{C}_i$, i = 1,...,6) and uncompressed (**U1**, **U2**) benchmarks. Here, $\Delta M_i = m_i - m_{\widetilde{\chi}_1^0}$ where $m_i$ represents the mass of the heaviest colored sparticle ($\widetilde{g}/\widetilde{q}_k$, (k = 1,2)) and $m_{\widetilde{\chi}_1^0}$, the mass of the NLSP. For all benchmarks, the gravitino mass, $m_{\widetilde{G}} = 1$ keV.

spectra produce similar event rates for our signal. In these spectra, the NLSP mass is around 700 and 1200 GeV respectively and the gluino is the lightest colored sparticle having a large ($\sim$ 1-1.4 TeV) mass gap with the NLSP. The squarks are chosen to be heavier (4-5 TeV) and are essentially decoupled from rest of the spectrum. The large mass gap between the NLSP and the colored sector ensures multiple hard jets from their decay cascades besides the hard photons. Thus with different mass gaps and squark-gluino hierarchy among the compressed and uncompressed spectra, the jet profiles are expected to be significantly different for the benchmark points. Following the existing ATLAS analysis [150], which provides the most stringent constraint on the SUSY spectrum with a light gravitino LSP, we determine the signal event rates for our choice of benchmark points. Since we have also chosen compressed and uncompressed spectra such that the final state event rates are equal or comparable after analysis, it is *a priori* difficult to determine which scenario such a signal reflects. Keeping this in mind, we propose a set of kinematic variables, besides the usual kinematic ones like $\not\!\!E_T$ and $M_{Eff}$, which highlight the distinctive features of compression in a SUSY spectra over an uncompressed one with $\widetilde{G}$ as the LSP, although both have comparable signal rates.

### 4.4.1 Simulation set up and Analysis

We consider the pair production and associated production processes of all colored sparticles at $\sqrt{s} = 13$ TeV LHC. Parton level events are generated using `Madgraph5` (v2.2.3) [123, 124] for the following processes with upto two extra partons at the matrix element level:

$$p\,p \to \widetilde{q}^*\,\widetilde{q},\ \widetilde{q}\,\widetilde{g},\ \widetilde{q}\,\widetilde{q},\ \widetilde{q}^*\,\widetilde{q}^*,\ \widetilde{q}^*\,\widetilde{g},\ \widetilde{g}\,\widetilde{g}$$

We reject any intermediate resonances at the matrix element level, which may arise in the decay cascades of the sparticles from two or more different processes, to avoid double counting of Feynman diagrams to the processes. The parton level events are then showered using `Pythia` (v6) [126]. To correctly model the hard ISR jets and reduce double counting of jets coming from the showers as well as the matrix element partons, MLM matching [127, 128] of the shower jets and the matrix element jets have been performed using the shower-k$_T$ algorithm with p$_T$ ordered showers by choosing a matching scale (QCUT) 120 GeV [163]. The default dynamic factorisation and renormalization scales [164] have been used in Madgraph whereas the PDF chosen is CTEQ6L [125]. After the showering, hadronisation and fragmentation effects performed by Pythia, subsequent detector simulation of the hadron level events are carried out by the fast simulator `Delphes`-v3.3.3 [129–131]. The jets are reconstructed using `Fastjet` [133] with a minimum $p_T$ of 20 GeV in a cone of $\Delta R = 0.4$

using the *anti-$k_t$* algorithm [132]. The charged leptons $(e, \mu)$ are reconstructed in a cone of $\Delta R = 0.2$ with the maximum amount of energy deposit allowed in the cone limited to 10% of the $p_T$ of the lepton. Photons are reconstructed in a cone of $\Delta R = 0.4$, with the maximum energy deposit in the cone as per ATLAS selection criteria [150].

For background estimation, we focus on the most dominant SM backgrounds for photon(s) + jets + $\not{E}_T$ signal at 13 TeV LHC, such as: $\gamma + \leq 4$ jets, $\gamma\gamma + \leq 3$ jets, $W\gamma + \leq 3$ jets, $Z\gamma + \leq 3$ jets and $t\bar{t}\gamma$ + jets. The sort of extremely hard $p_T$ photons that we expect in our signal events, are unlikely to be present in SM processes in abundance and the hard photons will arise mostly from the tails of the $p_T^\gamma$ distributions. Hence in order to obtain a statistically exhaustive event sample, we choose a hard $p_{T_\gamma} > 200$ GeV cut as a preselection for the parton level events for the leading photon while generating the background events. For MLM matching of the jets, the matching scale was chosen in the range 30-50 GeV as applicable for electroweak SM processes.

Some other SM processes, such as QCD, $t\bar{t}$+jets, $W$+jets, $Z$+jets, in spite of having no direct sources of hard photons, may also contribute to the background owing to their large production cross-sections coupled with mistagging of jets or leptons leading to fake photons. However, the cumulative effect of hard $p_T^\gamma$ as well as $\not{E}_T$ and $M_{Eff}$ requirement renders these contributions negligible.

### Primary Event selection criteria

We identify the charged leptons $(e, \mu)$, photons and jets as per the following selection criteria (**A0**) for signal and background events alike:

- Leptons ($\ell = e, \mu$) are selected with $p_T^\ell > 25$ GeV, $|\eta^e| < 2.37$ and $|\eta^\mu| < 2.70$ and excluding the transitional pseudorapidity window $1.37 < |\eta^\ell| < 1.52$ between the ECAL barrel and end cap of the calorimeter.

- Photons are identified with $p_T^\gamma > 75$ GeV and $|\eta^\gamma| < 2.47$ excluding $1.37 < |\eta^\gamma| < 1.52$.

- Reconstructed jets have $p_T^j > 30$ GeV and lie within $|\eta^j| < 2.5$.

- All reconstructed jets have a large azimuthal separation with $\vec{\not{E}}_T$, given by $\Delta\phi(\vec{\text{jet}}, \vec{\not{E}}_T) > 0.4$ to reduce fake contributions to missing transverse energy arising from hadronic energy mismeasurements.

- The jets are separated from other jets by $\Delta R_{jj} > 0.4$ and from the reconstructed photons by $\Delta R_{\gamma j} > 0.4$.

With these choices of final state selection criteria we now proceed to select the events for our analysis.

## Signal Region: $\geq 1\ \gamma + > 2$ jets + $\not{E}_T$

We look into final states with at least 1 photon, multiple jets and large $\not{E}_T$. Amongst the existing analyses for the same final state carried by the experimental collaborations, the ATLAS analysis imposes a more stringent constraint on the new physics parameter space and hence we have implemented the same set of cuts as enlisted below for our analysis:

- **A1**: The final state events comprise of at least one photon and the leading photon ($\gamma_1$) must have $p_T^{\gamma_1} > 400$ GeV.
- **A2**: There should be no charged leptons in the final state ($N_\ell$=0) but at least 2 hard jets ($N_j > 2$).
- **A3**: The leading and sub-leading jets must be well separated from $\vec{\not{E}}_T$, such that $\Delta\phi(j, \vec{\not{E}}_T) > 0.4$.
- **A4**: The leading photon must also be well separated from $\vec{\not{E}}_T$ with $\Delta\phi(\gamma_1, \vec{\not{E}}_T) > 0.4$.
- **A5**: As the light gravitinos would carry away a large missing transverse momenta, we demand that $\not{E}_T > 400$ GeV.
- **A6**: We further demand effective mass, $M_{Eff} > 2000$ GeV, with $M_{Eff} = H_T + G_T + \not{E}_T$, where $H_T = \Sigma_i\ p_T(j_i)$ is the scalar sum of $p_T$ of all jets and $G_T = \Sigma_j\ p_T(\gamma_j)$ is the scalar sum of $p_T$ of all photons in the event.

In Table 4.2 below we have summarised the effect of the cuts **A0**-**A6** for our signal on the respective benchmark points. All the production cross-sections in the table is scaled using `NLO+NLL` K-factors obtained from `NLL_Fast` [138, 165–168].

As evident from Table 4.2, cut efficiencies vary depending on the *compression* in the spectra. For example, the jet requirement affects the signal cross-section of **C6** the most, since it is the most compressed spectra among all. Naturally, one would expect jet multiplicity to be smaller in this case compared to the others. As a result, the requirement $N_j > 2$ reduces the corresponding signal cross-section by a significant amount, whereas, for the uncompressed spectra, **U1** and **U2**, this cut has no bearing. The hard photon(s) in the signal events and the presence of direct source of $\not{E}_T$ ensure that the $\not{E}_T$ and $M_{Eff}$ cuts are easily satisfied by the selected events.

| Signal | | Effective cross-section (in fb) after the cuts | | | | | |
|---|---|---|---|---|---|---|---|
| Benchmark Points | Production cross-section(fb) | **A0 + A1** | **A2** | **A3** | **A4** | **A5** | **A6** |
| C1 | 0.26 | 0.22 | 0.18 | 0.14 | 0.14 | 0.13 | 0.12 |
| C2 | 0.80 | 0.68 | 0.37 | 0.30 | 0.30 | 0.28 | 0.26 |
| C3 | 0.23 | 0.18 | 0.10 | 0.08 | 0.08 | 0.08 | 0.08 |
| C4 | 0.21 | 0.15 | 0.12 | 0.08 | 0.08 | 0.08 | 0.07 |
| C5 | 0.49 | 0.34 | 0.15 | 0.13 | 0.13 | 0.12 | 0.11 |
| C6 | 0.77 | 0.61 | 0.13 | 0.11 | 0.11 | 0.10 | 0.09 |
| U1 | 0.20 | 0.10 | 0.09 | 0.08 | 0.07 | 0.05 | 0.05 |
| U2 | 0.20 | 0.13 | 0.12 | 0.10 | 0.09 | 0.08 | 0.08 |

Table 4.2: Signal Cross-sections (NLO+NLL) for all the benchmark points listed in Table 4.1 corresponding to ($\geq 1\ \gamma + > 2$ jets $+ \not{E}_T$) final state. For all the points, $m_{\widetilde{G}} = 1$ keV.

For the corresponding background events, we use the observed number of background events at ATLAS, which is 1, for the same final state studied at an integrated luminosity of 13.3 fb$^{-1}$ at 13 TeV [150]. The statistical signal significance is computed using

$$\mathcal{S} = \sqrt{2[(s+b)\ln(1+\frac{s}{b}) - s]}$$

where $s$ and $b$ represent the remaining number of signal and background events after implementing all the cuts. In Table 4.3 below, we have shown the required integrated luminosity to obtain a $3\sigma$ and $5\sigma$ statistical significance for our signal corresponding to all the benchmark points.

The required luminosity for $3\sigma$ and $5\sigma$ statistical significance varies depending on the relative compression and heaviness of the spectra. As evident, **C2** has the best discovery prospects and is likely to be probed very soon. **C6** on the other hand, despite of having a similar squark-gluon spectra and a very similar production cross-section to that of **C2**, requires a much larger luminosity ($\sim$ 112 fb$^{-1}$) to be probed. This is because the high amount of compression in the spectra reduces the cut efficiency significantly due to the

[5] On the face of it, this benchmark may be ruled out by the current searches at LHC. However, this is to be taken with some caution, since the search criteria suggested by us are slightly different from the ones used in the current experimental searches.

| Signal | Luminosity $\mathcal{L}$ (in fb$^{-1}$) for | |
|---|---|---|
| | $\mathcal{S} = 3\sigma$ | $\mathcal{S} = 5\sigma$ |
| C1 | 68 | 189 |
| C2 [5] | 19 | 52 |
| C3 | 139 | 385 |
| C4 | 176 | 489 |
| C5 | 79 | 219 |
| C6 | 112 | 312 |
| U1 | 326 | 904 |
| U2 | 139 | 385 |

Table 4.3: Required luminosity ($\mathcal{L}$) to obtain $3\sigma$ and $5\sigma$ statistical Significance *($\mathcal{S}$)* of the signal at the 13 TeV run of the LHC corresponding to the benchmark points.

jet multiplicity requirement. The required integrated luminosity for **C1** and **C5** is very similar although **C5** has a relatively lighter colored sector and thus a larger production cross-section compared to **C1**, as can be seen from Table 4.2. However, the photon and jet selection criteria reduces the **C5** cross-section making it comparable to that of **C1**. The situation is different for **U1** which despite of having the lightest gluino, requires the largest luminosity ($\sim 326$ fb$^{-1}$) among all the benchmark points in order to be probed. The reason is two-fold. Firstly, the production cross-section in this case (and also for **U2**) is comprised of just the gluino-pair since the squarks are far too heavy to contribute. Secondly, the $\widetilde{\chi}_1^0$ being $\sim 700$ GeV, the photons arising from $\widetilde{\chi}_1^0$ decay are relatively on the softer side and hence the photon selection criteria further reduces the signal cross-section. A similar squark-gluon spectra in presence of a heavier $\widetilde{\chi}_1^0$ (**U2**) therefore is likely to be probed with a much smaller luminosity ($\sim 139$ fb$^{-1}$) than **U1**. Thus it is evident from Table 4.2 and 4.3, that given the present experimental constraints, a compressed spectra, unless it is too highly compressed such that the cut efficiency is reduced significantly, can improve the squark-gluino mass limits by a significant amount. For example, **C2** can be probed with slightly little more luminosity than 13.3 fb$^{-1}$ but with a colored spectra that lies in the vicinity of 2.5 TeV. This clearly suggests that a compressed spectra becomes much more quickly disfavoured over an uncompressed spectra with a gravitino LSP contrary to the case where a compressed SUSY spectrum appears as a saviour of low mass SUSY with a neutralino LSP. This is because of the hard photons that themselves act as a clear criterion to distinguish the signal over the SM background.

### 4.4.2 Distinction of Compressed and Uncompressed spectra

Given the inclusive hard photon + $\not{E}_T$ signals, supposedly due to a light gravitino, can one ascertain whether the MSSM part of the spectrum is compressed or uncompressed? With this question in view, it is worthwhile to compare signals of both types with various degree of compression in presence of a light ($\sim$ keV) gravitino as the LSP. We show that the kind of compressed spectra we have used enhances the existing exclusion limit on the colored sparticles. We consider different squark-gluino mass hierarchy represented by our choice of some sample benchmark points presented in Table 4.1. The $\widetilde{G}$ being almost massless in comparison to the $\widetilde{\chi}_1^0$ in consideration, the photons generated from the $\widetilde{\chi}_1^0$ decay into $\widetilde{G}$ are always expected to be very hard for both the compressed and uncompressed scenarios. This feature can be used to enhance the significance of the signal irrespective of the associated jets in the event. We provide a framework where one can use the properties of these jets in a novel way to distinguish between the two different scenarios in consideration even if they produce a similar event rate at the LHC. For illustration, let us consider the benchmark points, **C5**, **C4** and **U2** all of which result in nearly identical event rates for our signal and thus it is difficult to identify whether it is a signature of a compressed or an uncompressed spectra. It would be nice to have some kinematic variables which could be used to distinguish among the different kind of spectra. Subsequently, we have proposed few such variables which show distinctive features in their distributions depending on the relative hardness and multiplicity of the final state photon(s) and jets.

An uncompressed spectrum, such as **U2** is characterized by a large mass gap between the strong sector sparticles and the NLSP ($\widetilde{\chi}_1^0$). This ensures a large number of high $p_T$ jets from the cascades as compared to **C5** and **C4**. The difference in jet multiplicity in the two cases is clearly visible in Fig. 4.4 where we have presented both the jet and photon multiplicity distributions for some sample compressed and uncompressed spectra. The hard photons in the event are originated from the $\widetilde{\chi}_1^0$ decay and since for all our benchmark points the $\widetilde{\chi}_1^0$ is sufficiently heavy, the photon multiplicity peaks at a similar region for both the compressed and uncompressed spectra. However, the jets in the case of **U2** are generated from the three body decay of the gluino into a pair of quarks and $\widetilde{\chi}_1^0$. As evident from Fig. 4.1, for the choices of the sparticle masses of **U2**, the other decay mode is highly suppressed. Hence one would naturally expect to obtain a large number of jets in the final state as shown in Fig. 4.4. **C5** having a high degree of compression ($\Delta M_i = 48$ GeV) in the parameter space results in least number of jets in the final state. **C4**, on the other hand, has a more relaxed compression ($\Delta M_i = 198$ GeV) that gives rise to slightly harder cascade jets passing through the jet selection criteria resulting in a harder distribution than **C5**.

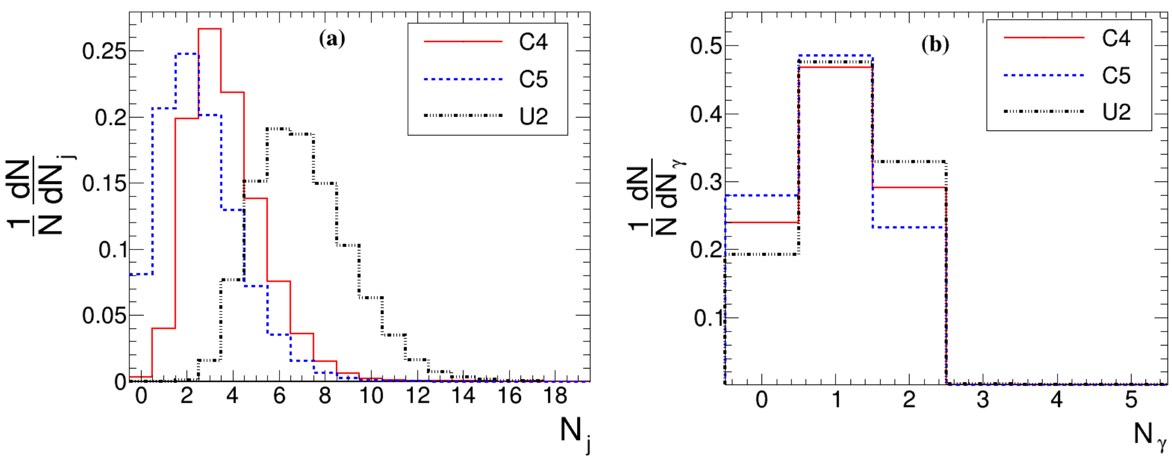


Figure 4.4: Normalized distributions for jet and photon multiplicity for the benchmark points **C4**, **C5** and **U2** representing moderately compressed, highly compressed and uncompressed scenarios respectively. Figure (a) has been prepared after implementing the selection cuts **A0+A1** and figure (b) after **A0**.

The relative differences in the compression factor ($\Delta M_i$) among the three benchmark points are also visible in the jet $p_T$ distributions shown in Fig. 4.5. As expected, the leading (Fig. 4.5(a)) and subleading (Fig. 4.5(b)) jet $p_T$ distributions predominantly show a harder peak for **U2** as compared to **C4**, **C5**. However, hard jets may also arise from the $\widetilde{\chi}_1^0$ decaying to a $Z$ boson and gravitino (BR $\sim 25\%$) as the $Z$ decays dominantly into two jets. The $Z$ boson is expected to be highly boosted and thus one can easily obtain additional hard jets from its decay. These jets populate a small fraction of the total number of events and thus for a compressed spectra one of these jets can turn out to be the hardest jet in the event. This feature can be observed by the subdominant peak at $\sim 1000$ GeV for the leading jet $p_T$ distribution in Fig. 4.5.

Fig. 4.5(c) and (d) show the leading and subleading photon $p_T$ distributions respectively for **C4**, **C5** and **U2**. The $\widetilde{\chi}_1^0$ mass in **C4**, **C5** being $\sim 2.5$ TeV, the photons produced

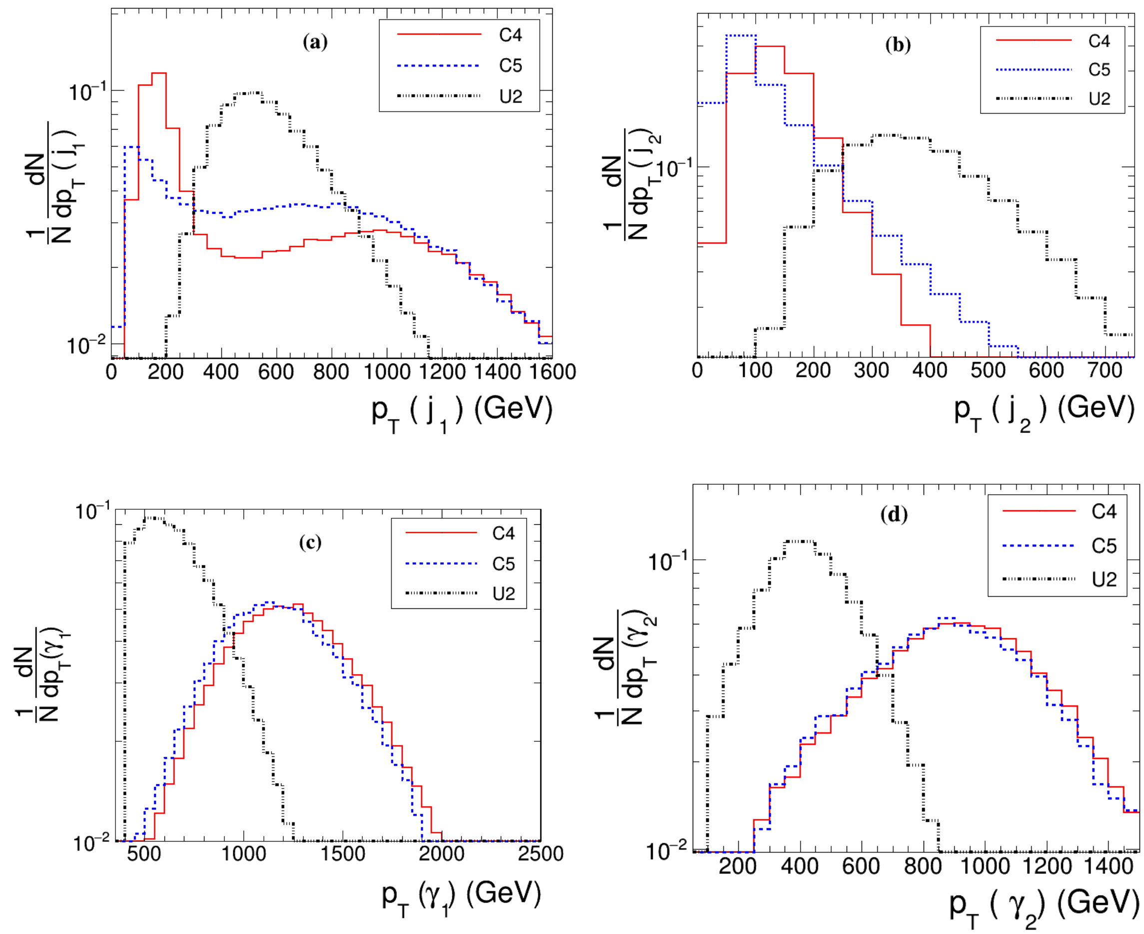


Figure 4.5: The leading and subleading jet and photon $p_T$ distributions for some of the benchmark points representing various compressed (**C4**), more compressed (**C5**) and uncompressed (**U2**) spectra after implementing the selection and analysis cuts **A0-A6**.

from their decay are much harder than the leading jets in the spectra as opposed to the uncompressed spectra (**U2**) and hence, the peak in the photon $p_T$ distribution is significantly shifted to lower values. Thus while the total hadronic energy, $H_T$ (Fig. 4.6(a)) peaks at a higher value for the uncompressed case owing to a large number of hard jets, $G_T$ (Fig. 4.6(b)) which is the scalar sum of all photon $p_T$, peaks at a lower value for the uncompressed case than the compressed cases. Among other kinematic variables, one can also look into the $\not{E}_T$ and $\mathrm{M}_{Eff}$ distributions to distinguish the compressed and uncompressed scenarios as shown in Fig. 4.6(c) and (d) respectively. Since the photons are almost always harder for the compressed spectra compared to the uncompressed cases, we have observed that the

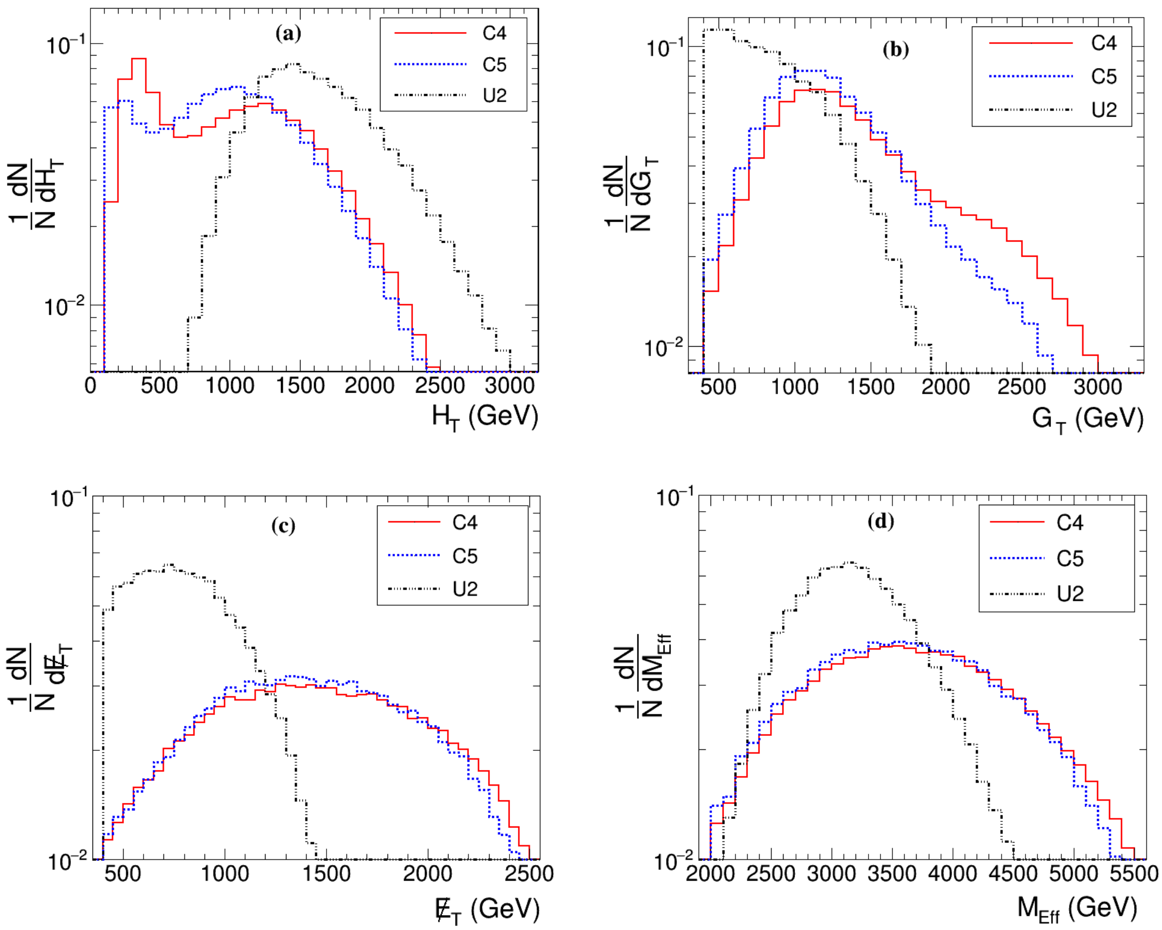


Figure 4.6: Normalized distributions of total hadronic energy deposit $H_T$,total photon energy deposit $G_T$, missing transverse energy $\not{E}_T$ and Effective Mass $M_{Eff}$, for benchmark points representing various compressed (**C4**), more compressed (**C5**) and uncompressed (**U2**) spectra after implementing the selection and analysis cuts **A0**-**A6**.

$\not{E}_T$, required to balance the total visible transverse energy, is much harder for the former. Effective mass, $M_{Eff}$ defined as the sum of $H_T$, $G_T$ and $\not{E}_T$, also shows some small difference in the peak value for both cases. In **U2**, $G_T$ and $\not{E}_T$ are softer than that for **C4**, **C5** but $H_T$ is much harder resulting in the $M_{Eff}$ peaking at similar values for the both cases. However, since the photons are considerably harder than the jets in all cases, the effect being more pronounced for the compressed over the uncompressed case, the $M_{Eff}$ distribution falls faster for **U2** than **C4** and **C5** as can be seen from Fig. 4.6(b) and 4.6(d) respectively.

Taking cue from the kinematic distributions in Fig. 4.5 and Fig. 4.6, we now proceed to formulate two observables

$$r_1 = \frac{p_T(j_1)}{p_T(\gamma_1)} \quad \text{and} \quad r_2 = \frac{p_T(j_2)}{p_T(\gamma_1)}$$

which capture the essence of the jet and photon transverse momenta behaviour in a way as to distinctly distinguish between the compressed and uncompressed scenarios. As seen in Fig. 4.7, for the compressed case, $r_1$ (Fig. 4.7(a)) peaks at rather small values ($\sim 0.1$ ) than the uncompressed case ($\sim 1.0$) since the leading jet $p_T$ is almost always softer than the leading photon for compressed spectra whereas for the uncompressed case there are hard jets with $p_T$ values comparable to the leading photon $p_T$. However for the compressed spectra, the collimated hard jet from the highly boosted $Z$ boson produced in the decay of the $\widetilde{\chi}_1^0$, lead to a subdominant peak at $\sim 0.7$ in $r_1$. The observable $r_2$ (Fig. 4.7(b)) constructed with the sub-leading jet and leading photon $p_T$, peaks at lower values ($\sim 0.1$) for **C4** and **C5** since the sub-leading jet, coming from the cascades or ISR in the compressed case is expected to be much softer than the photon. For **U2**, $r_2$ peaks at $\sim 0.5$ since the sub-leading jet also coming from the cascade is softer than the hardest photon. Thus we find that the above ratios seem to enhance the two major distinctive features between a compressed and an uncompressed scenario, namely the high/low $p_T$ for the photon/jet for the compressed as compared to the low/high $p_T$ of the photon/jet for the uncompressed case.

We further note that the jet multiplicity is another variable which shows a difference in the distributions for compressed spectra **C4** and **C5** when compared to that of the uncompressed spectra **U2** (Fig. 4.4(a)). Although the choice of our signal region involves $N_j > 2$, the compressed spectra, **C4** and **C5**, still retain a sufficient fraction of events with higher number of jets. In contrast, the uncompressed spectra **U2** has larger number of hard jets for all events, and thereby remains mostly unaffected by this selection criterion. We therefore define a modified ratio (scaled by the jet multiplicities) as

$$r_1' = N_j \; r_1 \quad \text{and} \quad r_2' = N_j \; r_2.$$

Notably the new variables $r_1'$ and $r_2'$ are able to significantly enhance the differences between a compressed and uncompressed spectra. Since the scale factor, $N_j$, is always greater for the uncompressed spectra **U2** than for the compressed spectra **C4** and **C5**, we find the peak values of $r_1'$ ($\sim 4.0$) and $r_2'$ ($\sim 2.5$) of the uncompressed spectra are shifted further away from that of compressed ones ($r_1' \sim 0.2$-$0.5$ and $r_2' \sim 0.1$-$0.3$). Quite importantly the visible overlap seen in $r_1$ for the sub-dominant peak is now completely disentangled in the new variable $r_1'$ as seen in Fig. 4.7(c). This is significant in the sense that when the event samples would retain a much harder criterion for the leading jet then the events for **U2**, **C4** and **C5** would all feature the overlap observed for the sub-dominant peak while the difference for low $r_1$ might be washed away for this particular choice of event selection.

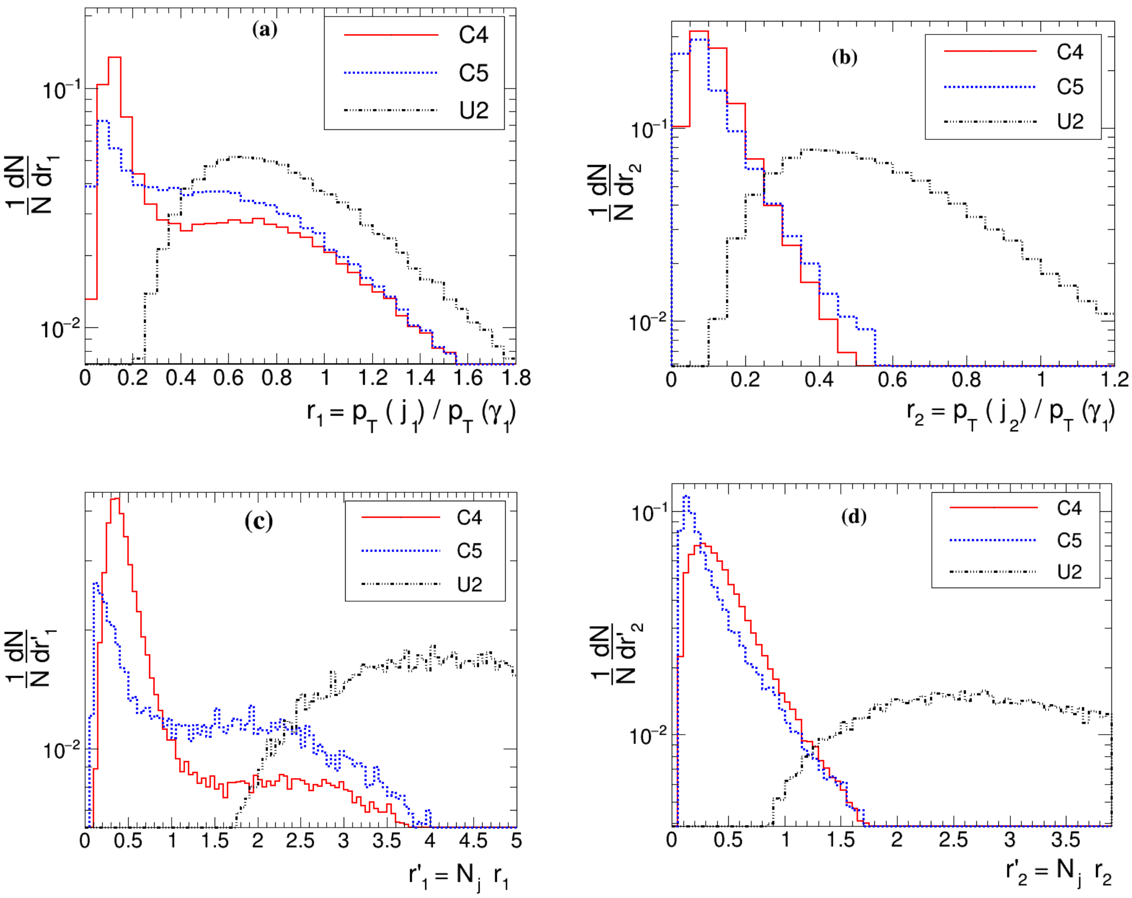


Figure 4.7: Normalized distributions of different kinematic variables $r_1$, $r_2$, $r'_1$ and $r'_2$ to distinguish compressed and uncompressed scenarios for some of the benchmark points representing various compressed (**C4**), more compressed (**C5**) and uncompressed (**U2**) spectra after implementing the selection and analysis cuts **A0-A6**.

Besides enhancing the differences between the compressed and uncompressed spectra, the differential distributions in $r_i$ and $r'_i$ can also be used to highlight the differences amongst the different compressed spectra themselves, depending on the level of compression in mass. For example, **C4**, has a larger mass separation $\Delta M_i$ than **C5**, and shows a peak in the jet multiplicity at $N_j = 3$ while for **C5**, the peak value of the differential cross section is at $N_j$

= 2. Thus a larger fraction of events survive after analysis for **C4** than **C5**. Again, since **C5** is relatively more compressed than **C4**, the jets from **C4** are considerably harder than the latter. However the NLSP mass for **C4** is larger than **C5**, since to probe lower values of compression, we require a heavier NLSP to meet current LHC bounds. This results in the photons being harder for **C4** than for **C5**. The combined effect of the two seem to be more prominent for both $r_1$ and $r_1'$, where the leading jet is either the ISR jet or cascade jet in case of **C4**. For $r_2$ this effect seems neutralised, owing to the sub-leading jets for both cases, being much softer than the leading photon $p_T$. However the scale factor $N_j$ shifts the peak value of $r_2'$, thus efficiently distinguishing amongst the two compressed spectra of varying degree of compression.

### 4.4.3 eV Gravitino

As pointed out earlier that the kinematic characteristics of events when the NLSP decays into a gravitino are independent of whether the $\widetilde{G}$ is in the keV or eV range. An eV gravitino cannot be the usual cold/warm DM candidate. Therefore such a scenario pertains to a situation where there is some other cold dark matter candidate. For an NLSP decaying into a $\widetilde{G}$ and a SM particle, the $\widetilde{G}$ remains practically massless. However, as discussed in Section 4.2.1, a lighter gravitino has a stronger coupling strength to the sparticles. Thus the decay of the sparticles into a SM particle and gravitino dominates over their decay to the NLSP. For a gravitino of mass 1 eV, we find that the gluino/squark almost always directly decays to the gravitino rather than to the NLSP. The branching fractions also depend on the mass gap between the colored sparticles and the NLSP. These features are highlighted in Figs. 4.1 and 4.2 where both compressed and uncompressed mass gaps are shown.

Therefore, an eV $\widetilde{G}$ does affect the overall event rates of the signal in the photon channel when compared to the keV $\widetilde{G}$ case. An immediate consequence which has gone unnoticed for such light eV $\widetilde{G}$ case would be a new competing signal which can become more relevant than the more popular photonic channel. This can be easily understood by taking a look at the resulting BR($\widetilde{g} \to g\widetilde{G}$) for some of our benchmark points in presence of an eV gravitino. As indicated by Fig. 4.1, this branching ratio is supposed to go up if the spectrum is more compressed. For the same benchmark points as in Table 3.1, now in the presence of an eV $\widetilde{G}$, we have observed that BR($\widetilde{g} \to g\widetilde{G}$) $\sim 13\%, 41\%$ and $99\%$ for **U1** ($\Delta m_{\widetilde{g}\widetilde{\chi}_1^0} = 1403$ GeV), **U2** ($\Delta m_{\widetilde{g}\widetilde{\chi}_1^0} = 911$ GeV) and **C1** ($\Delta m_{\widetilde{g}\widetilde{\chi}_1^0} = 78$ GeV) respectively. As a consequence, **C1** with an eV gravitino, is unlikely to yield a good event rate in the photonic channel since the gluino avoids decaying into the NLSP altogether. However, a small fraction of the squarks may still decay into the NLSP, $\sim 4\%$ and $\sim 24\%$ precisely for left and right squarks respectively. Hence, one would still expect a photon signal for such a scenario, but a much weaker one as presented in Table 4.4.

| Signal | Production | Cross-section (in fb) after cuts: | | | | | |
|---|---|---|---|---|---|---|---|
| | cross-section (in fb) | **A0+A1** | **A2** | **A3** | **A4** | **A5** | **A6** |
| C1 | 0.26 | 0.038 | 0.035 | 0.031 | 0.03 | 0.028 | 0.028 |

Table 4.4: Signal Cross-sections (NLO+NLL) for benchmark **C1** for $\geq 1$ photon + $> 2$ jets + $\not{E}_T$ final states ($m_{\widetilde{G}} = 1$ eV).

As expected, the photon signal weakens considerably when compared to one with a keV gravitino and requires an integrated luminosity $\sim 1000$ fb$^{-1}$ for observation at the LHC. However, much stronger signal would be obtained in the "n-jet+$\not{E}_T$" ($n \geq 2$) channel as the final state would have at least two very hard ($p_T$'s exceeding more than a TeV) jets and an equally hard $\not{E}_T$ signal for the eV-gravitino case. The conventional multi-jet search [169] rely upon the usual $\not{E}_T$, $M_{Eff}$, $\frac{\not{E}_T}{\sqrt{H_T}}$ and $\Delta\phi(j, \vec{\not{E}_T})$ cuts and in some cases, razor variables [143] to reduce the SM backgrounds. We have checked that with these cuts, a $3\sigma$ significance can be achieved for **C1** in the "n-jet+$\not{E}_T$" ($n \geq 2$) final state at an integrated luminosity of $\sim 1000$ fb$^{-1}$. However, in the presence of an eV gravitino, one can demand harder $p_T$ requirements of the jets and harder $\not{E}_T$, $M_{Eff}$ along with the other conventional cuts to increase signal significance further. We have checked that one can easily bring down the required luminosity to $\sim 728$ fb$^{-1}$ for a $3\sigma$ significance, which is a big improvement over the results obtained for the photon-associated final state. Thus the multi-jet channel is the more favorable one in order to explore an eV gravitino in presence of a $\sim$ TeV compressed color sector. However, as mentioned earlier, such a light gravitino may not be a viable dark matter candidate and would necessarily require the presence of other candidates to satisfy the constraints.

## 4.5 Summary and Conclusions

In this chapter, we have explored the compressed SUSY scenario in the presence of a light gravitino LSP within the framework of phenomenological MSSM. The question asked is:

since the light gravitino produced in the (neutralino) NLSP decays generates as much $\not{E}_T$ for compressed spectra as for uncompressed ones, are the former discernible?

The existing collider studies for such scenarios mostly account for the uncompressed parameter regions, and in some cases the NNLSP-NLSP compressed regions. However, compression in the entire colored sector of the sparticle spectrum can result in significantly different exclusion limits on the masses of squark, gluino and the lightest neutralino. The presence of a light gravitino in the spectrum affects the branching ratios of the colored sparticles into $\widetilde{\chi}_1^0$. We have studied the interplay of these relevant branching ratios for varying $\widetilde{G}$ mass and different amount of compression in the rest of the sparticle spectrum for a bino-like $\widetilde{\chi}_1^0$. Dictated by the DM constraints, we have mostly concentrated on the keV $\widetilde{G}$ scenario and have performed a detailed collider simulation and cut-based analysis for $\geq 1$ photon + $> 2$ jets + $\not{E}_T$ final states arising from the squark-gluino pair production channels in the context of the LHC. In our case, the squarks and the gluinos dominantly decay into the $\widetilde{\chi}_1^0$ which further decay into a $\widetilde{G}$ along with a $\gamma$ or a $Z$ resulting in the above mentioned final state. Hard $p_T$ photon requirement can be used along with other kinematic cuts to suppress the SM background very effectively. We have followed the existing ATLAS analysis for the same final state with the help of some benchmark points. We have shown that with the existing experimental data, the exclusion limits on the colored sparticle masses can increase by $\sim 500$ GeV for a highly compressed sparticle spectra. It is understood that similar signal event rates can be obtained from both uncompressed and compressed spectra depending on the choices of masses of squark, gluino and the lightest neutralino. However, the difference in the compression will be reflected in the kinematic distributions of the final state jets and photons. We have exploited this fact to construct some variables which can be used to good effect to differentiate between the two scenarios. We have also studied the collider prospects of SUSY spectra in the presence of sub-keV gravitinos. It turns out that in such cases, the $\widetilde{G}$-associated decay modes of the heavy ($\sim 2.5$ TeV) colored sparticles start to become relevant in the presence of high compression between the NNLSP and NLSP. Then the most suitable final state to look for such spectra would be multi-jets + $\not{E}_T$. However, the existing DM constraints strongly disfavour presence of such light gravitino in the spectrum.

# Chapter 5

# Identifying a Higgsino-like neutralino with a keV-scale dark matter

## 5.1 Introduction

We observe in Chapter 4 that the presence of non-standard LSP candidates, such as a light $\widetilde{G}$ as the lightest SUSY particle relaxes the DM constraints on the composition of the lightest neutralino $\widetilde{\chi}_1^0$, which now serves as the next-to-lightest sparticle (NLSP). Besides, it also provides additional channels of discovery of the MSSM part of the spectrum. For instance, a primarily bino-dominated $\widetilde{\chi}_1^0$ NLSP decays dominantly to a hard photon and $\widetilde{G}$ with a small fraction to a $Z$ boson and the light gravitino. This gives rise to hard photon signals along with large missing transverse energy carried away by the keV-scale LSP as was the subject of discussion in the last Chapter. However the final state signals are largely dependent on the composition of the NLSP. Therefore besides photon signals, there may be Higgs and/or $Z$ bosons in the final state as well for higgsino and/or gaugino dominated $\widetilde{\chi}_1^0$ NLSP's. In this chapter, we consider the LHC signals of a higgsino-dominated NLSP with a gravitino LSP. Our study would also apply to scenarios where an axino is the dark matter candidate. Such signals have been studied at the LHC by the experimental collaborations extensively. Since the light standard model (SM) like Higgs has the largest decay probability to $b\,\bar{b}$, this leads to a final state dominated by hard $b$-tagged jets along with large missing transverse momentum (MET) $\not{E}_T$ and additional light jets/leptons arising from accompanying $Z$ boson. Signatures for the higgsino-like NLSP's have been studied in the context of Tevatron [170, 171] and at the LHC where both CMS [172] and ATLAS [173] have looked at multiple $b$-jets + MET, dilepton and multilepton states to constrain a higgsino-like NLSP scenario.

We aim to study signatures of a low-lying higgsino sector in the presence of a light gravitino LSP with particular emphasis on determining how the NLSP nature can be convincingly identified. To do this one would like to reconstruct the decay products of the NLSP. As the higgsino NLSP would decay to a light Higgs or a $Z$ boson, we may be able to observe their properties by appropriately reconstructing the Higgs through the $b$-jets arising from its decay as well as the $Z$ boson through the opposite sign dilepton pair from the gauge boson's decay respectively. We note here a very important and interesting feature of the decay of the NLSP. It is expected that the $Z$ boson arising from the higgsino-like $\widetilde{\chi}_1^0$ decay would be dominantly *longitudinal* (Goldstone boson), primarily following the *equivalence theorem* where, after electroweak symmetry breaking the neutral Goldstone boson constitutes the longitudinal mode of the $Z$ boson responsible for its mass. This property if observed in the decay of the NLSP would exclusively point towards the presence of a higgsino-like $\widetilde{\chi}_1^0$, helping us identify the nature of the NLSP. The direct production of the electroweak neutralino NLSP would be limited at the LHC as their mass becomes larger. However, the property of the NLSP could still be studied if they are produced in cascade decays of strongly interacting sparticles. We therefore study the effect of including the strong sector in exploring the compositions of the NLSP as well as from the direct production of the low-lying electroweakinos (still allowed by experiments) and propose some new kinematic variables which help identify the NLSP. Thus, the salient points of our study as discussed in this chapter, the contents of which are based on [10], are as follows:

- We consider a naturally compressed low-lying higgsino sector as well as partially and/or fully compressed spectra with the strongly interacting sparticles sitting above the NLSP. The sparticles decay via cascades to the NLSP which further decays to a Higgs and a $Z$ boson thereby giving rise to at least 1 $b$-jet and opposite-sign same flavour dileptons along with missing transverse energy in the final state.

- The characteristic features of a longitudinal $Z$ boson arising from decay of the higgsino-like $\widetilde{\chi}_1^0$ are studied by utilising angular variables of the negatively charged lepton. In order to distinguish it from transversely polarised $Z$ bosons coming from other sources, we compare our results with the complementary admixture of NLSP, especially gaugino-dominated neutralinos as well as the SM background.

- We observe that for spectrum with a heavy NLSP, reflecting overall compression with respect to the strong sector leads to an increased fraction of the longitudinal mode in the $Z$ boson arising from the NLSP decay.

- New variables enhancing the asymmetry in the angular distributions of the negatively charged lepton have been proposed in order to characterize a longitudinally polarized $Z$ boson in comparison to a transversely polarized $Z$ boson. Such asymmetry variables distinctly vary depending on the higgsino-gaugino admixture of the NLSP and crucially capture the effect of the equivalence theorem for a heavy NLSP in a somewhat compressed spectrum.

The subsequent sections are organized as follows. In section 5.2 we discuss the current scenario with the higgsino NLSP and gravitino LSP followed by the decay properties of the higgsinos in section 5.3. In section 5.4, we discuss the experimental status of a higgsino-like NLSP with a light gravitino LSP at LHC. In section 5.5, we choose some benchmarks to study the available parameter space. We perform the collider study and discuss our results at the high luminosity run of LHC in section 5.6. In section 5.7, we distinguish between the features of longitudinal and transverse gauge bosons. Section 5.8 summarises the main conclusions of our work.

## 5.2 Higgsino-dominated NLSP with keV LSP

In the earlier chapters we have discussed signals of a predominatly bino-dominated NLSP. In this chapter, we discuss light higgsino-like NLSP as a possible consequence of general phenomenological MSSM. Since no hint of SUSY has yet shown up at direct searches, various possible configurations of the lightest neutralino, $\widetilde{\chi}_1^0$, leading to distinct signals at colliders are of interest. Such a light higgsino-like $\widetilde{\chi}_1^0$ is characterized by a light $\mu$ parameter and heavy bino, wino soft mass parameters, i.e, $|\mu| << M_1, M_2$. Besides, low $\mu$ parameter is also a preferred choice from naturalness perspective [174–179]. However $\widetilde{\chi}_1^0$ may not be the LSP in many situations. In such cases there can be several other candidates for LSP such as gravitinos, axinos, sneutrinos etc.

The gravitino is the spin-$\frac{3}{2}$ superpartner of the spin-2 graviton in local SUSY. Upon spontaneous SUSY breaking, there arises a massless Weyl fermion known as the goldstino ($\widetilde{G}$), owing to the breaking of the fermionic generators of SUSY. After electroweak symmetry breaking, the gravitino acquires mass by absorbing the goldstino which form the spin 1/2 components of the massive gravitino.

It is in fact the goldstino (which constitutes the longitudinal part of the gravitino) that is produced in processes at energy scales much higher than the gravitino mass. For a light gravitino, a TeV-scale sparticle then decays to an SM particle and the goldstino with a coupling enhanced by a factor of $(M_{Pl} m_{\widetilde{G}})^{-1}$ and hence may decay within the collider [38]. Hence, it is the goldstino mode of the gravitino that is important for collider phenomenology. The goldstino ($\widetilde{G}$) Lagrangian is [2]:

$$\mathcal{L}_{goldstino} = i\widetilde{G}^{\dagger}\bar{\sigma}^{\mu}\partial_{\mu}\widetilde{G} - \frac{1}{< F >}\widetilde{G}\partial_{\mu}j^{\mu} + c.c \tag{5.2.1}$$

where $< F >$ refers to the *vev* obtained by the SUSY breaking auxilliary field $F$ and $j^{\mu}$ refers to the current involving all other sparticles and SM particles. The couplings of the gravitino to fermion-sfermion, gauge boson-gauginos are computed in Ref. [38].

We now discuss the couplings and decays of a higgsino-like $\widetilde{\chi}_1^0$ NLSP in the presence of a gravitino ($\widetilde{G}$)[1] LSP before moving on to a numerical analysis in section 5.3. In addition, we briefly discuss the parameter space region where higgsinos could give rise to a prompt decay. Non-prompt searches (such as searches for charged tracks [180, 181]) for higgsinos would be relevant for $\widetilde{\chi}_1^{\pm}$ NLSP.[2]

Such a scenario is phenomenologically analogous to a scenario with axino LSP. However since axino couplings to MSSM particles differ from gravitino couplings, similar signals may arise for axino LSP depending on the NLSP masses. For similar mass values of an axino and gravitino, the NLSP decay width is much smaller for an axino LSP which may lead to a long lived NLSP signature, for e.g, charged tracks for $\widetilde{\chi}_1^{\pm}$ in the colliders [159].

## 5.3 Higgsino NLSP decays

A higgsino-like $\widetilde{\chi}_1^0$ is characterised by a large higgsino fraction with suppressed wino and bino fractions i.e, $\mu < M_1, M_2$. In the presence of a light $\widetilde{G}$ LSP, the higgsino-like $\widetilde{\chi}_1^0$ NLSP decays to either a Higgs ($h$) or a $Z$ boson and $\widetilde{G}$.[3] Absence of a large bino component leads to a rather suppressed photon mode unless there is substantial gaugino-bino-higgsino admixture [171]. However the photon mode may dominate in case of very light higgsinos where the decay to the Higgs or $Z$ boson is phase space suppressed. As the coupling of a

[1] We use $\widetilde{G}$ for the gravitino in the remaining part of the manuscript.

[2] Searches for displaced jets and leptons could be relevant for neutral higgsinos: $\widetilde{\chi}_2^0, \widetilde{\chi}_1^0$ in the presence of non-standard LSP candidates [159, 182].

[3] In presence of $M_A < \mu$, the NLSP may also decay into the heavy Higgses [156]. In this study, for simplicity the heavy Higgs masses are kept above the spectrum of interest.

gravitino to other particles are inversely proportional to its mass($m_{\widetilde{G}}$), a lighter gravitino has stronger couplings as compared to a heavier one. The decay width is proportional to $m^5_{\widetilde{X}}$, where $m_{\widetilde{X}}$ is the mass of the parent sparticle. Hence for a fixed gravitino mass and increasing NLSP mass, the decay width increases and leads to prompt decays. For any sparticle $\widetilde{X}$, its two-body decay to $X$ and a gravitino is given as [2]:

$$\Gamma(\widetilde{X} \to X\widetilde{G}) = \frac{m^5_{\widetilde{\chi}^0_1}}{48\pi M^2_{Pl} m^2_{\widetilde{G}}}(1 - \frac{m^2_X}{m^2_{\widetilde{X}}})^4 \tag{5.3.1}$$

where $m_X$ refer to the mass of the SM partner of $\widetilde{X}$. As we are interested in the decay of the neutralino NLSP to the gravitino, the composition of the lightest neutralino becomes an essential characteristic as it would determine what the NLSP finally decays to. The neutralino mass matrix in the basis $(\widetilde{B}, \widetilde{W}_3, \widetilde{H}^0_d, \widetilde{H}^0_u)$ is $M_{\widetilde{N}}$ as defined in Chapter 2, Eq. 2.3.20. Diagonalising the symmetric mass matrix using a unitary matrix $N$ lead to the neutralino mass eigenstates $\widetilde{\chi}^0_i$ $(i = 1, .., 4)$.

$$N M_{\widetilde{N}} N^T = diag(m_{\widetilde{\chi}^0_1}, m_{\widetilde{\chi}^0_2}, m_{\widetilde{\chi}^0_3}, m_{\widetilde{\chi}^0_4}) \tag{5.3.2}$$

where $m_{\widetilde{\chi}^0_1} < m_{\widetilde{\chi}^0_2} < m_{\widetilde{\chi}^0_3} < m_{\widetilde{\chi}^0_4}$.

The chargino mass matrix $M^c$ in the basis $(\widetilde{W}^+, \widetilde{H}^+_u)$ is as given in Chapter 2 Eq. 2.3.1. Since, $M_{\widetilde{C}}$ is not a symmetric matrix, we need two unitary matrices $U$ and $V$ to diagonalize the matrix. Hence,

$$U^* M_{\widetilde{C}} V^{-1} = diag(m_{\widetilde{\chi}^\pm_1}, m_{\widetilde{\chi}^\pm_2}) \tag{5.3.3}$$

where $m_{\widetilde{\chi}^\pm_1} < m_{\widetilde{\chi}^\pm_2}$. Thus, in the limit where $\mu << M_1, M_2$, ie. the lightest neutralino is dominantly higgsino-like with small gaugino fractions, there are two nearly degenerate higgsino-like neutralinos $\widetilde{\chi}^0_1, \widetilde{\chi}^0_2$ and higgsino-like chargino, $\widetilde{\chi}^\pm_1$. Thus, a low-lying higgsino mass parameter leads to a naturally compressed spectra consisting of three closely lying particles $\widetilde{\chi}^0_1$, $\widetilde{\chi}^0_2$ and $\widetilde{\chi}^\pm_1$. The mass eigenvalues for the higgsinos at the tree-level are [183,184]:

$$\begin{aligned} m_{\widetilde{\chi}^\pm_1} &= |\mu|\left(1 - \frac{M^2_W \sin 2\beta}{\mu M_2}\right) + \mathcal{O}(M_2^{-2}) \\ m_{\widetilde{\chi}^0_{1,2}} &= \pm\mu - \frac{M^2_Z}{2}(1 \pm \sin 2\beta)\left(\frac{\sin\theta^2_W}{M_1} + \frac{\cos\theta^2_W}{M_2}\right) \end{aligned} \tag{5.3.4}$$

In the MSSM, the $\widetilde{\chi}^0_1$ is primarily the LSP with different mass hierarchies amongst the higgsinos. Owing to the natural compression in mass amongst the higgsinos, $\widetilde{\chi}^0_2$ and $\widetilde{\chi}^\pm_1$ primarily decay via off-shell gauge bosons $(W^\pm, Z)$ to the LSP. $\widetilde{\chi}^0_2$ may also decay via a photon to the LSP at one-loop level. In cases, where $\widetilde{\chi}_2^0$ is the heaviest amongst all the higgsinos, the following are the relevant decay modes of the higgsinos:

$$\begin{aligned} \widetilde{\chi}_2^0 &\to f\bar{f}\widetilde{\chi}_1^0, f\bar{f}'\widetilde{\chi}_1^{\pm}, \gamma\widetilde{\chi}_1^0 \\ \widetilde{\chi}_1^{\pm} &\to f\bar{f}'\widetilde{\chi}_1^0 \end{aligned} \tag{5.3.5}$$

where $f$ and $f'$ are SM fermions. There may be regions in the parameter space where $\widetilde{\chi}_1^{\pm}$ is heavier than $\widetilde{\chi}_2^0$, the decays of the $\widetilde{\chi}_2^0$ and $\widetilde{\chi}_1^{\pm}$ are modified as follows:

$$\begin{aligned} \widetilde{\chi}_1^{\pm} &\to f\bar{f}'\widetilde{\chi}_1^0, f\bar{f}'\widetilde{\chi}_2^0 \\ \widetilde{\chi}_2^0 &\to f\bar{f}\widetilde{\chi}_1^0, \gamma\widetilde{\chi}_1^0 \end{aligned} \tag{5.3.6}$$

In some regions of the parameter space, $\widetilde{\chi}_1^{\pm}$ may become the lightest of all the higgsinos [183], thereby opening up the following are the decay modes of $\widetilde{\chi}_1^0, \widetilde{\chi}_2^0$:

$$\begin{aligned} \widetilde{\chi}_2^0 &\to f\bar{f}\widetilde{\chi}_1^0, f\bar{f}'\widetilde{\chi}_1^{\pm}, \gamma\widetilde{\chi}_1^0 \\ \widetilde{\chi}_1^0 &\to f\bar{f}\widetilde{\chi}_1^{\pm} \end{aligned} \tag{5.3.7}$$

However with the charged state being the lightest an alternative light LSP candidate is preferred, which in our case happens to be the gravitino. In the presence of $\widetilde{G}$ LSP, new decay modes open up for the higgsinos. The presence of a non-zero higgsino fraction in $\widetilde{\chi}_1^0$ and $\widetilde{h} - h - \widetilde{G}$ vertex ensures the presence of a Higgs boson arising from the decay of $\widetilde{\chi}_1^0$ to a Higgs and $\widetilde{G}$. Suppressed gaugino fractions imply reduced decay to photons or $Z$ along with the gravitino which would otherwise proliferate for bino/wino dominated NLSP. However there is substantial branching fraction of $\widetilde{\chi}_1^0$ into $Z$ and $\widetilde{G}$ in the case of a higgsino-like NLSP as well [170, 171]. This is because after electroweak symmetry breaking, the Goldstone boson forms the longitudinal component of the $Z$ boson. Similarly, $\widetilde{\chi}_1^{\pm}$ may also decay to a longitudinal $W$ along with the $\widetilde{G}$ in cases where $\widetilde{\chi}_1^{\pm}$ is the NLSP. Thus, depending on the various possible hierarchies amongst the higgsinos, the following are the possible decay channels of the higgsino-dominated electroweakinos:

$$\begin{aligned} \widetilde{\chi}_2^0 &\to f\bar{f}\widetilde{\chi}_1^0, f\bar{f}'\widetilde{\chi}_1^{\pm}, h\widetilde{G}, Z\widetilde{G} \\ \widetilde{\chi}_1^{\pm} &\to f\bar{f}'\widetilde{\chi}_1^0, f\bar{f}'\widetilde{\chi}_2^0, W^{\pm}\widetilde{G} \\ \widetilde{\chi}_1^0 &\to h\widetilde{G}, Z\widetilde{G} \end{aligned} \tag{5.3.8}$$

where the $Z$ boson from neutralino decay is mostly longitudinal. The couplings of the neutral higgsinos $\widetilde{\chi}_1^0, \widetilde{\chi}_2^0$ and charged higgsino, $\widetilde{\chi}_1^{\pm}$, to the gravitino ($\widetilde{G}$) LSP are [43]:

$$\begin{aligned} |g_{\widetilde{G}\widetilde{\chi}_i^0 H_k}|^2 &= |e_k N_{i3} + d_k N_{i4}|^2 (M_{Pl} m_{\widetilde{G}})^{-2}, \\ |g_{\widetilde{G}\widetilde{\chi}_1^{\pm} H_k^{\pm}}|^2 &= (|V_{12}^2| \cos^2\beta + |U_{12}^2| \sin^2\beta)(M_{Pl} m_{\widetilde{G}})^{-2} \end{aligned} \tag{5.3.9}$$

for $i = 1, 2$ corresponding to $\widetilde{\chi}_1^0$, $\widetilde{\chi}_2^0$ and $k = 1, 2, 3$ corresponding to the CP-even scalars $h, H$ and CP-odd pseudoscalar $A$. The coefficients $e_k$ and $d_k$ are as below:

$$\begin{aligned} e_1 = \cos\alpha, e_2 = -\sin\alpha, e_3 = -\sin\beta \\ d_1 = -\sin\alpha, d_2 = -\cos\alpha, d_3 = \cos\beta \end{aligned} \tag{5.3.10}$$

and $N_{ij}$ refer to the $(ij)^{th}$ entry of the neutralino mixing matrix $N$, $\alpha$ is the mixing angle between the CP-even Higgses, $h$ and $H$. In the decoupling limit, i.e, $m_A >> m_h$, $\beta - \alpha \sim \pi/2$ ( where, $0 < \beta < \pi$ and $-\pi < \alpha < 0$ ), the lightest CP-even Higgs ($h$) behaves like the SM Higgs boson [2][4]. The coupling of the $Z$ boson to $\widetilde{\chi}_1^0$ and $\widetilde{G}$ is as follows:

$$|g_{\widetilde{G}\widetilde{\chi}_i^0 Z}|^2 = (|N_{11}\sin\theta_W - N_{12}\cos\theta_W|^2 + \frac{1}{2}|N_{i4}\cos\beta - N_{i3}\sin\beta|^2)(M_{Pl}m_{\widetilde{G}})^{-2} \tag{5.3.11}$$

for $i = 1, 2$. Thus, the partial decay widths of a higgsino-like neutralino $\widetilde{\chi}_1^0$ are as follows [2, 156, 170]:

$$\Gamma(\widetilde{\chi}_1^0 \to Z\widetilde{G}) \propto (|N_{11}\sin\theta_W - N_{12}\cos\theta_W|^2 + \frac{1}{2}|N_{14}\cos\beta - N_{13}sin\beta|^2)(M_{Pl}m_{\widetilde{G}})^{-2}$$

$$\Gamma(\widetilde{\chi}_1^0 \to h\widetilde{G}) \propto |N_{14}\sin\alpha - N_{13}\cos\alpha|^2 (M_{Pl}m_{\widetilde{G}})^{-2}$$

The terms proportional to $N_{14}$ and $N_{13}$ denote the Goldstone couplings; which we discuss in detail later in section 5.7. In the decoupling limit, $\sin\alpha = -\cos\beta$ and $\cos\alpha = \sin\beta$, thus

$$\Gamma(\widetilde{\chi}_1^0 \to h\widetilde{G}) \propto |N_{14}\cos\beta + N_{13}\sin\beta|^2 (M_{Pl}m_{\widetilde{G}})^{-2} \tag{5.3.12}$$

For $|N_{11}|, |N_{12}| << |N_{13}|, |N_{14}|$, $\Gamma(\widetilde{\chi}_1^0 \to h\widetilde{G}) \sim \Gamma(\widetilde{\chi}_1^0 \to Z\widetilde{G})$. For the higgsino-like $\widetilde{\chi}_1^0$, $N_{13} \simeq N_{14}$ for $\mu > 0$, whereas for $\mu < 0$, ie, $N_{13} \sim -N_{14}$ [170]. This leads to an increase in $\Gamma(\widetilde{\chi}_1^0 \to h\widetilde{G})$ as evident from Eq. 5.3.12.

## Branching Ratios

We consider a higgsino-like $\widetilde{\chi}_1^0$ as the NLSP with a light $\widetilde{G}$ LSP. As discussed in section 5.3, the branching ratios of the NLSP are governed by the composition of the NLSP as well as the values of $\tan\beta$ and $\mu$. In Fig. 5.1 we plot the branching ratios of $\widetilde{\chi}_1^0$'s decay to a $h\,\widetilde{G}$ or a $Z\,\widetilde{G}$ as a function of $\tan\beta$ and $\mu$. Among other parameters, the bino, wino and gluino soft mass parameters are $M_1$, $M_2, M_3 \sim 2$ TeV respectively, whereas squarks and sleptons masses are kept at $\sim$2 TeV. The light stop masses are kept at 2.8 TeV to fit the lightest CP-even Higgs mass in the range 122-128 GeV [16, 185] for $\mu$ parameter values in the range [0.2:1.5] TeV. The relevant parameter ranges for the scan which is carried out using `SPheno-v3.3.6` [120, 121] are summarised in Table 5.1.

[4]We assume $M_A >> \mu$ for simplicity, therefore disallowing decays of $\widetilde{\chi}_i^0$ to heavy Higgses.

| Parameters | $\lvert\mu\rvert$ (GeV) | sign($\mu$) | $\tan\beta$ |
|---|---|---|---|
| Values | 0.2-1.5 | $\pm 1$ | 2-45 |

Table 5.1: Relevant range of the input parameters for the parameter-space scan to study the decay probabilities of the lightest neutralino is shown. We keep other parameters at fixed values which include: $M_1 = 2$ TeV, $M_2 = 2$ TeV, $M_3 = 1.917$ TeV, $M_{Q_3} = 2.8$ TeV, $M_{U_3} = 2.8$ TeV, $M_A = 2.5$ TeV, $A_t = 3$ TeV and $m_{\widetilde{G}} = 1$ keV.

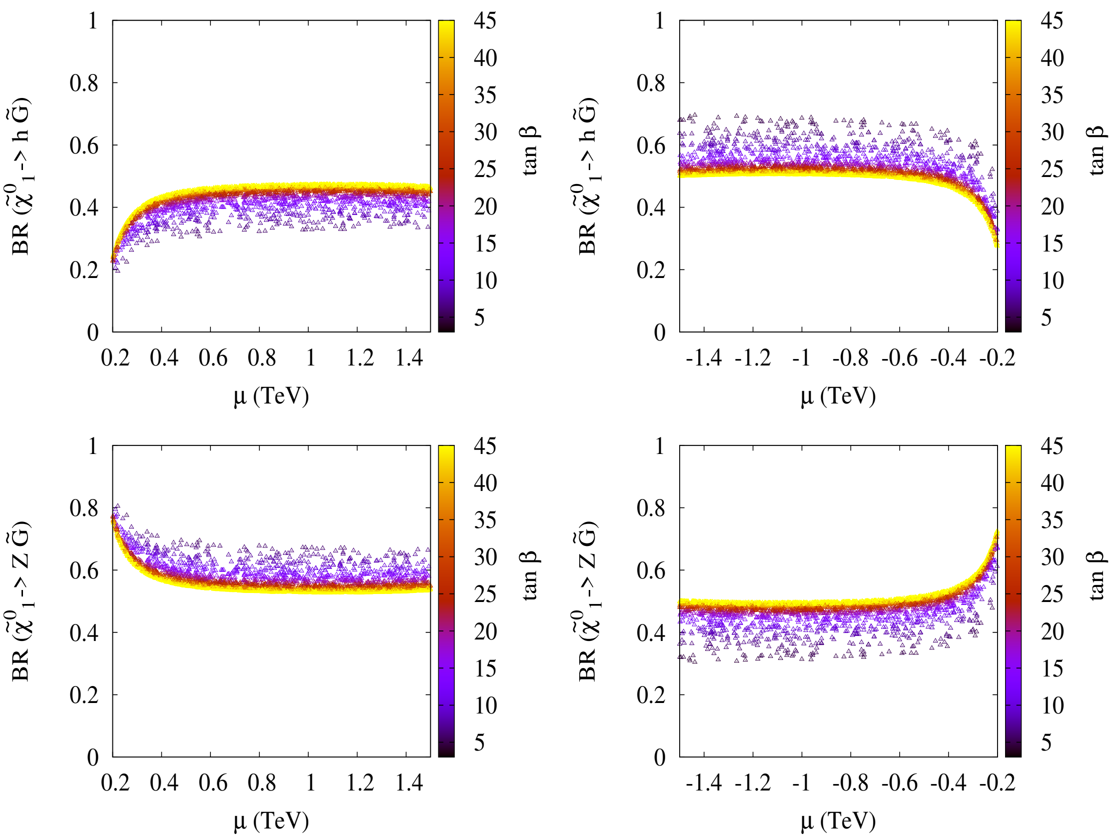


Figure 5.1: Variation of $\widetilde{\chi}_1^0$ decay into a Higgs (top panel) or $Z$ boson (bottom panel) along with the $\widetilde{G}$ LSP with $\mu$ and $\tan\beta$ in the coloured palette. The parameters of the scan are listed in Table 5.1.

The decay branching ratios of the higgsino-dominated $\widetilde{\chi}_1^0$ NLSP are governed mainly by values of $\mu$ and $\tan\beta$ and hence the composition of the NLSP. Fig. 5.1 clearly shows that there exist three distinct regions of the parameter space, namely the Higgs dominated region, the $Z$ boson dominated region and the region of parameter space where both the Higgs and the $Z$ boson modes are comparable. The Higgs dominated $BR(\widetilde{\chi}_1^0 \to h\widetilde{G}) \simeq 0.8$ occurs for negative values of the $\mu$ parameter whereas the $Z$ boson dominated $BR(\widetilde{\chi}_1^0 \to Z\widetilde{G}) \simeq 0.8$ is for positive $\mu$ parameter, both at low $\tan\beta$ values. In the former case, $N_{13} = N_{14}$ whereas in the latter case there is a relative sign between $N_{13}$ and $N_{14}$ in a small region of the parameter space where the Higgs mode takes over the $Z$ mode. Although the Higgs mode dominates over the $Z$ mode throughout the negative $\mu$ parameter space (see Eq. 5.3.12), it decreases with increase in the gaugino admixture in the NLSP at higher values of $\mu$ and $\tan\beta$ (as $\mu$ gets closer to the choice of $M_1$ and $M_2$ shown in Table 5.1), which defines a range of the parameter space with comparable branching ratios for the Higgs and $Z$ boson decay modes of the $\widetilde{\chi}_1^0$ NLSP. In addition, as the $\widetilde{\chi}_1^0$ becomes more gaugino-like the additional decay mode of $\gamma\,\widetilde{G}$ would also open up and subsequently dominate the branching probabilities.

## 5.4 Existing LHC limits

The current bounds on the light higgsinos as NLSP and $\widetilde{G}$ LSP are well studied at LHC for a light gravitino ( $m_{\widetilde{G}} = 1$ GeV) assuming prompt decays. The relevant analyses are summarised in Table 5.2. We discuss in detail the implications of the constraints from LHC on the higgsinos as well as on the strong sector sparticles as relevant for our study below:

- **Higgsinos:** ATLAS and CMS impose stringent limits on the mass of the higgsinos from searches involving multible b-jets/leptons along with large missing transverse energy $\not{E}_T$ assuming specific branching probabilities for its decay. The following are the exclusion limits on the higgsino masses [172, 186] :

$$BR(\widetilde{\chi}_1^0 \to h\widetilde{G}) \sim 1.0: \quad m_{\widetilde{\chi}_1^0} \geq 880 \text{ GeV (ATLAS)}; \quad m_{\widetilde{\chi}_1^0} \geq 760 \text{ GeV (CMS)}.$$
$$BR(\widetilde{\chi}_1^0 \to Z\widetilde{G}) \sim 1.0: \quad m_{\widetilde{\chi}_1^0} \geq 340 \text{ GeV (ATLAS)}.$$

  Combined exclusion limits on the higgsino mass from multiple searches at CMS are as follows [172]:

$$BR(\widetilde{\chi}_1^0 \to h\widetilde{G}) \sim 1.0: \qquad m_{\widetilde{\chi}_1^0} \geq 775 \text{ GeV (CMS)}.$$
$$BR(\widetilde{\chi}_1^0 \to Z\widetilde{G}) \sim 1.0: \qquad m_{\widetilde{\chi}_1^0} \geq 650 \text{ GeV (CMS)}.$$

- **Strong Sector:** Direct limits for a massless gravitino LSP scenario are placed on strong sector sparticles with $\widetilde{G}$ LSP from opposite-sign dilepton + missing energy searches in ATLAS [191] excluding $m_{\widetilde{g}} \leq 1.8$ TeV for $m_{\widetilde{\chi}_1^0} < 600$ GeV. Stringent limits

| Final State | Production mode | ATLAS | CMS |
|---|---|---|---|
| $2/3/4b + \not\!\!E_T$ | $\widetilde{\chi}_1^0\widetilde{\chi}_1^\pm, \widetilde{\chi}_2^0\widetilde{\chi}_1^\pm, \widetilde{\chi}_1^\mp\widetilde{\chi}_1^\pm, \widetilde{\chi}_1^0\widetilde{\chi}_2^0$ | [186] | [172] |
| $\ell^+\ell^- + \not\!\!E_T$ | $\widetilde{\chi}_1^0\widetilde{\chi}_1^\pm, \widetilde{\chi}_2^0\widetilde{\chi}_1^\pm, \widetilde{\chi}_1^\mp\widetilde{\chi}_1^\pm, \widetilde{\chi}_1^0\widetilde{\chi}_2^0$ | | [172] |
| $\geq 3\ell + \not\!\!E_T$ | $\widetilde{\chi}_1^0\widetilde{\chi}_1^\pm, \widetilde{\chi}_2^0\widetilde{\chi}_1^\pm, \widetilde{\chi}_1^\mp\widetilde{\chi}_1^\pm, \widetilde{\chi}_1^0\widetilde{\chi}_2^0$ | | [172] |
| $hh + \not\!\!E_T$ | $\widetilde{g}\widetilde{g}$ | | [187] |
| $4\ell + \not\!\!E_T$ | $\widetilde{\chi}_1^\pm\widetilde{\chi}_1^\pm, \widetilde{\chi}_1^\pm\widetilde{\chi}_2^0$ | [188] | |
| $\geq 2j + \not\!\!E_T$ | $\widetilde{g}\widetilde{g}, \widetilde{q}\widetilde{q}$ | [189] | |
| $b\bar{b} + \not\!\!E_T$ | $\widetilde{\chi}_2^0\widetilde{\chi}_1^\pm$ | [190] | |
| $1\ell + b\bar{b} + \not\!\!E_T$ | $\widetilde{\chi}_2^0\widetilde{\chi}_1^\pm$ | [190] | |
| $3\ell + \not\!\!E_T$ | $\widetilde{\chi}_2^0\widetilde{\chi}_1^\pm$ | [190] | |
| $\ell^\pm\ell^\pm + \not\!\!E_T$ | $\widetilde{\chi}_2^0\widetilde{\chi}_1^\pm$ | [190] | |

Table 5.2: List of experimental searches from LHC relevant for our current study with $\widetilde{G}$ LSP.

also arise from boosted Higgs searches [192] interpreted in terms of a simplified scenario with a light $\widetilde{\chi}_1^0$ LSP excluding $m_{\widetilde{g}} \leq 2.2$ TeV for $m_{\widetilde{\chi}_1^0} = 1$ GeV. Other indirect searches which constrain the above mentioned scenario are multi-jets and/or multileptons + $\not\!\!E_T$ searches [188, 189], owing to the presence of $h/Z$ from the NLSP decay which give rise to leptons or jets in the final state.

## 5.5 Benchmarks for our analysis

We choose representative benchmark points of the allowed parameter space to probe a low-lying higgsino-like $\widetilde{\chi}_1^0$ NLSP with light $\widetilde{G}$ LSP, focusing primarily on promptly decaying $\widetilde{\chi}_1^0$ signals. Our choice of benchmarks is motivated by the underlying aim of uncovering the characteristics of a higgsino-like $\widetilde{\chi}_1^0$ NLSP in the presence of a light $\widetilde{G}$ LSP. Decays of the strong sector sparticles occur via the following decay modes for a keV $\widetilde{G}$ as discussed in Chapter 4: for gluinos, with squarks and electroweakinos decoupled, the possible decay modes to the NLSP,

$$\widetilde{g} \to t\bar{t}\widetilde{\chi}_1^0, \quad b\bar{b}\widetilde{\chi}_1^0, \quad t\bar{b}\widetilde{\chi}_1^-, \quad q\bar{q}\widetilde{\chi}_1^-, q\bar{q}\widetilde{\chi}_1^0$$

Among these decay modes, owing to the higgsino-like nature of the NLSP, the interaction strengths are governed by the Yukawa couplings. Hence the third generation squark channels dominate. Whereas for the first and second generation squarks, the possible decay modes are:

$$\widetilde{q} \rightarrow q\widetilde{\chi}_1^0, \quad q\widetilde{\chi}_2^0, \quad q'\widetilde{\chi}_1^{\pm}$$

As discussed in section 5.3, the dominant decay mode of the $\widetilde{\chi}_1^0$ NLSP is to either a Higgs or a $Z$ boson along with the $\widetilde{G}$ LSP which constributes to the missing energy. This is because, for a keV $\widetilde{G}$ the sparticles decay primarily to the $\widetilde{\chi}_1^0$ NLSP, either directly or via cascade decays through the intermediate sparticles [9]. We wish to study the collider prospects of observing the final state: $\geq 1b + \ell^+\ell^- + \not{E}_T$ in the context of the upcoming high luminosity run of the LHC and explore kinematic variables reflecting the composition of the NLSP. We discuss below the characteristic features of each of the chosen benchmarks which follow:

- Squarks and keV $\widetilde{G}$ (**BP1**) with higgsino-like $\widetilde{\chi}_1^0$ NLSP.
- Squarks and keV $\widetilde{G}$ (**BP2**) with gaugino-like $\widetilde{\chi}_1^0$ NLSP.
- Light higgsinos only and keV $\widetilde{G}$ (**BP3**) with $\widetilde{\chi}_1^0$ NLSP.
- Squarks and keV $\widetilde{G}$ (**BP4**) with a heavy gaugino-higgsino mixed $\widetilde{\chi}_1^0$ NLSP.

For simplicity, $M_1, M_2 \sim 2.3 - 2.4$ TeV such that their contribution directly or via cascade decays of strong sector sparticles to the signal region under study is negligible. Among the constraints on the parameter space, light Higgs mass is within the range 122-128 GeV [16, 185]. In all cases, both $\widetilde{t}_1$ and/or $\widetilde{t}_2$ are heavy or the trilinear coupling, $A_t$, is large to fit the lightest CP-even Higgs mass, $m_h$ in the range 122-128 GeV [16, 185, 193]. Also, $m_{\widetilde{\chi}_1^{\pm}}$ adheres to LEP limit of 103.5 GeV [105]. We focus primarily on the following cases:

- **BP1**: We choose this benchmark with squark lighter in mass than the gluinos, i.e, $m_{\widetilde{q}} = 2.3$ TeV while $m_{\widetilde{g}} \sim 2.8$ TeV respectively. We choose $\mu = 800$ GeV and $\tan\beta = 25$ such that $BR(\widetilde{\chi}_1^0 \rightarrow h\widetilde{G}) \sim 0.45$ whereas $BR(\widetilde{\chi}_1^0 \rightarrow Z\widetilde{G}) \sim 0.55$. The lightest chargino, $\widetilde{\chi}_1^{\pm}$ decays primarily via $\widetilde{\chi}_1^0$, i.e, $\text{BR}(\widetilde{\chi}_1^{\pm} \rightarrow f\bar{f}'\widetilde{\chi}_1^0) \sim 0.98$.
- **BP2**: This benchmark is quite similar to **BP1** except with a major difference in the composition of the NLSP. Here the $\widetilde{\chi}_1^0$ NLSP is dominantly zino-like, i.e, $M_1 = M_2 =$ 800 GeV and $\mu = 2$ TeV. Thus, $\widetilde{\chi}_1^0 \rightarrow \gamma\widetilde{G} \sim 0.75$ and $\widetilde{\chi} \rightarrow Z\widetilde{G} \sim 0.25$. The sole pupose of choosing this benchmark is to compare the difference in distributions referred to in

section 5.7 which gives a clear indication of the NLSP composition. Note that the dominant signal for this benchmark is via hard photon signals along with jets and large missing energy, as discussed in Chapter 4.

- **BP3**: For this benchmark we consider a more simplified spectra with only a light higgsino sector where we have decoupled squarks and gauginos by making them ultra heavy and out of reach of the LHC. To achieve this we choose $\mu = 700$ GeV whereas $M_1, M_2 \sim 7$ TeV and $M_3, M_Q \sim 7$ TeV. We have chosen $\tan\beta = 25$ which gives a $BR(\widetilde{\chi}_1^0 \to h\widetilde{G}) \sim 0.45$ and $BR(\widetilde{\chi}_1^0 \to Z\widetilde{G}) \sim 0.55$ as in **BP1**.

- **BP4**: We choose here an overall heavy spectra with a significantly heavier NLSP with $\mu = 2.2$ TeV and with $M_1, M_2 = 2.3$ TeV. This makes the gauginos out of direct reach of LHC but accessible via cascades of strongly produced squarks which are around 2.3 TeV too. This benchmark also ensures a large gaugino-higgsino admixture in the $\widetilde{\chi}_1^0$ as compared to **BP1** which can test the efficacy of our analysis in unravelling the composition of the NLSP.

Finally we also include a benchmark **BP5** similar to **BP1** with a larger branching fraction into the Higgs boson and gravitino mode which would represent the low $\tan\beta$ and negative $\mu$ region of the parameter space. We choose the benchmarks after passing them through the public software `CheckMATE` [194]. Among the searches implemented in `CheckMATE`, stringent constraints come from multijet searches by ATLAS [189]. The benchmark points are generated using the spectrum generator `SPheno-v3.3.6` [120, 121] and shown in Table 5.3.

## 5.6 LHC Signals

We now discuss in detail the possible LHC signals arising in the current scenario with a higgsino-like $\widetilde{\chi}_1^0$ NLSP and keV $\widetilde{G}$ LSP. Strong sector sparticles pair produced at $\sqrt{s} = 13$ TeV LHC cascade down to the $\widetilde{\chi}_1^0$ NLSP along with additional jets arising from the cascade. In situations where the strong sector is not kinematically accessible, it is worthwhile to explore signals from the direct production of the low-lying higgsinos decaying promptly to the NLSP $\widetilde{\chi}_1^0$ which then further decays to a Higgs/$Z$ gauge boson and the $\widetilde{G}$ LSP. As discussed in section 5.3, such a scenario would lead to $hh/hZ/ZZ$ final states with/without extra hard jets arising from the strong sector cascade.

Motivated by the characteristics of a higgsino NLSP spectra, among the multifarious signatures possible we focus on a final state consisting of a Higgs and $Z$ boson along with

| Parameters | **BP1** | **BP2** | **BP3** | **BP4** | **BP5** |
|---|---|---|---|---|---|
| $M_1$ | 2400 | 800 | 7000 | 2300 | 2400 |
| $M_2$ | 2400 | 800 | 7000 | 2300 | 2400 |
| $\mu$ | 800 | 2400 | 700 | 2250 | -800 |
| $\tan\beta$ | 25 | 25 | 25 | 25 | 3.8 |
| $A_t$ | 3200 | 3200 | 100 | 3200 | 3740 |
| $m_A$ | 2500 | 2500 | 2500 | 2500 | 3000 |
| $m_h$ | 125.3 | 125.3 | 127.1 | 124.5 | 122.2 |
| $m_{\widetilde{g}}$ | 2806.4 | 2807.1 | 7271.2 | 2840.1 | 2663.3 |
| $m_{\widetilde{q}_L}$ | 2303.3 | 2300.2 | 7156.4 | 2313.3 | 2280.6 |
| $m_{\widetilde{q}_R}$ | 2302.2 | 2302.5 | 7155.4 | 2312.5 | 2283.7 |
| $m_{\widetilde{t}_1}$ | 2357.5 | 2184.8 | 7057.0 | 2509.1 | 1581.1 |
| $m_{\widetilde{t}_2}$ | 2340.9 | 2370.8 | 7104.0 | 2666.0 | 2271.4 |
| $m_{\widetilde{b}_1}$ | 2260.9 | 2266.4 | 7102.2 | 2583.4 | 2237.5 |
| $m_{\widetilde{b}_2}$ | 2299.0 | 2323.9 | 7129.0 | 2630.3 | 2295.6 |
| $m_{\widetilde{l}_L}$ | 3331.8 | 3326.8 | 7337.2 | 3332.6 | 3329.4 |
| $m_{\widetilde{l}_R}$ | 3335.6 | 3333.7 | 7336.3 | 3336.3 | 3334.1 |
| $m_{\widetilde{\chi}_1^0}$ | 810.9 | 797.9 | 718.8 | 2211.0 | 1214.8 |
| $m_{\widetilde{\chi}_2^0}$ | -814.4 | 837.8 | -723.7 | -2254.8 | -1217.2 |
| $m_{\widetilde{\chi}_1^\pm}$ | 812.5 | 837.9 | 720.9 | 2223.1 | 1216.4 |
| $m_{\widetilde{\chi}_2^\pm}$ | 2415.7 | 2397.3 | 1925.9 | 2350.5 | 2420.9 |
| $m_{\widetilde{\chi}_3^0}$ | 2386.3 | -2394.8 | 1923.6 | 2290.1 | 2392.2 |
| $m_{\widetilde{\chi}_4^0}$ | 2415.6 | 2397.4 | 1925.8 | 2350.5 | 2420.9 |
| $m_{\widetilde{G}}$ (keV) | 1.0 | 1.0 | 1.0 | 1.0 | 1.0 |
| $BR(\widetilde{\chi}_1^0 \to h\widetilde{G})$ | 0.45 | 0.0 | 0.44 | 0.23 | 0.27 |
| $BR(\widetilde{\chi}_1^0 \to Z\widetilde{G})$ | 0.55 | 0.25 | 0.56 | 0.75 | 0.73 |
| $BR(\widetilde{\chi}_1^0 \to \gamma\widetilde{G})$ | 0 | 0.75 | 0 | 0.02 | 0 |
| $BR(\widetilde{\chi}_1^\pm \to W\widetilde{G})$ | 0.024 | 0.0 | 0.003 | 0.0001 | 0.15 |
| $BR(\widetilde{\chi}_1^\pm \to W^*\widetilde{\chi}_1^0)$ | 0.976 | 1.0 | 0.997 | 0.9999 | 0.85 |

Table 5.3: List of benchmarks chosen for our study. Mass parameters are in GeV unless specified otherwise.

large $\not{E}_T$ as the primary signature of such a scenario. Although both Higgs and $Z$ dominantly decay to hadronic final states, (i.e, $BR(h \to b\bar{b}) \sim 0.58$ and $BR(Z \to jj) \sim 0.67$), the corresponding hadronic background would be clearly overwhelming for the all hadronic signal. In addition, to study the characteristic polarization of the $Z$ boson coming from the decay of the NLSP we require an efficient and cleaner mode of reconstruction which can only come through the leptonic decay of the weak gauge boson. We therefore choose a final state that includes atleast one $b$-jet and two same flavour opposite-sign leptons along with $\not{E}_T$. Owing to the presence of leptons in the final state, this is a relatively clean channel to observe at LHC as compared to an all hadronic final state. Since the LSP is a very light $\widetilde{G}$, the ensuing $h/Z$ from the NLSP decay and hence, the $b$-jets and/or leptons have large transverse momentum ($p_T$), thereby leading to a large $\not{E}_T$, where $\vec{\not{E}}_T = -\vec{p}_{T_{vis}}$ (balancing the net transverse momenta, $\vec{p}_{T_{vis}}$ of the visible particles). No specific criteria is imposed on the number of light jets in the scenario as will be present if the signal arises from the decay of the squarks or gluinos to the NLSP. This is because our choice of an inclusive final state signal would be able to highlight the presence of a higgsino-like NLSP irrespective of the rest of the underlying MSSM spectrum, *i.e.* with/without the strong sector placed above the low-lying higgsinos.

## Signal, Background and Event selection criteria

We consider the following SUSY production processes involving the first and second generation squarks as well as the low-lying higgsinos to be pair produced when kinematically accessible:

$$pp \to \widetilde{q}_i\widetilde{q}_j, \widetilde{q}_i\widetilde{q}_j^*, \widetilde{q}_i^*\widetilde{q}_j^*, \widetilde{\chi}_1^0\widetilde{\chi}_2^0, \widetilde{\chi}_1^\pm\widetilde{\chi}_1^0, \widetilde{\chi}_1^\pm\widetilde{\chi}_2^0, \widetilde{\chi}_1^\pm\widetilde{\chi}_1^\pm$$

For a keV $\widetilde{G}$ LSP with substantial mass difference between the NLSP and LSP, the following decay modes are in order:

$$\begin{aligned}
&\widetilde{q} \to q\widetilde{\chi}_1^0, \quad \widetilde{\chi}_1^0 \to h/Z\ \widetilde{G} \\
&\widetilde{q} \to q\widetilde{\chi}_2^0, \quad \widetilde{\chi}_2^0 \to f\bar{f}\widetilde{\chi}_1^0 \\
&\widetilde{q} \to q'\widetilde{\chi}_1^\pm, \quad \widetilde{\chi}_1^\pm \to f\bar{f}'\widetilde{\chi}_1^0
\end{aligned}$$

where $f$and $f'$ refer to the SM fermions. Thus when the signal is generated from the pair production of the strongly interacting sparticles, the final state consists of at least two hard jets in the $hh/hZ/ZZ$ final state along with a pair of invisible gravitinos which contribute to the large $\not{E}_T$. Among the possible combinations of the decay products of $h$ and $Z$, we primarily focus on the $\geq 1b+\ell^+\ell^-$ final state along with $\not{E}_T$. Since the $Z$ decays leptonically, it gives a cleaner channel and better control over the SM backgrounds as compared to a hadronic final state.

We generate the signal events in `Madgraph_v5` [123] using the model UFO files available from `Feynrules` [195]. Subsequently, parton level events are showered and hadronised using `Pythia` [126, 196] and detector simulation is performed using `Delphes` [129]. Jets (including b-jets) are reconstructed using the anti-kT algorithm [132] using `Fastjet` [133] with minimum transverse momentum, $p_T > 20$ GeV within a cone $\Delta R = 0.4$. Charged leptons are reconstructed in a cone of $\Delta R = 0.2$ with a maximum energy deposit in the cone from all other particles limited to 10% of the $p_T$ of the lepton. The significant contributions to the SM background for the given final state come from

- $t\bar{t}$, $(t \to bW^+,\ W^+ \to \ell^+\nu)$
- $hZ+$ jets, $(\ h \to b\bar{b},\ Z \to \ell^+\ell^-)$
- $t\bar{t}Z$, $(\ Z \to \ell^+\ell^-)$
- $ZZ$, $(\ Z \to b\bar{b},\ Z \to \ell^+\ell^-)$
- $W^\pm W^\pm Z$, $(Z \to \ell^+\ell^-)$
- $Zb\bar{b} + \not{E}_T$, $(Z \to \ell^+\ell^-)$

Although the QCD background has a large cross-section, it has negligible contribution to the signal region characterized by large $\not{E}_T$ as well as effective mass, $M_{Eff}$ which helps probe the heavy mass scale of the SUSY particles and would serve as an effective discriminator between the SUSY signal and SM background. For SM background, we have performed showering and hadronisation using `Pythia` [126, 196] and perform `MLM` matching [123] when needed with `QCUT`=20−30 GeV.

## Primary selection criteria

We choose the following basic selection criteria to identify leptons $(e^-, \mu^-)$ and $(b)$-jets in the signal and background:

- The charged leptons are identified with $p_T > 10$ GeV and $|\eta| < 2.5$.

- All reconstructed jets and $b$-jets have $p_T > 30$ GeV and $|\eta| < 2.5$.

- Jets and leptons are isolated with $\Delta R_{ij} > 0.4$ and $\Delta R_{\ell\ell} > 0.2$.

## Signal Analysis

We look at final states with at least one $b$-jet and a pair of opposite-sign same flavour leptons $(e^-, \mu^-)$ along with large $\not{E}_T$ carried away by the LSP. We also veto events with a photon with $p_T > 10$ GeV and $|\eta| < 2.5$. The missing transverse energy, $\not{E}_T = |\vec{p}_{T_{vis}}|$, where $\vec{p}_{T_{vis}} = \sum_j \vec{p}_T(j) + \vec{p}_T(\ell^+) + \vec{p}_T(\ell^-)$ is the net transverse momentum of the signal ($b$)-jets and charged leptons in the final state. Since the NLSP-LSP mass gap is large, the transverse momenta carried by the decay products are large thereby ensuring a large amount of $\not{E}_T$ in the event.

Fig. 5.2 shows the normalized differential distrubution of a few kinematic variables ($M_{Eff}$ and $\not{E}_T$) for **BP1** and **BP4** along with the background. The SUSY signal distributions for the missing transverse energy ($\not{E}_T$) and effective mass ($M_{Eff}$) are widely separated from the SM background for **BP4** in the presence of a heavy NLSP. However the signal events peak at a much lower value $\sim$ 600 GeV for **BP1** while significant events of the signal are found at large $M_{Eff}$ values $\sim$ 2.0 TeV for **BP4**. Note that for **BP4** this is due to the high transverse momentum of the jets, and leptons arising from the decay cascades of the heavy $\mathcal{O}(2)$ TeV range sparticles. However for **BP1** with a light NLSP, there is considerable overlap of the kinematic distributions with the background while differing in the tail of the distribution. This happens because the dominant contribution to the signal comes from the direct production of the light higgsino sector as compared to the strong production cross-section. We break our analysis in two parts to study different scenarios that can present themselves at LHC. The signal from a heavy spectrum of $\mathcal{O}(2)$ TeV including the NLSP, that can only have relevant signal contribution through the production of strongly interacting sparticles at the LHC is optimised using cuts in **Analysis 1** while the signal for relatively lighter electroweakino states being directly accessible at LHC with smaller contributions from the strong sector is analysed in **Analysis 2**. Appropriate cuts on the relevant kinematic variables will be crucial to remove SM background in the subsequent collider analyses to study the two scenarios discussed above.

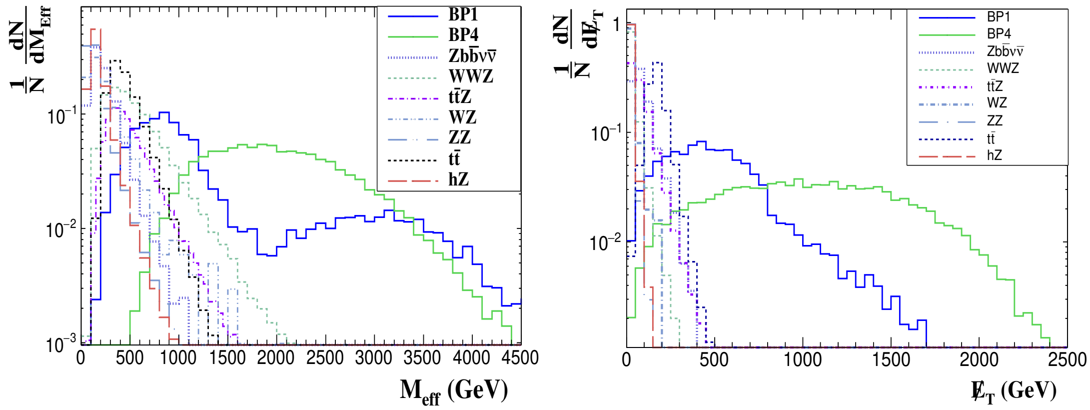


Figure 5.2: Distribution of few useful kinematic variables before application of any selection cuts.

## Analysis 1

As a crucial part of our analysis is dependent on the reconstruction of the $Z$ boson in the events through the dilepton mode, the event rate for the signal will suffer due to the small brancing fraction of the gauge boson to charged leptons. In addition, if we intend to reconstruct the light Higgs boson too using double $b$-tag jets, we will end up restricting our search sensitivity significantly. We therefore need to select events using proper cuts to be able to identify the $Z$ boson as well as imply a Higgs like event. In order to select such a final state we implement the following event selection criterion to retain a significant amount of signal against the SM background:

- **D1**: We select a final state with up to two opposite sign leptons of same flavour ($N_\ell = 2$ with $p_T > 20$ GeV) and at least one $b$-jet with $p_T > 30$ GeV.

- **D2**: To reconstruct the $Z$ boson we demand that the invariant mass of a dilepton pair (opposite-sign same-flavour) in the signal events is within the $Z$ mass window satisfying $76 < M_{\ell^+\ell^-} < 106$ GeV.

Another kinematic variable of importance is the *stransverse* mass $M_{T_2}$ [197]. It is reconstructed using the leading and sub-leading lepton $p_T$ along with $\not{E}_T$. For SM processes such as $t\bar{t}$, $M_{T_2}$ shows an end point value $\sim M_W$, the mass of the $W$ boson decaying leptonically thereby yielding an invisible neutrino. For SUSY processes, the end-point is determined by the mass difference between the NLSP and LSP. For a light keV scale LSP and TeV NLSP, the end-point is large compared to $M_W$ and can serve as an effective discriminator between SUSY signals and the dominant SM background subprocesses.

- **D3**: We demand a cut on the kinematic variable $M_{T_2} > 90$ GeV to remove backgrounds from $t\bar{t}$.

An important kinematic variable is the effective mass, $M_{Eff} = p_T(\ell^+) + p_T(\ell^-) + \not{E}_T + \sum p_{T_i}(j)$, the scalar sum of the transverse momenta of the visible jets, leptons and $\not{E}_T$ in the event. $M_{Eff}$ reflects the mass scale of the heavy SUSY particles and hence is an efficient variable to suppress SM background. However a strong cut on $M_{Eff}$ would choose to retain contributions from a very heavy spectrum and therefore in this case we focus on the benchmarks that contribute mainly through the production of the strong sector sparticles, *viz.* **BP4** and **BP5**. Note that the strong sector for **BP1** is of similar value to **BP4** and **BP5** and therefore the signal rates coming from the strong sector would be very similar. However, as the dominant fraction of signal events would be from the light higgsino production, the cuts given below are not particularly optimised to study **BP1** while **BP3** signal becomes very small. We shall discuss these benchmarks in **Analysis 2**.

- **D4**: Since nearly all the SUSY particles except LSP are very heavy for **BP4** and **BP5**, a large $M_{Eff}$ is expected for the signal over the SM background as shown in Fig. 5.2. We therefore demand a strong cut of $M_{Eff} > 2$ TeV. This cut renders the signal for other benchmarks to a relatively smaller value.

- **D5**: In addition we also put a strong cut on missing transverse energy, $\not{E}_T > 300$ GeV to further remove remaining contributions from SM background processes.

We show the cut-flow result of our analysis for the signal and SM background in Table 5.4. As expected the signal rates coming from a 2 TeV squark sector yields quite small numbers, even with an integrated luminosity of 3000 fb$^{-1}$. The overwhelmingly huge SM background is brought in control by primarily using the $M_{T_2}$ cut and is then rendered negligibly small using the combination of $M_{Eff}$ and $\not{E}_T$ cuts. We find that the sequence of cuts shown in Table 5.4 affects the signal slightly with a suppression of the signal rate of less than 50% for **BP4** and **BP5**. Thus we find a significant number of SUSY signal events surviving the event selection. Note that the relative suppression of events in **BP1** after the cuts is less compared to **BP3**. However the number of events after cuts in **BP1** is still quite large compared to the SM background.

We compute the statistical significance ($\mathcal{S}$) of the above signals using the formula in Chapter 3 Eq. 3.3.1 and show the required integrated luminosities to observe and discover the signal in Table 5.5:

$$\mathcal{S} = \sqrt{2 \times \left[(s+b)\ln(1+\frac{s}{b}) - s\right]}.$$

| Signal | **D1** | **D2** | **D3** | **D4** | **D5** |
|---|---|---|---|---|---|
| **BP1** | 112 | 92 | 81 | 24 | 21 |
| **BP3** | 98 | 83 | 74 | 2 | 2 |
| **BP4** | 15 | 12 | 12 | 10 | 10 |
| **BP5** | 24 | 17 | 15 | 15 | 14 |
| SM Background | **D1** | **D2** | **D3** | **D4** | **D5** |
| $t\bar{t}$ | 365125 | 64968 | 186 | - | - |
| $hZ$ | 29348 | 28360 | 781 | 1.76 | 0.16 |
| $ZZ$ | 178581 | 172636 | 2124 | 15 | 2.3 |
| $t\bar{t}Z$ | 3043.3 | 2111 | 287 | 6.14 | 0.98 |
| $t\bar{t}W$ | 9121 | 1802 | 13.6 | - | - |
| $WWZ$ | 159 | 153 | 13 | 0.65 | 0.074 |
| Total Background | | | | | 3 |

Table 5.4: Number of signal and background events for $\geq 1\ b + \ell^+\ell^- + \not{E}_T$ at $\sqrt{s} = 13$ TeV LHC for $\mathcal{L} = 3000$ fb$^{-1}$ using cuts **D1-D5**. Note that the events have been rounded-off to the nearest integer. Cross-sections for SUSY signals have been scaled using NLO K-factors [134] and wherever available, NLO+NLL K-factors [168]. Cross-sections for SM background processes have been scaled using NLO K-factors [123] and wherever available, NNLO K-factors [198–202] have been used.

where $s$ and $b$ refer to the number of signal and background events respectively. We observe

| Benchmark | $\mathcal{L}$ (in $fb^{-1}$) for $3\sigma$ excess | $\mathcal{L}$ (in $fb^{-1}$) for $5\sigma$ excess |
|---|---|---|
| **BP1** | 508 | 1409 |
| **BP4** | 1647 | 4575 |
| **BP5** | 956 | 2654 |

Table 5.5: Required luminosities for observing the SUSY signal for the different benchmarks at $\sqrt{s} = 13$ TeV LHC run.

that benchmarks **BP4** and **BP5** require large integrated luminosities whereas **BP3** with a decoupled squark sector is out of reach of LHC. Although **BP1** is observable at LHC, the large $M_{Eff}$ cut reduces the contribution from the light higgsino sector which is directly accessible at LHC. Therefore, this analysis is more sensitive to the case of heavier spectra that also includes the NLSP to be quite heavy, such as **BP4** and **BP5**. However with a light higgsino sector and similar squark masses to **BP4** such as in **BP1** we are still able to get a relatively healthy number for the signal albeit after losing a large part of the signal events. A more optimised set of cuts is used in **Analysis 2** to study the scenario with lighter NLSP mass.

Note that for simplicity we have looked at the presence of light squarks in the spectrum. Significant contribution to the signal region under study may also arise in the presence of gluinos from a compressed $\widetilde{qg}$ sector mainly from squark-gluino associated production. The gluinos decay via the NLSP leading to a large number of b-jets in the final state besides the contribution from the NLSP decay to the LSP. Since we have studied an inclusive final state, $\geq 1b + \ell^+\ell^- + \not{E}_T$, the contribution from the gluino will enhance the SUSY signal cross-section. We also comment on the prospect of multijet searches as discovery channels for our scenario. Using the SM backgrounds of the multijet analyses [189] we estimate the reach of the squark masses to be 2.78 TeV to achieve a $5\sigma$ discovery at an integrated luminosity of 3000 fb$^{-1}$ at LHC. For such heavy spectra the final state channel of $\geq 1b + \ell^+\ell^- + \not{E}_T$ would not be within the LHC reach and therefore multijet channel would be the best discovery channel.

## Analysis 2

We now focus on the signal contribution arising dominantly from the electroweak sector of sparticles with/without the strong sector when accessible, as for benchmark **BP1** and **BP3**. Since the electroweakino sector is lighter, a strong cut on $M_{Eff}$ as used in **D4** will deplete the signal significantly in this case. Therefore, we employ a different set of cuts for investigating the signal region $\geq 1\ b + \ell^+\ell^- + \not{E}_T$ arising from the low-lying higgsino sector. We consider the contributions from the electroweak sector in addition to the strong sector for the benchmarks in our study when they are kinematically accessible and study the benchmarks **BP1** and **BP3**. The following cuts are implemented on both signal and background:

- **E1**: As in **Analysis 1**, we select a final state with up to two opposite sign leptons of same flavour ($N_\ell = 2$ with $p_T > 20$ GeV) and atleast one $b$-jet with $p_T > 30$ GeV.

- **E2**: To reconstruct the $Z$ boson we demand that the invariant mass of the dilepton pair in the signal events is within the $Z$ mass window satisfying $76 < M_{\ell^+\ell^-} < 106$ GeV.

- **E3**: As before, $M_{T_2}$ is an efficient cut to reduce background contributions from $t\bar{t}$ to the signal region. We demand a slightly stronger cut of $M_{T_2} > 120$ GeV in this case as it helps improve the signal-to-background ratio.

- **E4**: The large mass scales of SUSY particles again lead to a higher $M_{Eff}$ as compared to the backgrounds. Since $\mu \sim 700-800$ GeV, $M_{Eff} > 300$ GeV helps reduce background dominantly compared to signal.

- **E5**: The SUSY signal has a larger $\not{E}_T$ as compared to the SM background. Hence $\not{E}_T > 300$ GeV cut helps reduce a significant part of the remnant contributions from SM background.

The cut-flow table for the signal and SM background are as shown in Table 5.6. Since the higgsinos, with masses in the range $\mu = 700 - 800$ GeV are rather light compared to the heavy squarks, a large cut on variables such as $M_{Eff} \sim 2$ TeV is quite ineffective to search for a spectrum with a lighter higgsino sector since the signal will be depleted significantly. Therefore, in this case we rely on a much relaxed cuts on $M_{Eff}$ and a slightly stronger cut on $M_{T_2}$ to ensure substantial removal of the $t\bar{t}$ background while retaining the signal events. However other background contributions remain with a softer $M_{Eff}$ cut such as that from $Zb\bar{b} + \not{E}_T$. This still gives a significantly large event rate for the signal as compared to **Analysis 1** and thereby allowing a $\sim 8.6\,(10)\sigma$ discovery possible with $\mathcal{L} = 3000\ fb^{-1}$. Since both the benchmarks have similar branching fractions into the $Z$ and Higgs mode, the difference in the required integrated luminosity is primarily owing to the fact that the NLSP mass is heavier in **BP1** than in **BP3**. The required luminosity for observing a $3\sigma$ and $5\sigma$ significance at LHC are shown Table 5.7. We conclude that both **BP1** and **BP3** are well within the discovery reach of the high luminosity run of LHC.

We now are set to study the efficacy of the signal that we have analysed to identify the nature of the NLSP and its inherent composition with respect to the gaugino-higgsino admixture in the following section.

| **BP1** | **E1** | **E2** | **E3** | **E4** | **E5** |
|---|---|---|---|---|---|
| $\widetilde{\chi}_1^{\pm}\widetilde{\chi}_1^{\mp}$ | 16 | 13 | 11 | 11 | 9 |
| $\widetilde{\chi}_1^{\pm}\widetilde{\chi}_{1/2}^0$ | 65 | 54 | 47 | 47 | 36 |
| $\widetilde{\chi}_2^0\widetilde{\chi}_1^0$ | 16 | 14 | 12 | 12 | 9 |
| $\widetilde{q}\widetilde{q}$ | 30 | 24 | 19 | 19 | 18 |
| Total | | | | | 73 |
| **BP3** | **E1** | **E2** | **E3** | **E4** | **E5** |
| $\widetilde{\chi}_1^{\pm}\widetilde{\chi}_1^{\mp}$ | 33 | 27 | 24 | 24 | 18 |
| $\widetilde{\chi}_1^{\pm}\widetilde{\chi}_{1/2}^0$ | 126 | 107 | 87 | 87 | 65 |
| $\widetilde{\chi}_2^0\widetilde{\chi}_1^0$ | 33 | 28 | 24 | 24 | 18 |
| Total | | | | | 101 |
| **SM Background** | **E1** | **E2** | **E3** | **E4** | **E5** |
| $t\bar{t}$ | 365125 | 64968 | - | - | - |
| $hZ$ | 29348 | 28360 | 298 | 298 | 0.67 |
| $ZZ$ | 178581 | 172636 | 774 | 774 | 6.61 |
| $t\bar{t}Z$ | 3043 | 2111 | 151 | 151 | 8.6 |
| $t\bar{t}W$ | 9121 | 1802 | 1 | 1 | - |
| $WWZ$ | 159 | 153 | 6 | 6 | 0.23 |
| $Zb\bar{b} + \not{E}_T$ | 2933 | 2905 | 312 | 311 | 34.7 |
| Total | | | | | 51 |

Table 5.6: Number of signal and background events for $\geq 1\ b + \ell^+\ell^- + \not{E}_T$ at $\sqrt{s} = 13$ TeV LHC for $\mathcal{L} = 3000$ fb$^{-1}$ using cuts **E1-E5**. Note that the events have been rounded-off to the nearest integer. Cross-sections for SUSY signals have been scaled using NLO K-factors [134] and wherever available, NLO+NLL K-factors [168]. Cross-sections for SM background processes have been scaled using NLO K-factors [123] and wherever available, NNLO K-factors [198–202] have been used.

| Benchmark | $\mathcal{L}$ (in $fb^{-1}$) for $3\sigma$ excess | $\mathcal{L}$ (in $fb^{-1}$) for $5\sigma$ excess |
|---|---|---|
| **BP1** | 373 | 1034 |
| **BP3** | 208 | 577 |

Table 5.7: Required luminosities for observing the SUSY signal for the different benchmarks at $\sqrt{s} = 13$ TeV LHC run.

## 5.7 A Distinguishing Feature: Longitudinal vs Transverse Gauge bosons

The Goldstone boson equivalence theorem states that, at very high energies, i.e, $\sqrt{s} >> M_V$, (where $V = W^{\pm}, Z$), the longitudinal components of the weak gauge bosons can be approximated by the corresponding Goldstone bosons (with corrections up to factors $\frac{M_V}{E_V}$,where mass $M_V$ and energy $E_V$ are the mass and energy of the gauge bosons respectively). In this limit, $W^{\pm}, Z$ bosons are primarily produced in the transverse polarised state for SM processes. This is because for SM gauge bosons, couplings of the longitudinal modes are suppressed by factors $M_V/E_V$ at high energies (since $E_V >> M_V$ for $V = W^{\pm}, Z$). However vector bosons arising from decay of heavy particles (say, $X$ where $X$ may be a heavy Higgs, or heavy gauge boson or heavy fermion) have enhanced couplings of the longitudinal mode by factors $(M_X/M_W)^2$ [203]. Therefore distinguishing the properties of longitudinal gauge bosons from SM processes giving rise to dominantly transverse gauge bosons is a clear signature of Beyond Standard Model (BSM) scenarios.

After electroweak symmetry breaking, the three massless Goldstone bosons are absorbed by the $W^{\pm}$ and $Z$ bosons contributing to their longitudinal modes. The other five degrees of freedom form the physical Higgs bosons: $h$, $H$, $A^0$ and $H^{\pm}$. From section 5.3, we observe that there exists a substantial parameter space where the decay of the higgsino into a $Z$ and gravitino is comparable to the decay branching into a Higgs and gravitino as also discussed in earlier works [170, 171]. Since the Goldstone boson from the Higgs doublet (which obtains a *vev* after electroweak symmetry breaking) is responsible for the longitudinal component of the $Z$ boson, a higgsino-like NLSP decays predominantly to a longitudinally polarised $Z$ boson. This is evident from Eq. 5.3, where for a higgsino-like NLSP, $|N_{13}|, |N_{14}| >> |N_{11}|, |N_{12}|$. The higgsino fractions thus drive the $\widetilde{\chi}_1^0 \to Z\widetilde{G}$ decay, where $Z$ is dominated by the neutral Goldstone boson. It is important to note that the polarisation information of such a $Z$

boson can be a signature for the presence of a higgsino-like $\widetilde{\chi}_1^0$. Conversely, for a gaugino-like NLSP (a photino or zino-like) $\widetilde{\chi}_1^0$ NLSP, $|N_{11}|, |N_{12}| >> |N_{13}|, |N_{14}|$, thereby leading to a dominantly transverse $Z$ boson being produced from the NLSP decay. Thus, the polarisation of the $Z$ boson could be an efficient discriminator between a higgsino-like and gaugino-like NLSP.

Although our focus is on the polarisation of $Z$ boson in the context of SUSY in this work, the polarisation information of vector bosons may be extremely useful even for non-SUSY scenarios where a polarised gauge boson is likely to be produced from the decay of a heavy particle. Thus, the features of the longitudinal Z boson which will be discussed in detail in this work are also applicable for other scenarios as well. For example, the presence of longitudinal gauge bosons from heavy Higgs decays have been studied in earlier works in the context of Tevatron [204]. LHC analyses have also looked at features of longitudinal gauge bosons in the SM [205]. In case an excess over SM is observed, it is of crucial importance to extend current search strategies to characterize BSM scenarios by studying variables sensitive to the polarisation information of the gauge bosons via their decay products. Although there have been several studies in the context of $e^+e^-$ colliders focusing on studies of polarisations of the incoming electron-positron beams or polarisation of the final state particles, there are few analogous studies with respect to the LHC utilising these techniques [206]. The polarisation of a $Z$ boson has been studied briefly in [206] with respect to the LHC in a similar scenario however in displaced dilepton final states arising from the $Z$ boson decay using the angular variable $\cos\theta^*$ discussed below. We discuss analytically some basic variables found in the literature, which distinguish longitudinal and transverse gauge bosons. The differential decay rates for the transversely polarized and longitudinally polarized $Z$ boson in the rest frame of $Z$ boson are [204]:

$$\frac{d\Gamma_T}{d\cos\,\theta^*} \propto (1 \pm \cos\,\theta^*)^2 \tag{5.7.1}$$

$$\frac{d\Gamma_L}{dcos\,\theta^*} \propto \sin^2\,\theta^* \tag{5.7.2}$$

where $\Gamma_T = \Gamma(\widetilde{\chi}_1^0 \to Z_T\,\widetilde{G})$ and $\Gamma_L = \Gamma(\widetilde{\chi}_1^0 \to Z_L\,\widetilde{G})$ are the partial decay widths of the $\widetilde{\chi}_1^0$ to a transverse $Z$ boson ($Z_T$) and longitudinal $Z$ ($Z_L$) boson respectively. The angle $\theta^*$ is defined as the angle the outgoing lepton (arising from the $Z$ boson decay) makes with the $Z$ boson in its rest frame with the reference direction being the boost direction of the $Z$ boson in the laboratory frame. The dependence of the decay width, *i.e.* $(1 \pm cos\,\theta^*)^2$ corresponds to $k = \mp 1$ state and $\sin^2\,\theta^*$ corresponds to $k = 0$ state, where $k$ is the helicity of the $Z$

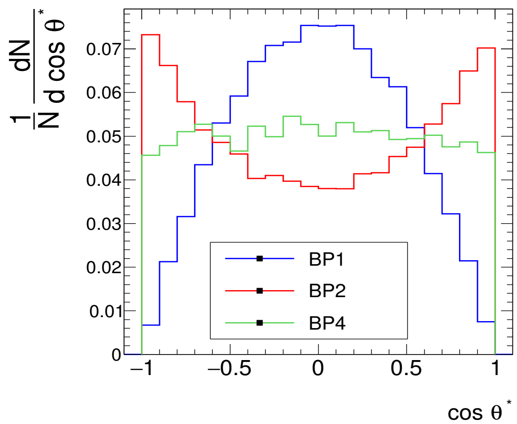


Figure 5.3: Normalized distribution of $\cos\theta^*$ of the negatively charged lepton ($\ell^-$) arising from the $\widetilde{\chi}_1^0$ NLSP decay at rest corresponding to the benchmarks **BP1**, **BP2** and **BP4** with the isolation variable $\Delta R > 0.2$ for the leptons.

boson. To highlight the difference we choose the NLSP from a few of the benchmarks we had chosen for our analysis and generate a normalized distribution for cos $\theta^*$ where the NLSP is decaying at rest and gives the $Z$ boson as its decay product. The simple illustration of this reconstruction is shown in Fig. 5.3 where **BP1** represents a dominantly higgsino-like NLSP, **BP2** represents a dominantly gaugino-like NLSP while **BP4** represents a somewhat democratic admixture of higgsinos and gauginos in the NLSP.

We now go ahead and consider the full analysis for the signal $\geq 1\,b + \ell^+\ell^- + \not{E}_T$ and focus on the negatively charged lepton. Note that we expect the nature of the NLSP as highlighted in Fig. 5.3 for the $Z$ polarisation to be robust against the energy smearings in the detector and the full detector simulation. To show this we compare both parton-level analysis to the signal events obtained after detector simulations. We plot the normalized distributions for $\cos\theta^*$ of the negatively charged daughter lepton of the $Z$ boson in Fig. 5.4 at the parton level (left) and detector level (right-panel) for our benchmarks **BP1**, **BP2** and **BP4** where one NLSP decays to a $Z$ boson along with a $\widetilde{G}$. Recall, **BP1** a purely higgsino-like NLSP ($\sim 99\%$), **BP2** purely gaugino-like NLSP ($\sim 100\%$) and **BP4** has $\sim 31\%$ gaugino admixture in the NLSP. Note that charge identification of the lepton ($\ell^-$) is important in determining the polarisation information of the parent $Z$ boson. We observe in Fig. 5.4 that the distributions for the negatively charged lepton (for **BP1** and **BP2**) bear significant resemblance at both parton and detector level simulations, to the expected distributions as shown in Fig. 5.3 and follows Eq 5.7.1 and Eq. 5.7.2 for the longitudinally polarised $Z$ boson

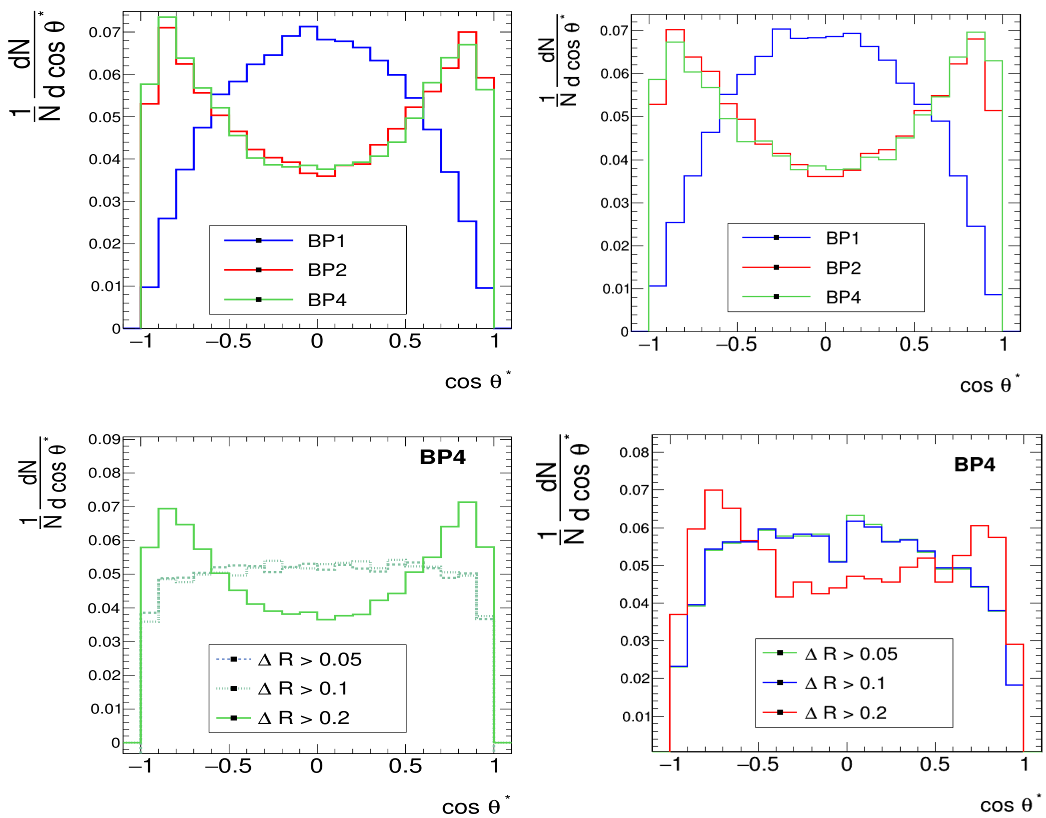


Figure 5.4: Normalized distribution of $\cos\theta^*$ of the negatively charged lepton ($\ell^-$) arising from the $\widetilde{\chi}_1^0$ NLSP at the parton level (top left panel) and after detector simulation (top right panel) using **Analysis 1**, corresponding to the benchmarks **BP1**, **BP2** and **BP4**. In the bottom panel we present the plots for **BP4** at the parton level (left) and at the detector level (right) for various $\Delta R$ values as discussed in the text.

($\cos\,\theta^* = 0$) and the transversely polarised $Z$ boson ($\cos\,\theta^* = \pm 1$). For **BP4** where the NLSP is a more democratic superposition of the higgsino and gaugino states, owing to the presence of a considerable fraction of gaugino admixture in the NLSP gives rise to a slightly flat and broad peak for $\cos\,\theta^*$ in Fig. 5.3. In addition, the NLSP mass is around 2 TeV which results in a very boosted $Z$ boson in the final state. The event selection criteria can in principle have adverse effects in this case and modify the distributions. The most notable effect for **BP4** that we find is that the distribution starts to resemble features similar to the gaugino-like NLSP (**BP2**) at both parton and detector-level simulations. This we find is due to the fact that when the $Z$ boson is highly boosted, the pair of charged leptons coming from the $Z$ boson decay get more collimated with a very small opening angle. This in turn would mean that a larger isolation requirement for the charged leptons would lead to loss of events and also affect the cos $\theta^*$ distribution. Note that in our analysis we have used the default Delphes card using a small cone radius $R = 0.2$ and a maximum energy deposit in the cone being 10% of the $p_T$ of the lepton as used for electron identification. An isolation cut on $\Delta R > 0.2$ when used seems to reduce the peak of the cos $\theta^*$ plot due to the leptons getting rejected under the isolation cut. To counter this, for **BP4** we find that a much loose lepton identification criterion can be useful for our purpose. To highlight this we identify the charged leptons with a much larger cone radius of $R = 0.5$ for lepton identification and also demand that a large energy deposit with respect to the $p_T$ of the lepton is allowed in the cone ($\sim$ 12% for electrons and 25% for muons). The distribution still retains the gaugino-like behaviour for an isolation of $\Delta R > 0.2$ as in the parton level but starts agreeing with the higgsino-like feature (as in the parton-level case) when the separation between the charged leptons is chosen to be loose with $\Delta R > 0.05$ or $\Delta R > 0.1$ as can be seen in the bottom-right panel of Fig. 5.4.

The qualitative differences observed in the distributions of the negatively charged lepton as the gaugino admixture increases in the NLSP amongst the three cases may be effectively captured by defining asymmetry variables in $\cos\theta^*$ which could clearly discriminate between a dominantly longitudinal and dominantly transverse $Z$ boson. Taking a cue from the features of $\cos\theta^*$, we construct a variable which enhances this difference through an asymmetry amongst the observed $\cos\theta^*$ values for the higgsino-like and gaugino-like NLSP. The asymmetry variable, $C_{\theta_Z}$, as defined in Eq. 5.7.3, serves to enhance the features of the longitudinally polarised $Z$ boson in comparison to the transversely polarised $Z$ boson such that they would be less affected if detector simulation effects smear the polarisation dependence of the angular or energy observables. We define

$$C_{\theta_Z} = \frac{N_A - N_B - N_C}{N_A + N_B + N_C} \tag{5.7.3}$$

where $N_I$'s stand for events whereas the subscript $I = A, B, C$ represent the angular regions in $\theta^*$ given by $A = [\pi/3, 2\pi/3]$, $B = [0, \pi/3]$ and $C = [2\pi/3, \pi]$. The numerator focuses only on the asymmetry features while the denominator is the total number of events for $-1 < \cos\theta^* < 1$. Based on the construction of $C_{\theta_Z}$ a positive value is indicative of a higgsino-like NLSP whereas negative values indicate a gaugino-like NLSP. Since $C_{\theta_Z}$ is the normalised difference in the number of events corresponding to $|\cos\theta^*| < 0.5$ and $|\cos\theta^*| > 0.5$, a higgsino-like NLSP which gives larger events around $\cos\theta^* = 0$, $N_A > (N_B + N_C)$ whereas for the gaugino-like NLSP the distribution peaks around $\cos\theta^* \sim \pm 0.8$ *i.e.* $(N_B + N_C) > N_A$. Therefore the latter shows a negative sign as compared to the former. We list the values

| Benchmark | $m_{\widetilde{\chi}_1^0}$ (GeV) | higgsino admixture (%) | Gaugino admixture (%) | $C_{\theta_Z}^{\text{rest}}$ | $C_{\theta_Z}^{\text{parton}}$ | $C_{\theta_Z}$ | $C_Z$ |
|---|---|---|---|---|---|---|---|
| **BP1** | 810.9 | 99.83 | 0.17 | 0.378 | 0.332 | 0.346 | 0.377 |
| | 1606.4 | 99.35 | 0.65 | 0.368 | 0.268 | 0.286 | 0.279 |
| | 1995.8 | 97.58 | 2.42 | 0.19 | 0.120 | 0.198 | 0.169 |
| **BP4** | 2211.0 | 68.31 | 31.69 | 0.021 | -0.309 | -0.214 | -0.209 |
| **BP2** | 797.9 | 0.05 | 99.95 | -0.18 | -0.078 | -0.054 | -0.025 |

Table 5.8: Variation of the asymmetry variables $C_{\theta_Z}^{\text{rest}}$, $C_{\theta_Z}^{\text{parton}}$, $C_{\theta_Z}$ and $C_Z$ as defined in the text, at the parton-level and detector level after cuts **D1-D5** for benchmarks **BP1**, **BP2**, **BP4** and some intermediate points with different gaugino-higgsino admixture.

of $C_{\theta_Z}$ for cases when the NLSP decays at rest ($C_{\theta_Z}^{\text{rest}}$) and compare this with parton-level ($C_{\theta_Z}^{\text{parton}}$) results and full detector-level simulation ($C_{\theta_Z}$) of our **Analysis 1** in Table 5.8 for the benchmarks **BP1**, **BP2** and **BP4**. We also include results for a few intermediate points with varying NLSP mass and compositions, after the selection cuts **D1-D5** are applied.[5]

Note that the values of $C_{\theta_Z}$ are in good agreement with the parton level $C_{\theta_Z}^{\text{parton}}$ results, from squark pair production. They also agree to almost all results from the NLSP decaying at rest as discussed in Fig. 5.3 with slight variations arising due to isolation cuts and smearing effects at the detector level, except for **BP4**. At the parton level, $C_{\theta_Z}^{\text{parton}}$ values range from [-0.08 : 0.33] as one varies the gaugino-higgsino admixture in the NLSP. For the pure higgsino-like NLSP (**BP1**), $C_{\theta_Z}$ is large and positive owing to the large higgsino-fraction in the NLSP whereas the pure gaugino-like NLSP **BP2** shows a negative value. For **BP1**, $C_{\theta_Z}$ is large and positive with the value decreasing as the gaugino admixture starts increasing. We illustrate this variation upon choosing a similar benchmark as **BP1** differing in the choice of $\mu$ ranging from 1.6 - 1.8 TeV to illustrate this effect. As one considers a dominantly gaugino-like NLSP as in **BP2**, $C_{\theta_Z}$ turns negative. Thus, with increasing gaugino admixture, the asymmetry value is negative and may be used as an estimate to determine the composition of the NLSP. The detector level estimates for $C_{\theta_Z}$ are similar to their parton level estimates. The most notable change is observed for the **BP4** with an intermediate gaugino-higgsino admixture. $C_{\theta_Z}$ value is $\sim 0.021$ when the NLSP decays at rest with the

[5]The results in Table 5.8 are produced by using only squark pair production. However the generic feature remains unchanged even when all production modes are included.

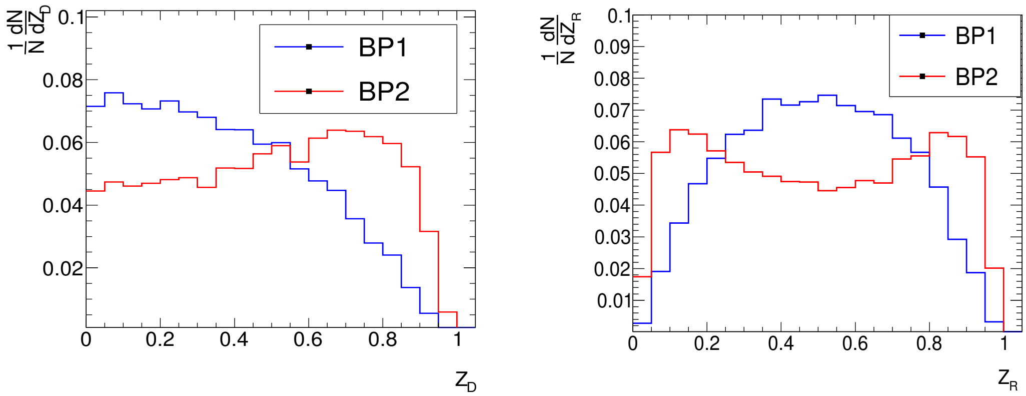


Figure 5.5: Normalized distributions of the kinematic variables $Z_D$ and $Z_R$ as defined in the text for distinguishing between a higgsino and gaugino-like $\widetilde{\chi}_1^0$ NLSP before cuts **D1-D5** The variables are as defined in the text. Here, we have plotted the observables for the process $\widetilde{q}\widetilde{q}$ with one of the squarks decaying as: $\widetilde{q} \to q\widetilde{\chi}_1^0 \to qZ\widetilde{G}, Z \to \ell^+\ell^-$.

small positive value still hinting at a larger higgsino admixture. However it turns negative for the analysis where the NLSP appears from cascade decays of the squark, both at the parton and the detector level owing largely to the effect of isolation cuts and detector smearing effects which modify the $\cos\theta^*$ distribution as seen in Fig 5.4 and discussed earlier. We note that the $C_{\theta_Z}^{\rm parton}$ value becomes positive giving $C_{\theta_Z}^{\rm parton} = 0.04, 0.05$ for the loose isolation requirement and identification of the charged lepton with $\Delta R > 0.05, 0.1$ as expected from Fig. 5.4 as against $C_{\theta_Z}^{\rm parton} = -0.214$ for the tighter isolation cut of $\Delta R > 0.2$. We expect that the same would be true when the events are passed through detector simulations which would be consistent with observations made in the lower panels of Fig. 5.4.

It is worth pointing out here that **BP4** has a very heavy higgsino NLSP, and the equivalence theorem [203] suggests that the couplings of the longitudinal mode are enhanced as the mass of the NLSP increases (which ensures a large fraction of the longitudinal polarisation mode in the $Z$ boson), the asymmetry variable is expected to capture this effect as one increases the mass of the NLSP. However, as the mass splitting becomes too large the $Z$ boson gets more boosted which makes the opening angle between the charged lepton pair very small leading to reduction of isolated dilepton events. Thus the asymmetry values in Table 5.8 for the heavier NLSP values are unable to reflect this feature.

An additional kinematic feature that can be used to study the polarisation of the $Z$ boson which in effect highlights the composition of the NLSP is the charged lepton energy. Among others, the ratio of the energy carried by the charged lepton and antilepton also show a dependence on the polarisation of the $Z$ boson with an energy $E$, via dependence on the angle $\theta^*$. The energy ($E_\ell$) of the leptons emitted at an angle $\theta^*$ with respect to the boost direction $\beta$ of the $Z$ boson in the laboratory frame [204] follows:

$$E_\ell \propto \frac{E}{2}(1 \pm \beta \cos\theta^*) \tag{5.7.4}$$

Using this we define two kinematic variables $Z_D$ and $Z_R$ (variations of such variables have been pointed out in earlier papers [207, 208] using jet substructure to study hadronic final states) :

$$Z_D = (E_{\ell^-} - E_{\ell^+})/(E_{\ell^-} + E_{\ell^+}); \qquad\qquad Z_R = E_{\ell_-}/(E_{\ell^-} + E_{\ell^+}) \tag{5.7.5}$$

We study the feasibility of these variables using simple cuts on kinematic variables and ascertain their efficacy after detector simulation effects are taken into account. Note that the energies of the leptons from $Z$ decay also carry the information of the polarisation of the parent. For a predominantly longitudinal $Z$ boson, there is an equal sharing of energy of the parent among its daughter particles whereas for a transverse $Z$ boson, the energy sharing is unequal. The asymmetry is evident in Fig 5.5 where the higgsino-like NLSP peaks at $Z_D = 0.1$ as compared to $Z_D = 0.8$ for the gaugino-like case. Similar effects are observed in the variable $Z_R$ which denotes the fraction of net leptonic energy carried away by the negatively charged lepton. The ratio peaks at $Z_R \simeq 0.5$ for **BP1** as compared to $Z_R \simeq 0.1$ and $Z_R \simeq 0.8$ for the **BP2** since for the former case, the leptons mostly have equal energy sharing whereas unequal energy sharing occurs for the latter case. We define an asymmetry variable similar to $C_{\theta_Z}$, now referred to as $C_Z$ to capture the asymmetry in the values of $Z_D$ at the detector level.

$$C_Z = \frac{N_A - N_B}{N_A + N_B} \tag{5.7.6}$$

where $N_A$ refers to the number of events for $Z_D < 0.5$ and $N_B$ represents events for $Z_D > 0.5$ respectively. We list the $C_Z$ values in Table 5.8 and observe that $C_Z$ is positive for the higgsino-like NLSP and negative for gaugino-like NLSP. Note that the effect observed for the highly boosted $Z$ boson in $C_{\theta_Z}$ also shows up for $C_Z$ highlighting the consistency and importance of the isolation of the charged leptons.

Therefore we emphasise that the distribution of $\cos\theta^*$ using charge identification of the leptons arising from the $Z$ boson decay as well as the associated asymmetry variables, $C_{\theta_Z}$ and $C_Z$ prove quite efficient in identifying the nature of the NLSP. The distinctive features of the variables discussed for distinguishing a longitudinal and transversely polarised $Z$ boson are also applicable for new physics scenarios where a polarised gauge boson is likely to be produced, and therefore can prove very important in studying BSM physics.

## 5.8 Summary and Conclusions

In this work, we have considered higgsino-like $\widetilde{\chi}_1^0$ NLSP in the presence of a light keV $\widetilde{G}$ LSP in the framework of phenomenological MSSM. The keV scale $\widetilde{G}$ serves as a warm dark matter candidate, significantly relaxing constraints from dark matter searches on the MSSM spectra and thereby allowing low $\mu$ parameter values. In addition, presence of a light $\widetilde{G}$ allows decay of $\widetilde{\chi}_1^0$ NLSP to a Higgs/$Z$ boson and $\widetilde{G}$ leading to hard $b$-jets and charged leptons in the final state along with large $\not{E}_T$ carried away by the $\widetilde{G}$. Such a scenario has been extensively explored by experiments, including the LHC with primary focus on the low-lying electroweak sector, leading to stringent constraints on the parameter space. The question that one ventures to answer in this study is as follows: *What are the future prospects of detecting a higgsino-like $\widetilde{\chi}_1^0$ NLSP at LHC? If detected, how can we ascertain the nature of the NLSP?*

We address this question by studying a specific final state: $\geq 1b + \ell^+\ell^- + \not{E}_T$ at $\sqrt{s} = 13$ TeV motivated by the presence of at least a couple of $b$-jets from the Higgs and an opposite-sign same flavour lepton pair from $Z$ boson decay besides large $\not{E}_T$. We choose a few representative benchmark points encompassing a light and heavy higgsino sector with/without strong sector sparticles within the reach of LHC. We find that such a signal is discoverable in the upcoming runs of the high luminosity LHC after suitable cuts are applied. It is important to emphasise that such a semi-leptonic channel will prove crucial in identifying the nature of the NLSP, being relatively clean compared to an all hadronic final state which may have a better discovery prospect since the semi-leptonic channel has a lower branching fraction. Thus simultaneous use of both channels could be advocated for the purpose of discovery and identifying the nature of the NLSP. We focus on the presence of a dominantly longitudinal $Z$ boson arising from the decay of a higgsino-like $\widetilde{\chi}_1^0$ owing to the presence of the Goldstone boson as the longitudinal mode of $Z$ after electroweak symmetry breaking. This is quite a striking identification criteria if observable for a higgsino-like NLSP in sharp contrast to a dominantly gaugino-like NLSP, which would dominantly decay to a transversely polarised $Z$. It is thus important to characterise the features of the longitudinally polarised $Z$ boson to ascertain the composition of the parent $\widetilde{\chi}_1^0$. The effects of polarisation of the $Z$ boson are carried by its decay products, namely, the leptons through their angular distributions. We construct several kinematic variables using the negatively charged lepton as reference and highlight its importance in observing the polarisation of the parent gauge boson. We also propose new variables which utilise the observed asymmetries between the angular variables for the charged lepton coming from a parent longitudinal and transverse $Z$ boson. We do a full detector level simulation of the events and study the asymmetries that show the characteristic features of a longitudinal $Z$ boson and observe substantial differences between a higgsino and gaugino-like NLSP, which highlights the robustness of the constructed asymmetries. Our analysis is equally applicable to other BSM scenarios and will prove useful in studying scenarios which project out the longitudinal nature of the weak gauge bosons and in the process highlight the veracity of the equivalence theorem in a relatively nonchalant way.

# Chapter 6

# Light Higgsinos at LHC with Right-Sneutrino LSP

## 6.1 Introduction

The TeV scale limits from LHC searches on the masses of strongly interacting supersymmetric particles have already set a dismal tone for naturalness concerns, a prime motivation for invoking SUSY in particle physics studies. While several studies in the literature attempt to quantify "naturalness" in a supersymmetric scenario, the interpretation and the measure of naturalness are often debated [174, 176, 209–212]. Nevertheless, in minimal supersymmetric extensions of the standard model (MSSM), a small value of the higgsino mass parameter $\mu$ and light stop squarks and gluinos ($\lesssim$ 1.5 TeV) [174–177, 209–212] remain desirable in "natural" scenarios at the electro-weak (EW) scale. However, even with not-so-light strong sector [213, 214], "natural" scenarios without much fine-tuning is possible impressing the fact that low $|\mu|$ is of more essence to the "natural" scenarios at EW scale.

While the constraints on stop squarks and gluinos are rather stringent due to their large production cross-section at the LHC, the weakly interacting sector with rather light electroweakinos in general, and higgsinos in particular, remain viable [215, 216]. There have been several analyses on light electroweakinos, assuming a simplified spectra with one or more specific decay channels [217–230]. Further, the constraints on the mass of the light higgsino-like states have been studied in detail because of their importance in a "natural" supersymmetric scenario [178, 223, 231–236]. However, note that these analyses assume the lightest neutralino as the LSP. In scenarios with conserved R-parity, the search strategies, and therefore the limits of various sparticle masses, depend on the nature of the LSP. This is because in such scenarios the LSP appears at the end of the decay chain of each sparticle, therefore dictating the possible search channels. This warrants investigation of supersymmetric scenarios with different types of LSP. While within the paradigm of the MSSM, the lightest neutralino is the LSP, and most supersymmetric searches are based on the same assumption. There have been studies with gravitino LSP, discussing implications on cosmology and signatures at the LHC [9, 67, 69, 158, 237–252]. In other simple extensions, axion and/or axino as the LSP [253–257] and right-sneutrino LSP have also been considered in minimal extensions of the MSSM [54–57, 61–63, 258–263]. While the former sets out to resolve the strong CP-problem, the latter provides a weak-scale solution to the neutrino mass generation issue, an important aspect missing in the MSSM.

In the same spirit as we have discussed in Chapter 4 and 5 that the study of alternate DM candidates opens up an avenue to study new signals of discovery for the MSSM spectra, we venture into an extension of the MSSM with a right-sneutrino as the LSP instead of a light gravitino. Note that while the presence of a light gravitino as the LSP serves to incorporate gravity in SUSY, the presence of a right-sneutrino in the spectrum incorporates masses for active neutrinos. Recall from our discussion in Chapter 2, Section 2.4, the MSSM in its minimal form does not explain light neutrino masses although simple extensions to the MSSM including right-sneutrino superfields resolve this issue and also accommodate a right-sneutrino as the LSP. For the former case, we look into hadronic and photonic signals as studied in Chapters 4 and 5 while in the latter case multileptonic channels dominate.

In this chapter, based on [11], we consider an extension to the MSSM with three generations of right-neutrino superfields. This scenario, which provides a weak-scale solution to the neutrino mass generation issue, has been widely studied in supersymmetric extensions. While the left-sneutrinos have been ruled out as a DM candidate long ago, thanks to the stringent limit from direct detection experiments (and also relic density constraints) [58], right-sneutrinos continue to be widely studied as a candidate for DM in simple extensions of the MSSM [55–57, 60–62, 258, 260, 261, 264]. In its simplest incarnation as ours, the right-sneutrinos at EW scale remain very weakly interacting, thanks to the small Yukawa coupling $\mathcal{O}(10^{-6}-10^{-7})$ determining their coupling strength to other particles. However, as in the case of charged sfermions, a rather large value of the corresponding trilinear soft supersymmtry breaking parameter can induce significant left-admixture in a dominantly right-sneutrino and therefore can substantially increase the interaction strengths [60, 61, 261]. In both of these scenarios, DM aspects as well as search strategies at LHC have been studied for certain choices of the SUSY spectra [259, 265–271].

We note that in the light of "naturalness", it becomes equally important to investigate the supersymmetric spectrum in such a scenario. In particular we focus on a minimalistic spectrum, motivated by "naturalness" at the EW scale, with light higgsino-like states and a right-sneutrino LSP. However, analysing collider signatures from the third generation squarks and gluinos will be beyond the scope of the present work and will be addressed in a subsequent extension. For the present case, the strongly interacting sparticles have been assumed to be very heavy adhering to the "naturalness" scheme proposed in Ref. [213, 214]. Further, we will also assume the gaugino mass parameters to be large enough ($\gtrsim \mathcal{O}(1)$ TeV). Thus the light electroweakinos are higgsino-dominated states. Note that the presence of a mixed right-sneutrino as the LSP can lead to a very different signature from the compressed higgsino-like states, mostly due to the leptonic decay of the light chargino. Although leptonic channels provide a cleaner environment for new physics searches at a hadron machine such as the LHC, one expects that the level of compression in the mass spectra of the electroweakinos would also play a major role in determining the efficacy of the leptonic channels. We investigate the prospects of discovery of such channels at the 13 TeV run of LHC. We focus on the following apsects in our study:

- We consider a right-sneutrino LSP along with a compressed electroweakino sector sitting above the LSP, where the lighter states are almost higgsino-like with a very small admixture of gauginos.

- We give a detailed account of how the decay of the light electroweakinos depend on the various supersymmetric parameters that govern the mixing, mass splitting and, in which region of the parameter space the decays are prompt. We also highlight how even the smallest gaugino admixture plays a significant role in their decays.

- We comment on the DM predictions for a thermal as well as non-thermal nature of the right-sneutrino DM candidate in regions of parameter space of our interest.

- We then look at possible leptonic signals that arise from such a spectrum and analyze the signal at LHC.

The subsequent sections are organized as follows. In section 6.2 we discuss the model and the underlying particle spectrum of interest in detail. In the following section 6.3 we focus on identifying the parameter space satisfying relevant constraints as well as implications on neutrino sector and a sneutrino as DM. In section 6.4 we discuss the possible signatures at

LHC and present our analysis for a few representative points in the model parameter space. We finally conclude in Section 6.5.

## 6.2 The Model

We consider an extension to the MSSM by introducing a right-chiral neutrino superfield for each generation. This extension addresses the important issue of neutrino mass generation which is otherwise absent in the MSSM. In particular, we adopt a phenomenological approach for "TeV Type-I seesaw mechanism". The superpotential, suppressing the generation indices, is given by [60, 258, 272]:

$$\mathcal{W} \supset \mathcal{W}_{\mathcal{MSSM}} + y_\nu \hat{L}\hat{H}_u\hat{N}^c + \frac{1}{2}M_R\hat{N}^c\hat{N}^c \tag{6.2.1}$$

where $y_\nu$ is the neutrino Yukawa coupling, $\hat{L}$ is the left-chiral lepton doublet superfield, $\hat{H}_u$ is the Higgs up-type chiral superfield and $\hat{N}$ is the right-chiral neutrino superfield. Besides the usual MSSM superpotential terms denoted by $\mathcal{W}_{\mathcal{MSSM}}$, we now have an added Yukawa interaction term involving the left-chiral superfield $\hat{L}$ coupled to the up-type Higgs superfield $\hat{H}_u$, and $\hat{N}$. SM neutrinos obtain a Dirac mass $m_D$ after electroweak symmetry breaking once the neutral Higgs field obtains a vacuum expectation value (*vev*) $v_u$, such that $m_D = y_\nu v_u$. The third term $\frac{1}{2}M_R\hat{N}^c\hat{N}^c$ is a lepton-number violating ($\not{L}$) term ($\triangle L = 2$).

In addition to the MSSM contributions, the soft-supersymmetry breaking scalar potential receives additional contributions as follows:

$$\mathcal{V}^{soft} \supset \mathcal{V}^{soft}_{MSSM} + m_R^2|\widetilde{N}|^2 + \frac{1}{2}B_M\widetilde{N}^c\widetilde{N}^c + (T_\nu\widetilde{L}.H_u\widetilde{N}^c + \text{ h.c.})$$

where $m_R^2$ is the soft-supersymmetry breaking mass parameter for the sneutrino, $B_M$ is the soft mass-squared parameter corresponding to the lepton-number violating term and $T_\nu$ is the soft-supersymmetry breaking L-R mixing term in the sneutrino sector. We have suppressed the generation indices both for the superpotential as well as for the soft supersymmetry-breaking terms so far.

Note that a small $\mu$-parameter is critical to ensure the absence of any fine-tuning at the EW scale ($\Delta_{\rm EW}$) [174–177]. Fine-tuning arises if there is any large cancellation involved at the EW scale in the right hand side of the following relation [209, 210] :

$$\frac{M_Z^2}{2} = \frac{m_{H_d}^2 + \Sigma_d - (m_{H_u}^2 + \Sigma_u)\tan\beta^2}{\tan\beta^2 - 1} - \mu^2, \tag{6.2.2}$$

where $m^2_{H_u}$, $m^2_{H_d}$ denote the soft-supersymmetry breaking terms for the up-type and the down-type Higgses at the supersymmetry breaking mass scale (which is assumed to be the geometric mean of the stop masses in the present context) and $\tan\beta$ denotes the ratio of the respective *vev*s while $\Sigma_u$ and $\Sigma_d$ denote the radiative corrections. Note that, since we are not considering any specific high-scale framework in the present context, we are only concerned about the EW fine-tuning. Typically $\Delta_{\rm EW} \lesssim 30$ is achieved with $|\mu| \lesssim 300$ GeV [174–177]. The assurance of EW naturalness is the prime motivation in exploring small $\mu$ scenarios. However it is quite possible that obtaining such a spectrum from a high-scale theory may require larger fine-tuning among the high-scale parameters and the corresponding running involved, especially considering that $m_{H_u}$ evolves significantly to ensure radiative EW symmetry breaking. Therefore, $\Delta_{\rm EW}$ can be interpreted as a lower bound on fine-tuning measure [174–177]. Note that, stop squarks and gluinos contribute to the radiative corrections to $m_{H_u}$ at one and two–loop levels respectively. It has been argued [213, 214] that an EW fine-tuning of less than about 30 can be achieved with $\mu \lesssim 300$ GeV and with stop squarks and (gluinos) as heavy as about 3 TeV (4 TeV). It is, therefore, important to probe possible scenarios with low $\Delta_{\rm EW}$ and therefore with low $|\mu|$.

### 6.2.1 The (s)neutrino sector

In presence of the soft-supersymmetry-breaking terms $B_M$, a split is generated between the CP-even and the CP-odd part of right-type sneutrino fields. In terms of CP eigenstates we can write: $\widetilde{\nu}_L = \dfrac{\widetilde{\nu}^e_L + i\widetilde{\nu}^o_L}{\sqrt{2}}$; $\widetilde{\nu}_R = \dfrac{\widetilde{\nu}^e_R + i\widetilde{\nu}^o_R}{\sqrt{2}}$, where superscripts $e$, $o$ denote "even" and "odd" respectively. The sneutrino ($\widetilde{\nu}$) mass-squared matrices in the basis $\widetilde{\nu}^e = \{\widetilde{\nu}^e_L, \widetilde{\nu}^e_R\}^T$ and $\widetilde{\nu}^o = \{\widetilde{\nu}^o_L, \widetilde{\nu}^o_R\}^T$ are given by,

$$\mathcal{M}^{j\ 2} = \begin{pmatrix} m^2_{LL} & m^{j2}_{LR} \\ & \\ m^{j\ 2}_{LR} & m^{j\ 2}_{RR} \end{pmatrix},$$

where,

$$\begin{aligned} m^2_{LL} &= m^2_L + \frac{1}{2} m^2_Z \cos 2\beta + m^2_D, \\ m^{j\ 2}_{LR} &= (T_\nu \pm y_\nu M_R) v \sin\beta - \mu m_D \cot\beta, \\ m^{j\ 2}_{RR} &= m^2_R + m^2_D + M^2_R \pm B_M, \end{aligned} \tag{6.2.3}$$

with $j \in \{e, o\}$ and the '+' and the '-' signs correspond to $j = e$ and $j = o$ respectively, and $v = \sqrt{v^2_u + v^2_d} = 174$ GeV, where $v_u$, $v_d$ denote the *vevs* of the up-type and the down-type CP-even neutral Higgs bosons. Further, we have assumed $T_\nu$ to be real and with no additional CP-violating parameters in the sneutrino sector. The physical masses and the mass eigenstates can be obtained by diagonalizing these matrices. The eigenvalues are given by :

$$m^{j\ 2}_{1,2} = \frac{1}{2}\left(m^2_{LL} + m^{j\ 2}_{RR} \pm \sqrt{(m^2_{LL} - m^{j\ 2}_{RR})^2 + 4m^{j\ 4}_{LR}}\right). \tag{6.2.4}$$

The corresponding mass eigenstates are give by,

$$\begin{aligned} \widetilde{\nu}^j_1 &= \cos\varphi^j \widetilde{\nu}^j_L - \sin\varphi^j \widetilde{\nu}^j_R \\ \widetilde{\nu}^j_2 &= \sin\varphi^j \widetilde{\nu}^j_L + \cos\varphi^j \widetilde{\nu}^j_R. \end{aligned} \tag{6.2.5}$$

The mixing angle $\theta = \frac{\pi}{2} - \varphi$ is given by,

$$\sin 2\theta^j = \frac{(T_\nu \pm y_\nu M_R) v \sin\beta - \mu m_D \cot\beta}{m^{j2}_2 - m^{j2}_1}, \tag{6.2.6}$$

where $j$ denotes CP-even ($e$) or CP-odd ($o$) states.

The off-diagonal term involving $T_\nu$ is typically proportional to the coupling $y_\nu$, ensuring that the left-right (L-R) mixing is small. However, the above assumption relies on the mechanism of supersymmetry-breaking and may be relaxed. The phenomenological choice of a large $T_\nu \sim \mathcal{O}(1)$GeV leads to increased mixing between the left and right components of the sneutrino flavor eigenstates in the sneutrino mass eigenstates [60, 61, 261]. Further, if the denominator in Eq. (6.2.6) is suitably small, it can also lead to enhanced mixing.

As for the neutrinos, at tree-level with $M_R \gg 1$ eV, their masses are given by $m_\nu \simeq \dfrac{y^2_\nu v^2_u}{M_R}$, as in the case of Type-I seesaw mechanism [20–22]. Thus, with $M_R \sim \mathcal{O}(100)$ GeV, neutrino masses of $\mathcal{O}(0.1)$ eV requires $y_\nu \sim 10^{-6} - 10^{-7}$. Although we have ignored the flavor indices in the above discussion of the sneutrino sector, the neutrino oscillation experiments indicate that these will play an important role in the neutrino sector. We will assume that the leptonic Yukawa couplings are flavor diagonal, and that the only source of flavor mixing arises from $y_\nu$ [273]; see also [274, 275].

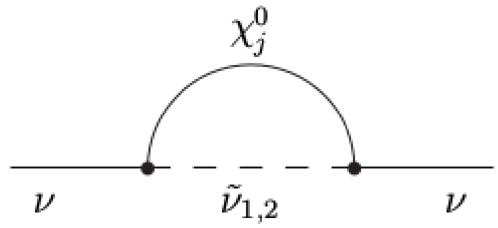


Figure 6.1: Schematic diagram showing the leading one-loop contribution to the light neutrino mass.

Further, at one-loop, flavor diagonal $B_M$ can also contribute to the neutrino mass matrix [272, 276] which can be quite significant in the presence of large $T_\nu$ in particular.[1] The dominant contribution to the Majorana mass of the active neutrino arises from the sneutrino-gaugino loop as shown in Fig. 6.1. The contributions from the loop are proportional to the mass splitting between the CP-even and the CP-odd left-sneutrino state which makes it significant in the presence of a rather large $T_\nu$ which is responsible for left-right mixing in the sneutrino sector (see Eq. 6.2.6). These additional contributions to the neutrino mass give significant constraints in the $\{T_\nu, B_M\}$ parameter space.

Finally, some comments on the scenario with $M_R = 0$ and $B_M = 0$ are in order. With $M_R = 0$ (and $B_M = 0$), only Dirac mass terms would be present for neutrinos, which is given by $y_\nu v_u$. The oscillation data for neutrinos can only be satisfied by assuming $y_\nu$ (and/or $T_\nu$, at one-loop order) to be flavor off-diagonal. In addition, $\mathcal{O}(0.1)$ eV neutrino mass, then, requires a very small $y_\nu \simeq 10^{-11}$.

In the sneutrino sector, the relevant mass eigenstates may be obtained simply by substituting $M_R = 0 = B_M$ in Eqs. (6.2.1, 6.2.3, 6.2.4). Since the mass matrices for both CP-even and the CP-odd sneutrinos are identical in this scenario, any splitting between the corresponding mass eigenstates would be absent. Consequently there will be only two complex-scalar mass eigenstates $\tilde{\nu}_1, \tilde{\nu}_2$. Also, there will be no large one-loop contribution to the Majorana neutrino mass, relaxing the constraint on large $T_\nu$ significantly.

[1]Note that flavor off-diagonal terms in $B_M$ can lead to flavor mixing in the neutrino sector via higher order effects which we avoid in our discussions for simplicity.

### 6.2.2 The Electroweakino sector

The other relevant sector for our study is the chargino-neutralino sector, in particular the higgsino-like states. This sector resembles the chargino-neutralino sector of the MSSM. The chargino mass matrix $M_{\widetilde{C}}$ is as given in Chapter 2 Eq. 2.3.1 with the eigenstates ordered in mass such that $m_{\tilde{\chi}_1^\pm} \leq m_{\tilde{\chi}_2^\pm}$. The left– and right–handed components of the corresponding Dirac mass eigenstates, the charginos $\tilde{\chi}_i^+$ with $i \in \{1, 2\}$, are

$$P_L \tilde{\chi}_i^+ = V_{ij} \psi_j^+ , \quad P_R \tilde{\chi}_i^+ = U_{ij}^* \overline{\psi_j^-} \, , \tag{6.2.7}$$

where $P_L$ and $P_R$ are the usual projectors, $\overline{\psi_j^-} = \psi_j^{-\dagger}$, and summation over $j$ is implied.

For the electrically neutral neutralino states, the neutralino mass matrix $M_{\widetilde{N}}$ can be written as discussed in Chapter 2 Eq. 2.3.20. Without loss of generality, we order the eigenvalues such that $m_{\tilde{\chi}_1^0} \leq m_{\tilde{\chi}_2^0} \leq m_{\tilde{\chi}_3^0} \leq m_{\tilde{\chi}_4^0}$.

The left–handed components of the corresponding mass eigenstates, described by four–component Majorana neutralinos $\tilde{\chi}_i^0$ with $i \in \{1, 2, 3, 4\}$, may be obtained as,

$$P_L \tilde{\chi}_i^0 = N_{ij} \psi_j^0 , \tag{6.2.8}$$

where summation over $j$ is again implied; the right–handed components of the neutralinos are determined by the Majorana condition $\tilde{\chi}_i^c = \tilde{\chi}_i$, where the superscript $c$ stands for charge conjugation.

Since the gaugino mass parameters do not affect "naturalness", for simplicity we have assumed $M_1, \ M_2 \gg |\mu|$. In this simple scenario there are only three low-lying higgsino-like states, $\tilde{\chi}_1^0$, $\tilde{\chi}_2^0$ and $\tilde{\chi}_1^\pm$. The EW symmetry breaking induces mixing between the gaugino and the higgsino-like states, via the terms proportional to $M_Z, \ M_W$ in the mass matrices above. The contributions of the right-chiral neutrino superfields to the chargino and neutralino mass matrices are negligible, thanks to the smallness of $y_\nu$ ($\simeq 10^{-6}$). Thus lightest neutralino and charginos are expected to be nearly the same as in the MSSM. Following [183] (see also [184]) in the limit $M_1, \ M_2 \gg |\mu|$, as discussed in Chapter 5, recall the analytical expression for the masses below,

$$\begin{aligned}
m_{\tilde{\chi}_1^\pm} &= |\mu| \left( 1 - \frac{M_W^2 \sin 2\beta}{\mu M_2} \right) + \mathcal{O}(M_2^{-2}) + \text{rad.corr.} \\
m_{\tilde{\chi}_{a,s}^0} &= \pm \mu - \frac{M_Z^2}{2} (1 \pm \sin 2\beta) \left( \frac{\sin \theta_W^2}{M_1} + \frac{\cos \theta_W^2}{M_2} \right) + \text{rad.corr.}
\end{aligned}$$

where the subscripts $s$ ($a$) denote symmetric (anti-symmetric) states respectively, and the sign of the eigenvalues have been retained. For the symmetric state $N_{i3}, \ N_{i4}$ share the same sign, while for the anti-symmetric state there is a relative sign between these two terms. Although the leading contribution to the mass eigenvalues are given by $|\mu|$ (which receives different radiative corrections in $M^n$ and $M^c$), $M_1$, $M_2$ and $\tan\beta$ affects the mass splitting between the three light higgsino-like states due to non-negligible gaugino-higgsino mixing. The radiative corrections, mostly from the third generation (s)quarks, contribute differently for $m_{\tilde{\chi}_1^\pm}$ and $m_{\tilde{\chi}_{1,2}^0}$ and have been estimated in [183, 277–279]. As we are interested in a spectrum where the lighter chargino and the neutralinos play a major role and the knowledge of their mass differences would become crucial, it is necessary to explore what role the relevant SUSY parameters have in contributing to the masses of the higgsino dominated states. It is quite evident for our choice of large $M_1$ and $M_2$ the three states would be closely spaced.

We now look at how the variation of the the above gaugino parameters affect the shift in mass of $m_{\tilde{\chi}_1^\pm}$ and $m_{\tilde{\chi}_{1,2}^0}$. Assuming $\mu = 300$ GeV, $\tan\beta = 5$, in Fig. 6.2 we show the

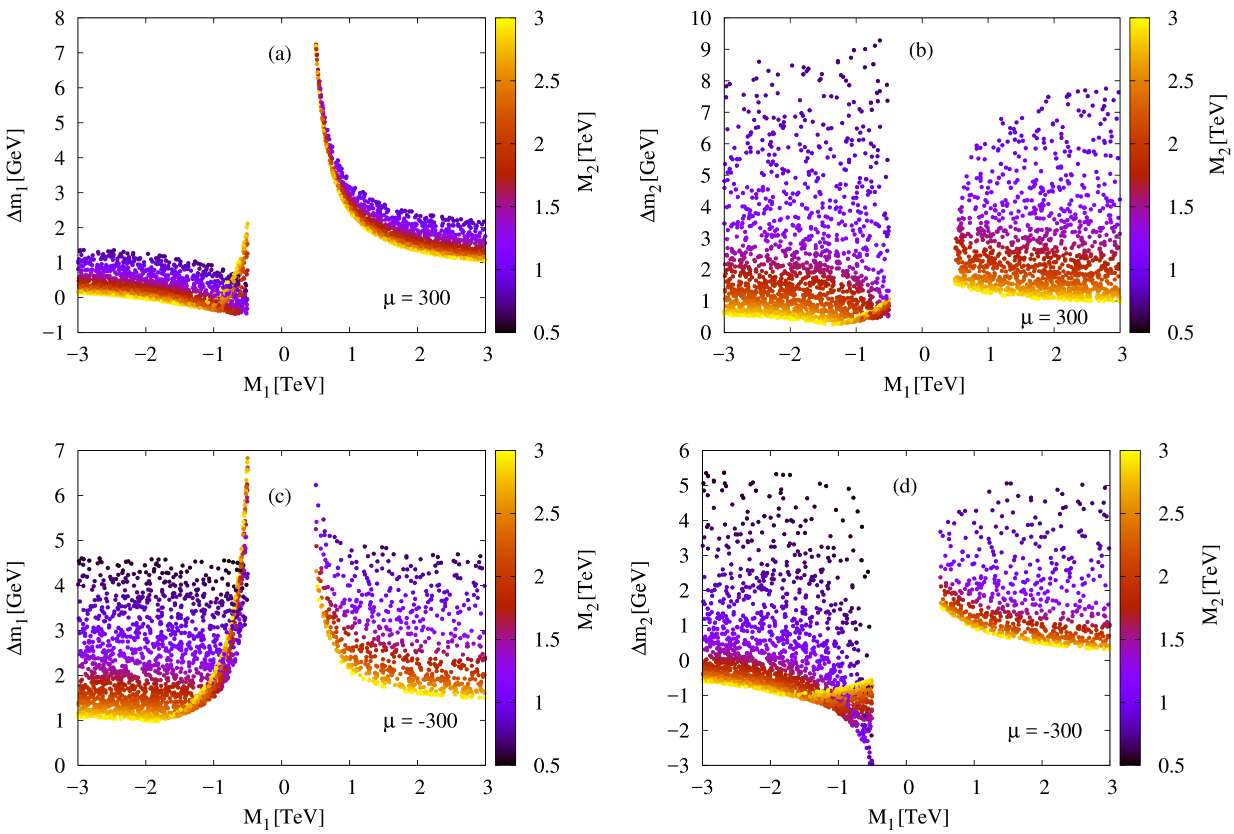


Figure 6.2: The left (right ) panel shows the variation of the mass difference $\Delta m_1 = m_{\tilde{\chi}_1^\pm} - m_{\tilde{\chi}_1^0}$ ($\Delta m_2 = m_{\tilde{\chi}_2^0} - m_{\tilde{\chi}_1^\pm}$) between $\tilde{\chi}_1^\pm$ and $\tilde{\chi}_1^0$ [$\tilde{\chi}_2^0$] for $\tan\beta = 5$ with respect to $M_1$, with $M_2$ on the palette.

variation of the mass differences $\Delta m_1 = m_{\tilde{\chi}_1^\pm} - m_{\tilde{\chi}_1^0}$ and $\Delta m_2 = m_{\tilde{\chi}_2^0} - m_{\tilde{\chi}_1^\pm}$ as a function of the gaugino mass parameters. $M_1$ and $M_2$ have been varied from 500 GeV to 3 TeV. Further, we have set $T_t = 2.9$ TeV, $M_{Q_3} = 1.3$ TeV, $M_{U_3} = 2$ TeV and $M_3 = 2$ TeV. We have used `SARAH` [280, 281] to generate model files for `SPheno` [120, 121], and have used the same to estimate the masses. Since `SLHA` [282] convention has been followed, the input parameters, as shown in the figures above, are interpreted as $\overline{\mathrm{DR}}$ parameters at $\sim 1.6$ TeV. Note that the same model and spectrum generators have been used for all subsequent figures. The following features are noteworthy from Fig. 6.2 :[2]

- For $\mu > 0$; $M_1, M_2 \gg \mu$: Here $\tilde{\chi}_2^0$ is the heaviest higgsino-like state while $\tilde{\chi}_1^\pm$ remains between the two neutralinos. For a fixed $M_1 \gg |\mu|$, the mass difference $\Delta m_1$ increases as $M_2$ decreases. This feature can be simply understood from Eq. 6.2.9. A similar conclusion also holds for $\Delta m_2$. Further, as shown in panels (a) and (b) of Fig. 6.2, the variation in $\Delta m_2$ is larger compared to $\Delta m_1$ in this case.

- For $\mu > 0; M_1 < 0$: We find that negative $M_1$ can lead to negative $\Delta m_1$, since the lightest chargino can become lighter than this state for a wide range of $M_2$ [233, 234, 241]. As shown in Fig. 6.2(a), such a scenario occurs for large $M_2$ values ($\gtrsim 2$ TeV) with $|M_1| \lesssim 1$ TeV. Further, for $|M_1| \ll M_2$, as $|M_1|$ decreases one observes an upward kink in the $\Delta m_1$ and $\Delta m_2$ plots as shown in Figs. 6.2(a) and 6.2(b) which can be attributed to the change in nature of the lightest neutralino state from anti-symmetric to the symmetric state.

- For $\mu < 0$; $M_1 > 0$: As shown in Figs. 6.2(c) and 6.2(d), similar to the $\mu > 0$ case, $\Delta m_i$ smoothly increases with decreasing $M_2$ in this region as well.

- For $\mu < 0$; $M_1 < 0$: In Fig. 6.2(c) we again see (due to the change in nature of LSP) a sharp rise of $\Delta m_1$ for large $M_2 \gtrsim 2$ TeV and $|M_1| \lesssim 1.5$ TeV. Note that in this case the $\tilde{\chi}_1^\pm$ can be the heaviest higgsino-like state in a substantial region of the parameter space for $M_2 \gtrsim 2$ TeV, as shown in Fig. 6.2(d).

[2] Although our numerical analysis, as shown in figure 6.2, includes radiative corrections, the generic features also appear at the tree-level for $|\mu| = 300$ GeV, $M_1,\ M_2 \gg |\mu|$ and $\tan\beta = 5$.We have checked this using a `Mathematica` code.

### 6.2.3 Compressed higgsino spectrum and its decay properties

As we have already emphasized, the focus of this work is on higgsino-like NLSPs in a scenario with a right-sneutrino LSP where the choice of small $|\mu|$ is motivated by the "naturalness" criteria [175, 176, 213]. Thus we will restrict our discussions to scenarios where the higgsino mass parameter $|\mu| \lesssim 500$ GeV. The gaugino mass parameters have been assumed to be heavy for simplicity; thus the light higgsino-like states are quite compressed in mass (Fig. 6.2).

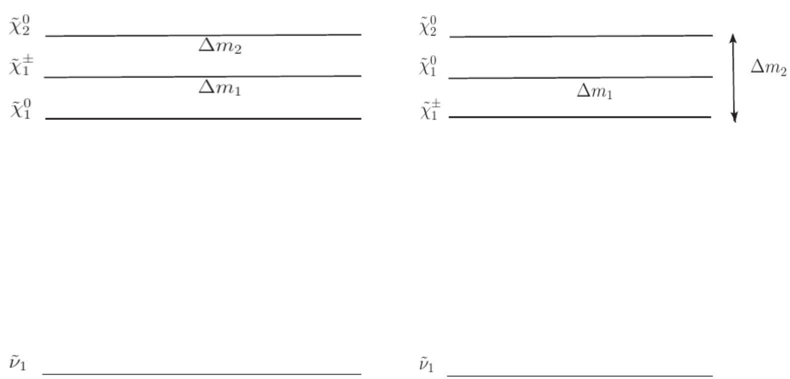


Figure 6.3: Schematic description of the mass spectrum with $|M_1|, M_2 \gg |\mu|$, and $m_{\tilde{\nu}_1} < |\mu|$. Here $|m_{\tilde{\chi}_2^0}| - m_{\tilde{\chi}_1^\pm} = \Delta m_2,\ m_{\tilde{\chi}_1^\pm} - |m_{\tilde{\chi}_1^0}| = \Delta m_1$.

Note that since the gaugino mass parameters are much heavier, the gaugino fraction in the higgsino–like states are small ($\mathcal{O}(10^{-2})$). However, $M_1$ and $M_2$ play significant role in determining $\Delta m_1$ and $\Delta m_2$ and also the hierarchy between the higgsino–like states. While for most parameter space the spectra shown in the left panel of Fig. 6.3 is realized, for $M_1 < 0$ (i.e. sign$(M_1 M_2) =$ -1), it is possible to achieve the chargino as the lightest higgsino-like state which leads to a spectra as shown in the right panel of Fig. 6.3. Further, with $\mu, M_1 < 0$ one can also have the chargino as the heaviest of the three higgsino-like state. However, as we will discuss subsequently in section 6.4, this does not contribute to any new signature. Fig. 6.3 schematically shows the mass hierarchies of our interest.

For the electroweakinos which are dominantly higgsino-like, their production rates and subsequent decay properties would have serious implications on search strategies at accelerator machines like LHC. This in turn would play an important role in constraining the higgsino mass parameter $\mu$ in the natural SUSY framework.

We now try to briefly motivate the compositions of the LSP as well as the higgsino-like

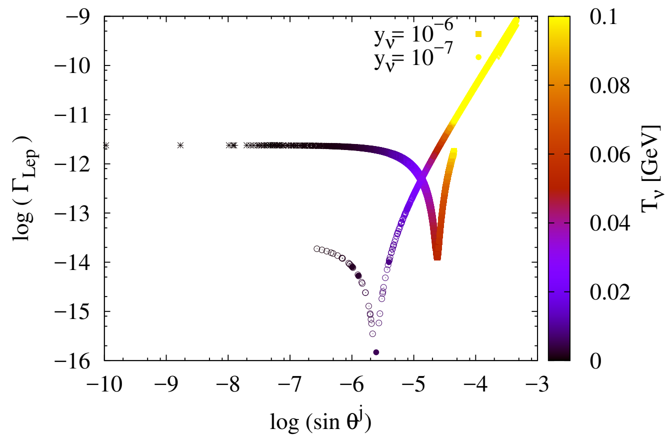


Figure 6.4: Variation of the partial decay width of $\widetilde{\chi}_1^{\pm} \to l\,\widetilde{\nu}$ versus $\sin(\theta^j)$ in logarithmic scale for $M_1 = -1.5$ TeV, $M_2 = 1.8$ TeV and gaugino fraction $\sim \mathcal{O}(10^{-2})$. Further, $M_R =$ 100 GeV, $M_{L_{1/2}} = 600$ GeV, $m_{\tilde{\nu}}^{soft} = 100$ GeV, $\mu = 300$ GeV and $\tan\beta = 5$. The colored palette corresponds to $T_\nu$, the soft left-right mixing parameter in the sneutrino sector. The plot shows the required $T_\nu$ and mixing angle $\sin(\theta^j)$ for prompt decay of the chargino. We focus on the values of $T_\nu$ in our study ensuring prompt decays of the chargino.

states of our interest and their decay properties. In the presence of $\tilde{\chi}_1^0$ as the lightest higgsino–like state, the decay modes available to the chargino are $\tilde{\chi}_1^{\pm} \to l\,\tilde{\nu}_k^j$ and $\tilde{\chi}_1^{\pm} \to \tilde{\chi}_1^0 W^{\pm *}$, where $j,\ k$ corresponds to a particular lighter sneutrino species. The partial width to the 3-body decay modes, mostly from the off-shell $W$ boson mediated processes, are suppressed by the small mass difference while small $y_\nu (\lesssim 10^{-6})$ suppresses the 2-body decay mode. In such a scenario, the gaugino fraction in $\tilde{\chi}_1^{\pm}$, can contribute to the 2-body mode significantly in the presence of small left-right mixing ($\sim \mathcal{O}(10^{-5})$) in the sneutrino sector.

We illustrate the decay properies of $\tilde{\chi}_1^{\pm}$ based on the composition of the LSP in Fig. 6.4.[3] As shown in Fig. 6.4, for small $T_\nu$ and therefore for small left admixture in the sneutrino sector, $y_\nu$ dominates the decay of $\tilde{\chi}_1^{\pm}$. As $T_\nu$ increases past $\mathcal{O}(10^{-2})$, the gaugino fraction plays a crucial role, which explains the rise of the partial width in the 2-body leptonic decay mode. With $y_\nu \sim 10^{-6}$ prompt decay of the lightest chargino to the sneutrino and lepton is always ensured. However, for $y_\nu \sim 10^{-7}$ prompt decay of the chargino in the leptonic channel

[3]The particular choice of gaugino mass parameters correspond to $\Delta m_1 \lesssim 1$ GeV, and the partial width in the corresponding hadronic channel is quite small ($\simeq 10^{-16}$ GeV). Thus, the leptonic partial width resembles the total width of $\tilde{\chi}_1^{\pm}$.

is not viable in the absence of adequate left admixture; $T_\nu \gtrsim \mathcal{O}(10^{-2})$ GeV is required to ensure prompt decay in the leptonic channel. The dip in Fig. 6.4 appears as a consequence of possible cancellation between the gaugino and the higgsino contributions to the vertex factor (e.g. $\propto (g_2 V_{11} \sin\theta^j - y_\nu V_{12} \cos\theta^j)$, $g_2$ is the $SU(2)$ gauge coupling). It is of our interest to study the scenario where the 2-body decay mode into $l\,\tilde{\nu}$ competes with the 3-body decay mode. Since the present work focuses on prompt decays, we ensure small left admixture with $T_\nu \gtrsim \mathcal{O}(10^{-2})$ GeV in the dominantly right-sneutrino LSP to ensure prompt decay of $\tilde{\chi}_1^\pm$ in the 2-body leptonic decay mode. The mass splitting $\Delta m_1 \gtrsim 1$ GeV has been considered to ensure a competing 3-body mode.

Since we have assumed a compressed higgsino spectrum, together with a mostly right-sneutrino LSP, the light higgsino states include $\tilde{\chi}_1^0$, $\tilde{\chi}_2^0$, $\tilde{\chi}_1^\pm$ and at least one generation of CP-odd and/or CP-even sneutrino LSP as described in section 6.2. In Fig. 6.2 we showed that for a fixed $|\mu|$, the hierarchy and the mass differences between the higgsino–like states are affected significantly by the choice of the gaugino mass parameters $M_1$, $M_2$, and sign$(\mu)$. In a similar compressed scenario within the MSSM, the higgsinos $\tilde{\chi}_2^0$ and $\tilde{\chi}_1^\pm$ decay into soft leptons or jets [283] and $\tilde{\chi}_1^0$, producing $\not{E}_T$. Scenarios with compressed higgsinos in MSSM have been studied in the light of recent LHC data [178, 231, 233–236]. For smaller mass differences, 130 MeV $\lesssim \Delta m_1 \lesssim 2$ GeV, the effective two-body process $\tilde{\chi}_1^\pm \to \pi^\pm \tilde{\chi}_1^0$ [284–286] can dominate the hadronic branching fraction. Further, when $\tilde{\chi}_2^0$ is also almost degenerate with $\tilde{\chi}_1^\pm$, for an even smaller mass difference $\Delta m_2$, $\tilde{\chi}_2^0 \to \gamma \tilde{\chi}_1^0$ can become significant [287–290]. Note that while the three-body decay modes (soft leptons/ jets and $\tilde{\chi}_1^0$) suffer from phase space suppression ($(\Delta m)^5$), the two-body mode ($\gamma \tilde{\chi}_1^0$) is also suppressed by a loop factor.

In addition to the above decay channels of the compressed higgsino-like states, the present scenario with a sneutrino LSP offers additional decay channels to the lighter sneutrinos. While a $\tilde{\chi}_1^0 \to \nu\,\tilde{\nu}$ would lead to missing transverse energy (as in the case for MSSM) without altering the signal topology if the neutralino was the LSP, $\tilde{\chi}_1^\pm \to l\,\tilde{\nu}$ would have a significant impact on the search strategies. For a pure right-sneutrino LSP this decay is driven by $y_\nu$. In the presence of large $T_\nu$ and therefore a large left-right mixing in the sneutrino LSP, a gaugino fraction of $\gtrsim \mathcal{O}(10^{-2})$ in the higgsino-like chargino begins to play a prominent role as the decay is driven by a coupling proportional to $g\delta\epsilon$ where $\delta$ represents the gaugino admixture and $\epsilon$ represents the L-R mixing in the sneutrino sector. The presence of multiple flavors of degenerate sneutrinos would lead to similar decay probabilities into each flavor and would invariably increase the branching to the two-body leptonic mode when taken together.

| Parameters | $\lvert M_1\rvert$ (GeV) | $\lvert M_2\rvert$ (GeV) | $\lvert\mu\rvert$ (GeV) | $\tan\beta$ | $T_\nu(GeV)$ |
|---|---|---|---|---|---|
| Values | (500-3000) | (500-3000) | 300 | 5 | 0.5 |

Table 6.1: Relevant input parameters for the parameter-space scan have been presented. Other parameters kept at fixed values include : $M_R = 100$ GeV, $B_M = 10^{-3}$ GeV$^2$, $M_3 = 2$ TeV, $M_{Q_3} = 1.3$ TeV, $M_{U_3} = 2$ TeV, $T_t = 2.9$ TeV, $M_{L_{1/2}} = 600$ GeV, $m_{\tilde{\nu}}^{soft} = 100$ GeV, $M_A = 2.5$ TeV, and $y_\nu = 10^{-7}$.

In the present context, as has been emphasized, only prompt decays into the leptonic channels such as $\tilde{\chi}_1^\pm \to l\,\tilde{\nu}$ and $\tilde{\chi}_i^0 \to \tilde{\chi}_1^\pm j_s j_s'$, where $j_s$, $j_s'$ denote soft-jets or soft-leptons can give us a signal with one or more hard charged leptons in the final state. Since the latter consists of $\tilde{\chi}_1^\pm$ in the cascade, it can also lead to leptonic final states. These branching fractions would be affected by any other available decay channels and therefore it is important to study the different regions of parameter space for all possible decay modes of the light electroweakinos. As shown in Fig. 6.2, while in most of the parameter space $\tilde{\chi}_1^0$ is the lightest higgsino-like state, and $\tilde{\chi}_1^\pm$ is placed in between the two neutralinos (i.e. $m_{\tilde{\chi}_1^0} < m_{\tilde{\chi}_1^\pm} < m_{\tilde{\chi}_2^0}$), it is also possible to have $\tilde{\chi}_1^\pm$ as the lightest or the heaviest higgsino-like state. The important competing modes for $\tilde{\chi}_1^\pm$ and $\tilde{\chi}_2^0$ where $m_{\tilde{\chi}_1^0} < m_{\tilde{\chi}_1^\pm} < m_{\tilde{\chi}_2^0}$ include

$$(a)\ \tilde{\chi}_1^\pm \to \tilde{\chi}_1^0 j_s j_s'/\pi^\pm, \qquad (b)\ \tilde{\chi}_2^0 \to \tilde{\chi}_1^0 j_s j_s/\gamma, \qquad (c)\ \tilde{\chi}_2^0 \to \tilde{\chi}_1^\pm j_s j_s'/\pi^\mp$$

where $(c)$ is usually small. However, if $\tilde{\chi}_1^\pm$ is the lightest higgsino-like state, decay modes $(b)$ and $(c)$, together with $\tilde{\chi}_1^0 \to \tilde{\chi}_1^\pm j_s j_s'/\pi^\mp$ can be present. Similarly, when $\tilde{\chi}_1^\pm$ is the heaviest higgsino-like state, decay modes $(a)$, $(b)$ and $\tilde{\chi}_1^\pm \to \tilde{\chi}_2^0 j_s j_s'/\pi^\pm$ can be present, although the latter would be sub-dominant.

In figures 6.5 ($\mu > 0$) and 6.6 ($\mu < 0$) we show the variation of branching fraction in the leptonic decay channels $\tilde{\chi}_1^\pm \to l\,\tilde{\nu}_i$ and $\tilde{\chi}_i^0 \to l\,\tilde{\nu}_i\,W^*$. The relevant parameters for the scan can be found in table 6.1.

Since the sneutrino masses and mixing matrices do not change in the scan, the two body partial decay widths $\Gamma(\tilde{\chi}_1^\pm \to l\,\tilde{\nu}_i)$ and $\Gamma(\tilde{\chi}_i^0 \to \nu\tilde{\nu}_j)$ are only affected by the variation of the gaugino-admixture in the higgsino-like states. However, the choice of gaugino mass parameters do affect the mass splittings $\Delta m_1$ and $\Delta m_2$ through mixing and can even alter the hierarchy. These alterations in the spectrum mostly affect the 3-body decay modes described above which has a significant effect on the branching ratio.

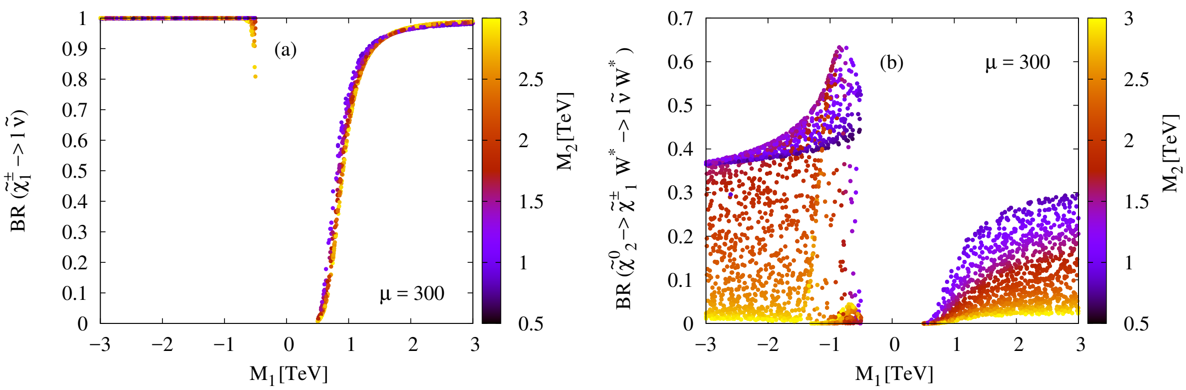


Figure 6.5: Variation of the leptonic branching ratios of $\widetilde{\chi}_1^{\pm} \to l\widetilde{\nu}$ and $\widetilde{\chi}_2^0 \to l\widetilde{\nu}W^*$ against the bino soft mass parameter, $M_1$ for the higgsino mass parameter, $\mu = 300$ GeV. The wino soft mass parameter $M_2$ is shown in the palette.

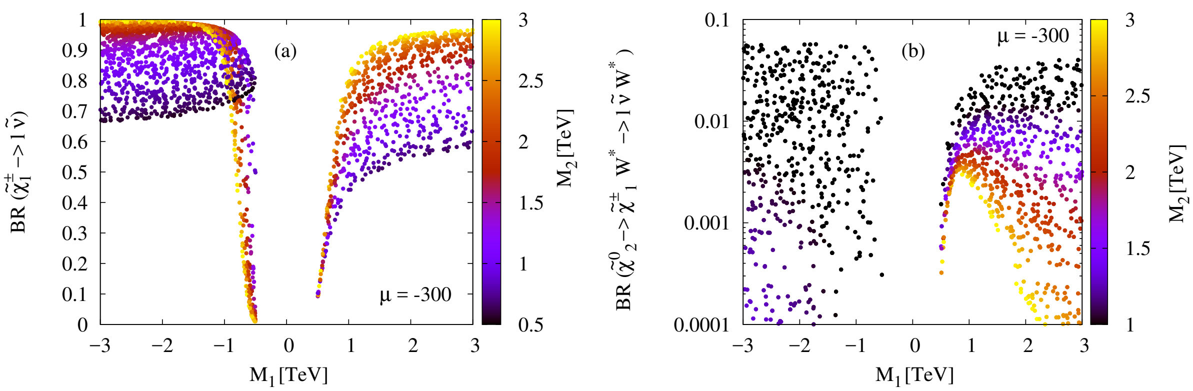


Figure 6.6: Variation of the leptonic branching ratios of $\widetilde{\chi}_1^{\pm} \to l\widetilde{\nu}$ and $\widetilde{\chi}_2^0 \to l\widetilde{\nu}W^*$ against the bino soft mass parameter, $M_1$ for the higgsino mass parameter, $\mu = -300$ GeV. The wino mass parameter $M_2$ is indicated in the palette.

As shown in Fig. 6.2(a), for $sgn(\mu) = +$ (i.e. $\mu = 300$ GeV) and for $M_1 < 0$, $\Delta m_1$ is almost entirely $\lesssim 1$ GeV. With large $M_2$ and $|M_1| \lesssim 2$ TeV, $\tilde{\chi}_1^{\pm}$ can become the lightest higgsino-like state making its leptonic branching probability close to 100% as shown in Fig. 6.5(a). However, for small $|M_1|$, and large $M_2$, where $\Delta m_1$ increases, this branching is somewhat reduced to about 0.8 and the 3-body decays start becoming relevant. For $M_1 > 0$ region the branching ratio increases as $M_1$ increases. This can be attributed to the consistent decrease in $\Delta m_1$ (Fig. 6.2(a)) and therefore of the three-body partial decay width.

Fig. 6.5(b) shows the variation of Br($\tilde{\chi}_2^0 \to \tilde{\chi}_1^{\pm} W^{\mp *}$) as a function of $M_1$ and $M_2$. For

$M_1 < 0$, generally the branching grows for larger $\Delta m_2$ (Fig. 6.2(b)) and decreases for smaller $M_2$ as the mass splitting goes down. It is again worth pointing out here that for large $M_2$ and with $|M_1| \lesssim 2$ TeV, $\Delta m_1 < 0$ and $\tilde{\chi}_1^\pm$ becomes the lightest state. Thus in this region the three-body mode into $\tilde{\chi}_1^0$ is more phase-space suppressed compared to the decay mode into $\tilde{\chi}_1^\pm$.[4] Further, as $|M_1|$ approaches $\mu$, the symmetric state, which mixes well with the bino, acquires larger bino fraction and there can be a cancellation in the vertex factor $\propto g_2(N_{22} - \tan\theta_W N_{21})$ for the two-body decay width into sneutrino. This can reduce the corresponding width and then increase again as $|M_1|$ decreases. Thus the branching ratio for the three-body decay shows a discontinuous behavior in such regions. For positive $M_1$, the branching ratio shows similar pattern as $\Delta m_2$ variation, as expected. Larger $\Delta m_1$ in this region implies that the three-body decay ($\tilde{\chi}_2^0 \to \tilde{\chi}_1^0 j_s j_s$) can be larger, and consequently $\mathrm{Br}(\tilde{\chi}_2^0 \to \tilde{\chi}_1^\pm j_s j_s')$ is rather small.

For $\mu = -300$ GeV, there are marked differences in the decay probabilities as the $\tilde{\chi}_1^\pm$ can become the heaviest when $M_1 < 0$, for large regions of the parameter space in contrast to what was observed for $\mu > 0$. Figure 6.6(a) shows the branching ratio of $\tilde{\chi}_1^\pm \to l\,\tilde{\nu}_j$ which decreases as $M_2$ increases. Although, for large $M_2$, the gaugino fraction in $\tilde{\chi}_1^\pm$ would be small, thus possibly reducing the partial width in this two-body decay mode; smaller $\Delta m_1$ in this region ensures that the competing three-body mode decreases even more. Therefore, the branching ratio in the two-body mode is enhanced. This holds true for almost the entire range of $M_1$. The feature in the negative $M_1$ region, as $|M_1|$ approaches $|\mu|$, where the branching ratio rises faster for larger $M_2$ values, corresponds to a similar fall in $\Delta m_1$ (see Fig. 6.2(c)).

In figure 6.6(b) we show the variation of $\mathrm{Br}(\tilde{\chi}_2^0 \to \tilde{\chi}_1^\pm j_s j_s')$ with $M_1,\ M_2$. For negative $M_1$, this branching ratio increases with decreasing $M_2$, since the corresponding mass difference $\Delta m_2$ also increases (see figure 6.2). The larger $M_2$ values are not shown for $M_1 < 0$, since $\tilde{\chi}_1^\pm$ becomes the heaviest higgsino-like state in this region. Thus, $\Delta m_2 < 0$ as shown in see Fig. 6.2(d), and this decay mode does not contribute. For $M_1 > 0$ smaller $M_2$ values correspond to larger branching fractions, since $\Delta m_2$ becomes larger, increasing the partial width. However, for large $M_2$ values, the partial width decreases rapidly as $\Delta m_2$ decreases.

[4]Note that, because of $\Delta m_i \lesssim 1.5$ GeV, decay modes involving $\pi^\pm$ can dominate the hadronic branching fractions in this region. While we have estimated the same to be significant using routines used in `SPheno-v4` [120, 121], see also ref. [284–286], the presence of large $T_\nu$ typically ensures that the two-body decay mode shares rather large branching fraction in these regions. In the plot we have only included three-body partial widths. A similar strategy has been adopted for regions with small $\Delta m_2$ as well.

Note that $T_\nu = 0.5$ GeV has been used in the figure. For smaller values of $T_\nu$ the leptonic branching ratio of $\tilde{\chi}_1^\pm$ would generally be reduced when it is not the lightest higgsino-like state. However, the generic features described above would remain similar. Note that, $y_\nu \sim 10^{-6}$ can lead to prompt decay even in the absence of large left-admixture, as induced by large $T_\nu$. Therefore, even for small $T_\nu \lesssim \mathcal{O}(10^{-2})$, for certain choice of the gaugino mass parameters, the leptonic branching can be competing, and thus would be relevant to probe such scenario at collider. The prompt region of decay for the charginos remain unchanged if $T_\nu$ is negative. For the non-prompt region there is some increase in the mixing angle for negative $T_\nu$.

## 6.3 Survey of the relevant parameter space

We now consider the model parameter space in light of various constraints.

### 6.3.1 General constraints

We implement the following general constraints on the parameter-space:

- The lightest CP-even Higgs mass $m_h$ has been constrained within the range : $122 \leq m_h$ (GeV) $\leq 128$ [1, 16, 89]. While the experimental uncertainty is only about 0.25 GeV, the present range of $\pm 3$ GeV is dominated by uncertainty in the theoretical estimation of the Higgs mass, see e.g. [104] and references there.[5]

- The lightest chargino satisfies the LEP lower bound: $m_{\tilde{\chi}_1^\pm} \geq 103.5$ GeV [105]. The LHC bounds, which depend on the decay channels of the chargino, will be considered only for prompt channels in more detail in section 6.4.

- The light sneutrino(s) (with small left-sneutrino admixture) can contribute to the non-standard decay channels of (invisible) Higgs and /or $Z$ boson. The latter requires the presence of both CP-even and CP-odd sneutrinos below $\simeq 45$ GeV. Constraints from the invisible Higgs decay ($\simeq 20\%$) [291] and the Z boson invisible width ($\simeq 2$ MeV) [292] can impose significant constraints on the parameter space where these are kinematically allowed.

- We further impose $B_s \to \mu^+\mu^-$ [293] and $b \to s\gamma$ constraints [106].

[5]Note that, besides the MSSM contributions, rather large $T_\nu$ can induce additional contributions to the Higgs mass [261]. Our numerical estimation takes this effect into account.

## Implication from neutrino mass

Recent analyses by PLANCK [294] impose the following constraint on the active neutrino masses: $\sum m_\nu^i \lesssim 0.7$ eV.

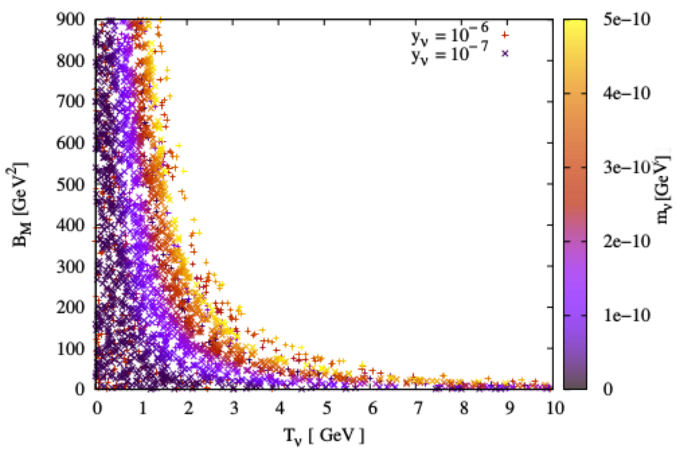


Figure 6.7: Allowed regions of $B_M$ and $T_\nu$ plane for $M_1 = 1.5$ TeV, $M_2 = 1.8$ TeV and gaugino fraction $\sim \mathcal{O}(10^{-2})$. The colored palette denotes the mass of the heaviest neutrino.

In the present scenario, the neutrinos can get a tree-level mass, as is usual in the Type-I see-saw scenario. For $y_\nu \sim 10^{-6}$, and $M_R \sim 100$ GeV, the active neutrino mass is of $\mathcal{O}(0.1)$ eV. Further, as discussed in section 6.2.1, a non-zero Majorana mass term $M_R$, and the corresponding soft-supersymmetry breaking term $B_M$ introduce a splitting between the CP-even and CP-odd mass eigenstates of right-sneutrinos. In the presence of sizable left-right mixing, significant contribution to the Majorana neutrino mass can be generated at one-loop level in such a scenario, the details depend on the gaugino mass parameters [272, 276]. Thus, regions of large $B_M$, in the presence of large left-right mixing in the sneutrino sector (induced by a large $T_\nu$) can be significantly constrained from the above mentioned bound on (active) neutrino mass. In Fig. 6.7 we show the allowed region in the $T_\nu - B_M$ plane. We consider $y_\nu \in \{10^{-6}, 10^{-7}\}$ while the other parameters are fixed as follows: $\mu = 300$ GeV, $M_3 = 2$ TeV, $M_{Q_3} = 1.5$ TeV, $T_t = 2.9$ TeV, $M_{L_{1/2}} = 600$ GeV, $m_{\tilde{\nu}}^{soft} = 100$ GeV and $M_A = 2.5$ TeV. While in the former case the tree-level and radiative contributions to the neutrino mass can be comparable (with each being $\mathcal{O}(0.1)$ eV), the radiative corrections often dominate for the latter. As shown in the figure, clearly larger $T_\nu$ values are consistent with neutrino mass for smaller $B_M$.

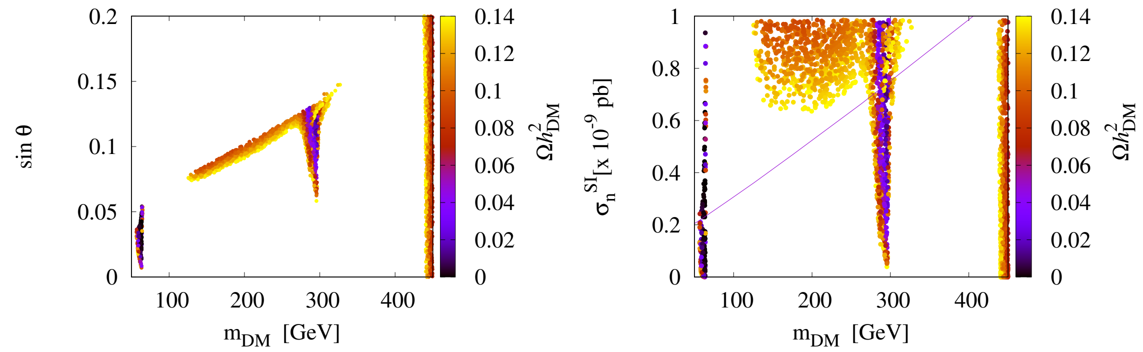


Figure 6.8: In the left panel, the dependence of the relic abundance of $\tilde{\nu}_1$ has been shown on its mass and left-fraction. The right panel shows the allowed region respecting the direct detection constraint from `XENON-1T`.

Within the paradigm of standard model of cosmology the relic abundance is constrained as $0.092 \leq \Omega h^2 \leq 0.12$ [294]. Stringent constraints from *direct* search constraints require the DM-nucleon (neutron) interaction to be less than about $10^{-9}$ pb, which varies with the mass of DM, see e.g. `LUX` [51], `PANDA-II` [295] and `Xenon-1T` [50].

In figure 6.8, with $y_\nu \in \{10^{-6}, 10^{-7}\},\ \tan\beta \in \{5, 10\},\ \mu = -450$ GeV, $m_A = 600$ GeV and all other relevant parameters are fixed as before, we scan over the set of parameters $\{T_\nu,\ m_{\tilde{\nu}},\ B_M\}$ (first generation only). We plot the left-admixture ($\sin\theta^j$) in the LSP required to obtain the thermal relic abundance and direct detection cross section against its mass in the left and the right panel respectively. We have used `micrOMEGAs-3.5.5` [122] to compute the thermal relic abundance and direct detection cross-sections.

With $T_\nu \gtrsim \mathcal{O}(10^{-3})$, which is the region of interest to allow left-right mixing in the sneutrino sector, the right-sneutrino LSP thermalizes with the (MS)SM particles via its interaction with left-sneutrino and Higgs bosons. The important annihilation processes involve s-channel processes mediated by Higgs bosons, as well as four-point vertices leading to $hh,\ W^\pm W^\mp,\ ZZ,\ t\bar{t}$ the final states. However, large left-right mixing induces large direct detection cross-section. In Fig.6.8 we have only shown parameter regions with a mass difference of at least 1 MeV between the CP-even and the CP-odd states to prevent the $Z$ boson exchange contribution to the direct detection [59, 258, 296].[6] There are t-channel

[6]We have checked that with 1 MeV mass splitting and a left-admixture of $\mathcal{O}(10^{-2})$, as is relevant for

contributions mediated by Higgs bosons, mostly from the D-term, as well as the tri-linear term $T_\nu$, and they are proportional to the left-right mixing ($\sin\theta$) in the sneutrino sector. Note that, we have only shown points with spin-independent direct detection cross-section less than $10^{-9}$ pb.

As shown in the left panel of Fig.6.8, $\sin\theta$ of $\mathcal{O}(0.1)$ is required to achieve the right thermal relic abundance. The right relic abundance is achieved soon after the dominant annihilation channels into the gauge bosons (and also Higgs boson) final states are open (i.e. $m_{\rm DM} \gtrsim 130$ GeV), while at the Higgs resonances ($m_h = 125$ GeV and $m_A \sim 600$ GeV) a lower admixture can be adequate. Further, co-annihilation with the low-lying higgsino-like states ($|\mu| \sim 450$ GeV), when the LSP mass is close to 450 GeV, can also be effective. As shown in the right panel of the same figure, for $m_{\rm DM} \lesssim 450$ GeV, most parameter space giving rise to the right thermal relic abundance is tightly constrained from direct searches (spin-independent cross-sections) from Xenon-1T [50] (similar constraints also arise from `LUX` [51], `PANDA-II` [295]), the exceptions being the resonant annihilation and co-annihilation regions.

Note that for very small $T_\nu$ and $y_\nu \lesssim 10^{-6}$, the effective interaction strength of right-sneutrinos may be smaller than the Hubble parameter at $T \simeq m_{\rm DM}$. In such a scenario, non-thermal production, especially from the decay of a thermal NLSP, can possibly generate the relic abundance [54–57]. Further, non-thermal productions can also be important in certain non-standard cosmological scenarios, e.g. early matter domination or low reheat temperature, see e.g. [297, 298]. In addition, large thermal relic abundance can be diluted if substantial entropy production takes place after the freeze-out of the DM. For such regions of parameter space our right-sneutrino LSP is likely to be a non-thermal DM candidate.

## 6.4 Signatures at LHC

We now focus on the LHC signal of the higgsino-like electroweakinos in the presence of a right-sneutrino LSP. As discussed, the various decay modes available to $\widetilde{\chi}_1^\pm$, $\widetilde{\chi}_2^0$ and $\widetilde{\chi}_1^0$ in presence of a right-sneutrino LSP depend not only on the mixing among the various sparticle components but also crucially on the mass splittings. The LHC signals would then reflect upon the above dependencies on the parameter space. We therefore look at all

thermal relic, the heavier of the CP-even and the CP-odd state has a decay width of $\sim 10^{-20}$ GeV, mostly into the LSP and soft leptons/quarks via off-shell $Z$ boson. This corresponds to a lifetime of $\lesssim 10^{-3}$ s. Thus it would decay well before the onset of Big Bang Nucleosynthesis (BBN) and is consistent with constraints from the same.

possible signals for different regions of $\Delta m_{1/2}$ and $T_\nu$. While there are regions of $\Delta m_{1/2}$ where the chargino decays non-promptly to pions that lead to the chargino traveling in the detector for some length and then decay into a soft pion and neutralino. In such cases, since both decay products are invisible, the relevant search channel at LHC is the *disappearing tracks* [235,236,299]. In cases where the chargino decay is long-lived, signals involving heavy stable charged tracks are of relevance [266,271,300,301,301]. Our focus however, is primarily on the prompt decay of the chargino to hard leptons (small $\Delta m_{1/2}$ and large $T_\nu$) which would be clean signals to observe at LHC.

The following production channels are of interest to us:

$$p\,p \to \widetilde{\chi}_1^{\pm}\,\widetilde{\chi}_2^0,\ \widetilde{\chi}_1^{\pm}\,\widetilde{\chi}_1^0,\ \widetilde{\chi}_1^{+}\,\widetilde{\chi}_1^{-},\ \widetilde{\chi}_1^0\,\widetilde{\chi}_2^0,\ \widetilde{\chi}_1^0\,\widetilde{\chi}_1^0\,\widetilde{\chi}_2^0\,\widetilde{\chi}_2^0,\ \widetilde{l}\,\widetilde{l},\ \widetilde{l}\,\widetilde{l}^*,\ \widetilde{l}\,\widetilde{\nu},\ \widetilde{\nu}\,\widetilde{\nu} \tag{6.4.1}$$

where the sleptons and sneutrinos are heavier than the electroweakinos here. The LSP pair production is excluded in the above list. The processes as given in Eq. 6.4.1 are in decreasing

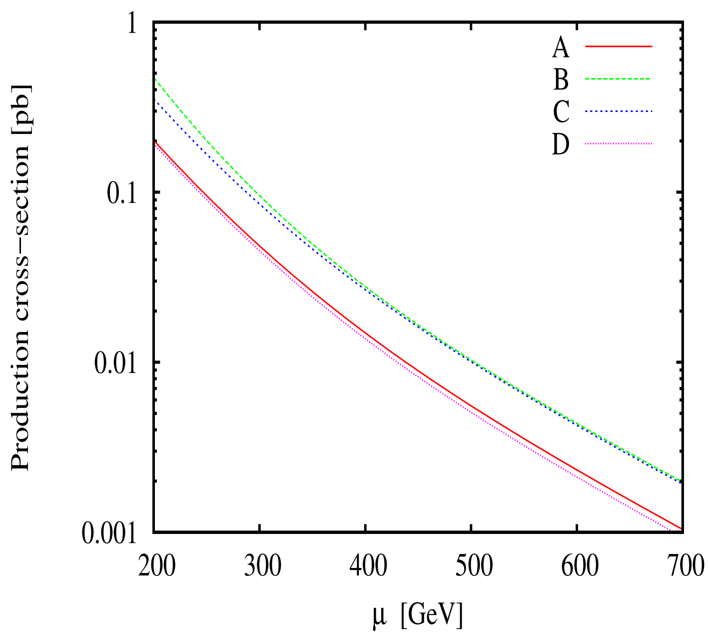


Figure 6.9: LO cross-sections of the different production channels at $\sqrt{s} = 13$ TeV. Here, A $= \widetilde{\chi}_1^+\widetilde{\chi}_1^-$, B $= \widetilde{\chi}_1^\pm\widetilde{\chi}_1^0$, C $= \widetilde{\chi}_1^\pm\widetilde{\chi}_2^0$ and D $= \widetilde{\chi}_1^0\widetilde{\chi}_2^0$. $\widetilde{t}_1$ and $\widetilde{b}_1$ are of mass $\sim 1.4$ TeV. The NLO cross-sections can be estimated by using a K factor $\sim 1.25$.

order of production cross-sections as obtained from `Prospino` [134–136]. The associated chargino neutralino pair, i.e $\widetilde{\chi}_1^\pm\,\widetilde{\chi}_{1/2}^0$ production has the largest cross-section followed by the chargino pair production, $\widetilde{\chi}_1^+ \, \widetilde{\chi}_1^-$. In the pure higgsino limit, the pair production cross-section of $\widetilde{\chi}_1^0 \, \widetilde{\chi}_1^0$ and $\widetilde{\chi}_2^0 \, \widetilde{\chi}_2^0$ are negligible compared to the other processes. Since the strong sector is kept decoupled and the compressed higgsino sector leads to soft jets and leptons, the only source of hard jets are from initial-state radiations (ISR). The suppressed jet multiplicity in the signal could prove to be a potent tool for suppressing SM leptonic backgrounds coming from the strongly produced $t\bar{t}$ and single top subprocesses which would give multiple hard jets in the final state in association with the charged leptons. Therefore we shall focus on the following leptonic signals with low hadronic activity:

- Mono-lepton + $\leq 1$ jet + $\not{E}_T$
- Di-lepton + 0 jet + $\not{E}_T$

The mono-lepton signals would come from the pair production of $\widetilde{\chi}_1^+\widetilde{\chi}_1^-$, ($\widetilde{\chi}_1^\pm \to l \, \widetilde{\nu}$ and $\widetilde{\chi}_1^\pm \to \widetilde{\chi}_1^0 \, W^{*\pm}$), and associated pair production, $\widetilde{\chi}_1^\pm \, \widetilde{\chi}_i^0$ with $i = 1, 2$ ($\widetilde{\chi}_1^\pm \to l \, \widetilde{\nu}$ and $\widetilde{\chi}_i^0 \to \nu\widetilde{\nu}$). A smaller contribution also comes from the production of $\widetilde{\chi}_1^0 \, \widetilde{\chi}_2^0$ ($\widetilde{\chi}_{2/1}^0 \to \widetilde{\chi}_1^\pm \, W^{*\mp}$ and $\widetilde{\chi}_{1/2}^0 \to \nu\widetilde{\nu}$) leading to missing energy. Among the di-lepton signals we look into both opposite sign leptons and same sign lepton signal with missing energy. Opposite sign leptons arise from the pair produced $\widetilde{\chi}_1^\pm \, \widetilde{\chi}_1^\pm$, with the chargino decaying leptonically as $\widetilde{\chi}_1^\pm \to l \, \widetilde{\nu}$. In regions of the parameter space where $\widetilde{\chi}_{2/1}^0$ is heavier than $\widetilde{\chi}_1^\pm$, $\widetilde{\chi}^\pm\widetilde{\chi}_i^0$, $i = 1, 2$ process may contribute to the di-lepton state via $\widetilde{\chi}_i^0 \to \widetilde{\chi}_1^\pm \, W^{*\mp}$ followed by $\widetilde{\chi}_1^\pm \to l \, \widetilde{\nu}$. In such cases, there could be either opposite sign di-lepton signal or same-sign di-lepton signal owing to the Majorana nature of the neutralinos ($\widetilde{\chi}_i^0$). A similar contribution to both channels come from $\widetilde{\chi}_1^0\widetilde{\chi}_2^0$ with $\widetilde{\chi}_{1/2}^0 \to \widetilde{\chi}_1^\pm \, W^{*\mp}$. Also there are sub-leading contributions from slepton pair productions which can become relevant if light sleptons are also present in the spectrum.

It is worth pointing out that in very particular regions of the parameter space $\widetilde{\chi}_1^\pm$ is the NLSP and therefore always decays to a hard lepton and sneutrino LSP. In such cases, signal rates for the di-lepton channel would be most interesting and dominant rates for same-sign di-lepton would be a particularly clean channel which will be important to probe high values of $\mu$ very effectively. This is very particular of the parameter region when $M_1$ is negative and one has a sneutrino LSP.

### 6.4.1 Constraints on electroweakino sector from LHC

Before setting up our analysis on the above signals we must consider the role of existing LHC studies that may be relevant for constraining the parameter space of our interest. LHC has already looked for direct production of lightest $\widetilde{\chi}_1^\pm$, $\widetilde{\chi}_2^0$ and $\widetilde{\chi}_1^0$ in both run 1 and run 2 searches at 7, 8 and 13 TeV respectively albeit assuming simplified models. Search results have been reinterpreted both in terms of non-prompt as well as prompt decays of the higgsinos. Since the focus of our study is on prompt decays of $\widetilde{\chi}_1^\pm$, we consider the prompt search results only.

The LHC results have been reinterpreted assuming simplified models with and without intermediate left and right sleptons with $\widetilde{\chi}_1^0$ LSP contributing to $\not{E}_T$ (see Table 6.3).

- Assuming 100% leptonic branching of the sparticles and an uncompressed spectra, CMS has ruled out degenerate wino-like $m_{\widetilde{\chi}_1^\pm}$, $m_{\widetilde{\chi}_2^0} < 1.2$ TeV for a bino-like $m_{\widetilde{\chi}_1^0} <$ 600 GeV from same-sign di-lepton, three lepton and four lepton searches with at most 1 jet [302]. The limits vary slightly depending on the choice of slepton masses. For the nearly compressed higgsino sector and assuming mass degeneracy of the lightest chargino ($\widetilde{\chi}_1^\pm$) and next-to-lightest neutralino ($\widetilde{\chi}_2^0$) the alternate channels probed by LHC are soft opposite sign di-leptons searches [303]. The mass limits on the compressed higgsino sector relax to $\sim 230$ (170) GeV for $m_{\widetilde{\chi}_1^0} \sim 210$ (162) GeV.

- ATLAS has also extensively looked for compressed higgsinos in opposite sign dilepton and trilepton final states excluding $m_{\widetilde{\chi}_2^0} \sim 150$ GeV for splittings as low as $\Delta m(\widetilde{\chi}_2^0 - \widetilde{\chi}_1^0) = 3$ GeV while the limit further improves by 20 GeV for degenerate $\widetilde{\chi}_2^0$ and $\widetilde{\chi}_1^\pm$ [304]. For the uncompressed case, searches with low hadronic activity [305] look for di-lepton and trilepton signal with up to 0 or 1 jet. The di-lepton search with no jet from chargino pair production, with charginos decaying to the neutralino LSP via intermediate sleptons sets a limit on the $m_{\widetilde{\chi}_1^\pm} > 720$ GeV for $m_{\widetilde{\chi}_1^0} < 200$ GeV. The trilepton channel excludes mass degenerate $m_{\widetilde{\chi}_2^0}$, $m_{\widetilde{\chi}_1^\pm} \sim 1.15$ TeV for $m_{\widetilde{\chi}_1^0}$ up to 580 GeV.

In Table 6.2, we list all relevant searches implemented in the public reinterpretation software `CheckMATE`. The ones, not implemented in `CheckMATE` have been recast in `Madanalysis-v5` as shown in table 6.3 and benchmarks have been chosen to pass all the relevant searches. Alternate results from LHC which constrain the compressed higgsino sector is the monojet + $\not{E}_T$ channel [306]. However no limits on the electroweak sector are yet placed from it. We ensure that our chosen benchmarks pass all of these discussed analyses.

### 6.4.2 Impact of additional related searches at LHC

For *monolepton* signal, multiple searches in both ATLAS and CMS look for single lepton final states with multiple (b) jets (refer Table 6.2 B.5) thus focussing on the production of coloured sparticles. However, there are not many dedicated SUSY search results for exploring low hadronic jet activity and low $\not{E}_T$. One of the closest analysis is [307], however employing a large cut on $\not{E}_T > 300$ GeV. Such a large cut on missing energy depletes the SUSY signal for low higgsino masses, ie., $\mu \sim 300-500$ GeV. Both ATLAS and CMS have also looked into resonant searches for heavy gauge bosons and considered monoleptonic channels with missing energy and placed limits on mass of heavy gauge bosons [308,309]. Since no reinterpretation exists on SUSY models in run 1 or run 2 so far, we reinterpret and take into account these limits in the context of our study and impose any constraints that apply on our parameter space. Few studies on soft leptons [307,310], involve high cuts on missing transverse energy ($\not{E}_T$) and hadronic energy ($H_T$) even though requiring up to two light jets and atmost one b jet. It is important to point out that since the signals from the higgsino sector here are devoid of sources of b jets, and only ISR jets are present, signal efficiency reduce substantially with cuts on large values of hadronic energy and hard b jet requirements. Further, owing to a light $\mu$ parameter, and consequently a low-lying higgsino state, a large missing energy cut of $\sim \mu$ reduces signals significantly. Hence, these searches would require large luminosity to probe the compressed higgsino sector. Reducing the hard cuts on $\not{E}_T$, b-veto and number of jets coupled with hadronic energy would allow better sensitivity to such signals and we have attempted to give an estimate of the results for the run 2 of LHC.

For *di-lepton* final states, both ATLAS and CMS have looked at stop searches or gluino searches giving rise to opposite sign or same sign leptons accompanied with multiple jets and b jets along with missing energy [191, 311]. As argued above, these searches weakly constrain the scenario we are interested in this study. However there are some searches specifically for soft leptons studied in 8 TeV [310] against which we check our benchmarks using `Madanalysis-v5`. For *opposite sign dileptons*, important searches from LHC which constrain our scenario are from ATLAS [305] and CMS [312]. Among other kinematic variables such as high lepton $p_T$ cuts, both studies focus on using large cuts on $M_{T_2}$ ($\geq 90$ GeV). We implement these analyses in `Madanalysis-v5` and choose benchmarks such that they are not excluded by current data. For *same sign dilepton*, the most constraining limit comes from CMS [313] with at most 1 jet. Other searches usually focus on the strong sector thus requiring large number of jets.

| A | $\sqrt{s} = 8$ TeV | | | |
|---|---|---|---|---|
| S.No. | Final State | Luminosity (in $\text{fb}^{-1}$) | ATLAS | CMS |
| 1 | 3 leptons + $\not{E}_T$ | 20.3 | [314] | - |
| 2 | Stop search with 2 leptons + $\not{E}_T$ | 20.3 | [97] | - |
| 3 | Stop search with Z boson and b jets + $\not{E}_T$ | 20.3 | [315] | - |
| 4 | 2 same-sign leptons or 3 leptons + $\not{E}_T$ | 20.3 | [316] | - |
| 5 | 1 lepton + (b) jets + $\not{E}_T$ | 20.3 | [95] | - |
| 6 | 2 leptons + jets + $\not{E}_T$ | 20.3 | [317] | - |
| 7 | Monojet + $\not{E}_T$ | 20.3,19.5 | [47] | [87] |
| 8 | 2 leptons + 2 b jets + $\not{E}_T$ | 20.3 | [318] | - |
| 9 | 1 lepton + $\geq$ 4 jets + $\not{E}_T$ | 20.5 | [319] | - |
| 10 | 3 leptons + $\not{E}_T$ | 20.3 | [320] | - |
| 11 | 2 leptons + $\not{E}_T$ | 20.3 | [321] | - |
| 12 | 0$-$1 lepton + $\geq$ 3 b jets + $\not{E}_T$ | 20.1 | [322] | - |
| 13 | 2 leptons + jets + $\not{E}_T$ | 20.3,19.5 | [323] | [324] |
| 14 | 1 lepton + $\geq$ 3 jets + $\geq$ 1 b jet+ $\not{E}_T$ (DM + 2 top) | 19.7 | - | [325] |
| 15 | Opposite sign leptons + 3 b tags | 19.5 | - | [326] |
| **B** | $\sqrt{s} = 13$ TeV | | | |
| S.No. | Final State | Luminosity (in $\text{fb}^{-1}$) | ATLAS | CMS |
| 1 | 2 same-sign or 3 leptons + jets + $\not{E}_T$ | 3.2 | [327] | - |
| 2 | Mono jet + $\not{E}_T$ | 3.2 | [328] | - |
| 3 | 1 lepton + jets + $\not{E}_T$ | 3.3 | [329] | - |
| 4 | 0$-$1 lepton + 3 b jets + $\not{E}_T$ | 3.3 | [330] | - |
| 5 | 1 lepton + (b) jets + $\not{E}_T$ | 3.2 | [331] | - |
| 6 | 2 leptons(Z) + jets + $\not{E}_T$ | 3.2 | [332] | - |
| 7 | 1 lepton + jets | 3.2 | [331] | |
| 8 | 2 leptons + jets + $\not{E}_T$ | 13.3 | [333] | - |
| 9 | 1 lepton + (b) jets + $\not{E}_T$ | 13.2 | [334] | - |
| 10 | 2 leptons + jets + $\not{E}_T$ | 2.2 | - | [335] |

Table 6.2: List of LHC analyses at $\sqrt{s} = 8,13$ TeV implemented in the public software Check-MATE. All the benchmarks considered in our study pass these analyses, without showing any excess above the observed number of events at 95% CL.

| Final State | ATLAS | CMS | Madanalysis−v5 |
|---|---|---|---|
| 1 lepton + $\not{E}_T$ | [308] | [307, 309] | Yes |
| 2 leptons + $\not{E}_T$ | [304, 305] | [312, 336, 337] | Yes |
| 2 same-sign leptons + $\not{E}_T$ | - | [313] | Yes |
| 3 or more leptons + $\not{E}_T$ | [305, 338, 339] | [172, 313, 340] | Not relevant for this study |

Table 6.3: Leptonic searches at $\sqrt{s} = 13$ TeV LHC with few jets (i,e, $N_j \leq 2$), as relevant for this study.

### 6.4.3 Benchmarks

In the context of natural supersymmetry with degenerate first and second generation sneutrino as LSP, we look into regions of parameter space allowed by neutrino physics constraints, LHC data and direct detection cross-section constraints. We select five representative points of the parameter space and analyze their signal at the current run of LHC. We check the viability of the chosen benchmarks for multi-leptonic signatures by testing the signal strengths against existing experimental searches implemented in the public software `CheckMATE` [194, 341]. Amongst the searches implemented in `CheckMATE`, mono-jet along with missing energy search [328] provides the most stringent constraint. Among the other 13 TeV searches as listed in Table 6.3, same-sign di-lepton and opposite-sign di-lepton searches also impose a stringent constraint on the current scenario. The allowed same-sign di-lepton branching is restricted to 4% or lower for $\mu = 300$ GeV for uncompressed scenarios. A higher value of $\mu$ and hence a lower production cross-section allows a larger same-sign di-lepton branching thereby allowing us to probe a wider range of the parameter space.

We choose parameters with $|\mu|$ in the range 300-500 GeV, $M_{1/2} \sim 2$ TeV and $\tan\beta \sim 5 - 10$ GeV as listed in Table 6.4. The choice of the benchmarks ensure prompt decay of the chargino to a hard lepton and LSP, i.e., $\Gamma > 10^{-13}$ GeV. The gaugino mass parameters $M_1$ and $M_2$ are large such that the spectrum consists of two light higgsino-like neutralinos $\widetilde{\chi}_1^0$, $\widetilde{\chi}_2^0$ and a nearly degenerate light higgsino-like $\widetilde{\chi}_1^\pm$ within $\mathcal{O}$(2-4) GeV. However there is considerable amount of freedom in choosing the relative sign among the soft parameters $M_1$, $M_2$ and $\mu$. Both the first and second generation squarks as well as gluino soft mass parameter are set to $\sim 2$ TeV. The stops are also kept heavy to ensure the light CP-even Higgs mass and signal strengths to be within the allowed experimental values. Both the first two generation left and right sleptons are kept above the higgsino sector and when possible within the reach of LHC, in the range 360−600 GeV, in the different benchmark points studied. Following our discussion in section 6.2.2 on the $M_1 - M_2$ dependence of the masses, the benchmarks represent points in the following regions of parameter space:

- **Region A**: $M_1 > 0$, $M_2 > 0$ and $\mu > 0$, with $\widetilde{\chi}_1^0$ as NLSP (**BP1**).
- **Region B**: $M_1 > 0$, $M_2 > 0$ and $\mu < 0$ , with $\widetilde{\chi}_1^0$ as NLSP (**BP2−a** and **BP2−b**).
- **Region C**: $M_1 < 0$, $M_2 > 0$ and $\mu > 0$, with $\widetilde{\chi}_1^\pm$ as NLSP (**BP3** and **BP4**).

**BP1** represents a point in the $M_1 M_2 > 0$ and $\mu > 0$ plane with $M_1 = 1.5$ TeV, $M_2 = 1.8$ TeV, $\tan\beta = 5$ and $\Delta m_{1/2} \sim 2$ GeV. The LSP mass is $\sim 140$ GeV and therefore there is a large mass gap between the higgsinos and the LSP, $\Delta M (= m_{\widetilde{\chi}_1^\pm} - m_{\widetilde{\nu}_{LSP}}) \sim 162$ GeV. The first two generation sleptons are of masses $\sim 360$ GeV to facilitate left-right mixing in the sneutrino sector. The mixing in the left-right sneutrino is $\mathcal{O}(10^{-5})$, such that for **BP1** the three body decay of $\widetilde{\chi}_1^\pm$, i.e. BR($\widetilde{\chi}_1^\pm \to \widetilde{\chi}_1^0\, W^{\pm *}$) dominates ($\sim 88\%$) over the two-body decay, BR($\widetilde{\chi}_1^\pm \to l\, \widetilde{\nu}$) ($\sim 12\%$). For a heavier slepton mass, a larger $T_\nu$ value is required for a similar left-right mixing angle and vice versa. Thus, we can fix the leptonic branching of the chargino either by lowering the left slepton mass or increasing $T_\nu$, and hence the left-right mixing in the sneutrino sector. Since the softer decay products from the three body decay produced from the off-shell $W$ pass undetected owing to the compression in the electroweakino sector, the two body leptonic decay is of interest, although subdominant. $\widetilde{\chi}_1^0$ and $\widetilde{\chi}_2^0$ dominantly decay to a $\nu\, \widetilde{\nu}$ pair contributing to missing energy signal. The dominant signals to look for in this case are mono-lepton + $\not{E}_T$ and to a lesser extent opposite-sign and same-sign di-lepton events owing to the small leptonic branching of chargino.

Further, we choose a benchmark **BP2−a**, consistent with current data and similar to **BP1**, but with an increased left-right mixing in the sneutrino sector and satisfying thermal relic density in presence of heavy Higgs resonance, of mass $\sim 824$ GeV. It represents a point in the $sgn(M_1 M_2) > 0$ and $\mu < 0$ plane with $M_1 = 1.5$ TeV and $M_2 = 1.8$ TeV with the chargino decaying completely to the lepton and sneutrino mode. Here $\Delta m_1 = 2.5$ GeV, $\Delta m_2 = 3.8$ GeV. We focus only on signals from the electroweakino sector and choose to keep the first and second generation left and right sleptons $\sim 600$ GeV such that their production cross-sections are negligible at 13 TeV LHC, thus reducing any additional contributions to the leptonic final states. Owing to the large left-right mixing in the sneutrino sector, the higgsinos decay entirely to the sneutrino final state. Thus, the dominant signals from this scenario are monolepton and opposite sign dileptons along with missing energy.

| Parameters | **BP1** | **BP2−a** | **BP2−b** | **BP3** | **BP4** |
|---|---|---|---|---|---|
| $\mu$ | 300 | -500 | -300 | 300 | 400 |
| $\tan\beta$ | 5 | 5 | 10 | 5 | 6.1 |
| $M_1$ | 1500 | 1500 | 2000 | -860 | -1150 |
| $M_2$ | 1800 | 1800 | 1000 | 2500 | 2500 |
| $M_3$ | 2000 | 2000 | 2000 | 2000 | 2000 |
| $M_A$ | 2500 | 803.2 | 2500 | 2500 | 2500 |
| $T_t$ | 2900 | 2900 | -2500 | 2950 | 2750 |
| $M_R$ | 100 | 100 | 100 | 100 | 100 |
| $BM_R$ (GeV$^2$) | $10^{-3}$ | 10.7 | 143 | $10^{-3}$ | $10^{-3}$ |
| $m_{\widetilde{\nu}}$ | 100 | 404 | 245 | 245 | 316.2 |
| $Y_\nu(\times 10^{-7})$ | 1 | 10 | 1 | 1 | 1 |
| $T_\nu$ | 0.02 | 140 | 0.8 | 4.0 | 0.06 |
| $m_{\widetilde{\chi}_1^\pm}$ | 303.6 | 510.9 | 307.5 | 305.4 | 407.2 |
| $m_{\widetilde{\chi}_1^0}$ | 301.7 | 508.4 | 303.5 | 305.5 | 407.3 |
| $m_{\widetilde{\chi}_2^0}$ | 305.8 | 512.2 | 311.5 | 305.8 | 407.5 |
| $m_{\widetilde{t}_1}$ | 1034.6 | 1528.3 | 1024.7 | 1514.8 | 1523.5 |
| $m_{\widetilde{b}_1}$ | 1064.3 | 1568.6 | 1057.8 | 1552.1 | 1555.2 |
| $m_{\widetilde{l}_L}$ | 380.3 | 627.3 | 617.5 | 617.9 | 618.7 |
| $m_{\widetilde{l}_R}$ | 364.5 | 611.8 | 606.7 | 608.5 | 610.6 |
| $m_{\widetilde{\nu}_L}$ | 372.4 | 624.5 | 611.7 | 612.9 | 613.5 |
| $m_{\widetilde{\nu}_R}$ | 141.4 | 412.2 | 264.1 | 264.6 | 331.7 |
| $m_h$ | 124.6 | 124.1 | 126.1 | 124.5 | 124.7 |
| $\Delta m_{CP}$ (MeV) | 0.004 | 25.7 | 900 | 0.004 | 0.003 |
| $\Delta m_1$ | 1.9 | 2.5 | 4.0 | -0.1 | -0.1 |
| $\Delta m_2$ | 2.2 | 3.8 | 4.0 | 0.4 | 0.2 |
| $\Delta M$ | 162.2 | 96.2 | 43 | 40.9 | 75.5 |
| $\Omega h^2$ | | 0.11 | | | |
| $\sigma_{SI}$ (pb) | | $1.4\times 10^{-10}$ | | | |
| $\sin\theta^j(\times 10^{-2})$ | 0.002 | 10.9 | 0.046 | 0.224 | 0.004 |
| $BR(\widetilde{\chi}_1^\pm \to l\,\widetilde{\nu})$ | 0.13 | 1.00 | 0.34 | 1.0 | 1.0 |
| $BR(\widetilde{\chi}_2^0 \to W^{\mp *}\,\widetilde{\chi}_1^\pm)$ | 0.12 | 0.0 | 0.0 | 0.0001 | 0.10 |
| $BR(\widetilde{\chi}_2^0 \to W^{\mp *}\,\widetilde{\chi}_1^\pm \to l\widetilde{\nu}\,W^{*\mp})$ | 0.015 | 0.0 | 0.031 | 0.0001 | 0.10 |

Table 6.4: Low energy input parameters and sparticle masses for the benchmarks used in the current study. All soft mass parameters and mass differences are in GeV. Mass differences amongst the different higgsino sector sparticles, $\Delta m_1$ and $\Delta m_2$, are as defined in Section 6.2.2. Additionally, $\Delta M = m_{\widetilde{\chi}_1^\pm} - m_{\widetilde{\nu}}$ represents the mass gap between the chargino and the sneutrino LSP and $\theta^j$ represents the mixing angle between the lightest left and right sneutrinos. The mass difference, $\Delta m_{CP} = m_{\widetilde{\nu}_e} - m_{\widetilde{\nu}_o}$ refers to the mass difference between the lightest CP-even and CP-odd sneutrino eigenstates.

We choose another spectrum **BP2−b** similar to **BP2−a** but for a lighter $\mu = 300$ GeV and LSP mass $\sim 264$ GeV such that $\Delta M \sim 40$ GeV. Thus, we choose a nearly compressed spectrum **BP2−b** where the leptons are much softer as compared to those of **BP2−a** in order to study the prospects of such a spectrum in presence of a $\widetilde{\nu}$ LSP. The dominant signals to look for are mono-lepton, opposite-sign di-lepton and same-sign di-lepton along with missing transverse energy.

| | | Luminosity (in $fb^{-1}$) for $3\sigma$ excess | | | | |
|---|---|---|---|---|---|---|
| Analyses | Reference | **BP1** | **BP2−a** | **BP2−b** | **BP3** | **BP4** |
| $l^{\pm}l^{\mp}$ (SF)+ 0 jet + $\not{E}_T$ | [305] | 13397 | 812 | - | - | 958 |
| $l^{\pm}l^{\mp}$ (DF)+ 0 jet + $\not{E}_T$ | [305] | 2191 | 162 | - | - | 104 |
| $l^{\pm}l^{\mp}$ + 0 jet + $\not{E}_T$ | [312] | - | 2223 | - | - | 385 |
| $l^{\pm}l^{\pm}$ + 0 jet + $\not{E}_T$ | [313] | - | - | 1997 | - | 2726 |
| $l^{\pm}l^{\pm}$ + 1 jet + $\not{E}_T$ | [313] | - | - | 4039 | - | 4901 |

Table 6.5: Forecast for luminosity for $3\sigma$ excess using present experimental searches using 36 $fb^{-1}$ of data at LHC. The blank spaces indicate that the benchmark is not sensitive to the final state analysis. We do not show the forecast from current monoleptonic searches as they show much weaker sensitivity to our scenario.

**BP3** and **BP4** represent spectra with $M_1 M_2 < 0$ and $\mu > 0$ with $M_1 = -860(-1150)$ GeV, $M_2 = 2.5$ TeV and $\tan\beta = 5$ such that the NLSP is the $\widetilde{\chi}_1^{\pm}$. For **BP3** we also choose a large left-right sneutrino mixing ($\mathcal{O}(10^{-3})$ while the LSP mass is 264 GeV. This leads to a tightly compressed electroweakino sector with $\widetilde{\chi}_1^{\pm}$ as the NLSP as discussed in section 6.2.2. Hence the only allowed decay of the chargino is the two body leptonic decay to the LSP with BR$(\widetilde{\chi}_1^{\pm} \to l\widetilde{\nu}) = 100\%$. Thus this region of parameter space favors the di-lepton channel with missing energy from chargino pair production. However the di-lepton channel suffers from a huge SM background and is much difficult to observe. Again the larger cross section for chargino-neutralino production only contributes to the mono-lepton channel as the decay of the heavier neutralinos to the chargino is rather suppressed for **BP3** in order to respect the bounds from existing same-sign di-lepton searches. Hence for this particular benchmark the dominant signal to look for is mono-lepton + $\not{E}_T$ and, to a lesser extent, opposite sign di-lepton + $\not{E}_T$. However, other choices of benchmark points in this region of parameter space would allow same-sign di-lepton signal along with missing energy making it very interesting and clean mode for discovery. This can be the preferred channel for much larger $\mu$. We demonstrate a single benchmark, **BP4**, with $\mu = 400$ GeV for this purpose.

Note that **BP2−a** is the only benchmark shown with the correct relic density ($\Omega h^2 = 0.11$) suggesting that the LSP in this case is a thermal DM candidate. While the other benchmarks are assumed to have non-thermal DM we could have made them thermal by adjusting the mass of one of the heavy Higgs to achieve resonant annihilations and satisfy the relic density criterion. However, from the collider point of view the relic value will not affect the signals at LHC for any of the benchmark points and in the process neither differentiate a thermal relic from a non-thermal one.

Before we propose our analysis for observing the signal at LHC we use the existing analyses and forecast the integrated luminosity that would be required to observe a $3\sigma$ excess at LHC for each of the benchmark points. We summarize our observations in table 6.5. For the above estimates, we have used the SM background events from the given references for respective analyses as shown in the table while we have computed the signal events in `Madanalysis-v5`.

### 6.4.4 Collider Analyses

### Simulation set-up and Analyses

Our focus in this study is on leptonic channels with up to one ISR jet ($p_T > 40$ GeV). We consider no extra partons at the matrix element level while generating the parton-level events for the signal using `MadGraph-v5` [123, 124, 126]. Following the event generation at parton-level, showering and hadronisation of the events are performed using `Pythia-v8` [342, 343]. Subsequently detector simulation is performed using `Delphes-v3` [129–131]. Default dynamic factorization and renormalization scales of `MadGraph-v5` have been used with `CTEQ6L` [125] as the parton distribution functions (PDF). Jets are reconstructed using `Fastjet` [133] with a minimum $p_T$ of 20 GeV in a cone of $\Delta R = 0.4$ using the *anti-*$k_t$ algorithm [132]. The charged leptons $(e, \mu)$ are reconstructed in a cone of $\Delta R = 0.2$ with the maximum amount of energy deposit from other objects in the cone limited to 10% of the $p_T$ of the lepton. Photons are also reconstructed similar to the leptons in a cone of $\Delta R = 0.2$, with the maximum energy deposit from other objects in the cone being at most 10% of the $p_T$ of the photon.

SM backgrounds have also been generated using `MadGraph-v5`, `Pythia-v6` [126] and visible objects reconstructed at the detector level using `Delphes-v3` [129–131]. Dominant

SM backgrounds such as $l\nu + 0, 1j$ and Drell Yan ($l^+l^- + 0, 1$ j) with large production cross-sections have been generated up to 1 extra parton. The matching between shower jets and jets produced at parton level is done using MLM matching with *showerKT* algorithm using $p_T$ ordered showers and a matching scale `QCUT` = 20 GeV. Signal and background analysis has been performed using `MadAnalysis-v5` [344–346].

## Primary Selection Criteria

We choose the following basic criteria for leptons (only $e^\pm$ and $\mu^\pm$), jets and photons for both signal and background:

- We select leptons (e, $\mu$) satisfying $p_T > 10$ GeV and $|\eta| < 2.5$.
- We choose photons with $p_T > 10$ GeV and $|\eta| < 2.5$.
- Reconstructed jets are identified as signal jets if they have $p_T > 40$ GeV and $|\eta| < 2.5$.
- Reconstructed b-tagged jets are identified with $p_T$ >40 GeV and $|\eta| < 2.5$.
- Jets and leptons are isolated such that $\Delta R_{lj} > 0.4$ and $\Delta R_{ll} > 0.2$.

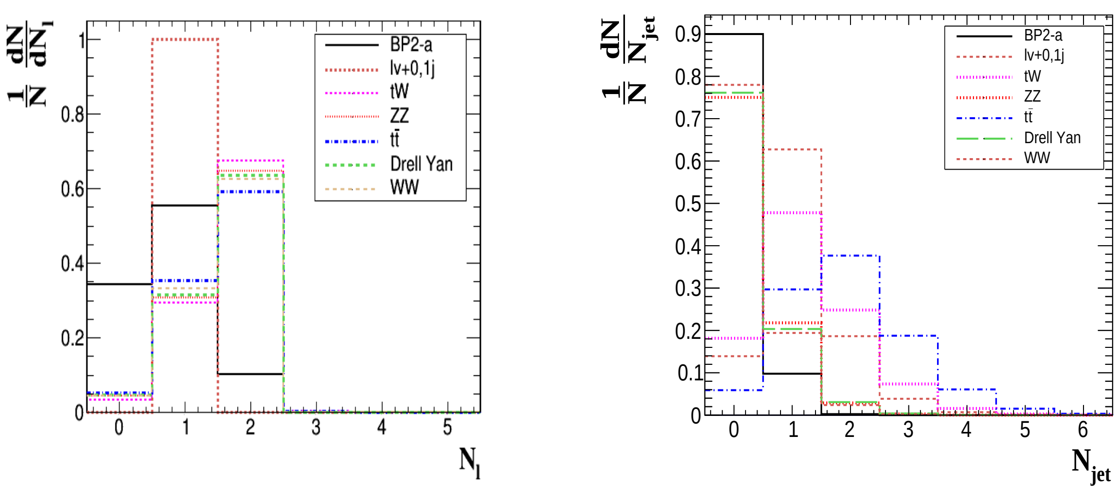


Figure 6.10: Normalized distributions for lepton and jet multiplicity for benchmark **BP2** and dominant SM backgrounds channels, respectively.

### 6.4.5 Mono-lepton + $\leq 1$ jet + $\not{E}_T$ signal

The presence of a sneutrino LSP opens up decay channels of the lightest chargino (neutralino) to a lepton (neutrino) and sneutrino. In such cases, mono-lepton signals with missing energy and few jets (mainly from ISR) arise dominantly from $\widetilde{\chi}_1^{\pm}\widetilde{\chi}_1^0$, $\widetilde{\chi}_1^{\pm}\widetilde{\chi}_2^0$ with $\widetilde{\chi}_1^{\pm} \to l\,\widetilde{\nu}$ and $\widetilde{\chi}_{1/2}^0 \to \nu\widetilde{\nu}$. Sub-dominant contributions to the signal may also arise from $\widetilde{\chi}_1^{\pm}\widetilde{\chi}_1^{\pm}$ pair production when one of the chargino decays to a soft lepton (via the three body decay to the neutralino) and the other one decays to a hard lepton and the LSP. Smaller contributions to the signal also come from $\widetilde{\chi}_1^0\widetilde{\chi}_2^0$ production with $\widetilde{\chi}_2^0$ decaying to a chargino and soft decay products while $\widetilde{\chi}_1^0$ decays invisibly or vice versa if the chargino is the lightest among the higgsinos.

Dominant background to this signal come from SM processes:

- $l^{\pm}\nu$+0,1 jets (including contributions from both on-shell and off-shell $W$ boson),
- $t\bar{t}$ (where one of the top quark decays hadronically and the other semi-leptonically).
- Single top quark production ($t(\bar{t})\,j,\ tW$).
- $W^+W^-$+ jets ($W \to l\nu$, $W \to jj$).
- $t\bar{t}W$+ jets (when both top quarks decay hadronically and $W \to l\nu$) and
- $WZ$ (with $W \to l\nu$, $Z \to \nu\bar{\nu}/jj$).

Other subdominant contributions come from $t\bar{t}$ (where both top quarks decaying semi-leptonically), Drell Yan process ($l^+l^-+0,1j$) and $ZZ,(Z \to l^+l^-, Z \to \nu\bar{\nu}/jj)$ from misidentification if one of the leptons fail to meet the isolation cuts required to identify signal leptons or even hadronic energy mismeasurements leading to jets faking leptons. Smaller contributions may also arise from triple gauge boson production with one of the gauge boson decaying leptonically and the others hadronically. However, these are negligible compared to the $l\nu+jets$ contribution. Other indirect contributions may arise from energy mismeasurements of jets as missing energy.

In order to select one lepton + missing energy signal, we implement the following criteria for both signal and backgrounds:

- **M1**: The final state consists of a single lepton with $p_T > 25$ GeV and no photons.
- **M2**: Since the dominant background contributions arise from W bosons, a large cut on the transverse mass, $M_T(l, \not{E}_T) > 150$ GeV, where

$$M_T(l, \not{E}_T) = \sqrt{2p_T(l)\not{E}_T(1 - \cos(\Delta\phi))}. \tag{6.4.2}$$

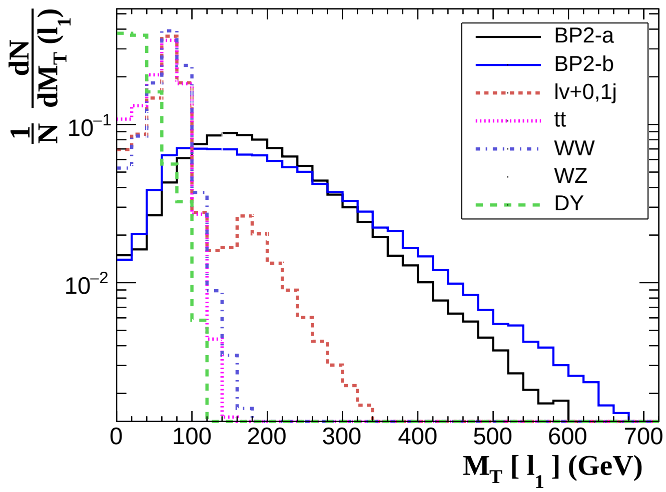


Figure 6.11: Normalized distribution for $M_T(l_1)$, the transverse mass of the leading lepton for SUSY signal **BP2−a** and **BP2−b** against the dominant SM backgrounds after preselection cut **M1.**

$\Delta\phi$ denotes the azimuthal angle separation between the charged lepton $\vec{p_T}$ and $\vec{\not{E}}_T$. A large cut on $M_T$ reduces SM background contributions from $l\nu + 0, 1$ jet, $WZ$, $WW$ and $t\bar{t}$ substantially as compared to the signal as seen in cut flow Table 6.6 and 6.7 .

| Signal | Number of events after cut | | | | | |
|---|---|---|---|---|---|---|
| | Preselection(**M1**) | **M2** | **M3** | **M4** | **M5** | **M6** |
| BP1 | 2543 | 1987 | 1946 | 1936 | 1601 | 1429 |
| BP2−a | 1495 | 944 | 922 | 916 | 706 | 611 |
| BP2−b | 6252 | 3194 | 3128 | 3118 | 2462 | 2215 |
| BP3 | $1.06\times10^4$ | 1664 | 1614 | 1601 | 1138 | 919 |
| BP4 | 3919 | 1793 | 1751 | 1740 | 1258 | 1074 |

Table 6.6: Mono-lepton + missing energy signal final state number of events at 100 fb$^{-1}$ for SUSY signals. Note that the events have been rounded-off to the nearest integer. Cross-sections have been scaled using NLO K-factors obtained from `Prospino`.

- **M3**: Events with atleast one b-tagged jet with $p_T$ > 40 GeV are rejected in order to reduce contribution from channels involving top quarks while leaving SUSY signals mostly unaffected.

- **M4**: As seen from Figure 6.10 the weakly produced SUSY signals have a comparatively lower jet multiplicity compared to SM background processes involving strong production such as $t\bar{t}$ or single top. Thus a cut on the jet multiplicity in the signal events help to suppress the large SM background from these sources. Thus, we demand jet multiplicity, $N_{jet} \leq 3$.

- **M5**: Since SUSY signals have a large missing energy compared to the SM background, $\not{E}_T > 100$ GeV helps to reduce contributions from background.

- **M6**: In addition the events are made quiet from hadronic activity by demanding at most 1 jet in the final state. This helps to further reduce backgrounds events from $t\bar{t}$ and single top production.

| SM | Number of events after cut | | | | | |
|---|---|---|---|---|---|---|
| Backgrounds | Preselection(**M1**) | **M2** | **M3** | **M4** | **M5** | **M6** |
| $l\nu + 0, 1j$ | $1.07\times10^7$ | $1.09\times10^6$ | $1.08\times10^6$ | $1.08\times10^5$ | $5.77\times10^5$ | $5.49\times10^5$ |
| Drell Yan | $3.52\times10^7$ | $3.47\times10^4$ | $3.34\times10^4$ | 5991 | 5272 | 3674 |
| $WW$ | $8.04\times10^5$ | 5696 | 5485 | 5446 | 1329 | 1130 |
| $WZ$ | $1.56\times10^5$ | $2.54\times10^4$ | $2.48\times10^4$ | $2.20\times10^4$ | $1.55\times10^4$ | 11523 |
| $ZZ$ | 4938 | 912 | 900 | 899 | 551 | 492 |
| $t\bar{t}$ | $2.04\times10^6$ | $5.97\times10^4$ | $1.79\times10^4$ | $1.68\times10^4$ | $1.17\times10^4$ | 6399 |
| Single top | $3.68\times10^6$ | $2.05\times10^4$ | 8517 | 8088 | 2659 | 1603 |
| Total | | | | | | $5.74\times10^5$ |

Table 6.7: Mono-lepton + missing energy signal final state number of events at 100 fb$^{-1}$ for SM background. Note that the events have been rounded-off to the nearest integer. Cross-sections scaled with K-factors at NLO [123] and wherever available, NNLO [199–201,347–349] have been used.

In Table 6.6 and 6.7 we list the number of events observable at 13 TeV LHC at 100 fb$^{-1}$, for the signal and SM background respectively. Although most of the SM background events could be suppressed, the continuum background from $l\,\nu + 0, 1\,j$ survives most of the cuts. The required luminosities for observing a $3\sigma$ and $5\sigma$ excess for the mono-lepton + $\not{E}_T$

channel are given in Table 6.8. The statistical significance is computed using:

$$\mathcal{S} = \sqrt{2[(s+b)\ln(1+\frac{s}{b}) - s]}$$

where $s$ and $b$ refer to the number of signal and background events after implementing the cuts **M1-M6** respectively.

| Signal | $\mathcal{L}_{3\sigma}$ (fb$^{-1}$) | $\mathcal{L}_{5\sigma}$(fb$^{-1}$) |
|---|---|---|
| BP1 | 254 | 704 |
| BP2−a | 1384 | 3485 |
| BP2−b | 106 | 293 |
| BP3 | 613 | 1701 |
| BP4 | 448 | 1245 |

Table 6.8: Required luminosities for discovery of mono lepton final states with missing energy at $\sqrt{s} = 13$ TeV LHC.

We find that the best signal significance is obtained by retaining at least one jet in the signal for all the benchmarks since the dominant background $l\nu + 0, 1j$ and signal both have only ISR jet contributions. We note that requiring large $M_T$, $\not{E}_T$ and one jet in the final state helps to improve the signal significance. Among all the benchmarks, **BP2−a** and **BP4** have highest leptonic branching fraction for the chargino (100%) as well as a large mass gap $\Delta M$ between the chargino and LSP. This leads to a relatively high cut efficiency for the signal. However since **BP2−a** corresponds to $|\mu| = 500$ GeV, the overall required luminosity for $3\sigma$ excess is $\sim 1400 fb^{-1}$. For **BP4** with $\mu = 300$ GeV and thus a higher production cross-section, the required luminosity is $\sim 500 fb^{-1}$. **BP1**, having a large $\Delta M$ but lower chargino leptonic branching fraction, i.e., $\sim$ 12% would require 254 fb$^{-1}$ of data for observing a $3\sigma$ excess at LHC. The relatively compressed spectra **BP2−b** and **BP3** although with large leptonic branching fractions of the chargino, i.e. $\sim$ 34% and 100% respectively, have a lower cut efficiency owing to a smaller $\Delta M \sim 40$ GeV. Thus the corresponding leptons would be soft compared to **BP1** and **BP2−a**. Therefore **BP2-b** requires 106 $fb^{-1}$ for observation.

### 6.4.6 Di-lepton + 0 jet +$\not{E}_T$ signal

The challenge in having a multi-lepton signal from the production of compressed higgsino-like electroweakinos comes from the fact that the decay products usually lead to soft final states. However, a sneutrino LSP and the possibility of the decay of the chargino to a hard lepton and the LSP lead to a healthy di-lepton signal with large missing energy (from $\widetilde{\chi}_1^+ \, \widetilde{\chi}_1^-$ as well as $\widetilde{\chi}_1^\pm \, \widetilde{\chi}_2^0$ pair production, provided the next-to-lightest neutralino decay yields a lepton via the chargino). A sub-dominant contribution also arises from $\widetilde{\chi}_1^0 \, \widetilde{\chi}_2^0$ with each of the neutralino decaying to a chargino and an off-shell $W$ boson which gives soft decay products. The chargino then decays to a charged lepton and sneutrino LSP. This happens most favorably when chargino is the lightest of the higgsinos. Owing to the Majorana nature of $\widetilde{\chi}_i^0$ we can have signals for opposite-sign and same-sign di-lepton final states with large missing transverse energy. Hence we look into both the possibilities:

- Opposite sign di-lepton + 0 jet + $\not{E}_T$
- Same sign di-lepton + 0 jet + $\not{E}_T$

**Opposite Sign di-lepton + 0 jet + $\not{E}_T$ signal**

Opposite sign di-lepton signal arises mainly from $\widetilde{\chi}_1^+\widetilde{\chi}_1^-$ production process. Sub-dominant contributions arise from $\widetilde{\chi}_1^\pm \, \widetilde{\chi}_1^0$, $\widetilde{\chi}_1^\pm \, \widetilde{\chi}_2^0$ and $\widetilde{\chi}_1^0 \, \widetilde{\chi}_2^0$ as discussed before. The dominant SM contributions to the opposite sign di-lepton signal with missing energy come from $t\bar{t}$, $tW$ and Drell-Yan production. Among the di-boson processes, $W^+W^-$ $(W^+ \to l^+\nu, W^- \to l^-\bar{\nu})$ , $ZZ$ ( $Z \to l^+l^-, Z \to jj/\nu\bar{\nu}$ ) and $WZ$+jets ($W \to jj, Z \to l^+l^-$) also contribute substantially to the opposite sign di-lepton channel. The triple gauge boson processes may also contribute. However, these have a small production cross-section and are expected to be subdominant. There could also be fake contributions to missing energy from hadronic energy mismeasurements.

In Figure 6.12 we show the normalized distributions for important kinematic variables for two benchmarks **BP2−a** and **BP2−b** with $\Delta M = 100,\ 40$ GeV respectively along with the dominant SM backgrounds after selecting the opposite sign-di-lepton state (**D1**). We find that as expected the lepton $p_T$ distribution for **BP2−a** is much harder than the SM backgrounds processes whereas for **BP2−b** with a lower mass gap between the chargino and LSP, the leptons are much softer and the distributions have substantial overlap with the backgrounds. We further use the other kinematic variables,

$$\not{E}_T = |\Sigma_i \vec{p}_{T_i}| \text{ and } M^2_{l^+l^-} = (p_{l_1} + p_{l_2})^2 \tag{6.4.3}$$

(where $i$ runs over all visible particles in the final state) represent the transverse missing energy and invariant mass-squared of the di-lepton final state respectively which peak at higher values for SUSY signals over backgrounds in **BP2−a** whereas **BP2−b** still retains a large overlap with the SM backgrounds. However, the largest source of background for the di-lepton background coming from Drell-Yan process can be removed safely by excluding the $Z$ boson mass window for $M_{l^+l^-}$. Since the SUSY signals do not arise from a resonance the exclusion of the $Z$ mass window is expected to have very little effect on the signal events. We further note that removing b-tagged jets would also be helpful in removing SM background contributions from the strongly produced top quark channels which have huge cross sections at the LHC.

Another kinematic variable of interest to discriminate between SUSY signals and SM backgrounds is the $M_{T_2}$ variable [197] constructed using the leading and sub-leading lepton $\vec{p_T}$ and $\vec{\not{E}}_T$. For processes with genuine source of $\not{E}_T$ there is a kinematic end point of $M_{T_2}$ which terminates near the mass of the parent particle producing the leptons and the invisible particle. In SM, channels such as $t\bar{t}, tW, W^+W^-$ involving a $W$ boson finally giving the massless invisible neutrino in the event, the end-point would be around 80 GeV. For SUSY events the invisible particle is not massless and therefore the visible lepton $p_T$ will depend on the mass difference. Thus the end-point in the signal distribution would not have a cut-off at the parent particle mass anymore. For **BP2−a** which has a large $\Delta M$ the end point is expected at larger values ($\sim 200$) GeV. However for **BP2−b**, where the available phase space is small for the charged lepton due to smaller $\Delta M$ the $M_{T_2}$ distribution is not very wide and has an end-point at a much lower value. Thus a strong cut on this variable is not favorable when the sneutrino LSP mass lies close to the electroweakino's mass.

Following the features of the kinematic distributions, we implement the following optimal selection criteria as follows for both signal and backgrounds:

- **D1**: The final state consists of two opposite sign leptons and no photons.
- **D2**: The leading lepton has $p_T > 20$ GeV and the sub-leading lepton has $p_T > 10$ GeV.
- **D3**: $M_{l^+l^-} > 10$ GeV helps remove contributions from photon mediated processes while the $Z$ mass window is also removed by demanding that the opposite-sign same flavor di-lepton invariant mass does not lie within the range $76 < M_{l^+l^-} < 106$ GeV. This helps to reduce a large resonant contribution form the $Z$ exchange in Drell-Yan process.

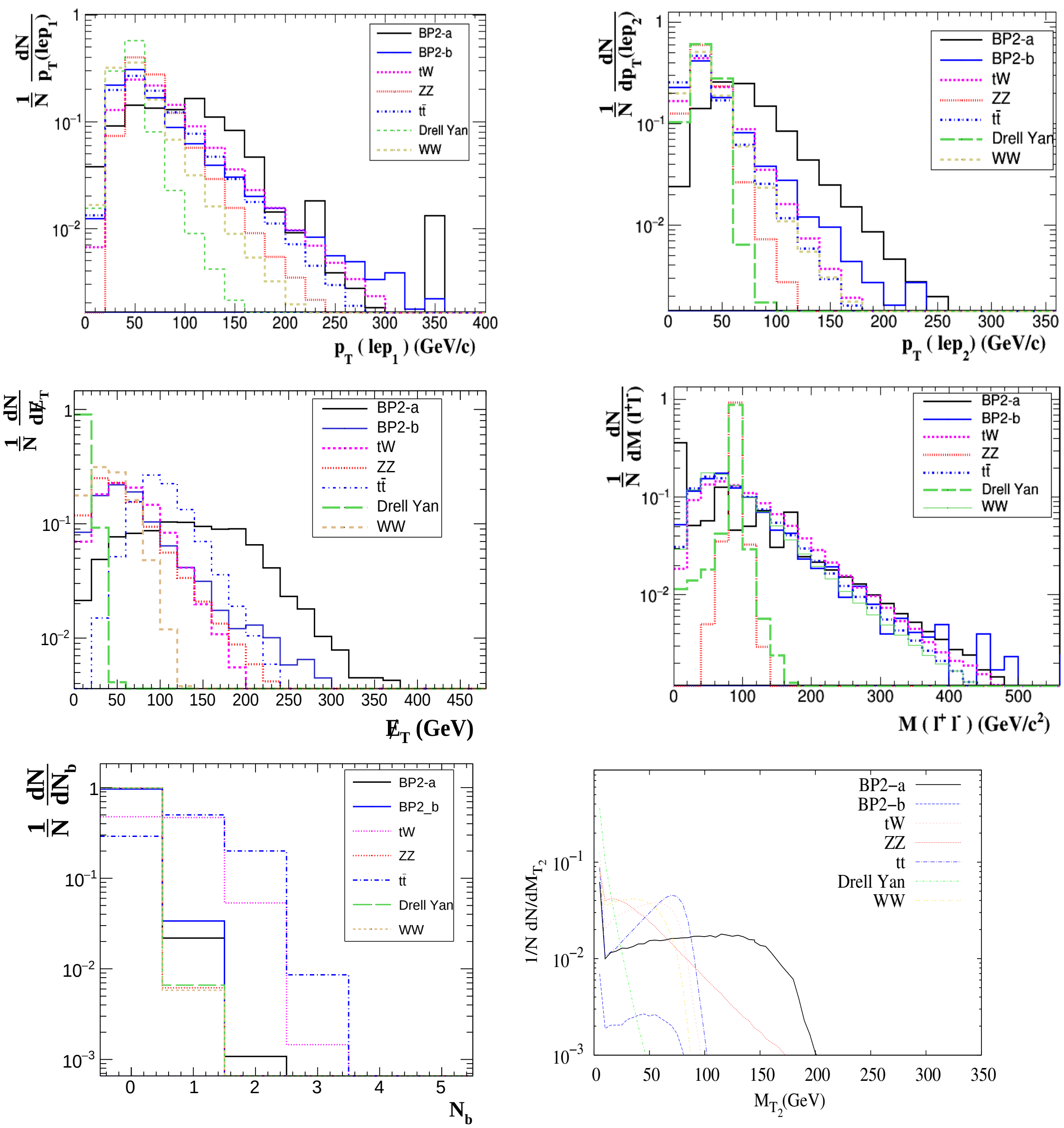


Figure 6.12: Normalized distributions of several kinematic variables after cut **D1.**

- **D4**: We reject any $b$-jet by putting a $b$-jet veto (for $p_T > 40$ GeV). This helps in suppressing background events coming from top quark production.

- **D5**: We demand a completely hadronically quiet event by choosing zero jet multiplicity ($N_{jet} = 0$) in the signal events. This is effective in suppressing contributions from background processes produced via strong interactions.

- **D6**: We demand $\not{E}_T > 80$ GeV to suppress the large Drell-Yan contribution.

- **D7**: We demand $M_{T2} > 90$ GeV which helps reduce a majority of the other SM backgrounds.

- **D8**: $\not{E}_T > 100$ GeV is implemented to further reduce the SM backgrounds.

| Signal | Number of events after cut | | | | | | |
|---|---|---|---|---|---|---|---|
| | Preselection (**D1**) | **D2** | **D3** | **D4** | **D5** | **D7** | **D8** |
| BP1 | 130 | 129 | 112 | 109 | 68 | 22 | 21 |
| BP2−a | 306 | 271 | 265 | 161 | 108 | 76 | 72 |
| BP4 | 209 | 298 | 246 | 241 | 153 | 81 | 40 |
| Signal | Number of events after cut | | | | | | |
| | Preselection (**D1**) | **D2** | **D3** | **D4** | **D5** | **D6** | |
| BP2−b | 455 | 452 | 351 | 345 | 230 | 45 | |
| BP3 | 2424 | 2394 | 1840 | 1805 | 1186 | 189 | |

Table 6.9: Opposite Sign di-lepton + $\not{E}_T$ final state number of events at 100 fb$^{-1}$ for SUSY signals. Note that the events have been rounded-off to the nearest integer. Cross-sections have been scaled using NLO K-factors obtained from `Prospino`.

In Table 6.9 we show the signal events that survive the above listed kinematic selections (cut-flow). We find that among all benchmarks, **BP2−a** is the most robust followed by **BP4**. Note that we avoid using the $M_{T2}$ cut on the benchmarks where the mass splitting between the chargino and the sneutrino LSP is small as **D7** cut makes the signal events negligible. As pointed out earlier, the end-point analysis in $M_{T2}$ is not favorable for small $\Delta M$ as seen in the signal and background distributions in Fig. 6.12. Thus **BP2−b** and **BP3** have cuts **D1-D6**. In Table 6.10 we give the SM background events after each kinematic cuts. Quite clearly up to cut **D6** the SM background numbers are quite large, and then drastically reduce after the $M_{T2}$ cut (**D7**) is imposed.

In Table 6.11 we give the required integrated luminosities to achieve a $3\sigma$ and $5\sigma$ statistical significance for the signal events of the benchmark points. **BP2−a** requires the least integrated luminosity and gives a $3\sigma$ significance for much lower luminosity compared to mono-lepton signal. However for the rest of the benchmarks mono-lepton channel is more favorable while the opposite-sign di-lepton can act as a complementary channel for **BP1** with higher luminosity and **BP3** with the very-high luminosity option of LHC. **BP2−b** type of spectrum for the model is strongly suppressed in the di-lepton channel. The signal rates can be attributed to the fact that the leptonic branching of the chargino is much larger for **BP2−a** ($\sim$ 100%) than **BP1** ($\sim$ 12%) and hence the signal is much more suppressed for **BP1** than in **BP2−a**. For **BP4** where the NLSP is the chargino, the opposite sign dilepton signal is a robust channel for discovery.

| Signal | Number of events after cut | | | | | | | |
|---|---|---|---|---|---|---|---|---|
| | Preselection (**D1**) | **D2** | **D3** | **D4** | **D5** | **D6** | **D7** | **D8** |
| Drell Yan | $1.16\times10^8$ | $1.14\times10^8$ | $8.89\times10^6$ | $8.80\times10^6$ | $6.89\times10^6$ | 506 | 293 | 53 |
| $W^+W^-$ | $1.44\times10^5$ | $1.43\times10^5$ | $1.13\times10^5$ | $1.13\times10^5$ | $1.00\times10^5$ | 5813 | 24 | 12 |
| $ZZ$ | $1.71\times10^4$ | $1.71\times10^4$ | 656 | 651 | 504 | 117 | 50 | 45 |
| $WZ$ | $6.0\times10^4$ | $6.0\times10^4$ | 5399 | 5208 | 1554 | 92 | 6 | 4 |
| $t\bar{t}$ | $6.19\times10^5$ | $6.16\times10^5$ | $4.96\times10^5$ | $1.48\times10^5$ | $3.5\times10^4$ | $2.63\times10^4$ | 132 | 106 |
| $tW$ | $1.77\times10^5$ | $1.74\times10^5$ | $1.40\times10^5$ | $6.76\times10^4$ | $2.99\times10^4$ | 8181 | 114 | 51 |
| Total | | | | | | 41009 | | 271 |

Table 6.10: Opposite Sign di-lepton + $\not{E}_T$ final state number of events at 100 fb$^{-1}$ for Standard Model backgrounds. Note that the events have been rounded-off to the nearest integer. Cross-sections scaled with K-factors at NLO [123] and wherever available, NNLO [199–201, 347–349] have been used.

Thus this channel is not a likely probe for benchmarks with a smaller phase space, like **BP2−b** and **BP3** in which cases, as seen in the previous section, mono-lepton signals fare better over di-lepton signals. Whereas for spectra like **BP2−a** and **BP4**, with a large phase space available, opposite sign di-lepton signals are much more sensitive than mono-lepton signals. In contrast spectra like **BP1** with a lower leptonic branching of the chargino, mono-lepton + missing energy signal is still a better channel to look for than opposite sign di-lepton channel.

| Signal | $\mathcal{L}_{3\sigma}$ (fb$^{-1}$) | $\mathcal{L}_{5\sigma}$(fb$^{-1}$) |
|---|---|---|
| BP1 | 568 | 1576 |
| BP2−a | 51 | 142 |
| BP2−b | $1.83 \times 10^4$ | $5.07\times10^4$ |
| BP3 | 1035 | 2875 |
| BP4 | 160 | 444 |

Table 6.11: Required luminosities for discovery of opposite sign di-lepton + $\not{E}_T$ final states at $\sqrt{s} = 13$ TeV LHC.

### Same Sign di-leptons + 0 jet + $\not{E}_T$ signal

A more interesting and unique new physics signal at LHC in the di-lepton channel is the same-sign di-lepton mode. The same-sign di-lepton in the absence of missing transverse energy is a clear signal for lepton number violation and forms the backbone for most studies of models with heavy right-handed Majorana neutrinos. Even with missing energy, the same-sign di-lepton is a difficult final state to find within the SM and therefore a signal with very little SM background. Thus finding signal events in this channel would give very clear hints of physics beyond the SM.

In our framework of SUSY model the same-sign di-lepton signal with missing energy and few jets come from the production modes $\widetilde{\chi}_1^{\pm}\widetilde{\chi}_2^0$ and/or $\widetilde{\chi}_1^{\pm}\widetilde{\chi}_1^0$ where the lepton number violating contribution comes from the decay of the Majorana-like neutralinos given by $\widetilde{\chi}_2^0 \to W^{\mp *}\widetilde{\chi}_1^{\pm}$ with $\widetilde{\chi}_1^{\pm} \to l\widetilde{\nu}$. We note that same-sign di-lepton backgrounds are rare in SM, with some small contributions coming from processes such as $p\,p \to WZ, ZZ, W^+W^+/W^-W^-$+jets, $t\bar{t}W$ and $t\bar{t}Z$ as well as from triple gauge boson productions such as $WWW$ where with two of the $W$ bosons being of same sign and the other decaying hadronically. Other indirect backgrounds can arise from energy mismeasurements, i.e, when jets or photons or opposite sign leptons fake a same sign di-lepton signal.[7]

[7] There may be additional contributions for same-sign di-lepton coming from non-prompt and conversions which we have not considered [302].

| Signal | Number of events after cut: | | | | |
|---|---|---|---|---|---|
| | Preselection (**S1**) | **S2** | **S3** | **S4** | **S5** |
| BP1 | 5 | 5 | 5 | 4 | 2 |
| BP2−a | 3 | 2.5 | 2.3 | 1.6 | 1 |
| BP2−b | 32 | 23 | 22 | 15 | 8 |
| BP3 | 2 | 0.5 | 0.5 | 0.2 | 0.1 |
| BP4 | 30 | 23 | 23 | 13 | 7 |

Table 6.12: Same sign di-lepton + $\not{E}_T$ final state number of events at 100 fb$^{-1}$ for SUSY signals. Note that the events have been rounded-off to the nearest integer where relevant. Cross-sections have been scaled using NLO K-factors obtained from `Prospino`.

For our analysis we select the same-sign di-lepton events using optimal cuts for both signal and background using the following kinematic criteria:

- **S1**: The final state consists of two charged leptons with same-sign and the leading lepton in $p_T$ must satisfy $p_T > 20$ GeV with the sub-leading lepton having $p_T > 15$ GeV. Additionally we ensure that there are no isolated photon and $b$-jets in the final state.

- **S2**: A minimal cut on the transverse mass constructed with the leading charged lepton $(l_1)$, $M_T(l_1, \vec{\not{E}}_T) > 100$ GeV is chosen to reject background contributions coming from $W$ boson.

- **S3**: To suppress background from $W^{\pm}W^{\pm}$jj as well as those from $t\bar{t}W$, $t\bar{t}Z$ with higher jet multiplicities than the SUSY signal, we keep events with only up to 2 jets.

- **S4**: A large missing energy cut, $\not{E}_T > 100$ GeV is implemented to reduce SM backgrounds.

- **S5**: Finally we choose the events to be completely hadronically quiet and demand zero jets in the event.

| SM Backgrounds | Number of events after cut | | | | |
|---|---|---|---|---|---|
| | Preselection (**S1**) | **S2** | **S3** | **S4** | **S5** |
| $WZ$ | 3856 | 1053 | 930 | 194 | 39 |
| $ZZ$ | 94 | 6 | 5 | 0.5 | 0.2 |
| $WWW$ | 60 | 29 | 21 | 7 | 0.6 |
| $W^+W^+jj$ | 416 | 175 | 116 | 56 | 2 |
| $W^-W^-jj$ | 188 | 82 | 57 | 18 | 0.5 |
| $tW$ | 40 | 20 | 19 | 7 | 4 |
| $t\bar{t}W$ | 128 | 60 | 30 | 13 | 1 |
| $t\bar{t}$ | 90 | 65 | 50 | 28 | 8 |
| Total background | | | | | 55 |

Table 6.13: Same sign di-lepton + $\not{E}_T$ final state number of events at 100 fb$^{-1}$ for SM background. Note that the events have been rounded-off to the nearest integer where relevant. Cross-sections scaled with K-factors at NLO [123] and wherever available, NNLO [199–201, 347–349] have been used.

In Tables 6.12 and 6.13 we show the signal and backgrounds events after each selection cuts are imposed. As the same-sign signal is strongly constrained by existing LHC data, our benchmarks have been chosen to comply with the existing limits. Thus we find that our benchmark choices do not seem too robust in terms of signal rates, especially **BP3** and **BP4** which has the chargino as the NLSP. It is therefore important to point out that **BP1** and **BP2−a** like spectra is naturally not favored to give a same-sign di-lepton signal while **BP3** and **BP4** are the most probable to give the same-sign signal but have been chosen to suppress the signal to respect existing constraints (by choosing very small branching for the neutralinos to decay to chargino) for two different $\mu$ values. However the spectra as reflected by **BP2−b** and **BP4** satisfying existing constraints do present us with a significant number of event rates when compared to the background after cuts.

From the above cuts, we find that a large $M_T(l_1)$ cut coupled with a large $\not{E}_T$ and the requirement of jet veto removes a large fraction of the dominant $WZ$ background as well as other fake contributions coming from $t\bar{t}$. Other genuine contributions to this channel from $W^\pm W^\pm jj$, $t\bar{t}W$ and $WWW$ having a lower production cross-section and are efficiently suppressed by cuts on $\not{E}_T$, $M_T$ and applying a jet veto. Amongst all benchmarks, the most sensitive to the same sign di-lepton analysis are **BP2−b** where BR($\widetilde{\chi}_2^0 \to \widetilde{\chi}_1^{\pm} W^{\mp} \to l\widetilde{\nu}$) $\sim$ 3.3% and **BP4** with BR($\widetilde{\chi}_2^0 \to \widetilde{\chi}_1^{\pm} W^{\mp} \to l\widetilde{\nu}$) $\sim$ 10%. Note that **BP2−b**, with a smaller $\Delta M$ gives soft leptons and is therefore slightly suppressed and requires larger integrated luminosity $\sim$ 810 fb$^{-1}$ of data. Although **BP4** has a larger branching fraction, it requires 1052 fb$^{-1}$ of data at LHC for observing a $3\sigma$ excess owing to a higher $\mu$ value compared to **BP2−b**. Thus the same-sign di-lepton can be a complementary channel to observe for benchmarks of **BP2−b** and **BP4**.

| Signal | $\mathcal{L}_{3\sigma}$ (fb$^{-1}$) | $\mathcal{L}_{5\sigma}$(fb$^{-1}$) |
|---|---|---|
| BP2−b | 811 | 2251 |
| BP4 | 1052 | 3845 |

Table 6.14: Required luminosities for discovery of same sign di-lepton final states with missing energy at $\sqrt{s} = 13$ TeV LHC.

We must again point out here that for **BP3**-like spectra with $\widetilde{\chi}_1^{\pm}$ NLSP the same-sign di-lepton would be the most sensitive channel of discovery, for large $|\mu|$ and small $M_2$, where the neutralino decay to chargino NLSP becomes large (see figs. 6.5 and 6.6) because of the small SM background. In such a case both $\widetilde{\chi}_1^0$ and $\widetilde{\chi}_2^0$ will decay to the NLSP along with soft jets or leptons. Thus both $\widetilde{\chi}_1^{\pm}\widetilde{\chi}_2^0$ and $\widetilde{\chi}_1^{\pm}\widetilde{\chi}_1^0$ production channels would have contributed to the signal leading to a two-fold increase of the number of signal events and would be more sensitive to detect a sneutrino LSP scenario.

We conclude that conventional channels such as mono-lepton or opposite sign di-lepton channels however with low hadronic activity, i.e, with at most 1 jet or no jet would be extremely useful channels to look for cases of a sneutrino LSP. Detecting same sign di-lepton signals at higher luminosities would further serve as a strong confirmatory channel for a sneutrino LSP scenario over a $\widetilde{\chi}_1^0$ LSP scenario as in the MSSM from the compressed higgsino sector and can exclude large portions of the regions with $M_1 < 0$. Our analyses also shows better signal significance for a given integrated luminosity, when compared to the forecast shown in table 6.5. Note that our estimates do not include any systematic uncertainties that may be present and would be dependent on the specific analysis of event topologies. However it is worthwhile to ascertain how our results fare in presence of such systematic uncertainties. To highlight this we assume a conservative 10% systematic uncertainty in each case. We find that the required integrated luminosities follow a similar scaling and our results for the luminosity vary by atmost 10% in most cases.

### Dependence on flavor of $\widetilde{\nu}_R$ LSP

LHC searches explore different search channels involving the flavor of the leptons owing to their high reconstruction efficiency at the detector, for instance, e+$\not{E}_T$, $\mu + \not{E}_T$ [308, 309], $ee/\mu\mu/e\mu$ final states associated with $\not{E}_T$ [303, 305]. As we have considered both first and second generation sneutrinos to be light in this study, we qualitatively analyze the prospects of the signals studied by tagging the flavor of the leptons as well as consequences of a single light generation of sneutrino LSP assuming the net leptonic branching to be the same in both cases.[8] Hence, for a single light sneutrino LSP, the observed events in the mono-lepton and di-lepton signals contribute to only a single choice of lepton flavor and vanish for the rest. We compare the signal and background in this case for the same luminosity as before and comment on the results obtained for our benchmarks.

For *mono-lepton* signals with degenerate sneutrino LSP (first two generations), say, we look at only an electron in the final state. This would lead to reduction of both signal and background in Table 6.6 and 6.7 by half such that the significance falls by a factor of $\sqrt{2}$. If a single generation of right-sneutrino was light, say $\widetilde{\nu}_e$, then only the background would reduce by a factor 1/2. Since the signal remains unchanged as the chargino now decays completely to an electron and the lightest sneutrino the signal significance increases by a factor of $\sqrt{2}$. Consequently no signal is observed for the other flavor lepton channel, in this case $\mu$, where although the background decreases by half, no signal events are present.

For the di-lepton signal there are three possible channels $ee$, $\mu\mu$ and $e\mu$ with net branching fraction of around 1/4, 1/4 and 1/2 respectively. We consider first the opposite-sign di-lepton channel. For $e\mu$ final states, only different flavor lepton backgrounds such as from $WW$, $t\bar{t}$ or $tW$ contribute with a BR $\simeq 2/3$. However contributions from same flavor di-lepton sources such as involving $Z$ boson fall. The total background thus reduces to nearly 70%. Since signal in this channel also reduces to half thereby the significance falls. For channels with same flavor (SF) leptons, i.e, $ee/\mu\mu$, dominant SF contributions are from $Z$ boson whereas sub-dominant contributions from top quark production channel reduce. Although SM background reduces so does the signal statistics and hence the significance. However, in presence of a single generation of light sneutrino we find that the signal significance improves

[8] This may not correspond to the same parameter point since the presence of the other decay modes of $\widetilde{\chi}_1^{\pm}$ affect the leptonic branching for the single light sneutrino LSP case. However, when $\widetilde{\chi}_1^{\pm}$ is the NLSP, the net leptonic branching is the same in both cases.

by a factor of about $\sqrt{2}$. Note that if the LSP is $\widetilde{\nu}_e$ then the chargino decays to an electron and the LSP. Therefore $ee + \not{E}_T$ channel significance improves whereas $\mu\mu$ and $e\mu$ channels vanish. Similarly, for an $\widetilde{\nu}_\mu$ LSP, $\mu\mu + \not{E}_T$ channels improve whereas the rest vanish. Similar conclusions may be drawn for *same sign di-lepton* channel, where the dominant backgrounds are $WZ$ and $W^\pm W^\pm$, the significance is expected to improve only for a single light generation of sneutrinos.

### Some comments on the prospect of $\tau$ flavor searches and other channels

In this context, we also explore the discovery prospects of a natural higgsino sector and a single light $\widetilde{\nu}_\tau$ as the LSP. LHC has looked at final states with tau leptons, decaying hadronically, in the context of electroweakino searches. The electroweakino mass limits considerably reduce for tau lepton searches owing to the reduced reconstruction efficiency of hadronically decaying $\tau$ leptons ($\sim$ 60%) [350] compared to that of the light leptons (e,$\mu$) ($\sim$ 95%). Searches with one or two hadronically decaying tau leptons associated with light leptons lead to stronger limits from $\widetilde{\chi}_1^\pm$,$\widetilde{\chi}_2^0$ production on $m_{\widetilde{\chi}_1^\pm}, m_{\widetilde{\chi}_2^0} > 800$ GeV for a bino-like $m_{\widetilde{\chi}_1^0} < 200$ GeV for stau mass midway between the $\widetilde{\chi}_1^\pm$ and $\widetilde{\chi}_1^0$. For stau closer to the $\widetilde{\chi}_1^\pm$, the limit [302], $m_{\widetilde{\chi}_1^\pm}, m_{\widetilde{\chi}_2^0} \sim 1000$ GeV for $m_{\widetilde{\chi}_1^\pm} \sim 200$ GeV. Limits on electroweakino searches from three tau lepton searches exclude wino-like degenerate $m_{\widetilde{\chi}_2^0}, m_{\widetilde{\chi}_1^\pm} > 600$ GeV for a bino-like $m_{\widetilde{\chi}_1^0} < 200$ GeV [302] for stau mass midway between the $\widetilde{\chi}_1^\pm$ and $\widetilde{\chi}_1^0$. Limits from opposite sign tau lepton searches [351] reinterpreted from $\widetilde{\chi}_1^\mp\widetilde{\chi}_2^0$ production and decaying via intermediate sleptons lead to $m_{\widetilde{\chi}_2^0}, m_{\widetilde{\chi}_1^\pm} > 760$ GeV for $m_{\widetilde{\chi}_1^0} < 200$ GeV. Opposite sign di-tau searches reinterpreted in context of chargino pair production lead to a bound close to 650 GeV on chargino for LSP masses up to 100 GeV [351] .

For the current scenario of a compressed electroweakino sector in presence of a light $\widetilde{\nu}_\tau$ LSP, the signals from the low-lying compressed higgsino sector would be:

- Mono-$\tau$ jet + $\not{E}_T$
- Di $\tau$ jets + $\not{E}_T$

For the mono-tau channel, both signal and background scale by the tau reconstruction efficiency, $\epsilon_R = 0.6$ is the tau reconstruction efficiency. Further a factor of $\frac{1}{2}$ comes in for the background since the branching of $W$ or $Z$ boson to light leptons is roughly twice that to the tau lepton as for a $\widetilde{\nu}_{e/\mu}$ LSP. However, owing to the reduced tau reconstruction efficiency, the signal significance falls by $\sim \sqrt{\epsilon_R} \sim 0.78$. Similarly, for the di-tau channels, the significance scales by $\epsilon_R \sim 0.6$. Hence, the estimated reach of the higgsino mass parameter, $\mu$ is expected to weaken for a $\widetilde{\nu}_\tau$ LSP compared to $\widetilde{\nu}_{e/\mu}$ LSP.

Note that, the pionic decay modes of the $\tilde{\chi}_1^\pm$ and $\tilde{\chi}_2^0$ can dominate among the hadronic modes as the respective mass differences become less than about a GeV. While we have used form factors to estimate the pionic branching fractions, we have not considered the possibility of late decay into pions in this work. This is because we have ensured that in the parameter space of our interest the two body mode to the lightest sneutrino(s) always remain prompt. Further, the potential of the loop-induced channel $\tilde{\chi}_2^0 \to \tilde{\chi}_1^0\gamma$ in deciphering the scenario has not been explored in the present work. While the photons, thus produced in the cascade, would be soft in the rest frame of $\tilde{\chi}_2^0$, it may be possible to tag hard photons in the lab frame. Note that the choice of light higgsinos are motivated by "naturalness" at the electroweak scale and we do not discuss the discovery potential for stop squarks and gluino in the present work which we plan to do in a subsequent extension.

## 6.5 Summary and Conclusions

Motivated by "naturalness" criteria at the electroweak scale, we have studied a simplified scenario with low $\mu$ parameter in the presence of a right-sneutrino LSP. For simplicity, we have assumed the gaugino mass parameters to be quite heavy $\gtrsim$ 1 TeV. In such a scenario, with $\mathcal{O}(100)$ GeV Majorana mass parameter the neutrino Yukawa coupling can be as large as $10^{-6} - 10^{-7}$. In contrast with the MSSM with light-higgsinos, in the present context, the higgsino-like states can decay to the sneutrino LSP. While the neutral higgsinos can decay into neutrino and sneutrino, the lightest chargino can decay into a lepton and sneutrino. We have demonstrated that the latter decay channel can lead to various leptonic final states with up to two leptons (i.e. mono-lepton, same-sign di-lepton and opposite-sign di-lepton) and missing transverse energy at the LHC, which can be important in searching for or constraining this scenario. We have only considered prompt decay into leptons, which require $y_\nu > 10^{-7}$ and/or small $\mathcal{O}(10^{-5} - 10^{-1})$ left-right mixing in the sneutrino sector. For smaller values of $y_\nu$, contribution from the latter dominates and the leptonic partial width on small gaugino-higgsino mixing ($\lesssim \mathcal{O}(10^{-2})$). Further, the mass split between the three states, the lightest chargino and the two lightest neutralinos depend on the choice of the gaugino mass parameters, as well as on one-loop contributions. We have shown how these mass differences significantly affect the three-body partial widths, thus affecting the branching ratios to the sneutrino. Therefore, even assuming the gaugino-like states to be above a TeV, as in our benchmark scenarios, the viability of a low $\mu$ parameter depends crucially on the choice of $M_1$, $M_2$. This has been emphasized in great detail. Consequently, there are regions of the parameter space where $BR(\widetilde{\chi}_1^{\pm} \to l\,\widetilde{\nu}) \sim 100\%$ especially in the negative $M_1$ parameter space. Such regions of parameter space would lead to enhanced leptonic rates, thereby a large fraction of negative $M_1$ parameter space can be excluded from current leptonic searches at LHC. For a given $|\mu|$, we check the existing constraints by recasting our signal in `CheckMATE` against existing LHC analysis relevant for our model parameters to search for a viable parameter region of the model. We then choose some representative benchmarks and observe that mono-lepton signals with large $\not{E}_T$ and little hadronic activity could successfully probe $\mu$ as low as 300 GeV at the ongoing run of LHC with 106 fb$^{-1}$ of data at $3\sigma$. Additional confirmatory channels for the $\widetilde{\nu}$ LSP scenario are opposite-sign di-lepton and same-sign di-lepton signal which require $\sim$ 50 fb$^{-1}$ and $\sim$ 800 fb$^{-1}$ for observing $3\sigma$ excess at LHC. While our benchmarks assume the first two generations of sneutrinos to be degenerate and consider only $e, \mu$ for the charged leptons which can be detected efficiently at the LHC, the reach may be substantially reduced if only tau-sneutrino appears as the lightest flavor due to the low tau reconstruction efficiency.

# Chapter 7

# Conclusions

In this thesis we have studied the phenomenological signatures of the MSSM and its different extensions, focusing on scenarios where the sparticles have significant compression as well as partial compression in their mass spectra. We present our study considering different LSP candidates. Among the potential candidates for LSP as well as cold/warm DM candidate, the ones chosen in this thesis are the lightest neutralino ($\widetilde{\chi}_1^0$), a light gravitino ($\widetilde{G}$) and a right-sneutrino ($\widetilde{\nu}_R$). Each of these scenarios have specific motivations to alleviate issues beyond the SM as discussed in Chapter 2. It turns out that the presence of $\widetilde{\chi}_1^0$ as the LSP and WIMP cold dark matter candidate allows contributions to the DM content of the universe, either fully or partially whereas a light $\widetilde{G}$ in the keV mass range is a more likely candidate for warm dark matter. Meanwhile a right-sneutrino LSP, invoked by adding an additional singlet chiral superfield in the MSSM fold, may behave as a thermal or non-thermal DM candidate in the $\mathcal{O}(100)$ GeV mass range depending on the model parameters. Besides being the dark matter candidate, the alternate LSP candidates provide complementary probes of the MSSM and its extensions. We study the prospects of discovering such scenarios by analysing signals comprising of multiple jets, monojets, multileptons as well as photonic channels along with missing energy after appropriate signal selection criteria have been implemented. We briefly summarise the salient features of the work done in the thesis as below.

The first chapter of the thesis deals with a brief introduction to the existing Standard Model of Particle Physics and the need to think beyond the SM. Although SM is successful in explaining most of the known phenomena in Nature, such as observed matter and the three fundamental forces, there are compelling reasons to believe that a complete underlying theory must exist. Supersymmetry is a prime BSM candidate and provides an elegant solution to the naturalness problem. In Chapter 2 we briefly introduce SUSY and discuss the MSSM. We conclude the chapter with a discussion on the phenomenological implications of MSSM and in cases one needs to think beyond the minimal version of SUSY. My thesis encompasses the phenomenological implications of both MSSM as well as extensions to the MSSM providing suitable dark matter candidates. Notably we do not rely on any underlying SUSY breaking mechanism in this thesis and focus on the phenomenological MSSM with 19 free parameters along with additional parameters in the extensions to the MSSM.

In Chapter 3, we explore the prospects of observing a compressed spectra in the MSSM with the full MSSM spectra within the compressed band. The presence of a light 125 GeV Higgs boson demands the presence of at least one heavy stop or large mixing in the stop sector and plays a crucial role in assessing the level of compression in the spectrum. We perform an exhaustive analysis of such compressed SUSY scenarios for the 13 TeV run of LHC, keeping the level of compression in the spectrum as high as possible. The rates of observable events in the high-energy run are obtained through detailed simulation of signal and backgrounds. We find that the multijet+ $\not{E}_T$ signal is a more robust channel for discovering compressed spectra besides the monojet and missing energy channel.

Although the MSSM in itself addresses issues like naturalness and provides a DM candidate, one needs to think beyond the MSSM for reasons already discussed in Chapter 2. We consider a simple extension to the MSSM with a light keV scale gravitino as the LSP. Such a light gravitino serves as a warm dark matter candidate. Chapter 4 studies the effects of including a light gravitino in the spectrum as the LSP candidate and keeping a bino-dominated $\widetilde{\chi}_1^0$ as the NLSP. The presence of the light gravitino as the LSP opens up interesting collider signatures consisting of one or more hard photons together with multiple jets and missing transverse energy from the cascade decay of the sparticles. We investigate such signals in the presence of both compressed and uncompressed SUSY spectra consistent with Higgs mass, collider and dark matter constraints. We analyse and compare the discovery potential in different benchmark scenarios consisting different levels of compression and intermediate decay modes. We find that a compressed spectrum is much more stringently constrained in such a scenario compared to the uncompressed case. We find through our analysis that compressed spectra up to $\sim 2.5$ TeV are likely to be probed even before the high luminosity run of the LHC. Some new kinematic variables are suggested to discriminate between an uncompressed and compressed spectra yielding similar event rates for photons + multi-jets + $\not{E}_T$ by probing the interplay between the transverse momentum associated with the hard photons and jets as well as the multiplicity of jets in the uncompressed case over the compressed scenario.

In Chapter 5 we further explore variants of the above scenario with the NLSP being a dominantly higgsino-like $\widetilde{\chi}_1^0$. Such a spectra may arise as a possible consequence of general phenomenological MSSM. The presence of a higgsino-like NLSP ensures the production of a large fraction of Higgs and/or $Z$ bosons along with missing energy in the final state. We focus on the prospects of observing $\geq 1b + l^+l^- + \not{E}_T$ signal at the LHC. A distinguishing feature of this scenario is the production of longitudinal $Z$ bosons in neutralino decays, unlike in the case of gaugino-like neutralinos, where the $Z$ is mostly transverse. The polarisation information of the parent $Z$ boson is reflected in the angular distributions of the decay leptons and in some other variables derived therefrom.

Chapter 6 deals with an extension to the MSSM with additional right-handed neutrino superfields. A prime motivation for such an extension to the MSSM is the possibility of generation of light neutrino masses via the Type-I Seesaw mechanism. It also opens up the possibility of a right-sneutrino LSP candidate. We focus on the viability of a light higgsino sector noting that in the light of "naturalness", it becomes equally important to investigate the supersymetric spectrum in such a scenario. The presence of small left-right mixing in the LSP can lead to a very different signature from the compressed higgsino-like states, mostly due to the leptonic decay of the light chargino leading to multileptonic channels along with $\not{E}_T$ strongly governed by the level of compression in the mass spectra of the higgsinos.

In conclusion, this thesis primarily looks into prospects of discovering largely or partially compressed spectra in the presence of different LSP candidates by analysing some phenomenological signals at the LHC as a possible probe of SUSY. Whether SUSY is a realistic theory remains to be observed as yet, however one must carry on a thorough search with the wealth of data produced and expected in the current and upcoming runs at LHC. We are continuing our work in this direction by working on some extensions of the work done in the thesis. We are working on signatures of late decaying higgsinos to the sneutrino LSP ( i.e, $T_\nu < 0.02$ region). Although in this thesis our focus has mainly been on SUSY phenomenology, certain aspects may be useful in search of non-SUSY BSM searches as well especially utilising the polarisation information of the final state gauge bosons as an indicator of the nature of the parent. We also intend to use machine learning techniques for further improvements in future studies.

# Bibliography


[1] **ATLAS** Collaboration, G. Aad et al., *Observation of a new particle in the search for the Standard Model Higgs boson with the ATLAS detector at the LHC*, *Phys. Lett.* **B716** (2012) 1–29, [arXiv:1207.7214].

[2] S. P. Martin, *A Supersymmetry primer*, hep-ph/9709356. [Adv. Ser. Direct. High Energy Phys.18,1(1998)].

[3] S. P. Martin, *Exploring compressed supersymmetry with same-sign top quarks at the Large Hadron Collider*, *Phys. Rev.* **D78** (2008) 055019, [arXiv:0807.2820].

[4] T. J. LeCompte and S. P. Martin, *Large Hadron Collider reach for supersymmetric models with compressed mass spectra*, *Phys. Rev.* **D84** (2011) 015004, [arXiv:1105.4304].

[5] T. J. LeCompte and S. P. Martin, *Compressed supersymmetry after 1/fb at the Large Hadron Collider*, *Phys. Rev.* **D85** (2012) 035023, [arXiv:1111.6897].

[6] **ATLAS** Collaboration, *Further searches for squarks and gluinos in final states with jets and missing transverse momentum at $\sqrt{s}$ =13 TeV with the ATLAS detector*, Tech. Rep. ATLAS-CONF-2016-078, CERN, Geneva, Aug, 2016.

[7] J. Dutta, P. Konar, S. Mondal, B. Mukhopadhyaya, and S. K. Rai, *A Revisit to a Compressed Supersymmetric Spectrum with 125 GeV Higgs*, *JHEP* **01** (2016) 051, [arXiv:1511.09284].

[8] G. F. Giudice and R. Rattazzi, *Theories with gauge mediated supersymmetry breaking*, *Phys. Rept.* **322** (1999) 419–499, [hep-ph/9801271].

[9] J. Dutta, P. Konar, S. Mondal, B. Mukhopadhyaya, and S. K. Rai, *Search for a compressed supersymmetric spectrum with a light Gravitino*, *JHEP* **09** (2017) 026, [arXiv:1704.04617].

[10] J. Dutta, B. Mukhopadhyaya, and S. K. Rai, *Identifying Higgsino-like neutralino with a keV-scale dark matter*, arXiv:1904.08906.

[11] A. Chatterjee, J. Dutta, and S. K. Rai, *Natural SUSY at LHC with Right-Sneutrino LSP*, *JHEP* **06** (2018) 042, [arXiv:1710.10617].

[12] E. G. J. Donoghue and B. Holstein, *Dynamics of the Standard Model (Cambridge Monographs on Particle Physics, Nuclear Physics and Cosmology).* Cambridge: Cambridge University Press., 1992.

[13] P. W. Higgs, *Broken symmetries and the masses of gauge bosons*, *Phys. Rev. Lett.* **13** (Oct, 1964) 508–509.

[14] G. S. Guralnik, C. R. Hagen, and T. W. B. Kibble, *Global conservation laws and massless particles*, *Phys. Rev. Lett.* **13** (Nov, 1964) 585–587.

[15] F. Englert and R. Brout, *Broken symmetry and the mass of gauge vector mesons*, *Phys. Rev. Lett.* **13** (Aug, 1964) 321–323.

[16] **CMS** Collaboration, S. Chatrchyan et al., *Observation of a new boson at a mass of 125 GeV with the CMS experiment at the LHC*, *Phys. Lett.* **B716** (2012) 30–61, [arXiv:1207.7235].

[17] **Particle Data Group** Collaboration, M. Tanabashi et al., *Review of Particle Physics*, *Phys. Rev.* **D98** (2018), no. 3 030001. http://pdg.lbl.gov/2019/reviews/rpp2018$-\tilde{b}$rev-$\tilde{b}$phys-$\tilde{b}$constants.pdf.

[18] I. Esteban, M. C. Gonzalez-Garcia, A. Hernandez-Cabezudo, M. Maltoni, and T. Schwetz, *Global analysis of three-flavour neutrino oscillations: synergies and tensions in the determination of $\theta 23$, $\delta cp$, and the mass ordering*, *Journal of High Energy Physics* **2019** (Jan, 2019) 106.

[19] S. Weinberg, *Baryon- and lepton-nonconserving processes*, *Phys. Rev. Lett.* **43** (Nov, 1979) 1566–1570.

[20] P. Minkowski, *$\mu \to e\gamma$ at a rate of one out of 109 muon decays?*, *Physics Letters B* **67** (1977), no. 4 421 – 428.

[21] T. Yanagida, *HORIZONTAL SYMMETRY AND MASSES OF NEUTRINOS*, *Conf. Proc.* **C7902131** (1979) 95–99.

[22] R. N. Mohapatra and G. Senjanović, *Neutrino mass and spontaneous parity nonconservation*, *Phys. Rev. Lett.* **44** (Apr, 1980) 912–915.

[23] J. Schechter and J. W. F. Valle, *Neutrino masses in su(2) $\bigotimes$ u(1) theories*, *Phys. Rev. D* **22** (Nov, 1980) 2227–2235.

[24] M. Magg and C. Wetterich, *Neutrino mass problem and gauge hierarchy*, *Physics Letters B* **94** (1980), no. 1 61 – 64.

[25] R. Foot, H. Lew, X. G. He, and G. C. Joshi, *Seesaw Neutrino Masses Induced by a Triplet of Leptons*, *Z. Phys.* **C44** (1989) 441.

[26] E. Ma, *Pathways to naturally small neutrino masses*, *Phys. Rev. Lett.* **81** (1998) 1171–1174, [hep-ph/9805219].

[27] M. Drees, *An Introduction to supersymmetry*, in *Current topics in physics. Proceedings, Inauguration Conference of the Asia-Pacific Center for Theoretical Physics (APCTP), Seoul, Korea, June 4-10, 1996. Vol. 1, 2*, 1996. hep-ph/9611409.

[28] V. C. Rubin, N. Thonnard, and W. K. Ford, Jr., *Rotational properties of 21 SC galaxies with a large range of luminosities and radii, from NGC 4605 /R = 4kpc/ to UGC 2885 /R = 122 kpc/*, *Astrophys. J.* **238** (1980) 471.

[29] D. Clowe, M. Bradac, A. H. Gonzalez, M. Markevitch, S. W. Randall, C. Jones, and D. Zaritsky, *A direct empirical proof of the existence of dark matter*, *Astrophys. J.* **648** (2006) L109–L113, [astro-ph/0608407].

[30] **Planck** Collaboration, N. Aghanim et al., *Planck 2018 results. VI. Cosmological parameters*, arXiv:1807.06209.

[31] NASA, *Dark energy survey*, . https://map.gsfc.nasa.gov/.

[32] C. Balazs, *Baryogenesis: A small review of the big picture*, arXiv:1411.3398.

[33] M. Trodden, *Electroweak baryogenesis*, *Rev. Mod. Phys.* **71** (Oct, 1999) 1463–1500.

[34] A. D. Sakharov, *Violation of CP Invariance, C asymmetry, and baryon asymmetry of the universe*, *Pisma Zh. Eksp. Teor. Fiz.* **5** (1967) 32–35. [Usp. Fiz. Nauk161,no.5,61(1991)].

[35] M. B. Gavela, P. Hernandez, J. Orloff, and O. Pene, *Standard model CP violation and baryon asymmetry*, *Mod. Phys. Lett.* **A9** (1994) 795–810, [hep-ph/9312215].

[36] N. Craig, *The State of Supersymmetry after Run I of the LHC*, in *Beyond the Standard Model after the first run of the LHC Arcetri, Florence, Italy, May 20-July 12, 2013*, 2013. arXiv:1309.0528.

[37] M. Drees, R. Godbole, and P. Roy, *Theory and phenomenology of sparticles: An account of four-dimensional N=1 supersymmetry in high energy physics*. Hackensack, USA: World Scientific (2004) 555 p, 2004.

[38] H. Baer and X. Tata, *Weak scale supersymmetry: From superfields to scattering events*. Cambridge University Press, 2006.

[39] I. Aitchison, *Supersymmetry in Particle Physics: An Elementary Introduction*. Cambridge University Press, 2007.

[40] R. Haag, J. T. Lopuszanski, and M. Sohnius, *All possible generators of supersymmetries of the s-matrix*, *Nuclear Physics B* **88** (1975), no. 2 257 – 274.

[41] S. Coleman and J. Mandula, *All possible symmetries of the s matrix*, *Phys. Rev.* **159** (Jul, 1967) 1251–1256.

[42] G. C. Branco, P. M. Ferreira, L. Lavoura, M. N. Rebelo, M. Sher, and J. P. Silva, *Theory and phenomenology of two-Higgs-doublet models*, *Phys. Rept.* **516** (2012) 1–102, [arXiv:1106.0034].

[43] A. Djouadi, *The Anatomy of electro-weak symmetry breaking. II. The Higgs bosons in the minimal supersymmetric model*, *Phys. Rept.* **459** (2008) 1–241, [hep-ph/0503173].

[44] A. Arbey, M. Battaglia, A. Djouadi, F. Mahmoudi, and J. Quevillon, *Implications of a 125 GeV Higgs for supersymmetric models*, *Phys. Lett.* **B708** (2012) 162–169, [arXiv:1112.3028].

[45] M. A. Ajaib, I. Gogoladze, F. Nasir, and Q. Shafi, *Revisiting mGMSB in Light of a 125 GeV Higgs*, *Phys. Lett.* **B713** (2012) 462–468, [arXiv:1204.2856].

[46] A. Djouadi, *Implications of the Higgs discovery for SUSY*, *J. Phys. Conf. Ser.* **447** (2013) 012002.

[47] **ATLAS** Collaboration, G. Aad et al., *Summary of the searches for squarks and gluinos using $\sqrt{s} = 8$ TeV pp collisions with the ATLAS experiment at the LHC*, *JHEP* **10** (2015) 054, [arXiv:1507.05525].

[48] **ATLAS** Collaboration. https://atlas.web.cern.ch/Atlas/GROUPS/PHYSICS/CombinedSummaryPlots/SUSY/.

[49] **CMS** Collaboration, https://twiki.cern.ch/twiki/bin/view/CMSPublic/PhysicsResultsSUS.

[50] **XENON** Collaboration, E. Aprile et al., *First Dark Matter Search Results from the XENON1T Experiment*, arXiv:1705.06655.

[51] D. S. Akerib et al., *Results from a search for dark matter in the complete LUX exposure*, arXiv:1608.07648.

[52] A. Boyarsky, J. Lesgourgues, O. Ruchayskiy, and M. Viel, *Lyman-alpha constraints on warm and on warm-plus-cold dark matter models*, *JCAP* **0905** (2009) 012, [arXiv:0812.0010].

[53] J. Baur, N. Palanque-Delabrouille, C. Yèche, C. Magneville, and M. Viel, *Lyman-alpha Forests cool Warm Dark Matter*, *JCAP* **1608** (2016), no. 08 012, [arXiv:1512.01981].

[54] S. Gopalakrishna, A. de Gouvea, and W. Porod, *Right-handed sneutrinos as nonthermal dark matter*, *JCAP* **0605** (2006) 005, [hep-ph/0602027].

[55] T. Asaka, K. Ishiwata, and T. Moroi, *Right-handed sneutrino as cold dark matter*, *Phys. Rev.* **D73** (2006) 051301, [hep-ph/0512118].

[56] T. Asaka, K. Ishiwata, and T. Moroi, *Right-handed sneutrino as cold dark matter of the universe*, *Phys. Rev.* **D75** (2007) 065001, [hep-ph/0612211].

[57] V. Page, *Non-thermal right-handed sneutrino dark matter and the Omega(DM)/Omega(b) problem*, *JHEP* **04** (2007) 021, [hep-ph/0701266].

[58] T. Falk, K. A. Olive, and M. Srednicki, *Heavy sneutrinos as dark matter*, *Phys. Lett.* **B339** (1994) 248–251, [hep-ph/9409270].

[59] L. J. Hall, T. Moroi, and H. Murayama, *Sneutrino cold dark matter with lepton number violation*, *Phys. Lett.* **B424** (1998) 305–312, [hep-ph/9712515].

[60] C. Arina and N. Fornengo, *Sneutrino cold dark matter, a new analysis: Relic abundance and detection rates*, *JHEP* **11** (2007) 029, [arXiv:0709.4477].

[61] B. Dumont, G. Belanger, S. Fichet, S. Kraml, and T. Schwetz, *Mixed sneutrino dark matter in light of the 2011 XENON and LHC results*, *JCAP* **1209** (2012) 013, [arXiv:1206.1521].

[62] M. Kakizaki, E.-K. Park, J.-h. Park, and A. Santa, *Phenomenological constraints on light mixed sneutrino dark matter scenarios*, *Phys. Lett.* **B749** (2015) 44–49, [arXiv:1503.06783].

[63] A. Ghosh, T. Mondal, and B. Mukhopadhyaya, *Right sneutrino with $\Delta l = 2$ masses as nonthermal dark matter*, *Phys. Rev. D* **99** (Feb, 2019) 035018.

[64] R. Barbier et al., *R-parity violating supersymmetry*, *Phys. Rept.* **420** (2005) 1–202, [hep-ph/0406039].

[65] S. Dimopoulos, M. Dine, S. Raby, and S. D. Thomas, *Experimental signatures of low-energy gauge mediated supersymmetry breaking*, *Phys. Rev. Lett.* **76** (1996) 3494–3497, [hep-ph/9601367].

[66] F. Zwirner, *Effective interactions of a light gravitino*, *Fortsch. Phys.* **47** (1999) 325–332, [hep-th/9801003].

[67] J. L. Feng, M. Kamionkowski, and S. K. Lee, *Light Gravitinos at Colliders and Implications for Cosmology*, *Phys. Rev.* **D82** (2010) 015012, [arXiv:1004.4213].

[68] J. T. Ruderman and D. Shih, *General Neutralino NLSPs at the Early LHC*, *JHEP* **08** (2012) 159, [arXiv:1103.6083].

[69] J. S. Kim, M. E. Krauss, and V. Martin-Lozano, *Probing the Electroweakino Sector of General Gauge Mediation at the LHC*, arXiv:1705.06497.

[70] H. K. Dreiner, M. Hanussek, J. S. Kim, and S. Sarkar, *Gravitino cosmology with a very light neutralino*, *Phys. Rev.* **D85** (2012) 065027, [arXiv:1111.5715].

[71] B. C. Allanach, M. Badziak, G. Cottin, N. Desai, C. Hugonie, and R. Ziegler, *Prompt Signals and Displaced Vertices in Sparticle Searches for Next-to-Minimal Gauge Mediated Supersymmetric Models*, *Eur. Phys. J.* **C76** (2016), no. 9 482, [arXiv:1606.03099].

[72] H. Murayama, Y. Nomura, S. Shirai, and K. Tobioka, *Compact Supersymmetry*, *Phys. Rev.* **D86** (2012) 115014, [arXiv:1206.4993].

[73] K. Nakayama and T. T. Yanagida, *Anomaly mediation deformed by axion*, *Phys. Lett.* **B722** (2013) 107–110, [arXiv:1302.3332].

[74] D. S. M. Alves, E. Izaguirre, and J. G. Wacker, *It's On: Early Interpretations of ATLAS Results in Jets and Missing Energy Searches*, *Phys. Lett.* **B702** (2011) 64–68, [arXiv:1008.0407].

[75] E. Alvarez and Y. Bai, *Reach the Bottom Line of the Sbottom Search*, *JHEP* **08** (2012) 003, [arXiv:1204.5182].

[76] H. K. Dreiner, M. Kramer, and J. Tattersall, *How low can SUSY go? Matching, monojets and compressed spectra*, *Europhys. Lett.* **99** (2012) 61001, [arXiv:1207.1613].

[77] B. Bhattacherjee and K. Ghosh, *Degenerate SUSY search at the 8 TeV LHC*, arXiv:1207.6289.

[78] H. Dreiner, M. Krämer, and J. Tattersall, *Exploring QCD uncertainties when setting limits on compressed supersymmetric spectra*, *Phys. Rev.* **D87** (2013), no. 3 035006, [arXiv:1211.4981].

[79] B. Bhattacherjee, A. Choudhury, K. Ghosh, and S. Poddar, *Compressed supersymmetry at 14 TeV LHC*, *Phys. Rev.* **D89** (2014), no. 3 037702, [arXiv:1308.1526].

[80] G. Belanger, M. Heikinheimo, and V. Sanz, *Model-Independent Bounds on Squarks from Monophoton Searches*, *JHEP* **08** (2012) 151, [arXiv:1205.1463].

[81] T. Cohen, T. Golling, M. Hance, A. Henrichs, K. Howe, J. Loyal, S. Padhi, and J. G. Wacker, *SUSY Simplified Models at 14, 33, and 100 TeV Proton Colliders*, *JHEP* **04** (2014) 117, [arXiv:1311.6480].

[82] **ATLAS** Collaboration, *Search for squarks and gluinos with the ATLAS detector in final states with jets and missing transverse momentum and 20.3 fb*$^{-1}$ *of* $\sqrt{s} = 8$ *TeV proton-proton collision data*, Tech. Rep. ATLAS-CONF-2013-047, CERN, Geneva, May, 2013.

[83] **CMS** Collaboration, S. Chatrchyan et al., *Search for New Physics with a Mono-Jet and Missing Transverse Energy in pp Collisions at $\sqrt{s} = 7$ TeV*, *Phys. Rev. Lett.* **107** (2011) 201804, [arXiv:1106.4775].

[84] **ATLAS** Collaboration, G. Aad et al., *Search for new phenomena with the monojet and missing transverse momentum signature using the ATLAS detector in $\sqrt{s} = 7$ TeV proton-proton collisions*, *Phys. Lett.* **B705** (2011) 294–312, [arXiv:1106.5327].

[85] **ATLAS** Collaboration, G. Aad et al., *Search for squarks and gluinos with the ATLAS detector in final states with jets and missing transverse momentum using 4.7 fb$^{-1}$ of $\sqrt{s} = 7$ TeV proton-proton collision data*, *Phys. Rev.* **D87** (2013), no. 1 012008, [arXiv:1208.0949].

[86] S. Mukhopadhyay, M. M. Nojiri, and T. T. Yanagida, *Compressed SUSY search at the 13 TeV LHC using kinematic correlations and structure of ISR jets*, *JHEP* **10** (2014) 12, [arXiv:1403.6028].

[87] **CMS** Collaboration, V. Khachatryan et al., *Search for dark matter, extra dimensions, and unparticles in monojet events in proton–proton collisions at $\sqrt{s} = 8$ TeV*, *Eur. Phys. J.* **C75** (2015), no. 5 235, [arXiv:1408.3583].

[88] **ATLAS** Collaboration, G. Aad et al., *Search for new phenomena in final states with an energetic jet and large missing transverse momentum in pp collisions at $\sqrt{s}$ =8 TeV with the ATLAS detector*, *Eur. Phys. J.* **C75** (2015), no. 7 299, [arXiv:1502.01518]. [Erratum: Eur. Phys. J.C75,no.9,408(2015)].

[89] **ATLAS, CMS** Collaboration, G. Aad et al., *Combined Measurement of the Higgs Boson Mass in pp Collisions at $\sqrt{s} = 7$ and 8 TeV with the ATLAS and CMS Experiments*, *Phys. Rev. Lett.* **114** (2015) 191803, [arXiv:1503.07589].

[90] S. P. Martin, *Compressed supersymmetry and natural neutralino dark matter from top squark-mediated annihilation to top quarks*, *Phys. Rev.* **D75** (2007) 115005, [hep-ph/0703097].

[91] S. P. Martin, *The Top squark-mediated annihilation scenario and direct detection of dark matter in compressed supersymmetry*, *Phys. Rev.* **D76** (2007) 095005, [arXiv:0707.2812].

[92] H. Baer, A. Box, E.-K. Park, and X. Tata, *Implications of compressed supersymmetry for collider and dark matter searches*, *JHEP* **08** (2007) 060, [arXiv:0707.0618].

[93] **ATLAS** Collaboration, G. Aad et al., *Search for strong production of supersymmetric particles in final states with missing transverse momentum and at least three b-jets at $\sqrt{s}$= 8 TeV proton-proton collisions with the ATLAS detector*, *JHEP* **10** (2014) 024, [arXiv:1407.0600].

[94] **ATLAS** Collaboration, G. Aad et al., *Search for squarks and gluinos with the ATLAS detector in final states with jets and missing transverse momentum using $\sqrt{s} = 8$ TeV proton–proton collision data*, *JHEP* **09** (2014) 176, [arXiv:1405.7875].

[95] **ATLAS** Collaboration, G. Aad et al., *Search for top squark pair production in final states with one isolated lepton, jets, and missing transverse momentum in $\sqrt{s}$ =8 TeV pp collisions with the ATLAS detector*, *JHEP* **11** (2014) 118, [arXiv:1407.0583].

[96] **ATLAS** Collaboration, G. Aad et al., *Search for direct pair production of the top squark in all-hadronic final states in proton-proton collisions at $\sqrt{s} = 8$ TeV with the ATLAS detector*, *JHEP* **09** (2014) 015, [arXiv:1406.1122].

[97] **ATLAS** Collaboration, G. Aad et al., *Search for direct top-squark pair production in final states with two leptons in pp collisions at $\sqrt{s}$ = 8TeV with the ATLAS detector*, *JHEP* **06** (2014) 124, [arXiv:1403.4853].

[98] **ATLAS** Collaboration, G. Aad et al., *Search for pair-produced third-generation squarks decaying via charm quarks or in compressed supersymmetric scenarios in pp collisions at $\sqrt{s} = 8$ TeV with the ATLAS detector*, *Phys. Rev.* **D90** (2014), no. 5 052008, [arXiv:1407.0608].

[99] **ATLAS** Collaboration, G. Aad et al., *Search for direct third-generation squark pair production in final states with missing transverse momentum and two b-jets in $\sqrt{s}$ = 8 TeV pp collisions with the ATLAS detector*, *JHEP* **10** (2013) 189, [arXiv:1308.2631].

[100] CMS, *Summary of cms susy results in sms framework*, . https://twiki.cern.ch/twiki/pub/CMSPublic/SUSYSMSSummaryPlots8TeV/barplot_ICHEP2014.pdf.

[101] ATLAS, *Summary of atlas susy searches*, . https://atlas.web.cern.ch/Atlas/GROUPS/PHYSICS/CombinedSummaryPlots/SUSY/ATLAS_SUSY_Summary/ATLAS_SUSY_Summary.png.

[102] L. J. Hall, D. Pinner, and J. T. Ruderman, *A Natural SUSY Higgs Near 126 GeV*, *JHEP* **04** (2012) 131, [arXiv:1112.2703].

[103] A. Djouadi, *Implications of the Higgs discovery for supersymmetry*, *EPJ Web Conf.* **95** (2015) 03006.

[104] M. Carena, S. Heinemeyer, O. Stål, C. E. M. Wagner, and G. Weiglein, *MSSM Higgs Boson Searches at the LHC: Benchmark Scenarios after the Discovery of a Higgs-like Particle*, *Eur. Phys. J.* **C73** (2013), no. 9 2552, [arXiv:1302.7033].

[105] LEP2SUSYWG et al., *Lep2 joint susy working group*, . http://lepsusy.web.cern.ch/lepsusy/,b̃http://lepsusy.web.cern.ch/lepsusy/www/inoslowdmsummer02/charginolowdm_pub.html,b̃http://lepsusy.web.cern.ch/lepsusy/www/inos_moriond01/charginos_pub.html.

[106] **Heavy Flavor Averaging Group** Collaboration, Y. Amhis et al., *Averages of B-Hadron, C-Hadron, and tau-lepton properties as of early 2012*, arXiv:1207.1158.

[107] **LHCb collaboration** Collaboration, R. Aaij et al., *Measurement of the $B_s^0 \to \mu^+\mu^-$ branching fraction and search for $B^0 \to \mu^+\mu^-$ decays at the LHCb experiment*, *Phys.Rev.Lett.* **111** (2013) 101805, [arXiv:1307.5024].

[108] **CMS** Collaboration, S. Chatrchyan et al., *Measurement of the B(s) to mu+ mu- branching fraction and search for B0 to mu+ mu- with the CMS Experiment*, *Phys.Rev.Lett.* **111** (2013) 101804, [arXiv:1307.5025].

[109] **WMAP** Collaboration, G. Hinshaw et al., *Nine-Year Wilkinson Microwave Anisotropy Probe (WMAP) Observations: Cosmological Parameter Results*, *Astrophys.J.Suppl.* **208** (2013) 19, [arXiv:1212.5226].

[110] Z. Berezhiani and M. Y. Khlopov, *Cosmology of Spontaneously Broken Gauge Family Symmetry*, *Z.Phys.* **C49** (1991) 73–78.

[111] C. Boehm, P. Fayet, and J. Silk, *Light and heavy dark matter particles*, *Phys.Rev.* **D69** (2004) 101302, [hep-ph/0311143].

[112] E. Ma, *Supersymmetric Model of Radiative Seesaw Majorana Neutrino Masses*, *Annales Fond.Broglie* **31** (2006) 285, [hep-ph/0607142].

[113] P.-H. Gu, *Unified mass origin at TeV for dark matter and Dirac neutrinos*, *Phys.Lett.* **B661** (2008) 290–294, [arXiv:0710.1044].

[114] T. Hur, H.-S. Lee, and S. Nasri, *A Supersymmetric U(1)-prime model with multiple dark matters*, *Phys.Rev.* **D77** (2008) 015008, [arXiv:0710.2653].

[115] Q.-H. Cao, E. Ma, J. Wudka, and C.-P. Yuan, *Multipartite dark matter*, arXiv:0711.3881.

[116] T. Hambye, *Hidden vector dark matter*, *JHEP* **0901** (2009) 028, [arXiv:0811.0172].

[117] M. Aoki, M. Duerr, J. Kubo, and H. Takano, *Multi-Component Dark Matter Systems and Their Observation Prospects*, *Phys.Rev.* **D86** (2012) 076015, [arXiv:1207.3318].

[118] J. Heeck and H. Zhang, *Exotic Charges, Multicomponent Dark Matter and Light Sterile Neutrinos*, *JHEP* **1305** (2013) 164, [arXiv:1211.0538].

[119] **LUX Collaboration** Collaboration, D. Akerib et al., *First results from the LUX dark matter experiment at the Sanford Underground Research Facility*, *Phys.Rev.Lett.* **112** (2014), no. 9 091303, [arXiv:1310.8214].

[120] W. Porod, *SPheno, a program for calculating supersymmetric spectra, SUSY particle decays and SUSY particle production at e+ e- colliders*, *Comput. Phys. Commun.* **153** (2003) 275–315, [hep-ph/0301101].

[121] W. Porod and F. Staub, *SPheno 3.1: Extensions including flavour, CP-phases and models beyond the MSSM*, *Comput. Phys. Commun.* **183** (2012) 2458–2469, [arXiv:1104.1573].

[122] G. Belanger, F. Boudjema, A. Pukhov, and A. Semenov, *micrOMEGAs-3: A program for calculating dark matter observables*, *Comput. Phys. Commun.* **185** (2014) 960–985, [arXiv:1305.0237].

[123] J. Alwall, R. Frederix, S. Frixione, V. Hirschi, F. Maltoni, O. Mattelaer, H. S. Shao, T. Stelzer, P. Torrielli, and M. Zaro, *The automated computation of tree-level and next-to-leading order differential cross sections, and their matching to parton shower simulations*, *JHEP* **07** (2014) 079, [arXiv:1405.0301].

[124] J. Alwall, M. Herquet, F. Maltoni, O. Mattelaer, and T. Stelzer, *MadGraph 5 : Going Beyond*, *JHEP* **06** (2011) 128, [arXiv:1106.0522].

[125] J. Pumplin, D. R. Stump, J. Huston, H. L. Lai, P. M. Nadolsky, and W. K. Tung, *New generation of parton distributions with uncertainties from global QCD analysis*, *JHEP* **07** (2002) 012, [hep-ph/0201195].

[126] T. Sjostrand, S. Mrenna, and P. Z. Skands, *PYTHIA 6.4 Physics and Manual*, *JHEP* **05** (2006) 026, [hep-ph/0603175].

[127] M. L. Mangano, M. Moretti, F. Piccinini, and M. Treccani, *Matching matrix elements and shower evolution for top-quark production in hadronic collisions*, *JHEP* **01** (2007) 013, [hep-ph/0611129].

[128] S. Hoeche, F. Krauss, N. Lavesson, L. Lonnblad, M. Mangano, A. Schalicke, and S. Schumann, *Matching parton showers and matrix elements*, in *HERA and the LHC: A Workshop on the implications of HERA for LHC physics: Proceedings Part A*, 2006. hep-ph/0602031.

[129] **DELPHES 3** Collaboration, J. de Favereau, C. Delaere, P. Demin, A. Giammanco, V. Lemaître, A. Mertens, and M. Selvaggi, *DELPHES 3, A modular framework for fast simulation of a generic collider experiment*, *JHEP* **02** (2014) 057, [arXiv:1307.6346].

[130] M. Selvaggi, *DELPHES 3: A modular framework for fast-simulation of generic collider experiments*, *J. Phys. Conf. Ser.* **523** (2014) 012033.

[131] A. Mertens, *New features in Delphes 3*, *J. Phys. Conf. Ser.* **608** (2015), no. 1 012045.

[132] M. Cacciari, G. P. Salam, and G. Soyez, *The Anti-k(t) jet clustering algorithm*, *JHEP* **04** (2008) 063, [arXiv:0802.1189].

[133] M. Cacciari, G. P. Salam, and G. Soyez, *FastJet User Manual*, *Eur. Phys. J.* **C72** (2012) 1896, [arXiv:1111.6097].

[134] W. Beenakker, R. Hopker, and M. Spira, *PROSPINO: A Program for the production of supersymmetric particles in next-to-leading order QCD*, hep-ph/9611232. http://www.thphys.uni-b̃heidelberg.de/~plehn/index.php?show=prospino&visible=tools.

[135] T. Plehn, *Measuring the MSSM Lagrangean*, *Czech. J. Phys.* **55** (2005) B213–B220, [hep-ph/0410063].

[136] M. Spira, *Higgs and SUSY particle production at hadron colliders*, in *Supersymmetry and unification of fundamental interactions. Proceedings, 10th International Conference, SUSY'02, Hamburg, Germany, June 17-23, 2002*, pp. 217–226, 2002. hep-ph/0211145.

[137] W. Beenakker, M. Kramer, T. Plehn, M. Spira, and P. M. Zerwas, *Stop production at hadron colliders*, *Nucl. Phys.* **B515** (1998) 3–14, [hep-ph/9710451].

[138] W. Beenakker, R. Hopker, M. Spira, and P. M. Zerwas, *Squark and gluino production at hadron colliders*, *Nucl. Phys.* **B492** (1997) 51–103, [hep-ph/9610490].

[139] http://moriond.in2p3.fr/QCD/2019/TuesdayMorning/Strobbe.pdf. Talk by Nadja Strobbe, Moriond 2019.

[140] **CMS** Collaboration, S. Chatrchyan et al., *Search for new physics in the multijet and missing transverse momentum final state in proton-proton collisions at $\sqrt{s}$= 8 TeV*, *JHEP* **06** (2014) 055, [arXiv:1402.4770].

[141] **ATLAS** Collaboration, *Search for new phenomena in final states with an energetic jet and large missing transverse momentum in pp collisions at $\sqrt{s} = 13$ TeV using the atlas detector*, *Phys. Rev. D* **94** (Aug, 2016) 032005.

[142] **ATLAS** Collaboration, M. Aaboud et al., *Search for squarks and gluinos in final states with jets and missing transverse momentum at $\sqrt{s}$ = 13 TeV with the ATLAS detector*, *Eur. Phys. J.* **C76** (2016), no. 7 392, [arXiv:1605.03814].

[143] **CMS** Collaboration, *An inclusive search for new phenomena in final states with one or more jets and missing transverse momentum at 13 TeV with the AlphaT variable*, Tech. Rep. CMS-PAS-SUS-16-016, CERN, Geneva, 2016.

[144] **ATLAS** Collaboration, G. Aad et al., *Search for diphoton events with large missing transverse momentum in 7 TeV proton-proton collision data with the ATLAS detector*, *Phys. Lett.* **B718** (2012) 411–430, [arXiv:1209.0753].

[145] **ATLAS** Collaboration, G. Aad et al., *Search for photonic signatures of gauge-mediated supersymmetry in 8 TeV pp collisions with the ATLAS detector*, *Phys. Rev.* **D92** (2015), no. 7 072001, [arXiv:1507.05493].

[146] **CMS** Collaboration, V. Khachatryan et al., *Search for supersymmetry in events with photons and missing transverse energy in pp collisions at 13 TeV*, *Phys. Lett. B* **769** (Nov, 2016) 391–412. 22 p.

[147] **CMS** Collaboration, V. Khachatryan et al., *Search for supersymmetry in electroweak production with photons and large missing transverse energy in pp collisions at sqrt(s) = 8 TeV*, *Phys. Lett.* **B759** (2016) 479–500, [arXiv:1602.08772].

[148] **CMS** Collaboration, *Search for supersymmetry in final states with at least one photon and MET in pp collisions at sqrt(s)=13 TeV*, Tech. Rep. CMS-PAS-SUS-16-023, CERN, Geneva, 2016.

[149] **ATLAS** Collaboration, M. Aaboud et al., *Search for supersymmetry in a final state containing two photons and missing transverse momentum in $\sqrt{s}$ = 13 TeV pp collisions at the LHC using the ATLAS detector*, *Eur. Phys. J.* **C76** (2016), no. 9 517, [arXiv:1606.09150].

[150] **ATLAS** Collaboration, *Search for Supersymmetry in events with photons, jets and missing transverse energy with the ATLAS detector in 13 TeV pp collisions*, Tech. Rep. ATLAS-CONF-2016-066, CERN, Geneva, Aug, 2016.

[151] **CMS** Collaboration, V. Khachatryan et al., *Search for supersymmetry in events with photons and missing transverse energy in pp collisions at 13 TeV*, *Phys. Lett.* **B769** (2017) 391–412, [arXiv:1611.06604].

[152] A. Albaid and K. S. Babu, *Higgs boson of mass 125 GeV in GMSB models with messenger-matter mixing*, *Phys. Rev.* **D88** (2013) 055007, [arXiv:1207.1014].

[153] P. Byakti and T. S. Ray, *Burgeoning the Higgs mass to 125 GeV through messenger-matter interactions in GMSB models*, *JHEP* **05** (2013) 055, [arXiv:1301.7605].

[154] E. A. Baltz and H. Murayama, *Gravitino warm dark matter with entropy production*, *JHEP* **05** (2003) 067, [astro-ph/0108172].

[155] M. Viel, J. Lesgourgues, M. G. Haehnelt, S. Matarrese, and A. Riotto, *Constraining warm dark matter candidates including sterile neutrinos and light gravitinos with WMAP and the Lyman-alpha forest*, *Phys. Rev.* **D71** (2005) 063534, [astro-ph/0501562].

[156] L. Covi, J. Hasenkamp, S. Pokorski, and J. Roberts, *Gravitino Dark Matter and general neutralino NLSP*, *JHEP* **11** (2009) 003, [arXiv:0908.3399].

[157] L. Covi, M. Olechowski, S. Pokorski, K. Turzynski, and J. D. Wells, *Supersymmetric mass spectra for gravitino dark matter with a high reheating temperature*, *JHEP* **01** (2011) 033, [arXiv:1009.3801].

[158] A. Arbey, M. Battaglia, L. Covi, J. Hasenkamp, and F. Mahmoudi, *LHC constraints on Gravitino Dark Matter*, *Phys. Rev.* **D92** (2015), no. 11 115008, [arXiv:1505.04595].

[159] L. Covi, *DARK MATTER CANDIDATES: AXINO AND GRAVITINO*, in *Proceedings, 46th Rencontres de Moriond on Electroweak Interactions and Unified Theories: La Thuile, Italy, March 13-20, 2011*, pp. 381–388, 2011.

[160] W. Porod, *The decays $\widetilde{g} \to \widetilde{t}_1\ \bar{b}W$ and gluino $\to \widetilde{t}_1\ \bar{c}$ and phenomenological implications in supersymmetric theories*, *JHEP* **05** (2002) 030, [hep-ph/0202259].

[161] **ATLAS** Collaboration, *Combined measurements of the Higgs boson production and decay rates in $H \to ZZ^* \to 4\ell$ and $H \to \gamma\gamma$ final states using pp collision data at $\sqrt{s} = 13$ TeV in the ATLAS experiment*, Tech. Rep. ATLAS-CONF-2016-081, CERN, Geneva, Aug, 2016.

[162] **CMS** Collaboration, V. Khachatryan et al., *Search for supersymmetry in events with photons and missing transverse energy*, .

[163] https://cp3.irmp.ucl.ac.be/projects/madgraph/wiki/IntroMatching.

[164] https://cp3.irmp.ucl.ac.be/projects/madgraph/wiki/FAQ-b̃General-b̃13.

[165] A. Kulesza and L. Motyka, *Threshold resummation for squark-antisquark and gluino-pair production at the lhc*, *Phys. Rev. Lett.* **102** (Mar, 2009) 111802.

[166] A. Kulesza and L. Motyka, *Soft gluon resummation for the production of gluino-gluino and squark-antisquark pairs at the lhc*, *Phys. Rev. D* **80** (Nov, 2009) 095004.

[167] W. Beenakker, S. Brensing, M. Krämer, A. Kulesza, E. Laenen, and I. Niessen, *Soft-gluon resummation for squark and gluino hadroproduction*, *Journal of High Energy Physics* **2009** (2009), no. 12 041.

[168] W. Beenakker, C. Borschensky, M. Krämer, A. Kulesza, E. Laenen, S. Marzani, and J. Rojo, *NLO+NLL squark and gluino production cross-sections with threshold-improved parton distributions*, *Eur. Phys. J.* **C76** (2016), no. 2 53, [arXiv:1510.00375].

[169] **ATLAS** Collaboration, *Further searches for squarks and gluinos in final states with jets and missing transverse momentum at $\sqrt{s}$ =13 TeV with the ATLAS detector*, .

[170] P. Meade, M. Reece, and D. Shih, *Prompt Decays of General Neutralino NLSPs at the Tevatron*, *JHEP* **05** (2010) 105, [arXiv:0911.4130].

[171] K. T. Matchev and S. D. Thomas, *Higgs and Z boson signatures of supersymmetry*, *Phys. Rev.* **D62** (2000) 077702, [hep-ph/9908482].

[172] **CMS** Collaboration, A. M. Sirunyan et al., *Combined search for electroweak production of charginos and neutralinos in proton-proton collisions at $\sqrt{s}$ = 13 TeV*, *JHEP* **03** (2018) 160, [arXiv:1801.03957].

[173] **ATLAS** Collaboration, https://atlas.web.cern.ch/Atlas/GROUPS/PHYSICS/CombinedSummaryPlots/SUSY/ATLAS_SUSY_EWSummary_GGM/ATLAS_SUSY_EWSummary_GGM.png.

[174] H. Baer, V. Barger, P. Huang, D. Mickelson, A. Mustafayev, and X. Tata, *Radiative natural supersymmetry: Reconciling electroweak fine-tuning and the Higgs boson mass*, *Phys. Rev.* **D87** (2013), no. 11 115028, [arXiv:1212.2655].

[175] H. Baer, V. Barger, P. Huang, D. Mickelson, A. Mustafayev, and X. Tata, *Naturalness, Supersymmetry and Light Higgsinos: A Snowmass Whitepaper*, in *Proceedings, Community Summer Study 2013: Snowmass on the Mississippi (CSS2013): Minneapolis, MN, USA, July 29-August 6, 2013*, 2013. arXiv:1306.2926.

[176] A. Mustafayev and X. Tata, *Supersymmetry, Naturalness, and Light Higgsinos*, *Indian J. Phys.* **88** (2014) 991–1004, [arXiv:1404.1386].

[177] H. Baer, V. Barger, P. Huang, A. Mustafayev, and X. Tata, *Radiative natural SUSY with a 125 GeV Higgs boson*, *Phys. Rev. Lett.* **109** (2012) 161802, [arXiv:1207.3343].

[178] H. Baer, V. Barger, M. Savoy, and X. Tata, *Multichannel assault on natural supersymmetry at the high luminosity LHC*, *Phys. Rev.* **D94** (2016), no. 3 035025, [arXiv:1604.07438].

[179] H. Baer, V. Barger, J. S. Gainer, P. Huang, M. Savoy, D. Sengupta, and X. Tata, *Gluino reach and mass extraction at the lhc in radiatively-driven natural susy*, *The European Physical Journal C* **77** (Jul, 2017) 499.

[180] **CMS** Collaboration, *Search for disappearing tracks in proton-proton collisions at* $\sqrt{s} = 13\,\mathrm{TeV}$, Tech. Rep. CMS-PAS-EXO-16-044, CERN, Geneva, 2018.

[181] **ATLAS** Collaboration, M. Aaboud et al., *Search for metastable heavy charged particles with large ionization energy loss in pp collisions at* $\sqrt{s} = 13$ *TeV using the ATLAS experiment*, *Phys. Rev.* **D93** (2016), no. 11 112015, [arXiv:1604.04520].

[182] S. Raby, *Long-lived gluinos and stable axinos*, *Phys. Rev. Lett.* **115** (Dec, 2015) 231801.

[183] M. Drees, M. M. Nojiri, D. P. Roy, and Y. Yamada, *Light Higgsino dark matter*, *Phys. Rev.* **D56** (1997) 276–290, [hep-ph/9701219]. [Erratum: Phys. Rev.D64,039901(2001)].

[184] G. F. Giudice and A. Pomarol, *Mass degeneracy of the Higgsinos*, *Phys. Lett.* **B372** (1996) 253–258, [hep-ph/9512337].

[185] **CMS** Collaboration, A. M. Sirunyan et al., *Combined measurements of Higgs boson couplings in proton-proton collisions at* $\sqrt{s} = 13$ *TeV*, *Submitted to: Eur. Phys. J.* (2018) [arXiv:1809.10733].

[186] **ATLAS** Collaboration, M. Aaboud et al., *Search for pair production of higgsinos in final states with at least three b-tagged jets in* $\sqrt{s} = 13$ *TeV pp collisions using the ATLAS detector*, *Submitted to: Phys. Rev.* (2018) [arXiv:1806.04030].

[187] **CMS** Collaboration, A. M. Sirunyan et al., *Search for Physics Beyond the Standard Model in Events with High-Momentum Higgs Bosons and Missing Transverse Momentum in Proton-Proton Collisions at 13 TeV*, *Phys. Rev. Lett.* **120** (2018), no. 24 241801, [arXiv:1712.08501].

[188] **ATLAS** Collaboration, M. Aaboud et al., *Search for supersymmetry in events with four or more leptons in* $\sqrt{s} = 13$ *TeV pp collisions with ATLAS*, arXiv:1804.03602.

[189] **ATLAS** Collaboration, M. Aaboud et al., *Search for squarks and gluinos in final states with jets and missing transverse momentum using 36 fb$^{-1}$ of $\sqrt{s} = 13$ TeV pp collision data with the ATLAS detector*, *Phys. Rev.* **D97** (2018), no. 11 112001, [arXiv:1712.02332].

[190] **ATLAS** Collaboration, M. Aaboud et al., *Search for chargino and neutralino production in final states with a Higgs boson and missing transverse momentum at $\sqrt{s} = 13$ TeV with the ATLAS detector*, arXiv:1812.09432.

[191] **CMS** Collaboration, A. M. Sirunyan et al., *Search for new phenomena in final states with two opposite-charge, same-flavor leptons, jets, and missing transverse momentum in pp collisions at $\sqrt{s} = 13$ TeV*, *JHEP* **03** (2018) 076, [arXiv:1709.08908].

[192] **CMS** Collaboration, *Search for physics beyond the standard model in events with high-momentum higgs bosons and missing transverse momentum in proton-proton collisions at 13 tev*, *Phys. Rev. Lett.* **120** (Jun, 2018) 241801.

[193] A. Arbey, M. Battaglia, A. Djouadi, F. Mahmoudi, and J. Quevillon, *Implications of a 125 gev higgs for supersymmetric models*, *Physics Letters B* **708** (2012), no. 1 162 – 169.

[194] M. Drees, H. Dreiner, D. Schmeier, J. Tattersall, and J. S. Kim, *CheckMATE: Confronting your Favourite New Physics Model with LHC Data*, *Comput. Phys. Commun.* **187** (2015) 227–265, [arXiv:1312.2591].

[195] N. D. Christensen, P. de Aquino, N. Deutschmann, C. Duhr, B. Fuks, C. Garcia-Cely, O. Mattelaer, K. Mawatari, B. Oexl, and Y. Takaesu, *Simulating spin-3/2particles at colliders*, *The European Physical Journal C* **73** (Oct, 2013) 2580.

[196] Pythia. http://home.thep.lu.se/~torbjorn/pythia81html/Welcome.html.

[197] H.-C. Cheng and Z. Han, *Minimal Kinematic Constraints and m(T2)*, *JHEP* **12** (2008) 063, [arXiv:0810.5178].

[198] L. H. V. cross-sections Working Group. https://twiki.cern.ch/twiki/bin/view/LHCPhysics/LHCHXSWG1HELHCXsecs.

[199] M. Grazzini, S. Kallweit, D. Rathlev, and M. Wiesemann, *$W^{\pm}Z$ production at hadron colliders in NNLO QCD*, *Phys. Lett.* **B761** (2016) 179–183, [arXiv:1604.08576].

[200] F. Cascioli, T. Gehrmann, M. Grazzini, S. Kallweit, P. Maierhöfer, A. von Manteuffel, S. Pozzorini, D. Rathlev, L. Tancredi, and E. Weihs, *ZZ production at hadron colliders in NNLO QCD*, *Phys. Lett.* **B735** (2014) 311–313, [arXiv:1405.2219].

[201] M. Czakon, P. Fiedler, and A. Mitov, *Total Top-Quark Pair-Production Cross Section at Hadron Colliders Through* $O(\alpha_S^4)$, *Phys. Rev. Lett.* **110** (2013) 252004, [arXiv:1303.6254].

[202] L. T. NNLO. https://twiki.cern.ch/twiki/bin/view/LHCPhysics/TtbarNNLO#Top_quark_pair_cross_sections_at.

[203] V. D. Barjer and R. J.N.Philips, *Collider Physics*. ABP, Westview Press, 276 p, 1991.

[204] M. Duncan, G. Kane, and W. Repko, *Ww physics at future colliders*, *Nuclear Physics B* **272** (1986), no. 3 517 – 559.

[205] **ATLAS** Collaboration, M. Aaboud et al., *Measurement of* $W^{\pm}Z$ *production cross sections and gauge boson polarisation in pp collisions at* $\sqrt{s} = 13$ *TeV with the ATLAS detector*, arXiv:1902.05759.

[206] P. Meade, M. Reece, and D. Shih, *Long-Lived Neutralino NLSPs*, *JHEP* **10** (2010) 067, [arXiv:1006.4575].

[207] G. Brooijmans et al., *Les Houches 2017: Physics at TeV Colliders New Physics Working Group Report*, in *10th Les Houches Workshop on Physics at TeV Colliders (PhysTeV 2017) Les Houches, France, June 5-23, 2017*, 2018. arXiv:1803.10379.

[208] J. R. Andersen et al., *Les Houches 2017: Physics at TeV Colliders Standard Model Working Group Report*, in *10th Les Houches Workshop on Physics at TeV Colliders (PhysTeV 2017) Les Houches, France, June 5-23, 2017*, 2018. arXiv:1803.07977.

[209] R. Barbieri and G. F. Giudice, *Upper Bounds on Supersymmetric Particle Masses*, *Nucl. Phys.* **B306** (1988) 63–76.

[210] J. R. Ellis, K. Enqvist, D. V. Nanopoulos, and F. Zwirner, *Observables in Low-Energy Superstring Models*, *Mod. Phys. Lett.* **A1** (1986) 57.

[211] J. L. Feng, *Naturalness and the Status of Supersymmetry*, *Ann. Rev. Nucl. Part. Sci.* **63** (2013) 351–382, [arXiv:1302.6587].

[212] G. F. Giudice, *Naturalness after LHC8*, *PoS* **EPS-HEP2013** (2013) 163, [arXiv:1307.7879].

[213] H. Baer, V. Barger, and M. Savoy, *Upper bounds on sparticle masses from naturalness or how to disprove weak scale supersymmetry*, *Phys. Rev.* **D93** (2016), no. 3 035016, [arXiv:1509.02929].

[214] H. Baer, V. Barger, J. S. Gainer, P. Huang, M. Savoy, D. Sengupta, and X. Tata, *Gluino reach and mass extraction at the LHC in radiatively-driven natural SUSY*, *Eur. Phys. J.* **C77** (2017), no. 7 499, [arXiv:1612.00795].

[215] **ATLAS** Collaboration, https://atlas.web.cern.ch/Atlas/GROUPS/PHYSICS/CombinedSummaryPlots/SUSY/.

[216] **CMS** Collaboration, https://twiki.cern.ch/twiki/bin/view/CMSPublic/PhysicsResultsSUS.

[217] A. Choudhury and A. Datta, *Many faces of low mass neutralino dark matter in the unconstrained MSSM, LHC data and new signals*, *JHEP* **06** (2012) 006, [arXiv:1203.4106].

[218] G. Bélanger, G. Drieu La Rochelle, B. Dumont, R. M. Godbole, S. Kraml, and S. Kulkarni, *LHC constraints on light neutralino dark matter in the MSSM*, *Phys. Lett.* **B726** (2013) 773–780, [arXiv:1308.3735].

[219] A. Choudhury and A. Datta, *Neutralino dark matter confronted by the LHC constraints on Electroweak SUSY signals*, *JHEP* **09** (2013) 119, [arXiv:1305.0928].

[220] C. Boehm, P. S. B. Dev, A. Mazumdar, and E. Pukartas, *Naturalness of Light Neutralino Dark Matter in pMSSM after LHC, XENON100 and Planck Data*, *JHEP* **06** (2013) 113, [arXiv:1303.5386].

[221] M. Chakraborti, U. Chattopadhyay, A. Choudhury, A. Datta, and S. Poddar, *The Electroweak Sector of the pMSSM in the Light of LHC - 8 TeV and Other Data*, *JHEP* **07** (2014) 019, [arXiv:1404.4841].

[222] G. Grilli di Cortona, *Hunting electroweakinos at future hadron colliders and direct detection experiments*, *JHEP* **05** (2015) 035, [arXiv:1412.5952].

[223] M. Drees and J. S. Kim, *Minimal natural supersymmetry after the LHC8*, *Phys. Rev.* **D93** (2016), no. 9 095005, [arXiv:1511.04461].

[224] M. Chakraborti, U. Chattopadhyay, A. Choudhury, A. Datta, and S. Poddar, *Reduced LHC constraints for higgsino-like heavier electroweakinos*, *JHEP* **11** (2015) 050, [arXiv:1507.01395].

[225] M. Badziak, A. Delgado, M. Olechowski, S. Pokorski, and K. Sakurai, *Detecting underabundant neutralinos*, *JHEP* **11** (2015) 053, [arXiv:1506.07177].

[226] J. Cao, Y. He, L. Shang, W. Su, and Y. Zhang, *Testing the light dark matter scenario of the MSSM at the LHC*, *JHEP* **03** (2016) 207, [arXiv:1511.05386].

[227] M. Beneke, A. Bharucha, A. Hryczuk, S. Recksiegel, and P. Ruiz-Femenia, *The last refuge of mixed wino-Higgsino dark matter*, arXiv:1611.00804.

[228] H. Baer, V. Barger, P. Huang, D. Mickelson, M. Padeffke-Kirkland, and X. Tata, *Natural SUSY with a bino- or wino-like LSP*, *Phys. Rev.* **D91** (2015), no. 7 075005, [arXiv:1501.06357].

[229] M. Abdughani, L. Wu, and J. M. Yang, *Status and prospects of light bino–higgsino dark matter in natural SUSY*, *Eur. Phys. J.* **C78** (2018), no. 1 4, [arXiv:1705.09164].

[230] M. R. Buckley, D. Feld, S. Macaluso, A. Monteux, and D. Shih, *Cornering natural susy at lhc run ii and beyond*, *Journal of High Energy Physics* **2017** (Aug, 2017) 115.

[231] H. Baer, V. Barger, and P. Huang, *Hidden SUSY at the LHC: the light higgsino-world scenario and the role of a lepton collider*, *JHEP* **11** (2011) 031, [arXiv:1107.5581].

[232] C. Han, A. Kobakhidze, N. Liu, A. Saavedra, L. Wu, and J. M. Yang, *Probing Light Higgsinos in Natural SUSY from Monojet Signals at the LHC*, *JHEP* **02** (2014) 049, [arXiv:1310.4274].

[233] Z. Han, G. D. Kribs, A. Martin, and A. Menon, *Hunting quasidegenerate Higgsinos*, *Phys. Rev.* **D89** (2014), no. 7 075007, [arXiv:1401.1235].

[234] D. Barducci, A. Belyaev, A. K. M. Bharucha, W. Porod, and V. Sanz, *Uncovering Natural Supersymmetry via the interplay between the LHC and Direct Dark Matter Detection*, *JHEP* **07** (2015) 066, [arXiv:1504.02472].

[235] H. Fukuda, N. Nagata, H. Otono, and S. Shirai, *Higgsino Dark Matter or Not: Role of Disappearing Track Searches at the LHC and Future Colliders*, arXiv:1703.09675.

[236] R. Mahbubani, P. Schwaller, and J. Zurita, *Closing the window for compressed Dark Sectors with disappearing charged tracks*, *JHEP* **06** (2017) 119, [arXiv:1703.05327]. [Erratum: JHEP10,061(2017)].

[237] S. Ambrosanio, B. Mele, S. Petrarca, G. Polesello, and A. Rimoldi, *Measuring the SUSY breaking scale at the LHC in the slepton NLSP scenario of GMSB models*, *JHEP* **01** (2001) 014, [hep-ph/0010081].

[238] J. R. Ellis, K. A. Olive, Y. Santoso, and V. C. Spanos, *Prospects for sparticle discovery in variants of the MSSM*, *Phys. Lett.* **B603** (2004) 51, [hep-ph/0408118].

[239] L. Roszkowski, R. Ruiz de Austri, and K.-Y. Choi, *Gravitino dark matter in the CMSSM and implications for leptogenesis and the LHC*, *JHEP* **08** (2005) 080, [hep-ph/0408227].

[240] J. R. Ellis, A. R. Raklev, and O. K. Oye, *Gravitino dark matter scenarios with massive metastable charged sparticles at the LHC*, *JHEP* **10** (2006) 061, [hep-ph/0607261].

[241] G. D. Kribs, A. Martin, and T. S. Roy, *Supersymmetry with a Chargino NLSP and Gravitino LSP*, *JHEP* **01** (2009) 023, [arXiv:0807.4936].

[242] S. Bailly, K.-Y. Choi, K. Jedamzik, and L. Roszkowski, *A Re-analysis of Gravitino Dark Matter in the Constrained MSSM*, *JHEP* **05** (2009) 103, [arXiv:0903.3974].

[243] T. Figy, K. Rolbiecki, and Y. Santoso, *Tau-Sneutrino NLSP and Multilepton Signatures at the LHC*, *Phys. Rev.* **D82** (2010) 075016, [arXiv:1005.5136].

[244] P. de Aquino, F. Maltoni, K. Mawatari, and B. Oexl, *Light Gravitino Production in Association with Gluinos at the LHC*, *JHEP* **10** (2012) 008, [arXiv:1206.7098].

[245] J. Barnard, B. Farmer, T. Gherghetta, and M. White, *Natural gauge mediation with a bino NLSP at the LHC*, *Phys. Rev. Lett.* **109** (2012) 241801, [arXiv:1208.6062].

[246] S. Bobrovskyi, J. Hajer, and S. Rydbeck, *Long-lived higgsinos as probes of gravitino dark matter at the LHC*, *JHEP* **02** (2013) 133, [arXiv:1211.5584].

[247] L. Roszkowski, S. Trojanowski, K. Turzynski, and K. Jedamzik, *Gravitino dark matter with constraints from Higgs boson mass and sneutrino decays*, *JHEP* **03** (2013) 013, [arXiv:1212.5587].

[248] R. H. Cyburt, J. Ellis, B. D. Fields, F. Luo, K. A. Olive, and V. C. Spanos, *Gravitino Decays and the Cosmological Lithium Problem in Light of the LHC Higgs and Supersymmetry Searches*, *JCAP* **1305** (2013) 014, [arXiv:1303.0574].

[249] J. D'Hondt, K. De Causmaecker, B. Fuks, A. Mariotti, K. Mawatari, C. Petersson, and D. Redigolo, *Multilepton signals of gauge mediated supersymmetry breaking at the LHC*, *Phys. Lett.* **B731** (2014) 7–12, [arXiv:1310.0018].

[250] J. Heisig, *Gravitino LSP and leptogenesis after the first LHC results*, *JCAP* **1404** (2014) 023, [arXiv:1310.6352].

[251] L. Covi and F. Dradi, *Long-Lived stop at the LHC with or without R-parity*, *JCAP* **1410** (2014), no. 10 039, [arXiv:1403.4923].

[252] F. Maltoni, A. Martini, K. Mawatari, and B. Oexl, *Signals of a superlight gravitino at the LHC*, *JHEP* **04** (2015) 021, [arXiv:1502.01637].

[253] H. Baer, R. Dermisek, S. Rajagopalan, and H. Summy, *Neutralino, axion and axino cold dark matter in minimal, hypercharged and gaugino AMSB*, *JCAP* **1007** (2010) 014, [arXiv:1004.3297].

[254] H. Baer, A. Lessa, S. Rajagopalan, and W. Sreethawong, *Mixed axion/neutralino cold dark matter in supersymmetric models*, *JCAP* **1106** (2011) 031, [arXiv:1103.5413].

[255] K. J. Bae, H. Baer, and E. J. Chun, *Mixed axion/neutralino dark matter in the SUSY DFSZ axion model*, *JCAP* **1312** (2013) 028, [arXiv:1309.5365].

[256] K. J. Bae, H. Baer, E. J. Chun, and C. S. Shin, *Mixed axion/gravitino dark matter from SUSY models with heavy axinos*, *Phys. Rev.* **D91** (2015), no. 7 075011, [arXiv:1410.3857].

[257] K. J. Bae, H. Baer, A. Lessa, and H. Serce, *Mixed axion-wino dark matter*, *Front.in Phys.* **3** (2015) 49, [arXiv:1502.07198].

[258] N. Arkani-Hamed, L. J. Hall, H. Murayama, D. Tucker-Smith, and N. Weiner, *Small neutrino masses from supersymmetry breaking*, *Phys. Rev.* **D64** (2001) 115011, [hep-ph/0006312].

[259] A. Kumar, D. Tucker-Smith, and N. Weiner, *Neutrino Mass, Sneutrino Dark Matter and Signals of Lepton Flavor Violation in the MRSSM*, *JHEP* **09** (2010) 111, [arXiv:0910.2475].

[260] K. Kadota and K. A. Olive, *Heavy Right-Handed Neutrinos and Dark Matter in the nuCMSSM*, *Phys. Rev.* **D80** (2009) 095015, [arXiv:0909.3075].

[261] G. Belanger, M. Kakizaki, E. K. Park, S. Kraml, and A. Pukhov, *Light mixed sneutrinos as thermal dark matter*, *JCAP* **1011** (2010) 017, [arXiv:1008.0580].

[262] A. Chatterjee, D. Das, B. Mukhopadhyaya, and S. K. Rai, *Right Sneutrino Dark Matter and a Monochromatic Photon Line*, *JCAP* **1407** (2014) 023, [arXiv:1401.2527].

[263] N. Cerna-Velazco, T. Faber, J. Jones-Perez, and W. Porod, *Constraining sleptons at the LHC in a supersymmetric low-scale seesaw scenario*, *Eur. Phys. J.* **C77** (2017), no. 10 661, [arXiv:1705.06583].

[264] S. Gopalakrishna, A. de Gouvêa, and W. Porod, *Right-handed sneutrinos as nonthermal dark matter*, *Journal of Cosmology and Astroparticle Physics* **2006** (may, 2006) 005–005.

[265] A. de Gouvêa, S. Gopalakrishna, and W. Porod, *Stop decay into right-handed sneutrino LSP at hadron colliders*, *Journal of High Energy Physics* **2006** (nov, 2006) 050–050.

[266] S. K. Gupta, B. Mukhopadhyaya, and S. K. Rai, *Right-chiral sneutrinos and long-lived staus: Event characteristics at the large hadron collider*, *Phys. Rev.* **D75** (2007) 075007, [hep-ph/0701063].

[267] D. Choudhury, S. K. Gupta, and B. Mukhopadhyaya, *Right sneutrinos in a supergravity model and the signals of a stable stop at the Large Hadron Collider*, *Phys. Rev.* **D78** (2008) 015023, [arXiv:0804.3560].

[268] J. Guo, Z. Kang, J. Li, T. Li, and Y. Liu, *Simplified Supersymmetry with Sneutrino LSP at 8 TeV LHC*, *JHEP* **10** (2014) 164, [arXiv:1312.2821].

[269] C. Arina and M. E. Cabrera, *Multi-lepton signatures at lhc from sneutrino dark matter*, *Journal of High Energy Physics* **2014** (Apr, 2014) 100.

[270] C. Arina, M. E. C. Catalan, S. Kraml, S. Kulkarni, and U. Laa, *Constraints on sneutrino dark matter from LHC Run 1*, *JHEP* **05** (2015) 142, [arXiv:1503.02960].

[271] S. Banerjee, G. Bélanger, B. Mukhopadhyaya, and P. D. Serpico, *Signatures of sneutrino dark matter in an extension of the CMSSM*, *JHEP* **07** (2016) 095, [arXiv:1603.08834].

[272] Y. Grossman and H. E. Haber, *Sneutrino mixing phenomena*, *Phys. Rev. Lett.* **78** (1997) 3438–3441, [hep-ph/9702421].

[273] J. A. Casas and A. Ibarra, *Oscillating neutrinos and muon $\to$ e, $\gamma$*, *Nucl. Phys.* **B618** (2001) 171–204, [hep-ph/0103065].

[274] M. Drewes, *The Phenomenology of Right Handed Neutrinos*, *Int. J. Mod. Phys.* **E22** (2013) 1330019, [arXiv:1303.6912].

[275] R. W. Rasmussen and W. Winter, *Perspectives for tests of neutrino mass generation at the GeV scale: Experimental reach versus theoretical predictions*, *Phys. Rev.* **D94** (2016), no. 7 073004, [arXiv:1607.07880].

[276] A. Dedes, H. E. Haber, and J. Rosiek, *Seesaw mechanism in the sneutrino sector and its consequences*, *JHEP* **11** (2007) 059, [arXiv:0707.3718].

[277] D. Pierce and A. Papadopoulos, *Radiative corrections to neutralino and chargino masses in the minimal supersymmetric model*, *Phys. Rev.* **D50** (1994) 565–570, [hep-ph/9312248].

[278] D. Pierce and A. Papadopoulos, *The Complete radiative corrections to the gaugino and Higgsino masses in the minimal supersymmetric model*, *Nucl. Phys.* **B430** (1994) 278–294, [hep-ph/9403240].

[279] A. B. Lahanas, K. Tamvakis, and N. D. Tracas, *One loop corrections to the neutralino sector and radiative electroweak breaking in the MSSM*, *Phys. Lett.* **B324** (1994) 387–396, [hep-ph/9312251].

[280] F. Staub, *SARAH*, arXiv:0806.0538.

[281] F. Staub, *SARAH 4 : A tool for (not only SUSY) model builders*, *Comput. Phys. Commun.* **185** (2014) 1773–1790, [arXiv:1309.7223].

[282] P. Z. Skands et al., *SUSY Les Houches accord: Interfacing SUSY spectrum calculators, decay packages, and event generators*, *JHEP* **07** (2004) 036, [hep-ph/0311123].

[283] A. Djouadi, Y. Mambrini, and M. Muhlleitner, *Chargino and neutralino decays revisited*, *Eur. Phys. J.* **C20** (2001) 563–584, [hep-ph/0104115].

[284] C. H. Chen, M. Drees, and J. F. Gunion, *Searching for invisible and almost invisible particles at e+ e- colliders*, *Phys. Rev. Lett.* **76** (1996) 2002–2005, [hep-ph/9512230].

[285] C. H. Chen, M. Drees, and J. F. Gunion, *A Nonstandard string / SUSY scenario and its phenomenological implications*, *Phys. Rev.* **D55** (1997) 330–347, [hep-ph/9607421]. [Erratum: Phys. Rev.D60,039901(1999)].

[286] C. H. Chen, M. Drees, and J. F. Gunion, *Addendum/erratum for 'searching for invisible and almost invisible particles at e+ e- colliders' [hep-ph/9512230] and 'a nonstandard string/SUSY scenario and its phenomenological implications' [hep-ph/9607421]*, hep-ph/9902309.

[287] H. E. Haber and D. Wyler, *RADIATIVE NEUTRALINO DECAY*, *Nucl. Phys.* **B323** (1989) 267–310.

[288] S. Ambrosanio and B. Mele, *Neutralino decays in the minimal supersymmetric Standard Model*, *Phys. Rev.* **D53** (1996) 2541–2562, [hep-ph/9508237].

[289] S. Ambrosanio and B. Mele, *Supersymmetric scenarios with dominant radiative neutralino decay*, *Phys. Rev.* **D55** (1997) 1399–1417, [hep-ph/9609212]. [Erratum: Phys. Rev.D56,3157(1997)].

[290] H. Baer and T. Krupovnickas, *Radiative neutralino decay in supersymmetric models*, *JHEP* **09** (2002) 038, [hep-ph/0208277].

[291] **CMS** Collaboration, V. Khachatryan et al., *Searches for invisible decays of the Higgs boson in pp collisions at sqrt(s) = 7, 8, and 13 TeV*, *JHEP* **02** (2017) 135, [arXiv:1610.09218].

[292] C. Patrignani and P. D. Group, *Review of particle physics*, *Chinese Physics C* **40** (2016), no. 10 100001.

[293] **LHCb** Collaboration, R. Aaij et al., *First Evidence for the Decay $B_s^0 \to \mu^+\mu^-$*, *Phys. Rev. Lett.* **110** (2013), no. 2 021801, [arXiv:1211.2674].

[294] **Planck** Collaboration, P. A. R. Ade et al., *Planck 2015 results. XIII. Cosmological parameters*, *Astron. Astrophys.* **594** (2016) A13, [arXiv:1502.01589].

[295] **PandaX-II** Collaboration, A. Tan et al., *Dark Matter Results from First 98.7 Days of Data from the PandaX-II Experiment*, *Phys. Rev. Lett.* **117** (2016), no. 12 121303, [arXiv:1607.07400].

[296] D. Tucker-Smith and N. Weiner, *Inelastic dark matter*, *Phys. Rev.* **D64** (2001) 043502, [hep-ph/0101138].

[297] H. Baer, K.-Y. Choi, J. E. Kim, and L. Roszkowski, *Dark matter production in the early Universe: beyond the thermal WIMP paradigm*, *Phys. Rept.* **555** (2015) 1–60, [arXiv:1407.0017].

[298] B. S. Acharya, P. Kumar, K. Bobkov, G. Kane, J. Shao, and S. Watson, *Non-thermal Dark Matter and the Moduli Problem in String Frameworks*, *JHEP* **06** (2008) 064, [arXiv:0804.0863].

[299] **ATLAS** Collaboration, M. Aaboud et al., *Search for long-lived, massive particles in events with displaced vertices and missing transverse momentum in $\sqrt{s} = 13$ TeV pp collisions with the ATLAS detector*, arXiv:1710.04901.

[300] A. Ghosh, T. Mondal, and B. Mukhopadhyaya, *Heavy stable charged tracks as signatures of non-thermal dark matter at the LHC : a study in some non-supersymmetric scenarios*, *JHEP* **12** (2017) 136, [arXiv:1706.06815].

[301] S. Biswas, *Reconstruction of the left-chiral tau-sneutrino in supersymmetry with a right-sneutrino as the lightest supersymmetric particle*, *Phys. Rev.* **D82** (2010) 075020, [arXiv:1002.4395].

[302] **CMS** Collaboration, *Search for electroweak production of charginos and neutralinos in multilepton final states in pp collision data at $\sqrt{s} = 13$ TeV*, Tech. Rep. CMS-PAS-SUS-16-039, CERN, Geneva, 2017.

[303] **CMS** Collaboration, *Search for new physics in events with two low momentum opposite-sign leptons and missing transverse energy at $\sqrt{s} = 13$ TeV*, Tech. Rep. CMS-PAS-SUS-16-048, CERN, Geneva, 2017.

[304] **ATLAS** Collaboration, M. Aaboud et al., *Search for electroweak production of supersymmetric states in scenarios with compressed mass spectra at $\sqrt{s} = 13$ TeV with the ATLAS detector*, *Phys. Rev.* **D97** (2018), no. 5 052010, [arXiv:1712.08119].

[305] **ATLAS** Collaboration, *Search for electroweak production of supersymmetric particles in the two and three lepton final state at $\sqrt{s} = 13$ TeV with the ATLAS detector*, Tech. Rep. ATLAS-CONF-2017-039, CERN, Geneva, Jun, 2017.

[306] **ATLAS** Collaboration, M. Aaboud et al., *Search for dark matter and other new phenomena in events with an energetic jet and large missing transverse momentum using the ATLAS detector*, *JHEP* **01** (2018) 126, [arXiv:1711.03301].

[307] **CMS** Collaboration, *Search for supersymmetry in events with at least one soft lepton, low jet multiplicity, and missing transverse momentum in proton-proton collisions at $\sqrt{s} = 13$ TeV*, Tech. Rep. CMS-PAS-SUS-16-052, CERN, Geneva, 2017.

[308] **ATLAS** Collaboration, M. Aaboud et al., *Search for a new heavy gauge boson resonance decaying into a lepton and missing transverse momentum in 36 $fb^{-1}$ of pp collisions at $\sqrt{s} = 13$ TeV with the ATLAS experiment*, arXiv:1706.04786.

[309] **CMS** Collaboration, V. Khachatryan et al., *Search for heavy gauge W' boson in events with an energetic lepton and large missing transverse momentum at $\sqrt{s} = 13$ TeV*, *Phys. Lett.* **B770** (2017) 278–301, [arXiv:1612.09274].

[310] **CMS** Collaboration, V. Khachatryan et al., *Search for supersymmetry in events with soft leptons, low jet multiplicity, and missing transverse energy in proton–proton collisions at $\sqrt{s}$=8 TeV*, *Phys. Lett.* **B759** (2016) 9–35, [arXiv:1512.08002].

[311] **CMS** Collaboration, A. M. Sirunyan et al., *Search for physics beyond the standard model in events with two leptons of same sign, missing transverse momentum, and jets in proton–proton collisions at $\sqrt{s} = 13$ TeV*, *Eur. Phys. J.* **C77** (2017), no. 9 578, [arXiv:1704.07323].

[312] **CMS** Collaboration, *Search for selectrons and smuons at $\sqrt{s} = 13$ TeV*, Tech. Rep. CMS-PAS-SUS-17-009, CERN, Geneva, 2017.

[313] **CMS** Collaboration, A. M. Sirunyan et al., *Search for electroweak production of charginos and neutralinos in multilepton final states in proton-proton collisions at $\sqrt{s} = 13$ TeV*, *JHEP* **03** (2018) 166, [arXiv:1709.05406].

[314] **ATLAS** Collaboration, G. Aad et al., *Search for direct production of charginos and neutralinos in events with three leptons and missing transverse momentum in* $\sqrt{s} =$ *8TeV pp collisions with the ATLAS detector*, *JHEP* **04** (2014) 169, [arXiv:1402.7029].

[315] **ATLAS** Collaboration, G. Aad et al., *Search for direct top squark pair production in events with a Z boson, b-jets and missing transverse momentum in sqrt(s)=8 TeV pp collisions with the ATLAS detector*, *Eur. Phys. J.* **C74** (2014), no. 6 2883, [arXiv:1403.5222].

[316] **ATLAS** Collaboration, G. Aad et al., *Search for supersymmetry at* $\sqrt{s}$*=8 TeV in final states with jets and two same-sign leptons or three leptons with the ATLAS detector*, *JHEP* **06** (2014) 035, [arXiv:1404.2500].

[317] **ATLAS** Collaboration, G. Aad et al., *Search for supersymmetry in events containing a same-flavour opposite-sign dilepton pair, jets, and large missing transverse momentum in* $\sqrt{s} = 8$ *TeV pp collisions with the ATLAS detector*, *Eur. Phys. J.* **C75** (2015), no. 7 318, [arXiv:1503.03290]. [Erratum: Eur. Phys. J.C75,no.10,463(2015)].

[318] **ATLAS** Collaboration, G. Aad et al., *ATLAS Run 1 searches for direct pair production of third-generation squarks at the Large Hadron Collider*, *Eur. Phys. J.* **C75** (2015), no. 10 510, [arXiv:1506.08616]. [Erratum: Eur. Phys. J.C76,no.3,153(2016)].

[319] **ATLAS** Collaboration, *Search for supersymmetry at* $\sqrt{s} = 8$ *TeV in final states with jets, missing transverse momentum and one isolated lepton*, Tech. Rep. ATLAS-CONF-2012-104, CERN, Geneva, Aug, 2012.

[320] **ATLAS** Collaboration, *Search for direct production of charginos and neutralinos in events with three leptons and missing transverse momentum in 21* $fb^{-1}$ *of pp collisions at* $\sqrt{s} = 8$ *TeV with the ATLAS detector*, Tech. Rep. ATLAS-CONF-2013-035, CERN, Geneva, Mar, 2013.

[321] **ATLAS** Collaboration, *Search for direct-slepton and direct-chargino production in final states with two opposite-sign leptons, missing transverse momentum and no jets in 20/fb of pp collisions at sqrt(s) = 8 TeV with the ATLAS detector*, Tech. Rep. ATLAS-CONF-2013-049, CERN, Geneva, May, 2013.

[322] **ATLAS** Collaboration, *Search for strong production of supersymmetric particles in final states with missing transverse momentum and at least three b-jets using 20.1 fb−1 of pp collisions at sqrt(s) = 8 TeV with the ATLAS Detector.*, Tech. Rep. ATLAS-CONF-2013-061, CERN, Geneva, Jun, 2013.

[323] **ATLAS** Collaboration, *Search for strongly produced supersymmetric particles in decays with two leptons at* $\sqrt{s}$ *= 8 TeV*, Tech. Rep. ATLAS-CONF-2013-089, CERN, Geneva, Aug, 2013.

[324] **CMS** Collaboration, V. Khachatryan et al., *Search for Physics Beyond the Standard Model in Events with Two Leptons, Jets, and Missing Transverse Momentum in pp Collisions at sqrt(s) = 8 TeV*, *JHEP* **04** (2015) 124, [arXiv:1502.06031].

[325] **CMS** Collaboration, V. Khachatryan et al., *Search for the production of dark matter in association with top-quark pairs in the single-lepton final state in proton-proton collisions at* $\sqrt{s}$ *= 8 TeV*, *JHEP* **06** (2015) 121, [arXiv:1504.03198].

[326] **CMS** Collaboration, *Search for supersymmetry in pp collisions at sqrt(s) = 8 Tev in events with two opposite sign leptons, large number of jets, b-tagged jets, and large missing transverse energy.*, Tech. Rep. CMS-PAS-SUS-13-016, CERN, Geneva, 2013.

[327] **ATLAS** Collaboration, G. Aad et al., *Search for supersymmetry at* $\sqrt{s} = 13$ *TeV in final states with jets and two same-sign leptons or three leptons with the ATLAS detector*, *Eur. Phys. J.* **C76** (2016), no. 5 259, [arXiv:1602.09058].

[328] **ATLAS** Collaboration, M. Aaboud et al., *Search for new phenomena in final states with an energetic jet and large missing transverse momentum in pp collisions at* $\sqrt{s} = 13$ *TeV using the ATLAS detector*, *Phys. Rev.* **D94** (2016), no. 3 032005, [arXiv:1604.07773].

[329] **ATLAS** Collaboration, G. Aad et al., *Search for gluinos in events with an isolated lepton, jets and missing transverse momentum at* $\sqrt{s}$ *= 13 Te V with the ATLAS detector*, *Eur. Phys. J.* **C76** (2016), no. 10 565, [arXiv:1605.04285].

[330] **ATLAS** Collaboration, G. Aad et al., *Search for pair production of gluinos decaying via stop and sbottom in events with b-jets and large missing transverse momentum in pp collisions at* $\sqrt{s} = 13$ *TeV with the ATLAS detector*, *Phys. Rev.* **D94** (2016), no. 3 032003, [arXiv:1605.09318].

[331] **ATLAS** Collaboration, *Search for production of vector-like top quark pairs and of four top quarks in the lepton-plus-jets final state in pp collisions at* $\sqrt{s} = 13$ *TeV with the ATLAS detector*, Tech. Rep. ATLAS-CONF-2016-013, CERN, Geneva, Mar, 2016.

[332] **ATLAS** Collaboration, *A search for Supersymmetry in events containing a leptonically decaying Z boson, jets and missing transverse momentum in* $\sqrt{s} = 13$ *TeV pp collisions with the ATLAS detector*, Tech. Rep. ATLAS-CONF-2015-082, CERN, Geneva, Dec, 2015.

[333] **ATLAS** Collaboration, *Search for direct top squark pair production and dark matter production in final states with two leptons in* $\sqrt{s} = 13$ *TeV pp collisions using 13.3* $fb^{-1}$ *of ATLAS data*, Tech. Rep. ATLAS-CONF-2016-076, CERN, Geneva, Aug, 2016.

[334] **ATLAS** Collaboration, *Search for top squarks in final states with one isolated lepton, jets, and missing transverse momentum in* $\sqrt{s} = 13$ *TeV pp collisions with the ATLAS detector*, Tech. Rep. ATLAS-CONF-2016-050, CERN, Geneva, Aug, 2016.

[335] **CMS** Collaboration, V. Khachatryan et al., *Search for new physics in final states with two opposite-sign, same-flavor leptons, jets, and missing transverse momentum in pp collisions at sqrt(s) = 13 TeV*, *JHEP* **12** (2016) 013, [arXiv:1607.00915].

[336] **CMS** Collaboration, V. Khachatryan et al., *Search for narrow resonances in dilepton mass spectra in proton-proton collisions at* $\sqrt{s}$ *= 13 TeV and combination with 8 TeV data*, *Phys. Lett.* **B768** (2017) 57–80, [arXiv:1609.05391].

[337] **CMS** Collaboration, *Search for supersymmetry in events with tau leptons and missing transverse momentum in proton-proton collisions at sqrt(s)=13 TeV*, Tech. Rep. CMS-PAS-SUS-17-002, CERN, Geneva, 2017.

[338] **ATLAS** Collaboration, M. Aaboud et al., *Search for supersymmetry in final states with two same-sign or three leptons and jets using 36* $fb^{-1}$ *of* $\sqrt{s} = 13$ *TeV pp collision data with the ATLAS detector*, arXiv:1706.03731.

[339] **ATLAS** Collaboration, *Search for supersymmetry in events with four or more leptons in* $\sqrt{s} = 13\,\mathrm{TeV}$ *pp collisions using* $13.3\,\mathrm{fb}^{-1}$ *of ATLAS data.*, Tech. Rep. ATLAS-CONF-2016-075, CERN, Geneva, Aug, 2016.

[340] **CMS** Collaboration, V. Khachatryan et al., *Search for new phenomena with multiple charged leptons in proton–proton collisions at* $\sqrt{s} = 13$ *TeV*, *Eur. Phys. J.* **C77** (2017), no. 9 635, [arXiv:1701.06940].

[341] D. Dercks, N. Desai, J. S. Kim, K. Rolbiecki, J. Tattersall, and T. Weber, *CheckMATE 2: From the model to the limit*, arXiv:1611.09856.

[342] T. Sjostrand, S. Mrenna, and P. Z. Skands, *A Brief Introduction to PYTHIA 8.1*, *Comput. Phys. Commun.* **178** (2008) 852–867, [arXiv:0710.3820].

[343] T. Sjöstrand, S. Ask, J. R. Christiansen, R. Corke, N. Desai, P. Ilten, S. Mrenna, S. Prestel, C. O. Rasmussen, and P. Z. Skands, *An Introduction to PYTHIA 8.2*, *Comput. Phys. Commun.* **191** (2015) 159–177, [arXiv:1410.3012].

[344] E. Conte, B. Fuks, and G. Serret, *MadAnalysis 5, A User-Friendly Framework for Collider Phenomenology*, *Comput. Phys. Commun.* **184** (2013) 222–256, [arXiv:1206.1599].

[345] E. Conte, B. Dumont, B. Fuks, and C. Wymant, *Designing and recasting LHC analyses with MadAnalysis 5*, *Eur. Phys. J.* **C74** (2014), no. 10 3103, [arXiv:1405.3982].

[346] B. Dumont, B. Fuks, S. Kraml, S. Bein, G. Chalons, E. Conte, S. Kulkarni, D. Sengupta, and C. Wymant, *Toward a public analysis database for LHC new physics searches using MADANALYSIS 5*, *Eur. Phys. J.* **C75** (2015), no. 2 56, [arXiv:1407.3278].

[347] A. Giammanco and R. Schwienhorst, *Single top-quark production at the Tevatron and the LHC*, *Rev. Mod. Phys.* **90** (2018), no. 3 035001, [arXiv:1710.10699].

[348] M. Czakon and A. Mitov, *Top++: A Program for the Calculation of the Top-Pair Cross-Section at Hadron Colliders*, *Comput. Phys. Commun.* **185** (2014) 2930, [arXiv:1112.5675].

[349] N. Kidonakis, *Soft-gluon corrections for $tW$ production at $N^3LO$*, *Phys. Rev.* **D96** (2017), no. 3 034014, [arXiv:1612.06426].

[350] **CMS** Collaboration, *Performance of reconstruction and identification of tau leptons in their decays to hadrons and tau neutrino in LHC Run-2*, Tech. Rep. CMS-PAS-TAU-16-002, CERN, Geneva, 2016.

[351] **ATLAS** Collaboration, M. Aaboud et al., *Search for the direct production of charginos and neutralinos in $\sqrt{s} = 13$ TeV pp collisions with the ATLAS detector*, arXiv:1708.07875.